

## Control of stick-slip vibrations in drilling systems

**Citation for published version (APA):**

Vromen, T. G. M. (2015). *Control of stick-slip vibrations in drilling systems*. [Phd Thesis 1 (Research TU/e / Graduation TU/e), Mechanical Engineering]. Technische Universiteit Eindhoven.

**Document status and date:**

Published: 30/11/2015

**Document Version:**

Publisher's PDF, also known as Version of Record (includes final page, issue and volume numbers)

**Please check the document version of this publication:**

- A submitted manuscript is the version of the article upon submission and before peer-review. There can be important differences between the submitted version and the official published version of record. People interested in the research are advised to contact the author for the final version of the publication, or visit the DOI to the publisher's website.
- The final author version and the galley proof are versions of the publication after peer review.
- The final published version features the final layout of the paper including the volume, issue and page numbers.

[Link to publication](#)

**General rights**

Copyright and moral rights for the publications made accessible in the public portal are retained by the authors and/or other copyright owners and it is a condition of accessing publications that users recognise and abide by the legal requirements associated with these rights.

- Users may download and print one copy of any publication from the public portal for the purpose of private study or research.
- You may not further distribute the material or use it for any profit-making activity or commercial gain
- You may freely distribute the URL identifying the publication in the public portal.

If the publication is distributed under the terms of Article 25fa of the Dutch Copyright Act, indicated by the "Taverne" license above, please follow below link for the End User Agreement:

[www.tue.nl/taverne](http://www.tue.nl/taverne)

**Take down policy**

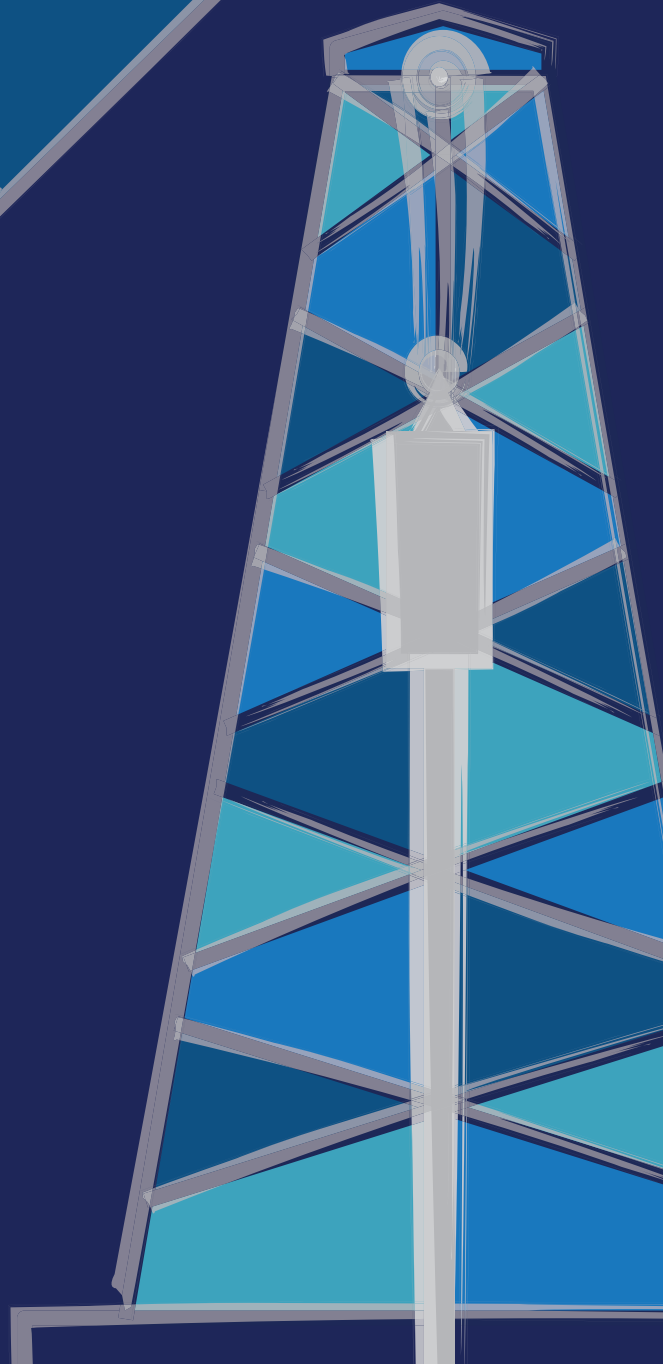
If you believe that this document breaches copyright please contact us at:

[openaccess@tue.nl](mailto:openaccess@tue.nl)

providing details and we will investigate your claim.

# Control of stick-slip vibrations in drilling systems

Thijs Vromen





# Control of stick-slip vibrations in drilling systems

Thijs Vromen





This research is supported by Shell Global Solutions International B.V., Rijswijk, the Netherlands.

T.G.M. Vromen, *Control of stick-slip vibrations in drilling systems*. PhD thesis, Eindhoven University of Technology, Eindhoven, the Netherlands, 2015.

A catalogue record is available from the Eindhoven University of Technology Library.  
ISBN: 978-90-386-3966-6

Printed by CPI - Koninklijke Wöhrmann, Zutphen, the Netherlands.

© 2015 by T.G.M. Vromen. All rights reserved.

# Control of stick-slip vibrations in drilling systems

PROEFSCHRIFT

ter verkrijging van de graad van doctor aan de  
Technische Universiteit Eindhoven, op gezag van de  
rector magnificus, prof.dr.ir. F.P.T. Baaijens, voor een  
commissie aangewezen door het College voor  
Promoties, in het openbaar te verdedigen  
op maandag 30 november 2015 om 16.00 uur

door

Thijs Godefridus Monica Vromen

geboren te Heerlen

Dit proefschrift is goedgekeurd door de promotoren en de samenstelling van de promotiecommissie is als volgt:

|                          |  |
|--------------------------|--|
| voorzitter:              | prof.dr.ir. A.A. van Steenhoven                              |
| 1 <sup>e</sup> promotor: | prof.dr. H. Nijmeijer  |
| 2 <sup>e</sup> promotor: | prof.dr.ir. N. van de Wouw                                   |
| leden:                   | prof.dr. S. Weiland  |
|                          | prof.dr. E.M. Detournay (University of Minnesota)            |
|                          | prof.dr. W. Lacarbonara (Sapienza Università di Roma)        |
| adviseur:                | dr.ir. P. Astrid (Shell Global Solutions International B.V.) |

Het onderzoek dat in dit proefschrift wordt beschreven is uitgevoerd in overeenstemming met de TU/e Gedragscode Wetenschapsbeoefening.

---

# Contents

---

|          |  |           |
|----------|--|-----------|
| <b>1</b> | <b>Introduction</b>  | <b>1</b>  |
| 1.1      | Stick-slip vibrations in drilling systems . . . . .            | 2         |
| 1.1.1    | Mitigation of stick-slip vibrations . . . . .                  | 3         |
| 1.2      | Objectives and contributions . . . . .                         | 5         |
| 1.2.1    | Contributions of the thesis . . . . .                          | 5         |
| 1.3      | Outline . . . . .  | 8         |
| <b>2</b> | <b>Modelling of the torsional drill-string dynamics</b>        | <b>11</b> |
| 2.1      | Introduction . . . . .   | 11        |
| 2.2      | Modelling of the drill-string dynamics . . . . .               | 11        |
| 2.2.1    | Modelling for control of torsional vibrations . . . . .        | 13        |
| 2.3      | Drill-string model . . . . .                                   | 16        |
| 2.3.1    | Different model representations . . . . .                      | 23        |
| 2.4      | Stability of the drill-string dynamics . . . . .               | 26        |
| 2.5      | Simulation of the drill-string dynamics . . . . .              | 27        |
| 2.6      | Summary . . . . .  | 28        |
| <b>3</b> | <b>Design of an observer-based output-feedback controller</b>  | <b>31</b> |
| 3.1      | Introduction . . . . .   | 31        |
| 3.1.1    | Preliminaries . . . . .  | 33        |
| 3.2      | Drill-string dynamics model . . . . .                          | 34        |
| 3.2.1    | Reduced-order model . . . . .                                  | 36        |
| 3.3      | Control problem formulation . . . . .                          | 39        |
| 3.3.1    | Controller objectives . . . . .                                | 39        |
| 3.3.2    | Model reformulation . . . . .                                  | 40        |
| 3.4      | Design of observer-based output-feedback controllers . . . . . | 41        |
| 3.4.1    | State-feedback controller design . . . . .                     | 42        |
| 3.4.2    | Observer design . . . . .                                      | 44        |
| 3.4.3    | Output-feedback control design . . . . .                       | 45        |

|          |   |            |
|----------|---|------------|
| 3.5      | A simulation case study . . . . .   | 45         |
| 3.6      | Controller design for the 18-DOF model . . . . .  | 52         |
| 3.6.1    | Stability analysis . . . . .  | 55         |
| 3.7      | Robustness of the closed-loop system . . . . .  | 57         |
| 3.7.1    | Different operating velocity . . . . .  | 58         |
| 3.7.2    | Changing bit-rock interaction model . . . . .   | 59         |
| 3.7.3    | Sensor and actuator noise disturbances . . . . .  | 63         |
| 3.7.4    | Changing length of the drill-string . . . . .   | 63         |
| 3.8      | Discussion . . . . .  | 68         |
| <b>4</b> | <b>Design of a linear robust output-feedback controller</b>                             | <b>69</b>  |
| 4.1      | Introduction . . . . .  | 69         |
| 4.2      | Drill-string dynamics model . . . . .   | 72         |
| 4.3      | Control problem formulation . . . . .   | 74         |
| 4.3.1    | Controller objectives . . . . .   | 74         |
| 4.3.2    | Model reformulation . . . . .   | 75         |
| 4.4      | Controller design methodology . . . . .   | 76         |
| 4.4.1    | Nominal stability and performance . . . . .   | 77         |
| 4.4.2    | Alternative robust performance . . . . .  | 79         |
| 4.4.3    | Skewed- $\mu$ DK-iteration . . . . .  | 81         |
| 4.4.4    | Closed-loop stability analysis . . . . .  | 83         |
| 4.5      | Controller synthesis . . . . .  | 84         |
| 4.5.1    | Weighting filter design . . . . .   | 85         |
| 4.5.2    | Controller synthesis results . . . . .  | 87         |
| 4.6      | Simulation results . . . . .  | 90         |
| 4.6.1    | Comparison with the observer-based output-feedback controller design strategy . . . . . | 93         |
| 4.7      | Robustness of the closed-loop system . . . . .  | 95         |
| 4.7.1    | Different operating velocity . . . . .  | 97         |
| 4.7.2    | Changing bit-rock interaction model . . . . .   | 99         |
| 4.7.3    | Sensor and actuator noise disturbances . . . . .  | 101        |
| 4.7.4    | Changing length of the drill-string . . . . .   | 103        |
| 4.8      | Summary . . . . .   | 108        |
| <b>5</b> | <b>Design of an experimental drill-string setup</b>                                     | <b>109</b> |
| 5.1      | Introduction . . . . .  | 109        |
| 5.2      | Modelling of the dynamics of the drill-string setup . . . . .                           | 110        |
| 5.2.1    | Reduced-order model . . . . .   | 113        |
| 5.2.2    | Dynamical model of the experimental setup . . . . .                                     | 114        |
| 5.2.3    | Parameter identification . . . . .  | 117        |
| 5.2.4    | Scaling of the drill-string model . . . . .   | 119        |
| 5.3      | The experimental drill-string setup . . . . .   | 123        |
| 5.4      | Summary . . . . .   | 128        |

---

|          |  |            |
|----------|--|------------|
| <b>6</b> | <b>Experimental results: identification and controller implementation</b>                                | <b>129</b> |
| 6.1      | Introduction . . . . .   | 129        |
| 6.2      | Parameter identification and compensation . . . . .  | 130        |
| 6.2.1    | Compensation of motor dynamics . . . . .   | 130        |
| 6.2.2    | Identification of the setup parameters . . . . .   | 133        |
| 6.3      | Emulation of additional dynamics . . . . .   | 138        |
| 6.3.1    | Drill-string borehole interaction torques . . . . .  | 140        |
| 6.3.2    | Bit-rock interaction torque . . . . .  | 142        |
| 6.3.3    | Additional damping term . . . . .  | 144        |
| 6.4      | Experimental controller validation . . . . .   | 145        |
| 6.4.1    | Startup scenario for experiments . . . . .   | 146        |
| 6.4.2    | SoftTorque controller . . . . .  | 148        |
| 6.4.3    | State-feedback controller . . . . .  | 149        |
| 6.4.4    | Observer-based output-feedback controller . . . . .  | 154        |
| 6.4.5    | $\mathcal{H}_\infty$ -based output-feedback controller . . . . .   | 156        |
| 6.5      | Summary . . . . .  | 159        |
| <b>7</b> | <b>Modelling and analysis of drilling systems for the assessment of a down-hole anti stick-slip tool</b> | <b>161</b> |
| 7.1      | Introduction . . . . .   | 161        |
| 7.2      | Anti stick-slip tool . . . . .   | 164        |
| 7.3      | Modelling of the drill-string dynamics . . . . .   | 166        |
| 7.3.1    | Modelling of the benchmark drill-string dynamics . . . . .   | 166        |
| 7.3.2    | Modelling of the drill-string dynamics including anti stick-slip tool . . . . .                          | 169        |
| 7.3.3    | Model reformulation . . . . .  | 171        |
| 7.4      | Simulation results . . . . .   | 174        |
| 7.4.1    | Simulation results of the benchmark model . . . . .  | 175        |
| 7.4.2    | Simulation results of the model including anti stick-slip tool . . . . .                                 | 176        |
| 7.4.3    | Investigation of the effect of the tool on the rate-of-penetration . . . . .                             | 179        |
| 7.5      | Detailed analysis of the drill-string dynamics including anti stick-slip tool . . . . .                  | 182        |
| 7.5.1    | Linearization of the drill-string dynamics . . . . .   | 183        |
| 7.5.2    | Two time-scale analysis . . . . .  | 188        |
| 7.6      | Discussion . . . . .   | 192        |
| 7.7      | Recommendations for future research . . . . .  | 194        |
| <b>8</b> | <b>Conclusions and recommendations</b>   | <b>195</b> |
| 8.1      | Conclusions . . . . .  | 195        |
| 8.2      | Recommendations . . . . .  | 198        |

---

|          |  |            |
|----------|--|------------|
| <b>A</b> | <b>Drill-string model settings</b>   | <b>203</b> |
| A.1      | FEM model drill-string configuration . . . . .   | 204        |
| <b>B</b> | <b>Proofs and technical results</b>  | <b>207</b> |
| B.1      | Proof of Theorem 3.1 . . . . .   | 207        |
| B.2      | Proof of Theorem 3.2 . . . . .   | 209        |
| B.3      | Proof of Theorem 3.3 . . . . .   | 210        |
| <b>C</b> | <b>Time-stepping scheme for first-order systems</b>  | <b>213</b> |
| <b>D</b> | <b>Derivation and parameters of the drill-string model including anti stick-slip tool</b>    | <b>217</b> |
| D.1      | Derivation equations of motion . . . . .   | 217        |
| D.2      | Parameters drill-string model including anti stick-slip tool . . . .                         | 219        |
| D.3      | Investigation of the effect of the tool on the rate-of-penetration:<br>50 rpm case . . . . . | 222        |
|          | <b>Bibliography</b>  | <b>225</b> |
|          | <b>Acronyms</b>  | <b>235</b> |
|          | <b>Summary</b>   | <b>237</b> |
|          | <b>Societal summary</b>  | <b>239</b> |
|          | <b>Samenvatting</b>  | <b>241</b> |
|          | <b>Dankwoord</b>   | <b>243</b> |
|          | <b>Curriculum vitae</b>  | <b>245</b> |

# Chapter 1

---

## Introduction

---

Drilling systems are used to drill wells in the earth's surface for the exploration and production of, for example, water, oil, natural gas, mineral resources and geo-thermal energy. In this work, the focus is on oil-field drilling systems. The earliest known oil wells were drilled in China in 347 AD. These wells were up to approximately 240 m deep and were percussion-drilled using bits attached to bamboo poles [113]. Although the main purpose for these wells was drilling for salt, incidentally oil was also discovered. In these days, both oil and gas were used for heating and lighting. Later, when oil was still mainly exploited from surface seeps, oil was also used for fuel and medicinal purposes [118]. However, it lasted till the 19<sup>th</sup> century until engineers began drilling deliberately for petroleum. This resulted in, what is reported as, the first modern oil well in 1859 [118]. The earliest oil wells in modern times were drilled percussively, by repeatedly raising and dropping a cable tool. In the 20<sup>th</sup> century cable tools were largely replaced with rotary drilling systems, which could drill boreholes to much greater depths and in less time.

At the beginning of the 20<sup>th</sup> century, the industrial revolution had progressed to the extent that the use of refined oil for illumination ceased to be of primary importance. The oil industry became the major supplier of energy largely because of the advent of the automobile. Although oil is also of great importance for the petrochemical industry (e.g. for the production of plastics, soaps and detergents, solvents, synthetic fibres and rubbers) its primary importance is as an energy source [95]. In both applications, it only became more important in the 20<sup>th</sup> century, resulting in an enormous increase of the oil production. Around 1900, the world oil production was nearly 410.000 barrels per day, surpassing 1 million barrels per day (Mmbpd) in 1913, 10 Mmbpd in 1950 and peaked at over 62 Mmbpd in 1979 [118]. After a drop, the world production again exceeded 60 Mmbpd in 1986 and 70 Mmbpd in 1995, 80 Mmbpd in 2004 and currently



(2014) the world oil production is over 93 million barrels per day [117]. This increasing demand for the production of oil and the fact that the “easier” areas of the world became intensively explored, resulted in increasing attention to harsher and more difficult environments. For example, until the 1970’s, most oil wells were vertical. However, modern directional drilling technologies allow for strongly deviated wells which can actually become horizontal. The use of deviated and horizontal wells made it possible to reach reservoirs several kilometers away from the drilling location. To reach these unconventional reservoir sections, deep and curved borehole geometries need to be drilled. This tendency towards drilling deeper and inclined wells increases the susceptibility to (torsional stick-slip) vibrations for currently used drilling systems. In the next section, stick-slip vibrations in drilling systems are discussed in more detail. The main focus of this thesis is on developing and analyzing (control) strategies to mitigate these vibrations in drilling systems.

This chapter forms a high-level introduction to this thesis as a whole and is written in a concise fashion to highlight the motivation and contributions of the thesis. More detailed literature surveys are presented in the individual chapters.

## 1.1 Stick-slip vibrations in drilling systems

Efficiency, reliability, performance, and safety are important aspects in the drilling of deep wells. One of the main limiting factors in maximizing the drilling performance is the presence of drill-string vibrations. These drill-string vibrations decrease the quality of the borehole, provoke premature wear of drilling equipment resulting in fatigue and induce failures such as drill pipe twist-off [98]. Due to the decreased performance and efficiency, drill-string vibrations can cost operations millions of dollars for each drilling campaign. Thus, mitigation of vibrations and therewith improving the drilling performance is of great economical interest for the oil industry. At the same time, safety remains the top priority and requirement in the drive for performance [47]. In other words, achieving improved performance (e.g. by reducing vibrations), and therewith reduced costs, may not be obtained at the expense of reduced reliability and safety.

Drilling systems are known to exhibit different types of self-excited vibrations, such as axial, lateral and torsional vibrations which lead to bit bouncing, whirling and torsional stick-slip, respectively. The focus in this work is on torsional stick-slip vibrations and in particular on the mitigation of torsional stick-slip vibrations. Torsional stick-slip is characterized by phases in which the bit comes to a complete stop (stick) and phases in which the bit rotates with several times the desired angular velocity (slip). A simulation result of a drill-string system, with a desired angular velocity of 100 rpm, that suffers from stick-slip vibrations is shown in Figure 1.1. The stick-slip limit cycles in the response of the bit angular velocity can be clearly recognized in this figure. In practice, the presence of stick-slip vibrations can be recognized in both down-hole and

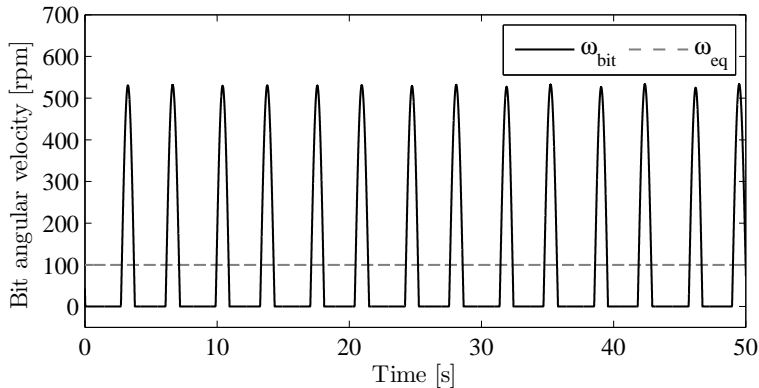


Figure 1.1: Simulation result of a drill-string model to illustrate the stick-slip behavior in the response of the bit angular velocity.

surface measurements [20, 69, 86]. Investigation of these vibrations in terms of modelling, analysis and stick-slip mitigation is an important aspect in the drilling industry. One of the first drill-string vibration models has been developed in [3], where predicted natural frequencies are compared with the frequencies present in (surface) measurements. In [18, 20], the presence of stick-slip vibrations in the drilling system has been reported based on measurements of a down-hole recording tool. The work in [5] presents one of the first analytical treatments of stick-slip vibrations in drill-strings. Extensive overviews regarding modelling of the drilling dynamics can be found in [65, 85, 98, 109, 131].

The main problem with stick-slip vibrations is the fact that it reduces the drilling efficiency, resulting in a decrease of the rate-of-penetration (ROP). In addition, this type of vibrations results in excessive bit wear, and it is detrimental for the tools in the bottom hole assembly (BHA) due to the high angular velocities which are reached during the slip phases. For these reasons, mitigation of stick-slip vibrations is of great interest.

### 1.1.1 Mitigation of stick-slip vibrations

Stick-slip mitigation methods for drilling systems can be divided in two main categories: passive stick-slip suppression and active stick-slip suppression. The first category can be grouped in three sub categories, that is, optimization of the BHA, bit selection and redesign, and the use of down-hole tools [131]. Active stick-slip suppression involves active control by means of feedback control strategies.

A detailed overview of passive stick-slip suppression methods is given in [131]. In the scope of passive solutions we only focus on the use of down-hole tools for stick-slip suppression in this thesis and, in particular, on the anti stick-slip tool

(AST) that has been developed by Tomax [102]. This is a mechanical down-hole tool which aims to adjust the drilling torque automatically and therewith to reduce stick-slip oscillations and to increase the drilling efficiency. Reported field results show that the tool indeed reduces the amount of vibration related failures and improves the drilling ROP [90, 91]. Although these field results provide evidence about the effectiveness of the tool, a fundamental physics-based explanation for these effects is lacking to this date.

The second solution to suppress stick-slip vibrations in drilling systems that is mentioned in literature, is the usage of active feedback control. Early feedback control strategies to actively damp torsional stick-slip vibrations can be found in [40, 51]. Based on these works, the well-known *Soft Torque Rotary System* (also referred to as SoftTorque) has been developed. The underlying idea of this control strategy is to make the top rotary system behave in a “soft” manner and this strategy is widely used in industry. In this controller design strategy, it is assumed that the drilling system behaves like a two degree-of-freedom torsional pendulum of which the first torsional mode can be damped using a PI-controller based on feedback of the surface angular velocity. However, the aforementioned tendency towards drilling deeper and inclined wells, results in drill-strings of several kilometers in length to transmit the axial force and torque necessary to drill the rock formations. The long and slender structure of current drill-string configurations makes drilling systems susceptible to torsional stick-slip vibrations. In contrast to wells drilled 20 to 30 years ago, in current wells the influence of multiple dynamical modes of the drill-string on torsional vibrations has increased [82, 96]. Therefore, current industrial controllers (such as SoftTorque) are not always able to eliminate stick-slip vibrations under the imposed operating conditions [30]. Another reason for the deficiency of current control strategies is the uncertainty in the (nonlinear) bit-rock interaction. In models concerning the torsional drill-string dynamics it is generally assumed that the resisting torque at the bit-rock interface can be modelled as a frictional contact with a velocity-weakening effect [11]. The interaction between the bit and the bottom of the borehole plays an important role in the onset of stick-slip vibrations. However, the cutting process depends, among other things, on the formation, wear state of the bit and the drilling dynamics. These aspects make the interaction process uncertain and varying over time due to changing conditions. Another important aspect in the design of controllers to mitigate stick-slip vibrations in drilling systems is the type of measurements used for feedback control. In literature, some controller design methodologies rely on down-hole measurements (see e.g. [19, 103]). However, down-hole measurements for real-time control purposes are not available in practice, due to limitations on the data rate, time delay of the measurements, and/or the high costs involved.

## 1.2 Objectives and contributions

The concise discussion in the previous section motivates the relevance of the stick-slip oscillation problem in drilling systems. Moreover, the main reasons for the deficiency of current control strategies under the imposed operating conditions are addressed. That is, the influence of multiple dynamical modes of the drill-string on torsional vibrations and the uncertainty in the bit-rock interaction law. Therefore, this thesis considers the design and implementation of controllers for oil-field drill-string systems to eliminate (torsional) stick-slip oscillations. Summarizing, the general objective of this thesis can be stated as follows.

*Develop and analyze (control) strategies to mitigate stick-slip vibrations in drilling systems, hereby addressing the following aspects:*

- 1. Development of controller design strategies for active feedback control of drilling systems with multiple dominant flexibility modes and severe velocity-weakening and uncertainty in the bit-rock interaction;*
- 2. Robustness analysis and validation on a lab-scale drill-string system of the proposed controller design methodologies;*
- 3. Modelling and analysis of passive down-hole tools for the mitigation of stick-slip vibrations and rate-of-penetration increase.*

The robustness of the designed controllers is investigated for operating conditions for which current industrial controllers fail to eliminate stick-slip vibrations. For the experimental validation of the designed control strategies a lab-scale drill-string system is developed. This system is used as an experimental benchmark system for the implementation of the designed controllers and serves as an intermediate step towards field implementation of the controllers on a real rig.

### 1.2.1 Contributions of the thesis

The main contributions of this thesis can be summarized in terms of contributions on modelling for control of torsional vibrations in drill-string systems, on novel controller design strategies for drill-string systems, on realization of a lab-scale drill-string system, on experimental validation of the proposed controllers, and on modelling and analysis for the assessment of a down-hole anti stick-slip tool:

- *Modelling for control of torsional vibrations in drill-string systems:* for the design of controllers to mitigate torsional vibrations in drilling systems, most studies rely on one- or two degree-of-freedom (DOF) models for the torsional drill-string dynamics only. However, as mentioned before,

the influence of multiple dynamical modes of the drill-string on torsional vibrations has increased. In Chapter 2, a multi-modal model of the torsional dynamics, exhibiting the most dominant torsional flexibility modes and based on a finite-element method representation of a realistic drilling system, is proposed as a basis for controller design. The model is based on a jack-up drilling rig used to drill wells of over 6000 m. During operations, stick-slip vibrations have been observed for this rig while it is equipped with a modern SoftTorque system. This motivates the use of this drill-string model as basis for the development of novel controller design methodologies;

- *Novel controller design strategies for drill-string systems:* two model-based output-feedback controller design methodologies are proposed in this thesis.

More specifically, in Chapter 3, a novel nonlinear observer-based output-feedback control strategy mitigating torsional stick-slip vibrations is developed. Using this controller, stick-slip vibrations can be mitigated and the controller has several benefits compared to existing controllers. Existing controllers often rely on one- or two degree-of-freedom (DOF) models for the torsional drill-string dynamics only and are therefore unable to mitigate stick-slip vibrations in drilling systems with multiple dominant flexibility modes. The particular benefits of the proposed nonlinear observer-based output-feedback controller can be summarized as follows. First, it can effectively deal with (realistic) drill-string models with multiple dominant torsional flexibility modes, second, it is robust with respect to severe velocity-weakening (and uncertainty) in the bit-rock interaction and, third, it only employs surface measurements (which is important because down-hole measurements are not available in practice). Additionally, a guarantee for (local) asymptotic stability of the closed-loop reduced-order system is given for bit-rock interaction laws satisfying a certain sector condition (which is beneficial as the bit-rock interaction is subject to uncertainty in practice).

In Chapter 4, a novel linear robust output-feedback controller methodology to eliminate stick-slip vibrations is developed. The same controller objectives as for the nonlinear observer-based output-feedback controller are met; in addition, the controller is optimized to have robustness with respect to uncertainty in the bit-rock interaction and closed-loop performance specifications regarding measurement noise sensitivity and actuator limitations are integrated in the controller design. Stability of the nonlinear closed-loop system is also investigated and conditions on the bit-rock interaction, in terms of a sector bound, for which the desired equilibrium is locally asymptotically stable, have been derived. The combination of robustness with respect to uncertainty in the bit-rock interaction and includ-

ing closed-loop performance specifications in the controller design while guaranteeing (local) stability of the desired setpoint is an important improvement in the design of controllers to mitigate stick-slip vibrations in drilling systems.

For both controllers, the robustness of the closed-loop system is investigated in model-based case studies. The following robustness aspects are key in the scope of practical applications, and are extensively studied in this thesis: robustness with respect to changes in the bit-rock interaction characteristics, increasing length of the drill-string, different desired angular velocities (i.e. increased operating envelope), and sensor and actuator noise.

- *Realization of a lab-scale drill-string system:* based on the drill-string models developed, a lab-scale oil-field drill-string system has been designed and realized, which exhibits the essential dynamics of a real drilling system. With the development and use of such an experimental drill-string system an improved understanding on the dynamical phenomena that occur while drilling can be obtained. Moreover, this system is used for the experimental validation of the proposed controller design strategies. The need for a new setup stems from the fact that the controllers proposed in this thesis focus on the robustness with respect to multiple dominant torsional flexibility modes in the drill-string dynamics. To investigate such robustness aspect, it is important that the experimental setup represents drill-string dynamics with multiple dominant flexibility modes.
- *Experimental validation of controllers for drill-string systems:* experimental validation of the designed controllers is an important intermediate step towards field implementation of the controllers on a real rig. Using the developed experimental setup, controllers can be extensively tested in different scenarios to validate the robustness of the controller design strategies. The industrial SoftTorque controller is implemented on the setup and used as a benchmark control system. The response of the experimental setup matches very well with the response of the drill-string model in simulations (i.e. stick-slip vibrations are observed), which illustrates that the setup is able to accurately emulate the drill-string dynamics to be investigated. The linear robust output-feedback controller and state-feedback controller (the latter representing a step towards implementation of the observer-based output-feedback controller) are also implemented and experimentally validated on the setup. Both controllers successfully stabilize the desired angular velocity and therewith mitigate stick-slip vibrations on the experimental setup in realistic scenarios in which the SoftTorque system can not.
- *Modelling and analysis of passive tools for the mitigation of stick-slip vibra-*

*tions and rate-of-penetration increase*: a modelling and analysis approach for a drill-string system including the anti stick-slip tool (AST) developed by Tomax (see [102]) is developed. Despite numerous successful applications of the tool in the field, a fundamental physics-based explanation of the working principle of the tool is lacking to this date. In this context, an existing drill-string model of the coupled axial and torsional dynamics is extended with a model of the anti stick-slip tool, resulting in a nonlinear (non-smooth) drill-string model with state-dependent delay. A simulation tool is developed to numerically obtain the response of the drill-string model and the dynamic behavior of the key variables of the drill-string system is investigated based on the simulation results. Moreover, we perform dynamic analyses on the drill-string dynamics including the anti stick-slip tool and compare the results with a benchmark model without the tool to assess the effectiveness of the tool in mitigating stick-slip vibrations. The analyses include a stability analysis based on a linearization approach for delay-differential equations with state-dependent delays and a two time-scale analysis. Finally, a (preliminary) study towards the effect of the AST on the rate-of-penetration (ROP) is performed based on the simulation results of the nonlinear model.

### 1.3 Outline

The chapters 3, 4 and 7 are written as research papers, and are therefore self contained. Each of these chapters can be read independently, which might cause some overlap between the chapters. The Chapters 5 and 6 contain a description of the designed lab-scale drill-string setup and the experimental results, respectively. The reading of these chapters requires some prerequisites from Chapters 2-4.

**Chapter 2** presents a model of the torsional dynamics of a drilling system. The model is based on a real drilling system and serves as a basis for the controller design methodologies that are presented in Chapters 3 and 4. Before going into detail on the specific drill-string model, a concise review about modelling of drilling dynamics is given.

In **Chapter 3**, a nonlinear observer-based output-feedback controller design methodology is proposed to mitigate torsional stick-slip vibrations in drilling systems. A complete proof regarding the stability of the closed-loop system is provided and the proposed control strategy is validated by application to a FEM model.

Another controller design methodology is proposed in **Chapter 4**, this controller design method is based on linear robust control techniques. A controller synthesis strategy is developed to optimize the robustness with respect to uncertainty in the bit-rock interaction, while at the same time satisfying performance objectives related to e.g. measurement noise sensitivity. A stability analysis

of the (nonlinear) closed-loop system is performed and the control strategy is validated by application to the same FEM model as used in Chapter 3.

**Chapter 5** presents the design of an experimental drill-string system. This system is designed to represent the dominant dynamics of an oil-field drill-string system. This system can be used for the experimental validation of the proposed controller design strategies and serve as an intermediate step towards field implementation of the controllers on a real rig.

The results of the experiments with the drill-string setup are presented in **Chapter 6**. First, identification experiments to determine the parameters of the setup are discussed. Subsequently, the results of the experiments to validate the controller design methodologies are presented.

**Chapter 7** presents the modelling and analysis approach for the assessment of a down-hole anti stick-slip tool. The dynamic behavior of the system including the tool is investigated based on simulation results and compared with a benchmark model without tool. Moreover, dedicated dynamic analyses on the drill-string dynamics including the anti stick-slip tool are performed to assess its effectiveness to mitigate stick-slip vibrations and to increase ROP.

Finally, conclusions and recommendations for future research are presented in **Chapter 8**.





# Modelling of the torsional drill-string dynamics

---

## 2.1 Introduction

In this chapter, a model of the torsional dynamics of a drilling system is presented. The model is based on a real drilling system and serves as a basis for the controller design methodologies that will be presented in the remainder of this work. Before going into detail on the specific drill-string model, first a concise review about modelling of drilling dynamics is given. Extensive overviews regarding modelling of the drilling dynamics can be found in [109] and [85,98,131], where the latter ones mainly focus on the modelling of torsional vibrations.

In Section 2.2, a short overview of different drill-string models is given, with a focus on models regarding the torsional dynamics suitable for controller design. In Section 2.3, the drill-string model is presented that will be used for controller design in later chapters. Stability properties of the model will be presented in Section 2.4 and a simulation result of the drill-string system in closed-loop with a currently used industrial controller is shown in Section 2.5. Finally, a short summary is given in Section 2.6.

## 2.2 Modelling of the drill-string dynamics

Drilling systems, as schematically shown in Figure 2.1, are used to drill deep wells for the exploration and production of oil and gas, mineral resources and geo-thermal energy. These drilling systems can be roughly divided in three parts; a drill bit at the bottom of the borehole for rock cutting, a drill-string to transmit torque to the bit and a top drive at surface to drive the system. The drill-string

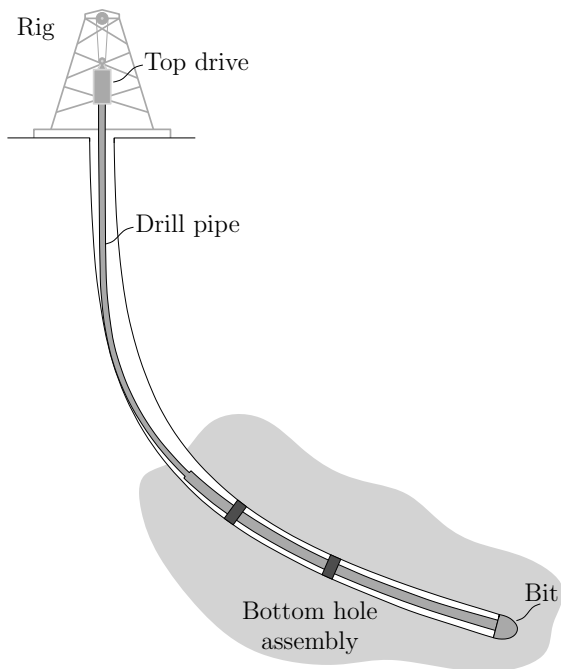


Figure 2.1: Schematic drilling system (adapted from [88]).

is a long and slender structure which can be several kilometers in length. The upper part of the drill-string consists of drill pipe and makes up the majority of the drill-string back up to the surface. The lower part of the drill-string is called the bottom hole assembly (BHA). Often the bit is considered as part of the BHA; in addition, the BHA consists of drill collars, which are heavy, thick-walled tubes used to apply weight to the bit and drilling stabilizers to keep the assembly centered in the hole. The BHA may also contain other components such as a down-hole motor, a rotary steerable system, vibration absorbers (shock subs), measurement while drilling (MWD), and logging while drilling (LWD) tools.

Surface and down-hole measurements [20, 69, 86] show that drilling systems experience different types of oscillations, which significantly decrease the drilling rate-of-penetration due to damage to the drill bit (e.g. bit tooth wear), the drill pipes (e.g. failure due to fatigue) and the bottom hole assembly. Different modes of vibration, such as axial, lateral and torsional vibrations, lead to bit bouncing, whirling and torsional stick-slip, respectively. Reduced drilling efficiency due to vibrations has led to a lot of research interest in this field, since it can cost operations millions of dollars for each drilling campaign. The different types of vibrations in drilling systems are generally quite complex in nature. They are intimately coupled together both linearly and nonlinearly, and occur

simultaneously [16]. Investigation of the fully coupled dynamics is treated in for example [16, 94]. Also several studies investigating the interaction between two of the three modes of vibration can be found in literature. Many studies investigated for example the coupling between the axial and torsional dynamics [6, 32, 37, 93, 100, 128], but also the coupled lateral-torsional dynamics (see e.g. [55, 67, 76, 127]) and axial-lateral dynamics (e.g. [15, 29, 126]) have been investigated. However, most studies focus on one of the modes of vibrations, such as in [33, 70] for the axial vibrations, in [31, 49, 59] for the lateral vibrations, while in [11, 14, 61, 63, 75, 77, 114] the focus is on torsional vibrations. The list of references given above is far from complete, but illustrates the interest in the modelling of drill-string dynamics for the purpose of analyzing different modes of vibration. For an extended overview of oil well drilling systems from a vibrations perspective the reader is referred to [109].

In this thesis, the focus is on torsional vibrations and mitigation of those torsional stick-slip oscillations (see Chapters 3-6), although also a model of the coupled axial-torsional dynamics is used and further developed for the analysis of a passive down-hole Anti Stick-slip Tool (AST) in Chapter 7. Modelling of the torsional drill-string dynamics for controller design purposes is discussed in more detail in the following section.

### 2.2.1 Modelling for control of torsional vibrations

Torsional stick-slip is characterized by phases in which the bit comes to a complete stop (stick) and phases in which the bit rotates with several times the desired angular velocity (slip). This type of vibrations results in excessive bit wear, but is also detrimental for the tools in the BHA due to the high angular velocities which are reached during the slip phases. Controllers for drilling systems therefore aim at drill-string rotation at a constant angular velocity and the mitigation of torsional (stick-slip) oscillations.

For the design of controllers to mitigate torsional vibrations in drilling systems, most studies rely on one- or two degree-of-freedom (DOF) models for the torsional drill-string dynamics only, see e.g. [19, 40, 51, 53, 103]. However, directional wells are nowadays common in the drilling industry and it is not evident that these torsional “pendulum-type” models are still accurate enough in inclined wells. Therefore, multi-DOF models or distributed-parameter models are needed to analyze torsional stick-slip in drilling systems [131]. Moreover, in models taking only the torsional dynamics into account it is generally assumed that the resisting torque at the bit-rock interface can be modelled as a frictional contact with a velocity-weakening effect. However, experiments using single cutters, aiming at the identification of the bit-rock interaction law, have not revealed any velocity-weakening effect [83]. Both these aspects in the modelling of the torsional drill-string dynamics are discussed below.

Let us first focus on the number of degrees of freedom employed in drill-string

models. Drill-string models vary from the 1 or 2-DOF pendulum models to infinite-dimensional partial differential equation (PDE) models and multi-DOF models, either extensions of the lumped parameter models or discretizations of PDE models. Due to their simplicity, the pendulum models are very well suited for controller design. Moreover, as the *Soft Torque Rotary System* [51] has shown, controllers based on these type of models are able to mitigate stick-slip oscillations and are therefore widely used in industry. On the other hand, these models are of course not able to describe all dynamical properties of a drill-string system. In fact, increasing demands on the operating envelope and a tendency towards drilling deeper and inclined wells impose higher demands on the controllers used in drilling systems and therewith, also on the drill-string models used for controller design. Two main reasons for the deficiency of currently used industrial controllers are the influence of multiple dynamical modes of the drill-string on torsional vibrations [82,96] and uncertainty in the bit-rock interaction.

A reported drawback of the use of finite-dimensional models is that these models neglect the time delay needed by the torsional waves to propagate in the drill-string. To solve this issue the drill-string torsional dynamics can be represented by a linear wave equation subject to (nonlinear) boundary conditions for the top drive and frictional processes, see e.g. [4,10,62,115]. Moreover, recent results as presented in e.g. [10,30] show that linear wave equation representations of the drill-string can also be used for controller design. However, these methods require assumptions on the bit-rock interaction and/or trivialize the BHA as a single inertia. On the other hand, discretizations of the wave equation (see [62]) result in a lumped parameter model, i.e. a finite-element representation of the drill-string dynamics, where, of course, a suitable choice for the number of elements in such discretization depends on the application at hand. Instead of discretizing an infinite-dimensional model to obtain a multi-DOF drill-string model, multi-DOF drill-string representations (i.e. FEM representations) can also be based on the properties of the drill-string. In fact, these multi-DOF models are extensions of the pendulum models, where only the BHA inertia (1-DOF models) or both the BHA and top drive inertia (2-DOF models) are taken into account. One can also think of models where the pipe sections and/or the BHA are divided in multiple sections, each section is then represented by an equivalent inertia and these inertias are lumped together to represent the entire drill-string. The simplest extension of the pendulum models is a 3-DOF model, with an additional inertia to represent the drill pipes, see [80], or a 4-DOF model with inertia representing the top drive, drill pipes, drill collars and the bit as in [81].

In this thesis, a multi-modal drill-string model is used and this finite-element model is based on a real drill-string configuration, in which elements represent equivalent pipe sections. This type of model is able to accurately describe the drill-string dynamics. The propagation time of torsional waves in the drill-string

is approximated (in the frequency range relevant for torsional vibrations) by the induced phase lag due to the lumped elements of the finite-element model. Additionally, the bit-rock interaction as well as drill-string borehole interactions can be readily included in the model. Moreover, this model form is suitable for model-based controller design techniques, such as  $\mathcal{H}_\infty$ -control and observer-based controller design approaches, as developed in this thesis in Chapters 3 and 4.

In models that only take the torsional drill-string dynamics into account, it is generally assumed that the resisting torque at the bit-rock interface can be modelled as a frictional contact with a velocity-weakening effect as reported in [11, 115]. This decrease in torque-on-bit for increasing rotational velocity is recognized as the cause of the stick-slip phenomenon. On the other hand, it has to be noted that these experimental results are obtained by averaging the torque-on-bit over multiple revolutions. As already mentioned, experiments with a single cutter [83] show that the rate effects are not a constitutive property of the bit-rock interface. Investigation of the axial and torsional dynamics, coupled using the rate-independent bit-rock interaction law developed in [22], led to the model as presented in [93]. In this approach, both the axial and torsional dynamics are included in the modelling of the drill-string dynamics and coupled via the bit-rock interaction law. In the original model, a characterization of the drilling structure by a 2-DOF system is used, while in [37] an extension is made by using a continuum representation of the drill-string. The used bit-rock interaction model in these models takes into account both cutting and frictional contact and the rate-independent laws are consistent with laboratory results from single cutter experiments. Analysis of this type of model is mainly based on the 2-DOF model representations, see e.g. [21, 38, 79, 93]. The analyses show that the axial dynamics exhibits a stick-slip limit cycle, whose properties are dependent on the rotational speed. This axial limit cycle generates an apparent velocity-weakening effect in the torsional dynamics, leading to torsional vibrations and stick-slip. Hence, the axial dynamics is responsible for the onset of torsional vibrations. This modelling approach is also used in Chapter 7 to analyze the Anti Stick-slip Tool (AST), since this down-hole tool is based on the coupling between the axial and torsional dynamics. However, the observation that such coupling still effectively leads to a velocity-weakening effect of the torque-on-bit with respect to the bit rotational velocity motivates to adopt a modelling-for-control approach for drill-string dynamics involving the torsional dynamics only, as pursued in Chapters 2-6. The drill-string model used in these chapters is a multi-DOF drill-string representation of the torsional dynamics, including a velocity-weakening bit-rock interaction model and resisting torques at multiple elements to model the interaction between the borehole and the drill-string. The modelling approach is discussed in more detail in Section 2.3.

## 2.3 Drill-string model

The system we will investigate is a realistic drill-string model of an offshore jack-up drilling rig and the reservoir sections of the wells are drilled with a 6" PDC bit to reach depths of >6000 m and with an inclination angle up to 60°, resulting in significant resistive torques along the drill-string. The rig is equipped with an AC top drive and fitted with a modern SoftTorque system [64]. However, for this depth and hole size, stick-slip vibrations have been observed in the field for this rig [39], as shown in Figure 2.2. In this figure, measurement data of the real rig is shown. The top drive angular velocity (RPM) and top drive torque (TQ) show severe oscillations, indicating stick-slip at the bit. In addition, the stick-slip severity indicator (*SS*) also shows high values which is a result of (stick-slip) oscillations of the BHA.

A finite-element model of this drilling system, which represents a drill-string of 6249 m in length, has been developed and the simulation results of this model have been validated with field data for a range of operational conditions (such as weight-on-bit (WOB) and angular velocity). The 18-DOF finite-element model is obtained by representing the drill-string by a number of equivalent pipe sections in order to accurately describe the torsional dynamics relevant for stick-slip vibrations. The model is validated by comparing the simulations of the nonlinear model (i.e. including interaction torques) with field measurements of the drill-string system. Figures 2.3 and 2.4 show two cases of this validation study, i.e. the simulation results of the finite-element model are compared with the field data under two different operating conditions, in both cases the drill-string system exhibited stick-slip vibrations at the bit. As can be seen from these figures, the simulation results match with the field data both in terms of the amplitude and the frequency of the oscillations. The latter observations further motivate the usage of the developed model as a basis for controller design in this thesis.

The finite-element method (FEM) representation of the drill-string is a model with 18 elements. The element at the top is a rotational inertia to model the top drive inertia, the subsequent elements are equivalent pipe sections based on the dimensions and material properties of the drill-string, see Appendix A.1 for more details. The resulting model can be written as

$$M\ddot{\theta} + D\dot{\theta} + K_t\theta_d = S_w T_w(\dot{\theta}) + S_b T_{bit}(\dot{\theta}_1) + S_t T_{td} \quad (2.1)$$

with the rotational displacement coordinates  $\theta \in \mathbb{R}^m$  with  $m = 18$ , the top drive motor torque input  $T_{td} \in \mathbb{R}$  being the control input, the bit-rock interaction torque  $T_{bit} \in \mathbb{R}$  and the interaction torques  $T_w \in \mathbb{R}^{m-1}$  between the borehole and the drill-string acting on the nodes of the FEM model. The coordinates  $\theta = [\theta_1 \ \cdots \ \theta_m]^\top$  represent the angular displacements of the nodes of the finite-element representation. Next, we define the difference in angular position between adjacent nodes as follows:  $\theta_d := [\theta_1 - \theta_2 \ \theta_2 - \theta_3 \ \cdots \ \theta_{m-1} - \theta_m]^\top$ . In (2.1), the mass, damping and stiffness matrices are, respectively, given by

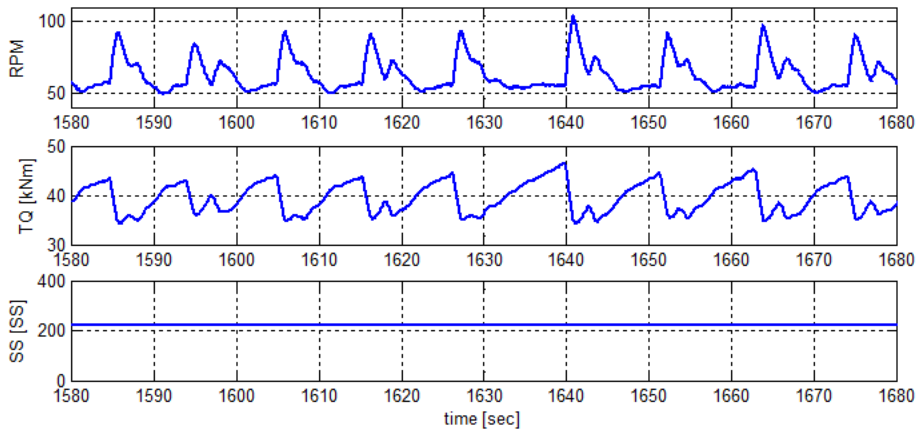


Figure 2.2: Field data of the drilling rig under investigation, indicating severe stick-slip oscillations [39] (desired angular velocity is approximately 50 rpm).

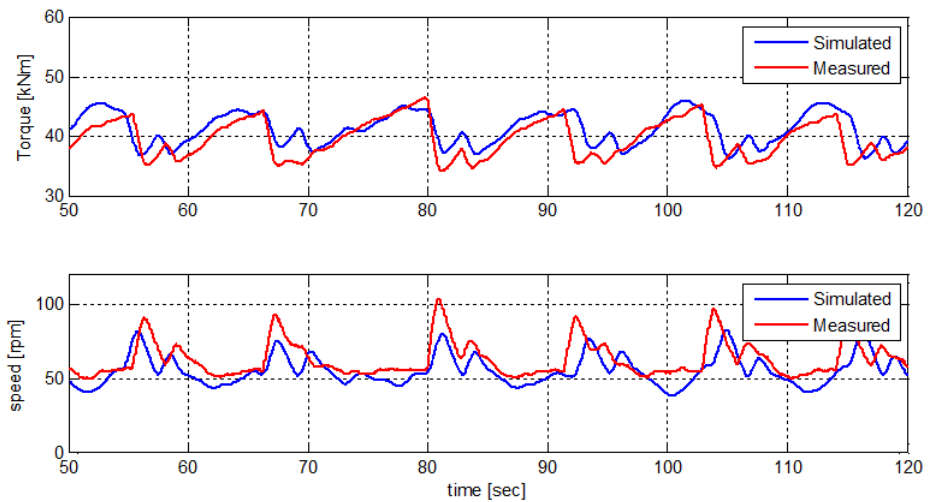


Figure 2.3: Comparison between a simulation result of the FEM model and actual field data of the rig (top drive torque and top drive velocity), the desired angular velocity is approximately 50 rpm [39].



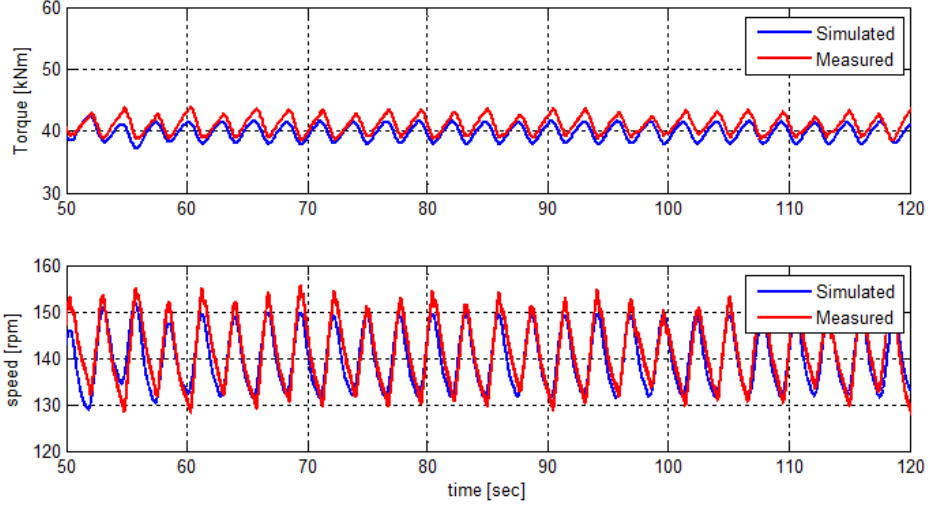


Figure 2.4: Comparison between a simulation result of the FEM model and actual field data of the rig (top drive torque and top drive velocity), the desired angular velocity is approximately 140 rpm [39].

$M \in \mathbb{R}^{m \times m}$ ,  $D \in \mathbb{R}^{m \times m}$  and  $K_t \in \mathbb{R}^{m \times m-1}$ , the matrices  $S_w \in \mathbb{R}^{m \times m-1}$ ,  $S_b \in \mathbb{R}^{m \times 1}$  and  $S_t \in \mathbb{R}^{m \times 1}$  represent the generalized force directions of the interaction torques, the bit torque and the input torque, respectively. The coordinates  $\theta$  are chosen such that the first element ( $\theta_1$ ) describes the rotation of the bit and the last element ( $\theta_{18}$ ) the rotation of the top drive at surface, as illustrated in Figure 2.5. The interaction between the borehole and the drill-string is modelled as Coulomb friction, that is

$$T_{w,i} \in T_i \text{Sign}(\dot{\theta}_i), \quad \text{for } i = 2, \dots, m, \quad (2.2)$$

with  $T_i$  representing the amount of friction at each element and the set-valued sign function defined as

$$\text{Sign}(y) \triangleq \begin{cases} -1, & y < 0 \\ [-1, 1], & y = 0 \\ 1, & y > 0. \end{cases} \quad (2.3)$$

Note that possible viscous effects between the drill-string and the borehole are captured in the damping matrix  $D$ , which motivates that only Coulomb effects are taken into account in the interaction torques  $T_w$ . The bit-rock interaction model is given by

$$T_{bit}(\dot{\theta}_1) \in \text{Sign}(\dot{\theta}_1) \left( T_d + (T_s - T_d) e^{-v_d |\dot{\theta}_1|} \right) \quad (2.4)$$

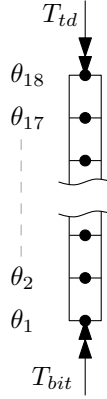


Figure 2.5: Schematic representation of the 18-DOF finite-element method model.

with  $T_s$  the static torque,  $T_d$  the dynamic torque and  $v_d := \frac{30}{N_d\pi}$  indicating the decrease from static to dynamic torque. A schematic representation of the bit-rock interaction is shown in Figure 2.6. For typical parameter settings the ratio between  $T_s$  and  $T_d$  is in the range 2-5, i.e. the static torque is 2 to 5 times higher than the dynamic torque. Moreover, typical parameter settings for  $N_d$  are such that the decrease from static to dynamic torque is mainly between 0 and 20-30 rpm, which results in a severe velocity-weakening effect in the bit-rock interaction for low angular velocities.

The model (2.1), (2.2) and (2.4) together forms a differential inclusion that we can write in state-space Lur'e-type form as follows:

$$\begin{aligned}
 \dot{x} &= Ax + Bu_t + Gv + G_2v_2 \\
 q &= Hx \\
 q_2 &= H_2x \\
 y &= Cx \\
 v &\in -\varphi(q) \\
 v_2 &\in -\phi(q_2)
 \end{aligned} \tag{2.5}$$

where  $x := [\theta_d \ \dot{\theta}]^\top \in \mathbb{R}^{2m-1}$  is the state,  $q = \dot{\theta}_1 \in \mathbb{R}$  and  $q_2 := [\dot{\theta}_2 \ \dots \ \dot{\theta}_m]^\top \in \mathbb{R}^{m-1}$  are the angular velocity arguments of the set-valued nonlinearities  $\varphi$  and  $\phi$ , respectively. The bit-rock interaction torque is given by  $v \in \mathbb{R}$  and the drill-string-borehole interaction torques are given by  $v_2 \in \mathbb{R}^{m-1}$ ,  $u_t := T_{td} \in \mathbb{R}$  is the control input and  $y := [\omega_{td} \ T_{pipe}]^\top \in \mathbb{R}^2$  is the measured output. Note that the latter implies that only surface measurements will be employed, which is an important requirement for the controllers to be designed in the following chapters. The angular velocities of the top drive and the bit are defined as  $\omega_{td} := \dot{\theta}_{18}$  and  $\omega_{bit} := \dot{\theta}_1$ , respectively, and the pipe torque  $T_{pipe}$  is the torque

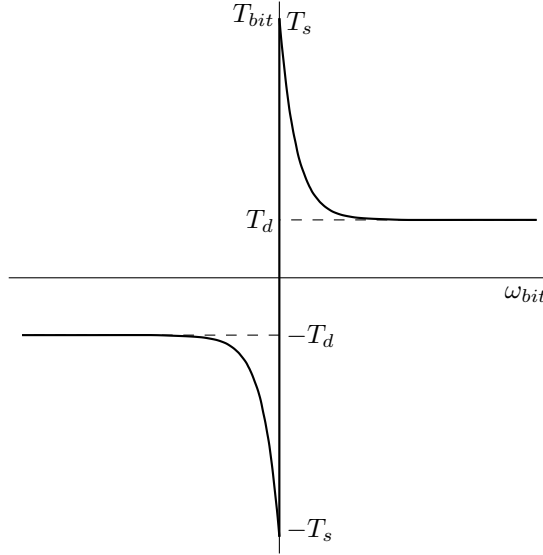


Figure 2.6: Schematic representation of the bit-rock interaction  $T_{bit}$  (2.4).

in the drill-string directly below the top drive. A block diagram of the system (2.5) is shown in Figure 2.7. The matrices  $A$ ,  $B$ ,  $C$ ,  $G$ ,  $G_2$ ,  $H$  and  $H_2$  in (2.5), with appropriate dimensions are given by

$$A = \begin{bmatrix} O_{m-1 \times m-1} & a \\ -M^{-1}K_t & -M^{-1}D \end{bmatrix}, \quad a = \begin{bmatrix} 1 & -1 & 0 & \cdots & 0 \\ 0 & \ddots & \ddots & \ddots & \vdots \\ \vdots & \ddots & \ddots & \ddots & 0 \\ 0 & \cdots & 0 & 1 & -1 \end{bmatrix}, \quad (2.6)$$

$$B = \begin{bmatrix} O_{m-1 \times 1} \\ M^{-1}S_t \end{bmatrix}, \quad (2.7)$$

$$C = \begin{bmatrix} O_{1 \times 2m-2} & 1 \\ J_{td}M^{-1}K_t & J_{td}M^{-1}D \end{bmatrix}, \quad (2.8)$$

$$G = \begin{bmatrix} O_{m-1 \times 1} \\ M^{-1}S_b \end{bmatrix}, \quad (2.9)$$

$$G_2 = \begin{bmatrix} O_{m-1 \times m-1} \\ M^{-1}S_w \end{bmatrix}, \quad (2.10)$$

$$H = [O_{1 \times m-1} \quad 1 \quad O_{1 \times m-1}], \quad (2.11)$$

$$H_2 = [O_{m-1 \times m} \quad I_{m-1}], \quad (2.12)$$

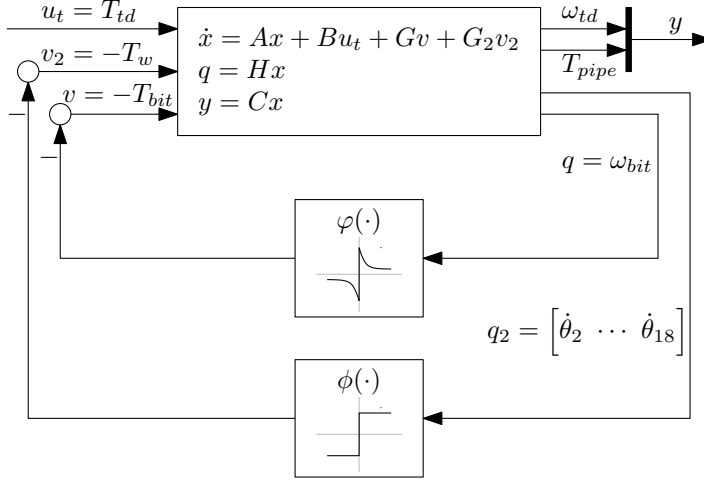


Figure 2.7: Block diagram of the open-loop system (2.5) in state-space Lur'e-type form.

with  $J_{td}$  the top drive inertia,  $I_k$  the  $k$  by  $k$  identity matrix and  $O_{k \times l}$  a  $k$  by  $l$  matrix with all zero entries. Note that  $\varphi(q) := T_{bit}(\omega_{bit})$  and  $\phi(q_2) := [T_{w,2}(\dot{\theta}_2) \cdots T_{w,m}(\dot{\theta}_m)]^\top$ . The relevant frequency response functions for the linear part of the drill-string dynamics (2.5), of the drill-string configuration given in Appendix A.1, are shown in Figures 2.8-2.10.

To facilitate controller synthesis, the drill-string dynamics (2.5) are rewritten in a specific form. The desired constant angular velocity  $\omega_{eq} > 0$  for the drill-string can be associated with a desired equilibrium  $x_{eq}$  for the state of the system. To ensure that  $x_{eq}$  is indeed an equilibrium of the closed-loop system, the control input  $u_t := u_c + \tilde{u}$  is decomposed in a constant feedforward torque  $u_c$  (inducing  $x_{eq}$ ) and the feedback control input  $\tilde{u}$ . Therefore, assume that the resistive torques along the drill-string are constant and can be compensated by  $u_c$ . From (2.2) it follows that the resistive torques along the drill-string ( $T_{w,i}$ ) are constant if  $\dot{\theta}_i > 0$ , for  $i = 2, \dots, m$ . Thus by assuming that  $\dot{\theta}_i$  is close (enough) to the desired velocity  $\omega_{eq} > 0$  the resistive torque along the drill-string can indeed be compensated for by  $u_c$ . In practical drilling situations this is a reasonable assumption, since the drilling system should operate at (or close to) a constant (positive) angular velocity. Especially, since a modelling-for-control approach is adopted in this work, i.e. the model has to be suitable for controller design, and the controllers aim at locally stabilization of the desired setpoint. The (constant) equilibrium  $x_{eq}$  and feedforward torque  $u_c$  can be obtained from the equilibrium inclusion of system (2.5):

$$Ax_{eq} - G\varphi(Hx_{eq}) - G_2\phi(H_2x_{eq}) + Bu_c \ni 0 \quad (2.13)$$

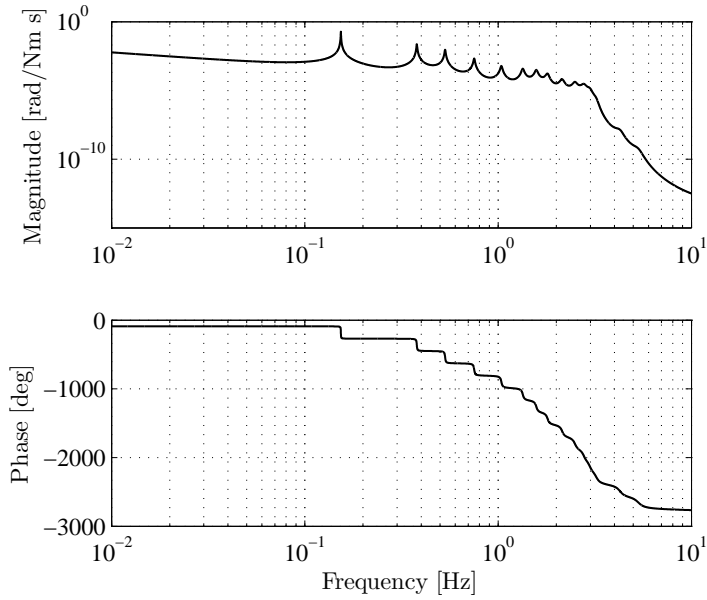


Figure 2.8: Frequency response function of the 18-DOF model from input torque  $T_{td}$  to bit velocity  $\omega_{bit}$ .

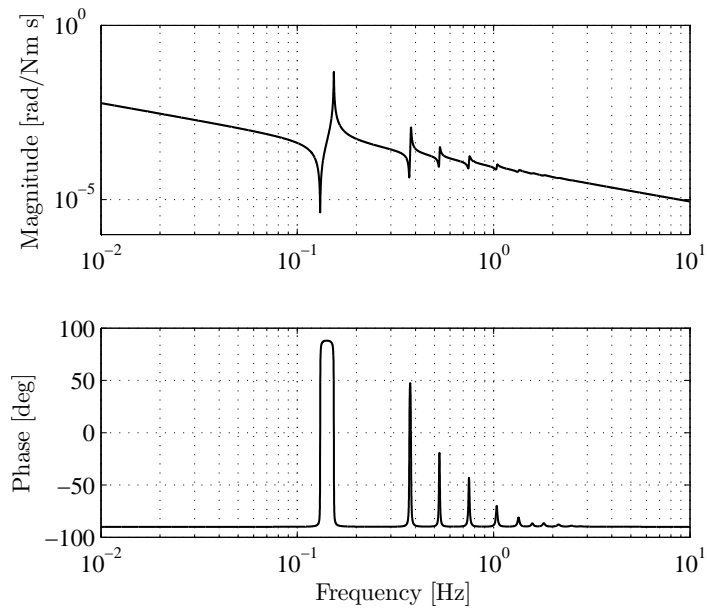


Figure 2.9: Frequency response function of the 18-DOF model from input torque  $T_{td}$  to top drive velocity  $\omega_{td}$ .

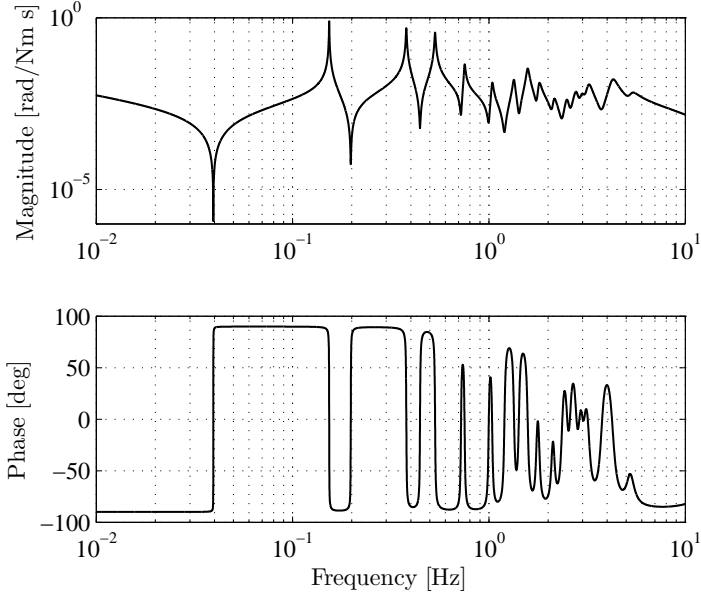


Figure 2.10: Frequency response function of the 18-DOF model from bit torque  $T_{bit}$  to bit velocity  $\omega_{bit}$ , i.e. bit-mobility.

Next, let  $\xi := x - x_{eq}$  be a perturbation coordinate with respect to the equilibrium and apply a linear loop transformation such that the slope of the nonlinearity  $\varphi$  at the equilibrium can be changed. This transformation is used in the controller design methodologies in Chapters 3 and 4. For the moment, assume that the slope of the nonlinearity is changed with a factor  $\delta$  and define the transformed nonlinearity  $\tilde{\varphi}(q) := \varphi(q) - \varphi(Hx_{eq}) + \delta(q - Hx_{eq})$ , as illustrated in Figure 2.11. This results in the following state-space representation of the transformed drill-string dynamics in perturbation coordinates:

$$\begin{aligned}
 \dot{\xi} &= A_t \xi + B \tilde{u} + G \tilde{v} \\
 \tilde{q} &= H \xi \\
 \tilde{y} &= C \xi \\
 \tilde{v} &\in -\tilde{\varphi}(\tilde{q})
 \end{aligned} \tag{2.14}$$

with  $A_t := A + \delta GH$ ,  $\tilde{y} := y - Cx_{eq}$ ,  $\tilde{q} := q - Hx_{eq}$ ,  $\tilde{\varphi}(\tilde{q}) = \varphi(\tilde{q} + Hx_{eq}) - \varphi(Hx_{eq}) + \delta \tilde{q}$  and  $\tilde{v} := v - v_{eq} - \delta \tilde{q}$ .

### 2.3.1 Different model representations

Different representations of the model, which is introduced in the previous section, are used in this thesis. In this section, an overview of the different model

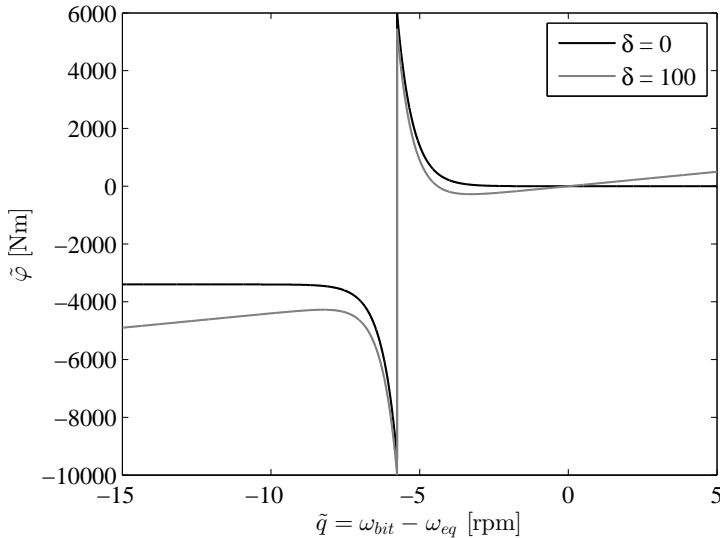


Figure 2.11: Transformed bit-rock interaction model with and without loop transformation to change the slope of the nonlinearity  $\tilde{\varphi}$ .

representations is given, without going into detail on the different models. Figure 2.12 shows the different representations of a drilling system that will be used.

The FEM model introduced in Section 2.3 is based on a real drilling system and field data is used to validate the FEM model. The FEM model has, as the name suggests, a finite number of degrees of freedom to model the infinite-dimensional real drilling system. The considered FEM model of the drill-string system has 18 elements and a state-space realization with 35 states (note that the absolute position of the drill-string omitted).

For multiple reasons, such as limiting controller complexity and feasibility of the lab-scale realization of a drilling system, reduced-order models will be used in this thesis. The purpose of these reduced-order models is to approximate the higher-order FEM model with a reduced number of states, while still preserving the key system properties. Typically, in this thesis, the reduced-order models have a model order (number of states) of 7 or 9. As mentioned before, previous studies investigating the torsional dynamics of a drill-string system often used 1 or 2-DOF models to represent a drilling system. In this thesis, models with at least 4 degrees of freedom are considered, because field observations have revealed that also higher flexibility modes of the drill-string play a role in the onset of stick-slip vibrations [82]. The choice to take at least 4 degrees of freedom into account stems from the fact that the first three resonance modes, with resonance frequencies  $f_1 \approx 0.15$ ,  $f_2 \approx 0.38$  and  $f_3 \approx 0.53$  Hz, are dominant in the drill-

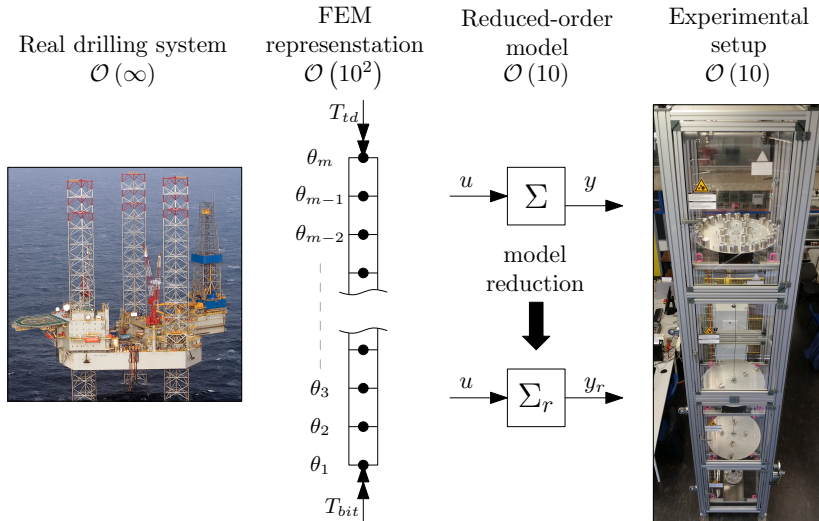


Figure 2.12: Schematic overview of the different system and model representations used in this thesis. The photo on the left shows a real drilling system, next the finite-element representation, as introduced in Section 2.3, is schematically shown, followed by a reduced-order model representation and on the right-hand side a photo of the lab-scale realization of the drill-string system is shown.

string dynamics (see Figures 2.8-2.9). Therefore, those first three modes and the rigid body mode need to be accurately captured by the reduced-order model.

For the controllers to have practical relevance they should be able to stabilize the desired setpoint of the 18-DOF FEM model. Validation of the controller design strategies is based on analysis of the closed-loop dynamics and simulation studies of the controller applied to the 18-DOF model. However, the step from a simulation study to implementation of the controller on a real rig is still quite large. Therefore, as an intermediate step, a lab-scale drill-string system has been developed. The design of this experimental setup is presented in Chapter 5. This setup is designed based on a reduced-order 4-DOF drill-string model and again represents the dominant flexibility modes of the 18-DOF model. The setup is used to experimentally validate the controller design methodologies developed in this thesis.

Summarizing, all the drill-string models used for controller design in this thesis take multiple flexibility modes of the drill-string into account. Moreover, all these models are designed such that they represent the most important dynamics of the real drilling system.



## 2.4 Stability of the drill-string dynamics

In this section, the stability of the desired equilibrium  $x_{eq}$  of the *open-loop* drill-string dynamics (2.5) is investigated. Investigation of the (local) stability of the equilibrium point of (2.5), with  $u_t = u_c$ , is equivalent to investigation of the stability of origin of the transformed system (2.14), with  $\delta = 0$  and  $\tilde{u} = 0$ . Since the main interest is in the local stability of the equilibrium point we linearize the nonlinear dynamics and determine the eigenvalues of the linearized system in order to investigate the stability.

The only nonlinear term in the transformed drill-string dynamics involves the transformed bit-rock interaction term  $\tilde{\varphi}$ . Hence, the system is written in Lur'e-type form with only the nonlinearity  $\tilde{\varphi}$  in a negative feedback loop. The linearization of

$$\dot{\xi} \in A\xi - G\tilde{\varphi}(\tilde{q}) \quad (2.15)$$

around the origin is obtained as follows:

$$\begin{aligned} \dot{\xi} &= A\xi - G \left. \frac{\partial \tilde{\varphi}}{\partial \tilde{q}} \frac{\partial \tilde{q}}{\partial \xi} \right|_{\xi=0} \xi \\ &= A\xi - GH \left. \frac{\partial \tilde{\varphi}}{\partial \tilde{q}} \right|_{\xi=0} \xi \\ &= (A + \delta_{lin}GH) \xi, \end{aligned} \quad (2.16)$$

where  $\delta_{lin} := - \left. \frac{\partial \tilde{\varphi}}{\partial \tilde{q}} \right|_{\xi=0}$ . Note that we linearize around a desired equilibrium  $x_{eq}$  associated with a desired constant angular velocity  $\omega_{eq} > 0$ , such that  $\tilde{\varphi}$  is continuously differentiable in a neighbourhood of the equilibrium. Due to the velocity-weakening effect in the bit-rock interaction,  $\left. \frac{\partial \tilde{\varphi}}{\partial \tilde{q}} \right|_{\xi=0}$  is typically smaller than zero, thus  $\delta_{lin} > 0$ . Note that the effect of  $\delta_{lin}$  is equivalent to the effect of  $\delta$  as defined in the transformed drill-string dynamics (2.14).

The eigenvalues  $\lambda_i$ ,  $i = 1, \dots, m$ , of  $(A + \delta_{lin}GH)$  are determined for different values of  $\delta_{lin}$  to investigate the stability of the open-loop dynamics. For  $\delta_{lin} = 0$  the system has an eigenvalue  $\lambda = 0$ , corresponding to the rigid body mode of the system. For increasing values of  $\delta_{lin}$  the right-most eigenvalue (corresponding to one of the flexibility modes of the system) moves further into the right-half-plane (RHP) of the complex plane, indicating an unstable mode of the system, see Figure 2.13. The fact that the right-most eigenvalue moves further into the RHP indicates that damping of this mode decreases for increasing values of  $\delta_{lin}$ . That is, increasing  $\delta_{lin}$  corresponds to adding negative damping to the system. This observation confirms that the velocity-weakening effect in the bit-rock interaction has a destabilizing effect on the drill-string dynamics. In other words, a steeper slope in the bit-rock interaction, typically at low angular velocities, destabilizes the system. As can be seen in Figure 2.6, the slope of the bit-rock interaction approaches zero for increasing angular velocities. Thus increasing the angular velocity reduces the effect of negative damping. This

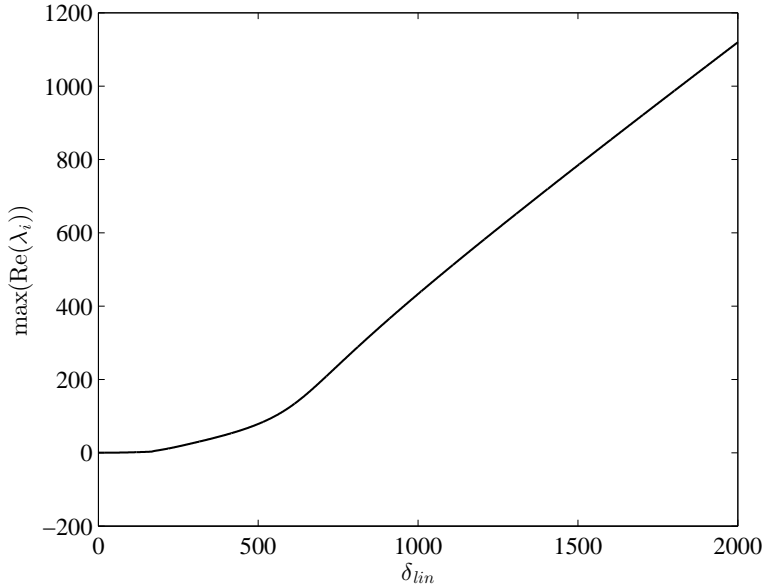


Figure 2.13: Real value of the right-most pole as function of  $\delta_{lin}$ ; if  $\text{Re}(\lambda_i) < 0, \forall i$  the equilibrium point is locally asymptotically stable.

corresponds to observations in the field where increasing the angular velocity often reduces the effect of stick-slip vibrations. In Chapters 3 and 4 of this thesis, stability properties of the nonlinear closed-loop drill-string system (i.e. including the proposed feedback controllers) are also investigated.

## 2.5 Simulation of the drill-string dynamics

The objective of the controller design strategies in Chapters 3 and 4 is to eliminate torsional stick-slip vibrations in drilling systems. An underlying objective is to enlarge the operating envelope of drilling systems in terms of rate-of-penetration (ROP) and angular velocity (RPM) we note that current industrial controllers are not always able to eliminate stick-slip vibrations under the imposed operating conditions. In this section, we will not go into detail on the controllers; however some simulation results of the drill-string system (2.5) in closed-loop with an existing industrial controller (based on [51]) will be shown to illustrate the typical response of the drilling system when stick-slip vibrations occur.

The industrial controller is a so-called classical SoftTorque system. This controller basically is a PI-controller based on feedback of the surface angular

velocity that aims at damping of (only) the first torsional mode of the drill-string. For the simulation results shown in Figure 2.14 the desired equilibrium velocity,  $\omega_{eq}$ , for the drilling system is 50 rpm. The top drive angular velocity, bit angular velocity and top drive torque are shown in this figure. From the bit angular velocity the stick-slip oscillations can be clearly recognized, i.e. the bit comes to a complete stop in the sticking phase and rotates with approximately 10 times the desired angular velocity during the slipping phase. This illustrates that the SoftTorque controller is not able to stabilize the desired equilibrium under the imposed operating conditions. A possible explanation could be the lack of damping of higher flexibility modes of the drill-string. Note that the stick-slip limit cycle in this simulation result consists of two successive slip phases relatively short after each other followed by a longer sticking period before the cycle is repeated. This clearly shows the effect of multiple dominant flexibility modes of the drill-string, because if only one flexibility mode would be responsible for stick-slip, the stick-slip limit cycle is characterized by one peak within a period associated to a single frequency. It has to be mentioned that the simulation results presented here match very well with the field data obtained from measurements during drilling operation for this drilling system (see Figures 2.3 and 2.4). During this drilling operation the presence of stick-slip vibrations could be recognized from the surface torque and angular velocity, even with the SoftTorque controller turned on.

## 2.6 Summary

In this thesis, the objective is to design controllers to mitigate stick-slip vibrations in drilling systems. A model-based control perspective is taken to design these controllers and therefore a modelling-for-control approach involving the torsional dynamics only, in combination with a velocity-weakening bit-rock interaction model, is adopted. In Section 2.3, the drill-string model is introduced and the stability analysis in Section 2.4 showed that the open-loop dynamics are unstable. Moreover, it is shown that the velocity-weakening effect in the bit-rock has a destabilizing effect. The simulation result in Section 2.5 shows that a currently used industrial controller is unable to stabilize the desired angular velocity, which shows the importance of novel controller design strategies to eliminate stick-slip vibrations in drilling systems.

In this thesis, two different controller design strategies are proposed to eliminate stick-slip oscillations in drilling systems. First, in Chapter 3, a nonlinear observer-based output-feedback controller design methodology is developed. This strategy allows to design an output-feedback controller for multi-modal drill-string systems while guaranteeing (local) asymptotic stability of the desired operating velocity. Second, a linear output-feedback controller design strategy, based on robust control techniques is considered in Chapter 4. With this strategy we can also design (locally) stabilizing controllers for multi-modal drill-string

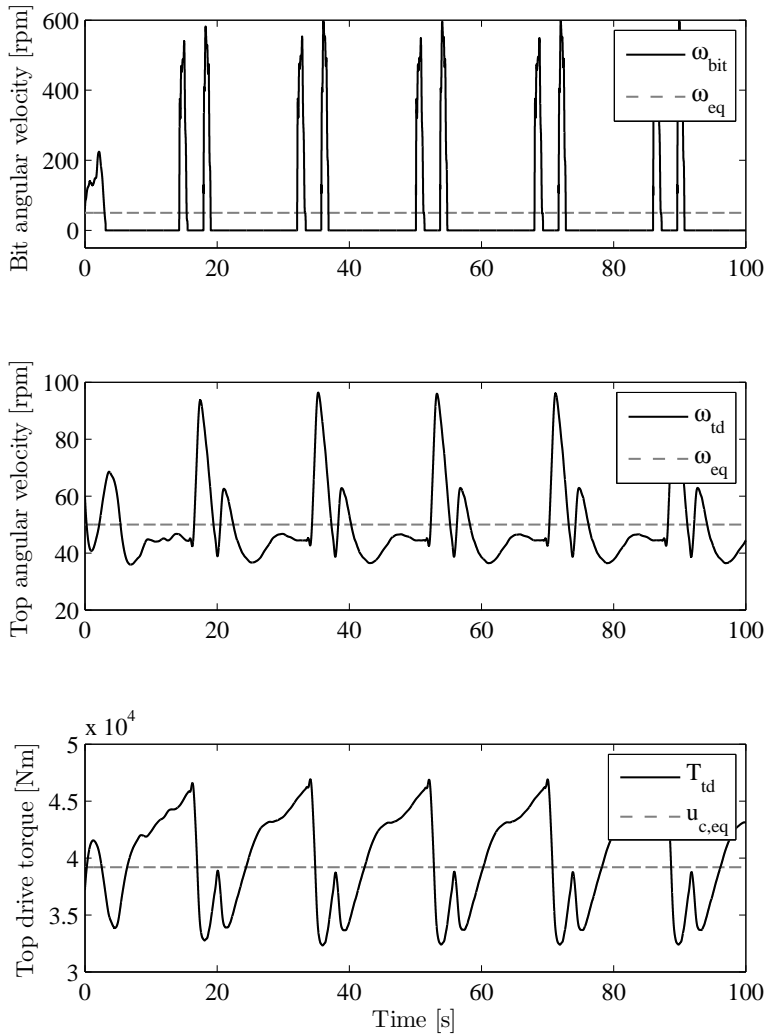


Figure 2.14: Simulation result of the drill-string model in closed-loop with a classic SoftTorque controller.

systems and in addition, performance specifications (e.g. measurement noise sensitivity and actuator limitations) can be taken into account in the controller design.

# Design of an observer-based output-feedback controller

---

### 3.1 Introduction

Drilling systems are used to drill deep wells for the exploration and production of oil and gas, mineral resources and geo-thermal energy. Such a drilling system is schematically shown in Figure 2.1. Surface and down-hole measurements [20, 69, 86] indicate that these systems experience different types of oscillations, which significantly decrease the drilling rate-of-penetration and can damage the drill bit (e.g. bit tooth wear), the drill pipes (e.g. twisted pipe) and the bottom hole assembly. Different modes of vibration, such as axial, lateral and torsional vibrations, lead to bit bouncing, whirling and torsional stick-slip, respectively. The focus of the current chapter is on the aspect of mitigation of torsional stick-slip oscillations by means of control as these vibrations are known to be highly detrimental to drilling efficiency, reliability and safety.

To support the design of controllers to eliminate torsional vibrations, most studies rely on one- or two degree-of-freedom (DOF) models for the torsional drill-string dynamics only, see e.g. [12, 19, 40, 51, 53, 103]. In these models, it is generally assumed that the resisting torque at the bit-rock interface can be modelled as a frictional contact with a velocity-weakening effect as reported in [11, 115]. In fact, modelling of the coupled axial and torsional dynamics, as for example in [93], shows that the velocity-weakening effect in the torque-on-bit (TOB) is a consequence of the drilling dynamics, rather than an intrinsic property of the bit-rock interface. The fact that such coupling effectively leads to a velocity-weakening effect of the TOB (see e.g. [6, 38]) motivates to adopt a

modelling-for-control approach for drill-string dynamics involving the torsional dynamics only, while including velocity-weakening in the bit-rock interaction law, as we will pursue in this chapter. To model the torsional drill-string dynamics we use a finite-element method (FEM) representation of the drill-string. A different modelling approach is taken in [34,37], where infinite-dimensional models, formulated in terms of partial differential equations, are considered. Using the same approach as a basis, models in terms of delay-differential equations are derived in [4,9,10,99]. In [62], it is shown that discretizations of the infinite-dimensional models resulting in a finite-element representation of the drill-string dynamics can accurately describe the underlying drill-string dynamics leading to torsional vibrations. Therefore, we will use such a finite-element method model of the drill-string dynamics for the model-based controller design methodology proposed in this chapter.

Different control strategies aiming to suppress torsional vibrations can be found in literature. In [40], the use of torque feedback in addition to a speed controller is investigated. The underlying idea is making the top rotary system behave in a “soft” manner, hence the name *Soft Torque Rotary System*, see also [51]. In these works, it is assumed that the drilling system behaves like a 2-DOF torsional pendulum of which the first torsional mode can be damped using a PI-controller based on feedback of the surface angular velocity. In [115,116], the above SoftTorque approach is compared with a control method based on torsional rectification, which outperforms the SoftTorque approach in simulation studies by using improved torque feedback based on the twist of the drill-string near the rotary table. Another type of PI-controller is developed in [80], where a 3-DOF drill-string model is used for controller design. To do so, it is assumed that the bit angular velocity can be measured; we note that down-hole measurements for real-time control purposes are not available in practice. A linear  $\mathcal{H}_\infty$  controller synthesis approach is presented in [103]. Herein, the bit-rock interaction, key in causing stick-slip, is not taken into account in the controller design and stability analysis of the closed-loop dynamics. A control design approach, where information of the nonlinear bit-rock interaction model is explicitly taken into account in the controller synthesis, is proposed in [19,24,25]. Drawbacks of the approaches in [19,103] are, firstly, the necessity of down-hole measurements reflecting the twist of the drill-string between surface and bit, which can not be measured in practice, and, secondly, the fact that only one torsional mode of the drill-string is taken into account.

Increasing demands on the operating envelope and a tendency towards drilling deeper and inclined wells impose higher demands on the controllers used in drilling systems. Industrial controllers (such as SoftTorque) are not always able to eliminate stick-slip vibrations under the imposed operating conditions [30,96]. Two main reasons for this deficiency are the influence of multiple dynamical modes of the drill-string on torsional vibrations [82,96] and the uncertainty in the bit-rock interaction law.

The main contribution of this chapter is a nonlinear output-feedback control strategy mitigating torsional stick-slip vibrations while 1) only using surface measurements, 2) taking into account a multi-modal drill-string model and 3) taking into account severe velocity-weakening and uncertainty in the bit-rock interaction. A preliminary version of this work has been presented in [122]. Additional contributions of the current chapter are, firstly, an extensive robustness analysis of the proposed controller, secondly, a validation of the proposed control strategy by application to a high-order FEM model of the drill-string dynamics and, thirdly, a complete proof regarding the stability of the closed-loop system. The robustness analysis mainly focuses on implementation issues essential in practice, such as measurement and actuator noise, changing dynamics due to the increasing length of the drill-string while drilling and changing conditions at the bit-rock interface (e.g. due to changing formation characteristics or bit wear).

This chapter is organized as follows. Section 3.2 introduces the drill-string model based on a finite-element model of a real-life rig and a reduced-order model is derived to facilitate controller design. Subsequently, in Section 3.3 the control problem is formulated. Next, in Section 3.4 we present a design approach for nonlinear output-feedback controllers including a robust stability analysis of the resulting (reduced-order) closed-loop system. Section 3.5 will present simulation results illustrating the effectiveness of the proposed approach applied to the reduced-order drill-string model. In Section 3.6 the controller design strategy is validated by application to the full-scale finite-element drill-string model and a stability analysis of the closed-loop system is performed. Next, in Section 3.7 the robustness of the controller is investigated by means of simulation case studies involving realistic drilling scenarios, for example increasing length of the drill-string and disturbances due to sensor and actuator noise. Finally, the main results of this work are discussed in Section 3.8.

### 3.1.1 Preliminaries

In support of the controller design result in Section 3.4.1, we present the following definitions on input-to-state-stability (ISS) and the strict passivity property.

The concept of input-to-state stability has been introduced in [107]. Its local version has first appeared in [108].

**Definition 3.1.** *The system  $\dot{x}(t) \in F(x(t), e(t))$  is locally input-to-state stable (LISS) if there exist constants  $c_1, c_2 > 0$ , a function  $\rho$  of class  $\mathcal{KL}$  and a function  $\mu$  of class  $\mathcal{K}$  such that for each initial condition  $x(0) = x_0$ , such that  $\|x_0\| \leq c_1$ , and each piecewise continuous bounded input function  $e(t)$  defined on  $[0, \infty)$  and satisfying  $\sup_{\tau \in [0, \infty)} \|e(\tau)\| \leq c_2$ , it holds that*

- all solutions  $x(t)$  exist on  $[0, \infty)$  and,
- all solutions satisfy



$$\|x(t)\| \leq \rho(\|x_0\|, t) + \mu \left( \sup_{\tau \in [0, t]} \|e(\tau)\| \right), \quad \forall t \geq 0. \quad (3.1)$$

Consider the linear time-invariant minimal state-space realization

$$\begin{aligned} \dot{x} &= Ax + Gv \\ q &= Hx + Dv \end{aligned} \quad (3.2)$$

with the state  $x \in \mathbb{R}^n$ , and input and output  $v, q \in \mathbb{R}$ .

**Definition 3.2.** *The system (3.2) or the quadruple  $(A, G, H, D)$  is said to be strictly passive if there exist an  $\varepsilon > 0$  and a matrix  $P = P^\top > 0$  such that*

$$\begin{bmatrix} A^\top P + PA + \varepsilon I & PG - H^\top \\ G^\top P - H & -D - D^\top \end{bmatrix} \leq 0. \quad (3.3)$$

## 3.2 Drill-string dynamics model

The system we will investigate is a realistic drill-string model of a jack-up drilling rig and the reservoir sections of the wells are drilled with a 6" bit to reach depths of >6000 m and with an inclination angle up to 60°, resulting in significant resistive torques along the drill-string. The rig is equipped with an AC top drive and fitted with a modern SoftTorque system [64]. However, for this depth and hole size stick-slip vibrations have been observed in the field for this rig [39]. A finite-element model of this drilling system has been developed and the simulation results of this model have been validated with field data under different conditions (such as weight-on-bit (WOB) and angular velocity), see Figures 2.3 and 2.4.

The finite-element method (FEM) is used to construct a multi-modal torsional drill-string model (with 18 elements). The element at the top is a rotational inertia to model the top drive inertia, the subsequent elements are equivalent pipe sections based on the dimensions and material properties of the drill-string. The resulting model can be written as

$$M\ddot{\theta} + D\dot{\theta} + K_t\theta_d = S_w T_w(\dot{\theta}) + S_b T_{bit}(\dot{\theta}_1) + S_t T_{td} \quad (3.4)$$

with the coordinates  $\theta \in \mathbb{R}^m$ , where  $m = 18$ , the top drive motor torque input  $T_{td} \in \mathbb{R}$  being the control input, the bit-rock interaction torque  $T_{bit} \in \mathbb{R}$  and the interaction torques  $T_w \in \mathbb{R}^{m-1}$  between the borehole and the drill-string acting on the nodes of the FEM model. The coordinates  $\theta$  represent the angular displacements of the nodes of the finite-element representation. Next, we define the difference in angular position between adjacent nodes as follows:  $\theta_d := [\theta_1 - \theta_2 \quad \theta_2 - \theta_3 \quad \cdots \quad \theta_{17} - \theta_{18}]^\top$ . In (3.4), the mass, damping and “stiffness” matrices are, respectively, given by  $M \in \mathbb{R}^{m \times m}$ ,  $D \in \mathbb{R}^{m \times m}$  and

$K_i \in \mathbb{R}^{m \times m-1}$ , the matrices  $S_w \in \mathbb{R}^{m \times m-1}$ ,  $S_b \in \mathbb{R}^{m \times 1}$  and  $S_t \in \mathbb{R}^{m \times 1}$  represent the generalized force directions of the interaction torques, the bit torque and the input torque, respectively. The coordinates  $\theta$  are chosen such that the first element ( $\theta_1$ ) describes the rotation of the bit and the last element ( $\theta_{18}$ ) the rotation of the top drive at surface. The interaction between the borehole and the drill-string is modelled as Coulomb friction, that is

$$T_{w,i} \in T_i \text{Sign}(\dot{\theta}_i), \quad \text{for } i = 2, \dots, 18, \quad (3.5)$$

with  $T_i$  representing the amount of friction at each element and the set-valued sign function defined as

$$\text{Sign}(y) \triangleq \begin{cases} -1, & y < 0 \\ [-1, 1], & y = 0 \\ 1, & y > 0. \end{cases} \quad (3.6)$$

The bit-rock interaction model, including the velocity-weakening effect, is given by

$$T_{bit}(\dot{\theta}_1) \in \text{Sign}(\dot{\theta}_1) \left( T_d + (T_s - T_d) e^{-v_d |\dot{\theta}_1|} \right) \quad (3.7)$$

with  $T_s$  the static torque,  $T_d$  the dynamic torque and  $v_d := \frac{30}{N_d \pi}$  indicating the decrease from static to dynamic torque. For this model, the parameters are tuned such that a match between the simulation results and the (surface) field data is obtained. The values of the parameters are given by  $T_s = 7700$  Nm,  $T_d = 1700$  Nm,  $N_d = 5$  rpm and the resulting bit-rock interaction model is shown in Figure 3.1. The model (3.4), (3.5) and (3.7) together forms a differential inclusion that we can write in state-space Lur'e-type form as follows:

$$\begin{aligned} \dot{x} &= Ax + Bu_t + Gv + G_2 v_2 \\ q &= Hx \\ q_2 &= H_2 x \\ y &= Cx \\ v &\in -\varphi(q) \\ v_2 &\in -\phi(q_2), \end{aligned} \quad (3.8)$$

where  $x := [\theta_d \ \dot{\theta}]^\top \in \mathbb{R}^{35}$  is the state,  $q := \omega_{bit} \in \mathbb{R}$  and  $q_2 := [\dot{\theta}_2 \ \dots \ \dot{\theta}_{18}]^\top \in \mathbb{R}^{17}$  are the angular velocity arguments of the set-valued nonlinearities  $\varphi$  and  $\phi$ , respectively. The bit-rock interaction torque is given by  $v \in \mathbb{R}$  and the drill-string-borehole interaction torques are given by  $v_2 \in \mathbb{R}^{17}$ ,  $u_t := T_{td} \in \mathbb{R}$  is the control input and  $y := \omega_{td} \in \mathbb{R}$  is the measured output. Note that the latter implies that only surface measurements will be employed in the output-feedback control strategy proposed in Section 3.4. The angular velocities of the top drive and the bit are defined as  $\omega_{td} := \dot{\theta}_{18}$  and  $\omega_{bit} := \dot{\theta}_1$ , respectively. The matrices

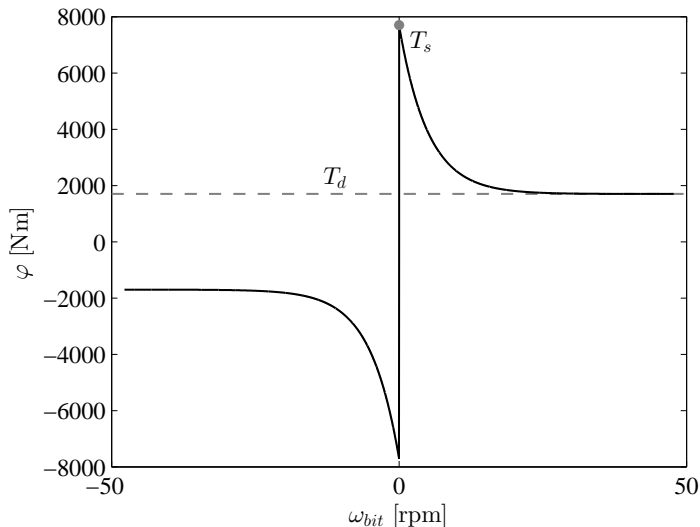


Figure 3.1: Bit-rock interaction model.

$A$ ,  $B$ ,  $G$ ,  $G_2$ ,  $H$  and  $H_2$  in (3.8), with appropriate dimensions, are given by

$$A = \begin{bmatrix} O_{17 \times 17} & a \\ -M^{-1}K_t & -M^{-1}D \end{bmatrix}, \quad a = \begin{bmatrix} 1 & -1 & 0 & \cdots & 0 \\ 0 & \ddots & \ddots & \ddots & \vdots \\ \vdots & \ddots & \ddots & \ddots & 0 \\ 0 & \cdots & 0 & 1 & -1 \end{bmatrix},$$

$$B = \begin{bmatrix} O_{17 \times 1} \\ M^{-1}S_t \end{bmatrix}, \quad G = \begin{bmatrix} O_{17 \times 1} \\ M^{-1}S_b \end{bmatrix}, \quad G_2 = \begin{bmatrix} O_{17 \times 17} \\ M^{-1}S_w \end{bmatrix},$$

$$H = [O_{1 \times 17} \quad 1 \quad O_{1 \times 17}], \quad H_2 = [O_{17 \times 18} \quad I_{17}]$$

and  $C \in \mathbb{R}^{35}$  indicates the measured output, where  $I_k$  the  $k$ -by- $k$  identity matrix and  $O_{k \times l}$  a  $k$ -by- $l$  matrix with all zero entries. Note that  $\varphi(q) := T_{bit}(\omega_{bit})$  and  $\phi(q_2) := [T_{w,2}(\dot{\theta}_2) \cdots T_{w,18}(\dot{\theta}_{18})]^\top$ . The relevant frequency response functions of (the linear part of) system (3.8) from inputs  $T_{td}$  and  $T_{bit}$  to the outputs  $\omega_{td}$  and  $\omega_{bit}$  are shown in Figures 3.2-3.4.

### 3.2.1 Reduced-order model

In order to both facilitate the design of and to decrease the implementation burden of the resulting observer-based output-feedback controllers (see Section 3.4), we apply model reduction to obtain a low-order approximation of the drilling system dynamics (3.8). Such reduced-order model approximates the input-output

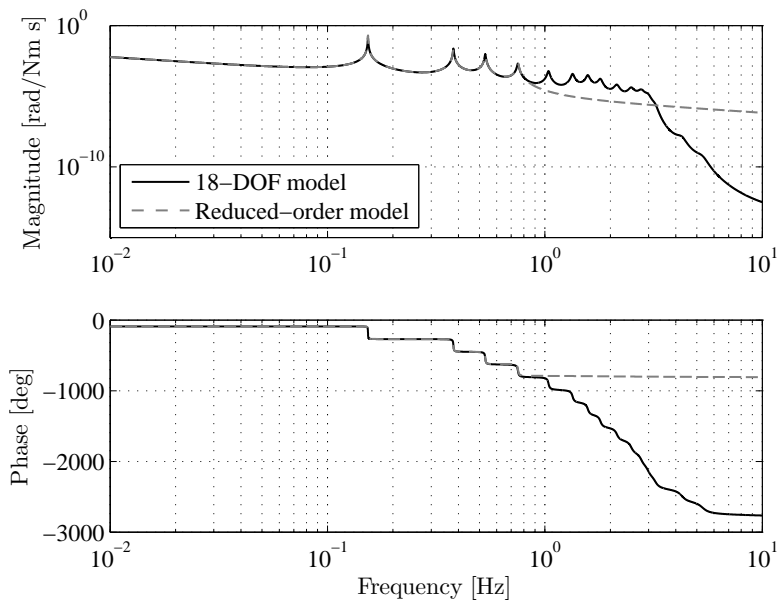


Figure 3.2: Frequency response function of the full-order and reduced-order model from input torque  $T_{td}$  to bit velocity  $\omega_{bit}$ .

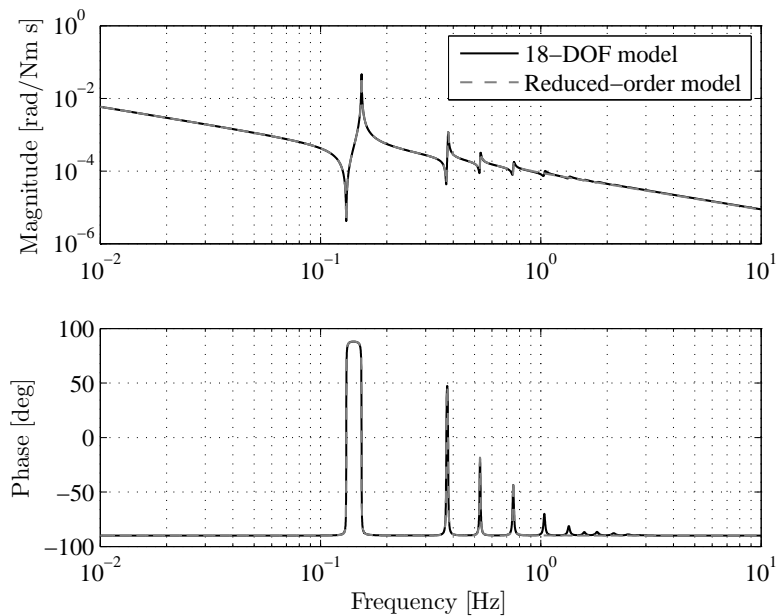


Figure 3.3: Frequency response function of the full-order and reduced-order model from input torque  $T_{td}$  to top drive velocity  $\omega_{td}$ .

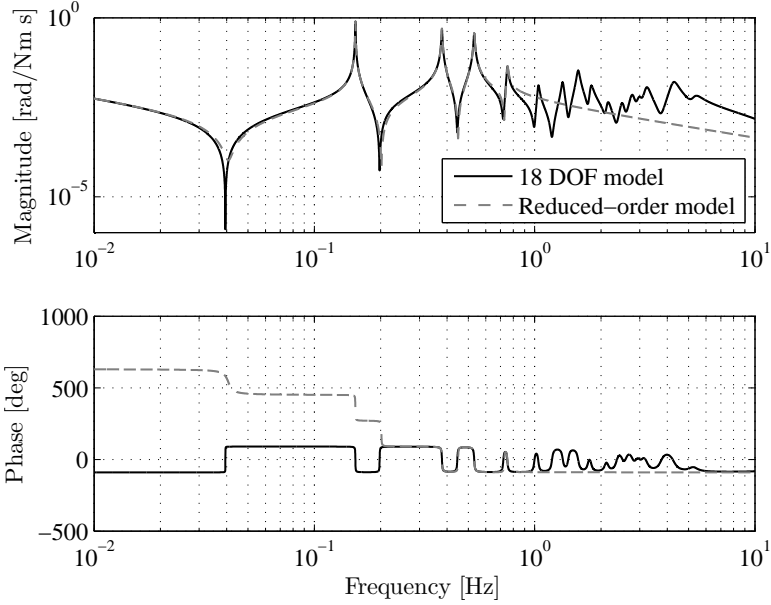


Figure 3.4: Frequency response function of the full-order and reduced-order model from bit torque  $T_{bit}$  to bit velocity  $\omega_{bit}$ , i.e. the bit-mobility.

behavior from inputs  $u_t$  and  $v$  to outputs  $y$  and  $q$ . The inputs and outputs related to the drill-string-borehole interaction ( $T_{w,i}$ ) are not taken into account in the reduction process, but can be approximated using the transformation matrix obtained from the reduction procedure. With this assumption, system (3.8) can be represented as a Lur'e type system  $\Sigma = (\Sigma^{lin}, \varphi)$ , consisting of high-order linear dynamics  $\Sigma^{lin}$  with a single static output-dependent nonlinearity  $\varphi$ , related to the bit-rock interaction, in the feedback loop. We will use the model reduction approach for Lur'e-type systems as proposed in [7], which employs a linear model reduction technique (such as balanced truncation) for the reduction of the linear part of the Lur'e-type system. In doing so, we combine the inputs  $u_t$  and  $v$  and the outputs  $y$  and  $q$ , yielding the new input matrix  $[B \ G]$  and the new output matrix  $[C^T \ H^T]^T$ . With these inputs and outputs, applying balanced truncation to the linear part of the Lur'e-type system results in the reduced-order linear system  $\Sigma_r^{lin}$ . Now, the reduced-order linear part is interconnected with the original nonlinearity yielding the reduced-order drill-string system model  $\Sigma_r = (\Sigma_r^{lin}, \varphi)$ .

Using the approach outlined above, we obtain a reduced-order model with state  $x_r \in \mathbb{R}^{m_r}$ . The equations of motion for the reduced-order system are

written as (now again taking into account drill-string borehole interactions):

$$\begin{aligned}
 \dot{x}_r &= A_r x_r + B_r u_t + G_r v_r + G_{2,r} v_{2,r} \\
 q_r &= H_r x_r \\
 q_{2,r} &= H_{2,r} x_r \\
 y_r &= C_r x_r \\
 v_r &\in -\varphi(q_r) \\
 v_{2,r} &\in -\phi(q_{2,r})
 \end{aligned} \tag{3.9}$$

and the bit-rock interaction as shown in Figure 3.1. The relevant frequency response functions for the linear part of the reduced-order dynamics in (3.8) and (3.9) are shown in Figures 3.2, 3.3 and 3.4. Clearly, the first four resonance modes (and the rigid-body mode) are accurately captured in the reduced-order model. The so-called bit-mobility, shown in Figure 3.4, describes the dynamics of the drill-string system from bit torque input ( $T_{bit}$ ) to bit angular velocity output ( $\omega_{bit}$ ). In other words, it indicates the sensitivity of the bit angular velocity for disturbances in the bit-rock interaction torque. A lower magnitude of the bit-mobility makes the drill-string system thus less sensitive for disturbances at the bit (induced by the bit-rock interaction including a destabilizing velocity-weakening effect) that could eventually lead to stick-slip oscillations. Therefore, the bit-mobility gives an indication of the most important resonance modes in the onset of stick-slip vibrations. It can be seen that the first three resonance modes are dominant, which motivates the choice to reduce to a model order of at least  $m_r = 7$ . In the remainder of this chapter, a reduced-order model with  $m_r = 9$  states is used. The choice for  $m_r = 9$  is such that it is sufficiently large to capture the dominant modes and to reduce the model error due to reduction as much as possible, while on the other hand, the model order is limited to obtain a feasible controller and observer design.

## 3.3 Control problem formulation

In Section 3.3.1, we formulate the control problem and specify the controller objectives. Additionally, in Section 3.3.2 we apply a loop transformation to the model in (3.9) to render it amendable for controller design, discussed in detail in Section 3.4.

### 3.3.1 Controller objectives

The desired operation of the drill-string system is a constant angular velocity  $\omega_{eq}$  for the entire drill-string. So, the objective is to regulate the nonlinear drill-string system to this setpoint by means of an observer-based output-feedback controller. The available measurement for the controller is the top drive angular velocity  $\omega_{td}$  and the system can be controlled by the top drive torque  $T_{td}$ . As briefly mentioned in the introduction, the controller should

1. locally stabilize the constant rotational velocity  $\omega_{eq}$  of the drill-string, therewith eliminating torsional (stick-slip) vibrations;
2. be able to deal with severe velocity-weakening and uncertainty in the non-linear bit-rock interaction  $\varphi$ ;
3. be applicable to multi-modal drill-string models, i.e. effectively deal with flexibility modes at higher frequencies.

### 3.3.2 Model reformulation

To facilitate controller synthesis, the drill-string dynamics (3.9) are rewritten in a specific form. The desired constant angular velocity  $\omega_{eq} > 0$  can be associated with a desired equilibrium  $x_{r,eq}$  for the state of the system. To ensure that  $x_{r,eq}$  is indeed an equilibrium of the closed-loop system, the control input  $u_t = u_c + \tilde{u}$  is decomposed in a constant feedforward torque  $u_c$  (inducing  $x_{r,eq}$ ) and the feedback control input  $\tilde{u}$ . If we assume that we can indeed operate the drill-string system at positive angular velocity, the Coulomb friction terms  $T_{w,i}$  along the drill-string do not affect the dynamics of the system, at least locally near the desired operating condition, and can consequently be represented by constant resistive torques. These constant resistive torques can then be compensated by the feedforward torque. The equilibrium  $x_{r,eq}$  and feedforward torque  $u_c$  can be obtained from the equilibrium condition of system (3.9) that has to satisfy the algebraic inclusion

$$A_r x_{r,eq} - G_r \varphi(H_r x_{r,eq}) - G_{2,r} \phi(H_{2,r} x_{r,eq}) + B_r u_c \ni 0. \quad (3.10)$$

Due to the reduction error introduced by the model reduction procedure (see Section 3.2.1) the outputs  $q_r$  and  $y_r$  of the reduced-order system (3.9) do not exactly match the outputs  $q$  and  $y$  of the original system (3.8). Moreover, the outputs  $q_r$  and  $y_r$  of the reduced-order model are not necessarily equal, although they represent the bit angular velocity and top drive angular velocity, respectively. To obtain a unique equilibrium  $x_{r,eq}$  associated to a specific desired angular velocity  $\omega_{eq}$ , we have to introduce an additional requirement. For the implementation of a reduced-order controller (as treated in Sections 3.5 and 3.6) we require that  $y_{r,eq}$  matches the desired equilibrium velocity  $\omega_{eq}$ . Therewith satisfying the drillers setpoint at the top drive. Consequently, the approximated bit angular velocity of the reduced-order model, i.e.  $q_{r,eq} = H_r x_{r,eq}$ , will be slightly different from the desired equilibrium velocity  $\omega_{eq}$ . In other words, for the reduced-order model,  $y_r$  is not necessarily equal to  $q_r$ . For the equilibrium  $x_{r,eq}$  of the reduced-order model we therefore require  $y_{r,eq} = \omega_{eq}$ , consequently,  $q_{r,eq}$  will probably not exactly match  $\omega_{eq}$ .

**Remark 3.1.** *In the case that the Coulomb friction due to the interaction between the drill-string and the borehole cannot be compensated for by the feedforward torque, these (nonlinear) interaction torques should be taken into account*

in the drill-string dynamics. Linear frictional effects (such as viscous damping) can be incorporated in the system matrices. Nonlinear effects can be included in a similar fashion as the bit-rock interaction, resulting in multiple nonlinearities instead of a single nonlinear interaction term. The controller design methodology presented in Section 3.4 is developed for a scalar nonlinearity; however, the method can also be extended to cope with multiple nonlinearities (see [19]).

Next, we write the reduced-order drill-string system (3.9) in perturbation states  $\xi_r$  with respect to the equilibrium, defined as  $\xi_r := x_r - x_{r,eq}$ . Furthermore, we apply a linear loop transformation to change the properties of the nonlinearity  $\varphi$  in order to satisfy certain conditions related to the controller design in Section 3.4. This results in the state-space representation of the dynamics in perturbation coordinates given by:

$$\begin{aligned}\dot{\xi}_r &= A_{r,t}\xi_r + B_r\tilde{u} + G_r\tilde{v}_r \\ \tilde{q}_r &= H_r\xi_r \\ \tilde{y}_r &= C_r\xi_r \\ \tilde{v}_r &\in -\tilde{\varphi}_r(\tilde{q}_r),\end{aligned}\tag{3.11}$$

where we define  $A_{r,t} := A_r + \delta G_r H_r$  with  $\delta > 0$  a constant to apply the linear loop transformation. Moreover,  $\tilde{q}_r := q_r - H_r x_{r,eq}$ ,  $\tilde{y}_r := y_r - C_r x_{r,eq}$ ,  $\tilde{\varphi}_r(\tilde{q}_r) := \varphi(\tilde{q}_r + H_r x_{r,eq}) - \varphi(H_r x_{r,eq}) + \delta \tilde{q}_r$  and  $\tilde{v}_r = v_r - v_{r,eq} - \delta \tilde{q}_r$ . Note that the first controller objective in Section 3.3.1 (stabilization) can now be formulated as the desire to stabilize the origin of (3.11) by the design of output-feedback controllers inducing the control input  $\tilde{u}$ . The latter is the topic of Section 3.4.

### 3.4 Design of observer-based output-feedback controllers

The control design strategy proposed here builds upon an observer-based controller for Lur'e-type systems with discontinuities as in [19, 26]. In these previous works, the controller and observer were designed for a drill-string model with a single flexibility mode and with the assumption on the availability of down-hole measurements, while in the current work we adopt more realistic multi-modal drill-string models (see Section 3.2) and develop controllers based on surface measurements only. Moreover, the conditions for controller synthesis as in [19] achieving *global* asymptotic stability are infeasible for the realistic drill-string model presented here for three reasons: firstly, the incorporation of multiple torsional flexibility modes of the drill-string, see Figures 3.2, 3.4 and 3.3, secondly, the incorporation of a bit-rock interaction model based on field data, which shows a rather severe velocity-weakening effect, see Figure 3.1, and, thirdly, the restriction on the availability of only surface measurements. Therefore, we employ a controller synthesis strategy to design *locally* stabilizing controllers and we show



that such local stability properties suffice to mitigate stick-slip oscillations in realistic drilling scenarios. In Section 3.4.1, we propose the state-feedback controller, in Section 3.4.2, the observer design and in Section 3.4.3, the resulting output-feedback control strategy, all including stability guarantees.

### 3.4.1 State-feedback controller design

In this section, we discuss the design of a state-feedback controller that stabilizes the origin  $\xi_r = 0$  of the system (3.11). Stabilization of the origin of (3.11) corresponds to the desired operation of constant angular velocity of the drilling system, as discussed in Section 3.3.2. The control input is given by  $\tilde{u} \in \mathbb{R}$ , the input and output of the set-valued nonlinearity  $\tilde{\varphi}_r$  are given by  $\tilde{q}_r \in \mathbb{R}$  and  $\tilde{v}_r \in \mathbb{R}$ , respectively, and the system matrices are  $A_{r,t} \in \mathbb{R}^{m_r \times m_r}$ ,  $B_r \in \mathbb{R}^{m_r \times 1}$ ,  $G_r \in \mathbb{R}^{m_r \times 1}$  and  $H_r \in \mathbb{R}^{1 \times m_r}$ . We introduce a linear static state-feedback law, where we take the “measurement” (or observer) error  $e := \xi_r - \hat{\xi}_r$  into account as follows:

$$\tilde{u} = K \hat{\xi}_r = K (\xi_r - e). \quad (3.12)$$

Herein,  $K \in \mathbb{R}^{1 \times m_r}$  is the control gain matrix and  $\hat{\xi}_r$  the observer estimate of the state  $\xi_r$ ; the observer will be treated in detail in Section 3.4.2. The resulting closed-loop system is described by the following differential inclusion:

$$\begin{aligned} \dot{\xi}_r &= (A_{r,t} + B_r K) \xi_r + G_r \tilde{v}_r - B_r K e \\ \tilde{q}_r &= H_r \xi_r \\ \tilde{v}_r &\in -\tilde{\varphi}_r(\tilde{q}_r). \end{aligned} \quad (3.13)$$

The transfer function  $G_{cl}(s)$  from the input  $\tilde{v}_r$  to the output  $\tilde{q}_r$  of system (3.13) is given by  $G_{cl} = H_r (sI - (A_{r,t} + B_r K))^{-1} G_r$ ,  $s \in \mathbb{C}$ . Now, let us state the following assumptions on the properties of the set-valued nonlinearity  $\tilde{\varphi}_r(\tilde{q}_r)$ . Hereto, we first define a set  $\mathcal{S}_a$  for which a particular sector condition is satisfied:  $\mathcal{S}_a := \{\tilde{q}_r \in \mathbb{R} \mid \tilde{q}_{r,a1} < \tilde{q}_r < \tilde{q}_{r,a2}\}$  with  $\tilde{q}_{r,a1} < 0 < \tilde{q}_{r,a2}$ .

**Assumption 3.1.** *The set-valued nonlinearity  $\tilde{\varphi}_r : \mathbb{R} \rightarrow \mathbb{R}$  satisfies the following conditions:*

- $0 \in \tilde{\varphi}_r(0)$ ;
- $\tilde{\varphi}_r$  is continuously differentiable and bounded for all  $\tilde{q}_r \in \mathcal{S}_a$ ;
- $\tilde{\varphi}$  locally satisfies the  $[0, k]$  sector condition, with  $k > 0$ , in the sense that

$$\tilde{v}_r [\tilde{v}_r + k \tilde{q}_r] \leq 0 \quad \forall \tilde{v}_r \in -\tilde{\varphi}_r(\tilde{q}_r), \text{ with } \tilde{q}_r \in \mathcal{S}_a. \quad (3.14)$$

**Remark 3.2.** *The case where  $\tilde{\varphi}_r$  is non-smooth or even discontinuous on the domain  $\mathcal{S}_a$  can also be treated using the approach presented in [19]. However, this is not necessary for the application presented in this chapter, since we pursue the design of controllers locally stabilizing a non-zero rotational velocity of the drill-string system.*

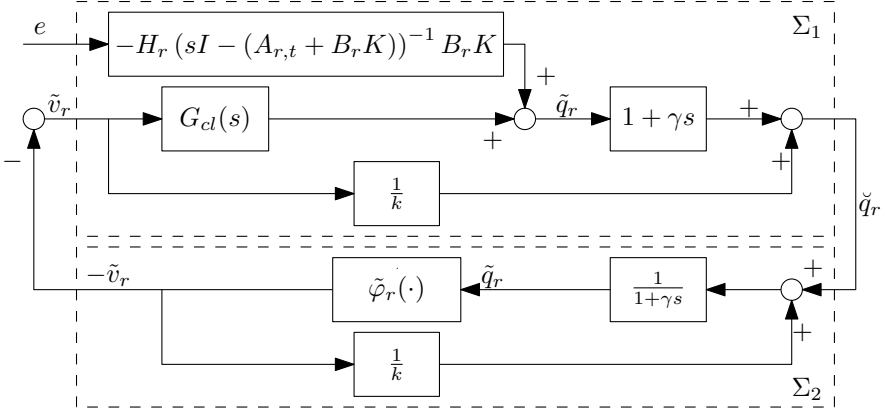


Figure 3.5: Schematic representation of system (3.13) after transformation using a dynamic multiplier.

The intended control goal is to render the closed-loop system (3.13) *locally input-to-state stable* (LISS) with respect to the input  $e$ , as formalized in Definition 3.1, by a proper design of the controller gain  $K$ . We use the concept of a dynamic multiplier to transform the original system into a feedback interconnection of two passive systems. In Figure 3.5, a block diagram of the system including the dynamic multiplier with transfer function  $M(s) = 1 + \gamma s$ ,  $s \in \mathbb{C}$ , is shown. Furthermore the loop transformation gain  $\frac{1}{k}$  is included given the fact that the nonlinearity  $\tilde{\varphi}_r(\cdot)$  belongs to the sector  $[0, k]$ . The linear system  $\Sigma_1$  in Figure 3.5 can be written in state-space form as follows:

$$\Sigma_1 : \begin{cases} \dot{\xi}_r = (A_{r,t} + B_r K) \xi_r + G_r \tilde{v}_r - B_r K e \\ \dot{\check{q}}_r = \check{H}_r \xi_r + \check{D}_r \tilde{v}_r + \check{Z}_r e \end{cases} \quad (3.15)$$

with  $\check{H}_r := H_r + \gamma H_r (A_{r,t} + B_r K)$ ,  $\check{D}_r := \frac{1}{k} + \gamma H_r G_r$  and  $\check{Z}_r := -\gamma H_r B_r K$ . For system  $\Sigma_2$  in Figure 3.5 we can write:

$$\Sigma_2 : \begin{cases} \dot{\check{q}}_r = -\frac{1}{\gamma} \check{q}_r + \frac{1}{\gamma} \check{q}_r - \frac{1}{\gamma k} \tilde{v}_r \\ \tilde{v}_r \in -\tilde{\varphi}_r(\check{q}_r). \end{cases} \quad (3.16)$$

The following theorem states sufficient conditions under which system (3.13) is LISS with respect to input  $e$ .

**Theorem 3.1.** *Consider system (3.13) and suppose that there exists a constant  $\gamma > 0$  such that  $(A_{r,t} + B_r K, G_r, \check{H}_r, \check{D}_r)$  is strictly passive. Then, system (3.13) is LISS, with respect to input  $e$  for any  $\tilde{\varphi}_r(\cdot)$  satisfying Assumption 3.1.*

*Proof.* The proof of Theorem 3.1 is given in Appendix B.1.  $\square$

### 3.4.2 Observer design

Next, an observer will be designed to construct an estimate of the states of system (3.11). Such a state estimate is needed since we only rely on surface measurements while, at the same time, aiming to employ the state-feedback controller of Section 3.4.1. The proposed observer design builds upon the result in [26]. In fact the observer itself is the same as the observer in [26]; however, due to the multi-modal dynamics, severe velocity-weakening in the bit-rock interaction and availability of surface measurements only, the global stability conditions for the equilibrium of the observer error dynamics are unfeasible. Therefore, we propose novel results providing feasible conditions for the *local* stability of the observer error dynamics, which is sufficient to mitigate stick-slip oscillations in realistic drilling scenarios. Therefore, we propose the following observer:

$$\begin{aligned}\dot{\hat{\xi}}_r &= (A_{r,t} - LC_r)\hat{\xi}_r + B_r\tilde{u} + G_r\hat{v}_r + L\tilde{y}_r \\ \hat{q}_r &= (H_r - NC_r)\hat{\xi}_r + N\tilde{y}_r \\ \hat{y}_r &= C_r\hat{\xi}_r \\ \hat{v}_r &\in -\tilde{\varphi}_r(\hat{q}_r),\end{aligned}\tag{3.17}$$

with measured output  $\tilde{y}_r = C_r\xi_r$  ( $\tilde{y}_r \in \mathbb{R}^{k_r}$  and  $C_r \in \mathbb{R}^{m_r \times k_r}$ ) and observer gain matrices  $L \in \mathbb{R}^{m_r \times k_r}$  and  $N \in \mathbb{R}^{1 \times k_r}$ . Next, we state an additional assumption on the nonlinearity  $\tilde{\varphi}_r(\cdot)$ . Hereto, we first define the set  $\mathcal{S}_b$  as  $\mathcal{S}_b := \{\tilde{q}_r \in \mathbb{R} | \tilde{q}_{r,b1} < \tilde{q}_r < \tilde{q}_{r,b2}\}$  with  $\tilde{q}_{r,b1} < 0 < \tilde{q}_{r,b2}$ , such that for all  $\tilde{q}_r \in \mathcal{S}_b$  the following monotonicity property holds.

**Assumption 3.2.** *The set-valued nonlinearity  $\tilde{\varphi}_r : \mathbb{R} \rightarrow \mathbb{R}$  is such that  $\tilde{\varphi}_r$  is monotone for all  $\tilde{q}_r \in \mathcal{S}_b$ , i.e. for all  $q_1 \in \mathcal{S}_b$  and  $q_2 \in \mathcal{S}_b$  with  $v_1 \in \tilde{\varphi}_r(q_1)$  and  $v_2 \in \tilde{\varphi}_r(q_2)$ , it holds that  $(v_1 - v_2)(q_1 - q_2) \geq 0$ .*

The observer error dynamics (with the observer error defined as  $e = \xi_r - \hat{\xi}_r$ ) can be written as

$$\begin{aligned}\dot{e} &= (A_{r,t} - LC_r)e + G_r(\tilde{v}_r - \hat{v}_r) \\ \tilde{v}_r &\in -\tilde{\varphi}_r(H_r\xi_r) \\ \hat{v}_r &\in -\tilde{\varphi}_r\left(H_r\hat{\xi}_r + N\left(\tilde{y}_r - C_r\hat{\xi}_r\right)\right).\end{aligned}\tag{3.18}$$

The following theorem provides sufficient conditions for the design of the observer gains  $L$  and  $N$  such that the origin  $e = 0$  is a locally exponentially stable equilibrium point of the observer error dynamics (3.18).

**Theorem 3.2.** *Consider system (3.11) and the observer (3.17) with  $(A_{r,t} - LC_r, G_r, H_r - NC_r, 0)$  strictly passive and the matrix  $G_r$  being of full column rank. If it holds that*

$$\|\tilde{\xi}_r(t)\| \leq e^{-\frac{\tilde{q}_{r,b,min}}{\|H_r\|}t}, \quad \forall t \geq 0,$$

for some  $\epsilon \in (0, 1)$  and  $\tilde{q}_{r,b,min} := \min(|\tilde{q}_{r,b1}|, |\tilde{q}_{r,b2}|)$ , then  $e = 0$  is a locally exponentially stable equilibrium point of the observer error dynamics (3.18) for any  $\tilde{\varphi}_r$  satisfying Assumptions 3.1 and 3.2 with the region of attraction containing the set

$$\left\{ e \in \mathbb{R}^{m_r} \left| \|e_0\| \leq (1 - \epsilon) \frac{\tilde{q}_{r,b,min}}{\|H_r - NC_r\|} \left( \frac{\lambda_{max}(P_o)}{\lambda_{min}(P_o)} \right)^{-\frac{1}{2}} \right. \right\}$$

with the initial observer error  $e(0) = e_0$ . The matrix  $P_o$  results from the existence of  $P_o = P_o^\top > 0$  and  $Q_o = Q_o^\top > 0$  such that  $P_o(A_{r,t} - LC_r) + (A_{r,t} - LC_r)^\top P_o = -Q_o$  and  $G_r^\top P_o = H_r - NC_r$ , which is equivalent to the strict passivity of  $(A_{r,t} - LC_r, G_r, H_r - NC_r, 0)$ .

*Proof.* The proof of Theorem 3.2 is given in Appendix B.2.  $\square$

### 3.4.3 Output-feedback control design

The state-feedback controller and the observer from the previous sections together form an observer-based output-feedback controller. We use the estimated state  $\hat{\xi}_r$  of the observer (3.17) in the feedback law (3.12) of system (3.13) and prove local asymptotic stability of the equilibrium  $(\xi_r, e) = (0, 0)$  of the interconnected system (3.13), (3.18).

**Theorem 3.3.** *Consider system (3.13) and observer (3.17). Suppose the conditions in Theorem 3.1 are satisfied for system (3.13) and that the observer error dynamics in (3.18) satisfies the conditions in Theorem 3.2. Then,  $(\xi_r, e) = (0, 0)$  is a locally asymptotically stable equilibrium point of the interconnected system (3.13), (3.18) for any  $\tilde{\varphi}$  satisfying Assumptions 3.1 and 3.2.*

*Proof.* The proof of Theorem 3.3 is given in Appendix B.3.  $\square$

## 3.5 A simulation case study

In this section, we will show the application of the observer-based output-feedback controller (see Section 3.4) to the reduced-order drill-string model presented in Section 3.2. To stabilize the desired equilibrium  $x_{r,eq}$  of system (3.9) we have to design the controller gain  $K$  and the observer gains  $L$  and  $N$  to apply the control torque

$$u_t = u_c + K\hat{\xi}_r, \quad (3.19)$$

with  $u_c$  the constant feedforward torque as determined in Section 3.3.2 and  $K\hat{\xi}_r$  the feedback torque based on the observer estimate  $\hat{\xi}_r$ .

For the design of the controller and observer gains, we consider the system in perturbation states (3.11). Therefore we also have to apply the linear loop transformation to change the properties of the set-valued nonlinearity such

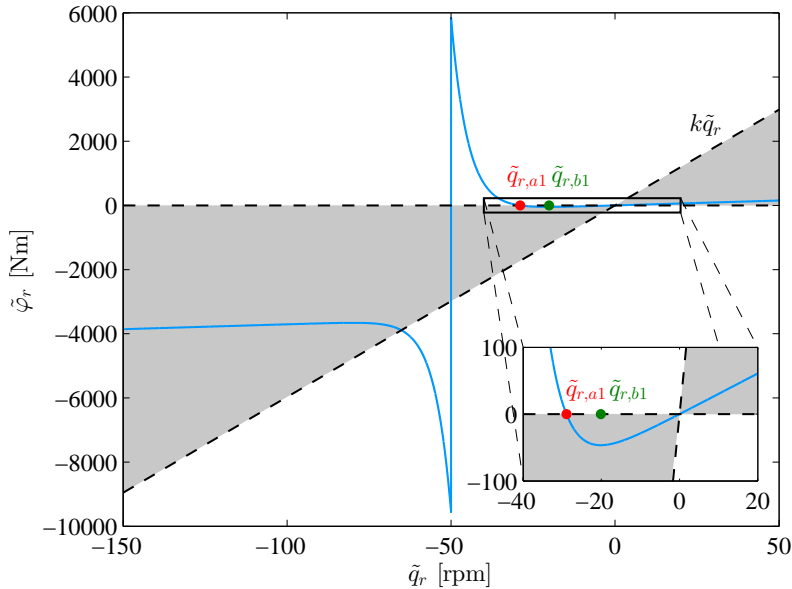


Figure 3.6: Transformed bit-rock interaction model  $\tilde{\varphi}_r(\tilde{q}_r)$ .

that it satisfies the conditions in Assumptions 3.1 and 3.2. Recall the transformed nonlinearity  $\tilde{\varphi}_r(\tilde{q}_r) = \varphi(\tilde{q}_r + H_r x_{r,eq}) - \varphi(H_r x_{r,eq}) + \delta \tilde{q}_r$ . By choosing  $\delta > 0$  appropriately,  $\tilde{\varphi}_r$  can be made locally monotonically increasing to satisfy Assumption 3.2. In addition and in combination with the fact that the system is written in perturbation states, the transformed nonlinearity also locally satisfies the sector condition as defined in Assumption 3.1. To illustrate both aspects, the transformed nonlinearity  $\tilde{\varphi}_r(\tilde{q}_r)$ , with  $\delta = 29.2$  Nms/rad, is shown in Figure 3.6. As can be seen in this figure,  $\tilde{\varphi}_r(\tilde{q}_r)$  belongs locally to the sector  $[0, k]$  with  $k = 570$  Nms/rad. The physical meaning of this condition is that the amount of velocity-weakening in the bit-rock interaction is limited for bit-rock interaction laws satisfying this sector condition. Moreover, the size of the sector indicates the amount of uncertainty in the bit-rock interaction for which the desired setpoint can be robustly stabilized. A larger sector, including the total nonlinearity  $\tilde{\varphi}_r(\tilde{q}_r)$ , results in an increased robustness with respect to uncertainty in the bit-rock interaction. However, it would also result in high control gains  $K$ . Such high gains result in high control torques  $\tilde{u}$  that can not be realized by the top drive and are therefore infeasible in practice. In Figure 3.6, we have also indicated the point  $\tilde{q}_{r,a1} = -28.9$  rpm for which it holds that for  $\tilde{q}_{r,a1} < \tilde{q}_r < \tilde{q}_{r,a2}$  the sector condition is satisfied ( $\tilde{q}_{r,a2}$  can be chosen arbitrarily large in this case) and hence Assumption 3.1 is satisfied. Moreover, the point  $\tilde{q}_{r,b1} = -20.1$  rpm such that for  $\tilde{q}_{r,b1} < \tilde{q}_r < \tilde{q}_{r,b2}$  it holds that  $\tilde{\varphi}_r$  is monotoni-

cally increasing ( $\tilde{q}_{r,b2}$  can also be chosen arbitrarily large in this case) and hence Assumption 3.2 is satisfied.

The controller and observer gains are designed according to the conditions given in Theorem 3.1 and Theorem 3.2, respectively. The results are obtained by using SeDuMi 1.3 [111], a linear matrix inequality (LMI) solver and the YALMIP interface [71]. The designed controller and observer gains are given by

$$K = [-276.9 \ 201.7 \ -228.1 \ -481.4 \ 370.6 \ 192.1 \ 549.1 \ 272.7 \ 68.79],$$

$$L = \begin{bmatrix} 40.14 \\ 64.19 \\ 87.96 \\ -187.3 \\ -239.9 \\ 183.5 \\ 428.0 \\ 347.5 \\ -6.515 \end{bmatrix}, \quad N = [0.502].$$

In this case study, we introduce a so-called startup scenario, which is based on practical startup procedures for drilling rigs. Herein, the drill-string is first accelerated to a low constant rotational velocity with the bit above the formation (off bottom) and, subsequently, the angular velocity and weight-on-bit (WOB) are gradually increased to the desired operating conditions. The startup scenario is built up as follows:

1. Start with zero WOB, which on a model level is reflected by the absence of a velocity-weakening effect in the bit-rock interaction model. Moreover, an industrial PI-controller, see (3.22) for details, is used to operate at relatively low velocity and build up torque in the drill-string to overcome static torques due to drag in the time window  $0 < t < 50$  s;
2. The controller (3.19) is activated at  $t = 50$  s and the reference angular velocity is slowly increased until the desired operating velocity ( $\omega_{eq}$ ) is reached (in the time window  $50 \leq t < 110$  s). At the same time, we emulate that the WOB slowly increases (by adaptation of the bit-rock interaction model as in (3.20), (3.21)) to engage the drilling process in order to generate the nominal operating condition in both the angular velocity and the WOB (and hence bit torque).

The change in the WOB is modelled as a change in the torque-on-bit  $T_{bit}$ . In particular, the bit-rock interaction model in (3.7) is scaled using a scaling factor  $\alpha(t)$  according to

$$T_{bit}(t) = \text{Sign}(\omega_{bit}) \left( T_{ini} + \alpha(t) \left( T_d - T_{ini} + (T_s - T_d) e^{-\frac{30}{N_d \pi} |\omega_{bit}|} \right) \right), \quad (3.20)$$

where

$$\alpha(t) = \begin{cases} 0, & t_0 \leq t \leq t_1 \\ \frac{t-t_1}{t_2-t_1}, & t_1 < t < t_2 \\ 1, & t \geq t_2 \end{cases} \quad (3.21)$$

with  $t_1 = 50$  and  $t_2 = 110$  in this case and  $T_{ini}$  is the amount of resisting torque that is still present at the bit-rock interface, even when the bit is off bottom (e.g. due to drilling mud and interactions with the bore hole).

Before we show the simulation results of the designed output-feedback controller, we will show a simulation result of the reduced-order drill-string system in closed loop with an existing industrial controller (based on [51]). The result of the simulation of the reduced-order model in closed loop with the industrial (SoftTorque) controller is shown in Figure 3.7. The simulations have been obtained numerically using the time-stepping method [66, 78]. When possible a Moreau time-stepping method, applicable to second-order dynamics, is used. However the observer is based on a reduced-order model which is not necessarily in second-order form. For the system in first-order state-space form the time-stepping scheme is adapted; the dedicated solver for first-order systems employed in this thesis is given in Appendix C.

The controller used for the simulation in Figure 3.7 is a properly tuned active damping system (i.e. PI-control of the angular velocity) which aims at damping the first torsional mode of the drill-string dynamics, based on the error  $e_y$  between the measured top drive velocity  $y = \omega_{td}$  and the reference angular velocity  $\omega_{td,ref}$ , i.e.  $e_y := \omega_{td,ref} - \omega_{td}$ . The controller is given in the Laplace domain by

$$\tilde{u}(s) = \left( c_t + \frac{k_t}{s} \right) e_y(s) \quad (3.22)$$

with  $c_t = 1829$  and  $k_t = 1177$  such that damping of the first torsional flexibility mode is obtained. The second plot shows the top drive velocity ( $\omega_{td}$ ) along with the reference velocity  $\omega_{td,ref}$  that starts at a velocity of 20 rpm and is gradually increased to the desired equilibrium velocity,  $\omega_{eq}$ , of 50 rpm. From the bit response, in the upper plot, we can clearly recognize stick-slip oscillations. The increasing amplitude of the oscillations in the top drive velocity demonstrates that these vibrations arise when the WOB is increased ( $50 \leq t < 110$  s). More specifically, when the bit is off bottom (in the first 50 seconds) and there is no velocity-weakening effect in the bit-rock interaction, the controller stabilizes the desired velocity, even though the bit initially sticks a couple of times due to transient oscillations. However, when the WOB is increased, modelled as an increase in  $T_s$  and  $T_d$  and therewith increasing the amount of velocity-weakening, the controller is no longer able to stabilize the desired equilibrium and eventually stick-slip oscillations appear. In the bottom plot, the applied torque at the top drive is also shown; the controller clearly acts on the oscillations in the top drive velocity, however the control action does not stabilize the desired velocity.

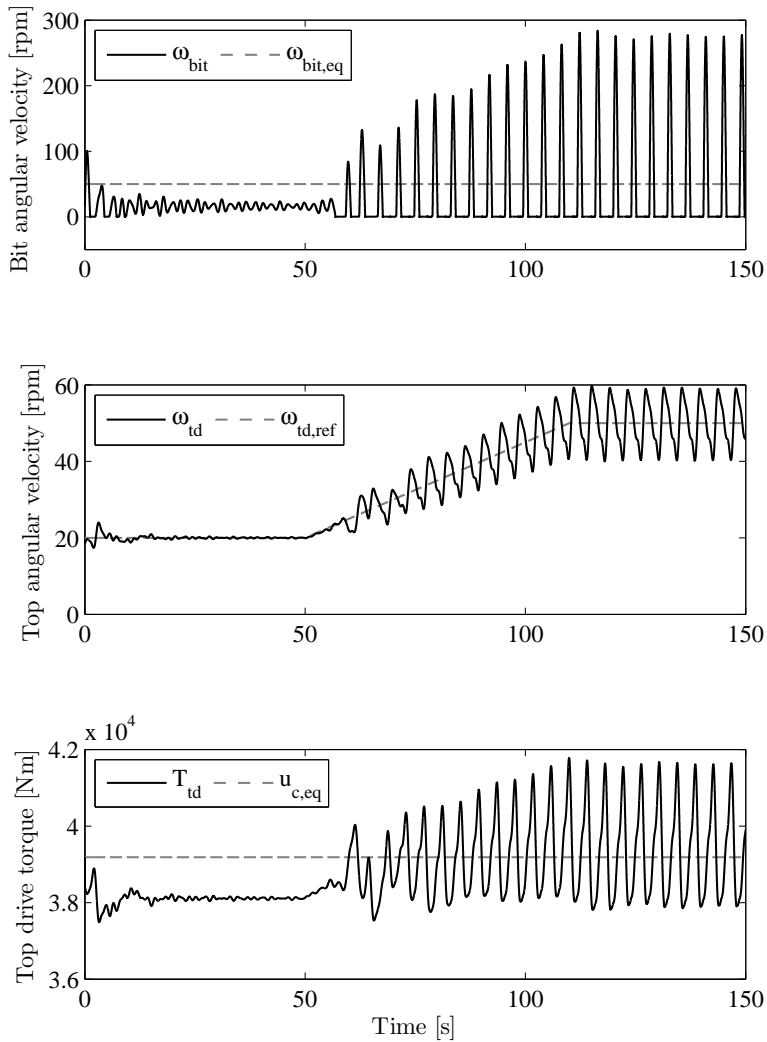


Figure 3.7: Simulation result of the reduced-order model with an existing industrial (SoftTorque) controller in the startup scenario.



For the designed output-feedback controller, we immediately activate (at  $t = 0$ ) the observer to obtain the state estimate  $\hat{\xi}_r$ ; however, this estimate is not used by the industrial PI-controller in the first 50 seconds (since this controller only uses the top drive velocity as a measured output). When the state-feedback controller is switched on at  $t = 50$ , it uses the state estimate  $\hat{\xi}_r$ , based on the surface measurement  $\omega_{td}$  only. Figure 3.8 shows a simulation result of the closed-loop system with output-feedback controller, where we used the same initial conditions  $\xi_{r,0}$  and startup scenario as for the previous simulation (Figure 3.7). Furthermore, the initial states for the observer  $\hat{\xi}_{r,0}$  have a 10% offset from the initial states  $\xi_{r,0}$ . It can be seen that after some transient behavior, the observer estimates converge to the actual states within approximately 5 seconds. For the sake of clarity, the scale of the plot is adapted such that the initial peaks of the observer estimate of the bit angular velocity are not totally visible. The amplitude of these oscillations peaks up to 300 rpm due to the initial observer error but this does not affect the control action because the PI-controller does not use the observer estimates. After 50 seconds the output-feedback controller is turned on and the WOB and desired velocity are increased. The simulation results show that the top drive and bit velocity converge to their equilibrium value and stick-slip oscillations are avoided. The equilibrium velocity of the bit  $\omega_{bit,eq} := H_r x_{r,eq} \approx 47$  rpm is slightly lower than the equilibrium velocity of the top drive  $\omega_{td,eq} = \omega_{eq} = 50$  rpm. This small mismatch is a consequence of the model reduction, as the outputs  $q_r$  and  $y_r$  of the reduced-order system slightly differ from the original outputs  $q$  and  $y$  and the feedforward is designed such that in equilibrium the top drive velocity of the reduced-order model matches the desired velocity. The lag between the desired velocity and the top drive velocity between 50 and 115 s in Figure 3.8 can be explained as follows. We have designed a low-gain controller to accommodate the practical limitations of the top drive actuator aiming at the stabilization of the desired equilibrium (not at achieving a high bandwidth). If desired, this could be compensated by designing additional (mass) feedforward.

Most importantly, it can be concluded that the stick-slip vibrations are eliminated with the designed controller. Besides (local) asymptotic stability of the desired setpoint, the controller is designed to obtain robustness with respect to uncertainty in the bit-rock interaction. As mentioned in Section 3.2.1, the bit-mobility can be used to investigate the sensitivity for disturbances in the bit-rock interaction. Therefore, we would like to analyze if indeed damping of the resonance modes in the bit-mobility is obtained with the designed observer-based controller. To do so, we use a linearized approximation of the reduced-order nonlinear closed-loop system to determine the closed-loop bit-mobility. The approximated closed-loop system in perturbation coordinates, and linearized

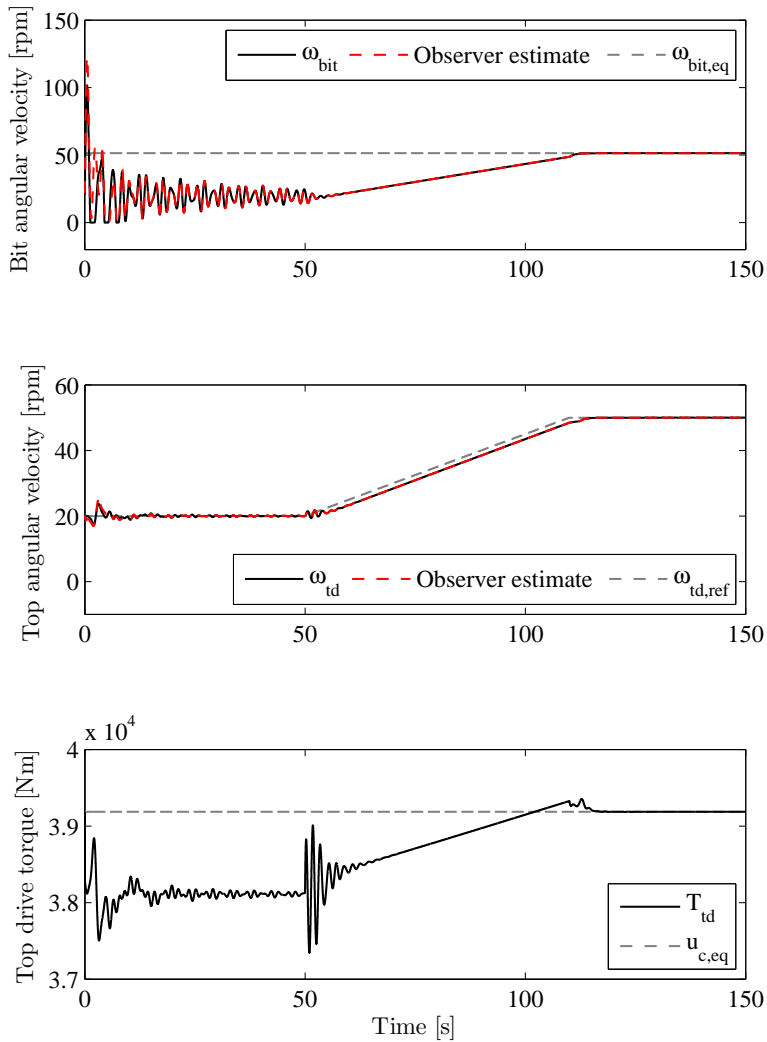


Figure 3.8: Simulation result of the reduced-order model with the designed output-feedback controller in the startup scenario.

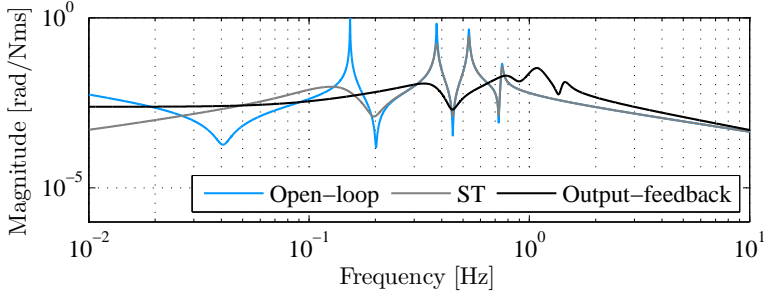


Figure 3.9: Closed-loop bit-mobility of the reduced-order model, i.e. the frequency response function from bit torque  $T_{bit}$  to bit velocity  $\omega_{bit}$  for the linearized system (3.23).

around  $(\xi_r, \hat{\xi}_r) = (0, 0)$  is given by

$$\begin{aligned} \dot{\xi}_r &= \left( A_r - G_r H_r \left. \frac{\partial \varphi}{\partial \dot{q}_r} \right|_{\xi_r=0, \hat{\xi}_r=0} \right) \xi_r + B_r K \hat{\xi}_r \\ \dot{\hat{\xi}}_r &= \left( A_r - LC_r + B_r K - G_r (H_r - NC_r) \left. \frac{\partial \varphi}{\partial \dot{q}_r} \right|_{\xi_r=0, \hat{\xi}_r=0} \right) \hat{\xi}_r \\ &\quad + \left( LC_r - G_r NC_r \left. \frac{\partial \varphi}{\partial \dot{q}_r} \right|_{\xi_r=0, \hat{\xi}_r=0} \right) \xi_r. \end{aligned} \quad (3.23)$$

Based on this linearized closed-loop system, we can determine the closed-loop bit-mobility as shown in Figure 3.9. For reference we have also shown closed-loop bit-mobility of the system with the industrial controller (ST). It can be observed that with the industrial controller only the first torsional flexibility mode is damped, which can be an explanation for the fact that the drill-string system still exhibits stick-slip oscillations when controlled by the SoftTorque controller. The designed observer-based controller, on the other hand, clearly achieves damping of all three flexibility modes of the reduced-order model. Clearly, damping of multiple flexibility modes can be achieved with the proposed controller design methodology.

### 3.6 Controller design for the 18-DOF model

In the previous sections, the controller design strategy is applied to a reduced-order model of the drill-string dynamics. Stability conditions to guarantee (local) asymptotic stability are derived and simulation results to illustrate that the desired velocity can indeed be stabilized are shown. The purpose of the reduced-order model is to reduce the controller complexity, such that the LMI-based design of the state-feedback controller and observer are feasible. Additionally, a controller of limited order is favorable for implementation reasons. However,

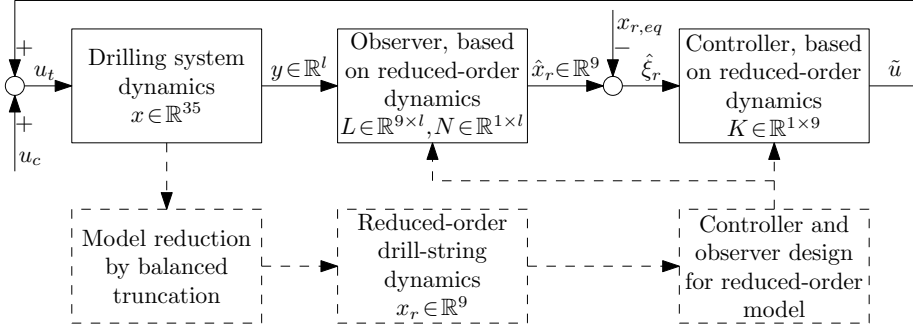


Figure 3.10: Block diagram of 1) the controller implementation for the 18-DOF drill-string model, and 2) the design steps for the controller.

in practice the plant (i.e. the drilling system) is of course not of reduced order. Therefore, the application of the controller design strategy to the 18-DOF drilling system dynamics (3.8) is investigated in this section.

The implementation of the controller and the design steps taken to obtain the controller are illustrated in the block diagram in Figure 3.10. The upper loop in the block scheme is the part that is running online, while the dashed blocks indicate the design steps that are performed offline before applying the controller to the drilling system. The controller design strategy can be summarized by the following steps. First, a reduced-order model, that captures the dominant dynamics to estimate the input-output behavior, is determined based on a (full-scale finite-element) model of the drill-string. This model can be obtained from the drill-string plan in practice. Next, a controller and observer are synthesized for the reduced-order model, according to the procedure presented in Section 3.4. Finally, this controller-observer combination is applied to the drilling system as visualized by the upper loop in Figure 3.10.

The closed-loop system, consisting of the finite-element model of the drill-string dynamics and the observer-based output-feedback controller based on the reduced-order model, is given by the drill-string dynamics (3.8):

$$\begin{aligned}
 \dot{x} &= Ax + Bu_t + Gv + G_2v_2 \\
 q &= Hx \\
 q_2 &= H_2x \\
 y &= Cx \\
 v &\in -\varphi(q) \\
 v_2 &\in -\phi(q_2),
 \end{aligned} \tag{3.24}$$

the observer, based on the reduced-order model:

$$\begin{aligned}
 \dot{\hat{x}}_r &= A_r \hat{x}_r + B_r u_t + G_r \hat{v}_r + G_{2,r} \hat{v}_{2,r} + L (y - \hat{y}_r) \\
 \hat{q}_r &= H_r \hat{x}_r + N (y - \hat{y}_r) \\
 \hat{q}_{2,r} &= H_{2,r} \hat{x}_r \\
 \hat{y}_r &= C_r \hat{x}_r \\
 \hat{v}_r &\in -\varphi(\hat{q}_r) \\
 \hat{v}_{2,r} &\in -\phi(\hat{q}_{2,r})
 \end{aligned} \tag{3.25}$$

and the state-feedback controller  $\tilde{u} = K \hat{\xi}_r = K (\hat{x}_r - x_{r,eq})$ .

**Remark 3.3.** *The stability conditions, as presented in Section 3.4, only hold for a closed-loop system where the controller and observer are designed for the plant model and also are applied to the same plant. For the application of the reduced-order controller and observer to a higher-order model (or real drilling system) stability is not necessarily guaranteed due to model mismatches. However, analysis of the closed-loop system and simulation results presented next show that the reduced-order controller and observer can still (locally) stabilize the desired equilibrium of the high-order finite-element model.*

As mentioned before, only the top drive angular velocity measurement is used and the measured output is given by  $y = Cx = \omega_{td}$ . The designed controller and observer gains for the closed-loop system (3.24)-(3.25), with the top drive angular velocity measurement is the measured output (i.e.  $y = Cx = \omega_{td}$ ), are given by

$$K = [-276.9 \ 201.7 \ -228.1 \ -481.4 \ 370.6 \ 192.1 \ 549.1 \ 272.7 \ 68.79],$$

$$L = \begin{bmatrix} 44.26 \\ 41.77 \\ 27.17 \\ -72.56 \\ -105.6 \\ 84.30 \\ 171.6 \\ 61.88 \\ 43.36 \end{bmatrix}, \quad N = [0.414]. \tag{3.26}$$

The controller gains are equal to the controller gains designed for the reduced-order model in Section 3.5, however the observer gains are slightly different. The observer has been re-tuned (by changing the sector bounds for the observer) to obtain more robustness with respect to the model mismatch due to reduction.

A simulation result of the designed controller applied to the 18-DOF drill-string model is shown in Figure 3.11. For comparison, also the response of the system in closed-loop with the industrial controller (indicated by the subscript

$ST$ ) is shown. In the first 50 seconds, in both strategies the same controller is used (as explained for the startup scenario), after 50 seconds the observer-based controller is switched on while for the industrial controller the same controller is used for the whole time range. Between 50 and 110 seconds the torque-on-bit and desired velocity are again changed according to the startup scenario explained earlier to obtain the desired operating conditions. This simulation shows that the observer-based output-feedback controller clearly stabilizes the desired setpoint of 50 rpm, while the industrial controller does not stabilize the equilibrium, resulting in stick-slip oscillations at the bit. It is also important to mention that the control action ( $T_{td}$ ) is limited as can be seen in the top drive torque in the bottom plot. Figure 3.11 shows that the stick-slip limit cycles consist of two successive slip phases relatively short after each other followed by a longer sticking period before the cycle is repeated, while in the response of the reduced-order model the stick-slip oscillations are characterized by a single peak. The response with the two peaks followed by a longer sticking period is recognized from field observations for this rig. Apparently, this behavior is not captured in the reduced-order model from Section 3.2.1. However, the main purpose of the reduced-order model is to capture the dominant dynamics in order to design controllers to mitigate stick-slip vibrations. Closed-loop simulations, using a controller and observer based on the reduced-order model, show that the model can be very well used for this purpose.

To conclude, the simulation result in Figure 3.11 shows that the controller is robust for the model mismatch introduced by the reduction procedure. In addition, this simulation result gives an indication that the controller can deal with unmodelled drill-string dynamics, since the controller only uses the reduced-order dynamics in which a part of the original dynamics is omitted. Both these aspects are important properties for practical implementation of the proposed controller design strategy. In Section 3.7, several other robustness aspects are investigated by means of simulation studies. In the next section, a stability analysis based on linearization is performed.

### 3.6.1 Stability analysis

For a controller to work properly in practice, i.e. mitigate stick-slip vibrations and stabilize the desired angular velocity, three main aspects should be satisfied. First, the desired setpoint should be a (locally) asymptotically stable equilibrium point of the closed-loop system. Second, the control action required to stabilize the equilibrium should satisfy actuator limitations and third, the closed-loop system has to be robust with respect to uncertainties (e.g. in the bit-rock interaction and the drill-string model) and disturbances (e.g. sensor and actuator noise). The first point is a necessary condition, while the latter two aspects are performance requirements from a practical point of view.

To investigate the stability of the equilibrium point of the closed-loop non-

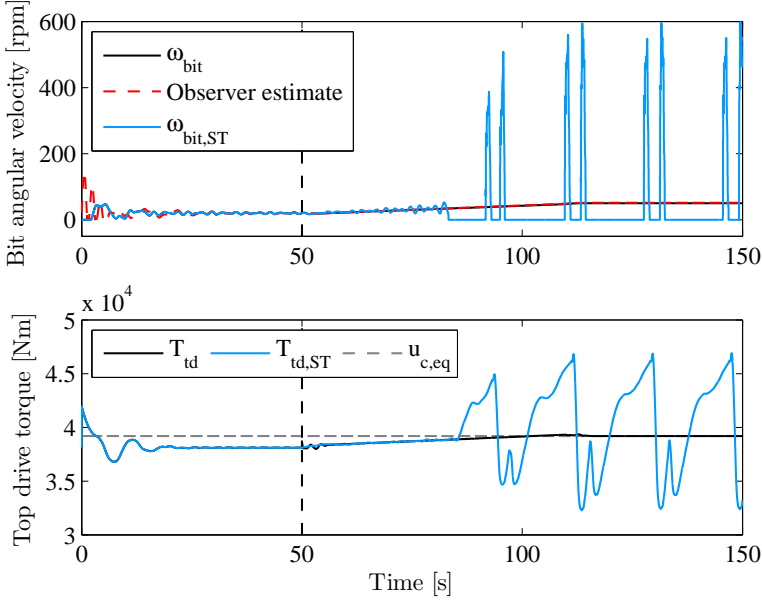


Figure 3.11: Simulation result of both the industrial (SoftTorque) controller and the designed observer-based output-feedback controller applied to the 18-DOF drill-string system.

linear system we linearize the closed-loop system around this equilibrium point and determine the eigenvalues of the linearized system. The linearized closed-loop system, in perturbation coordinates, and linearized around  $(\xi, \hat{\xi}_r) = (0, 0)$  is given by

$$\begin{aligned} \dot{\xi} &= \left( A - GH \left. \frac{\partial \varphi}{\partial q} \right|_{\xi=0, \hat{\xi}_r=0} \right) \xi + BK \hat{\xi}_r \\ \dot{\hat{\xi}}_r &= \left( A_r - LC_r + B_r K - G_r (H_r - NC_r) \left. \frac{\partial \varphi}{\partial q_r} \right|_{\xi=0, \hat{\xi}_r=0} \right) \hat{\xi}_r \\ &\quad + \left( LC - G_r NC \left. \frac{\partial \varphi}{\partial q_r} \right|_{\xi=0, \hat{\xi}_r=0} \right) \xi. \end{aligned} \quad (3.27)$$

As can be seen from this equation, both the nonlinearity in the plant and the nonlinearity in the observer are linearized. The desired equilibrium of the closed-loop system is (locally) exponentially stable if the eigenvalues  $\lambda_i$  of the system are in the open left-half-plane (LHP) of the complex plane. For a desired velocity of 50 rpm the real value of the right-most pole equals  $\max(\text{Re}(\lambda_i)) = -0.015$ , hence the desired setpoint is locally (exponentially) stable, which is in accordance to the simulation results shown in Figure 3.11. However, the equilibrium of the closed-loop with the industrial controller used for the simulation in the

same figure is also stable ( $\max(\text{Re}(\lambda_i)) = -0.022$ ). As we have observed in the simulation, the controller failed to stabilize the desired velocity. This is because the controller also needs to be robust with respect to disturbances, model mismatches, (measurement) noise etc. to work properly in practice, while the linearization only indicates local stability of the desired equilibrium. Some of these robustness aspects, such as changing operating conditions and measurement noise are investigated in the next section. Moreover, investigation of the closed-loop system has revealed that robustness with respect to the bit-rock interaction is particularly important for the stability of the desired setpoint of the nonlinear closed-loop system and is therefore further analyzed here.

As mentioned before, the velocity-weakening effect in the bit-rock interaction has a destabilizing effect on the drill-string dynamics. Therefore, a controller should be designed such that the robustness with respect to this negative damping effect is “optimized”. An indication of such robustness property is given by the closed-loop bit-mobility transfer function. That is, damping of the resonance modes in the bit-mobility results in a decreased sensitivity with respect to variations in the bit-rock interaction. The open-loop bit-mobility function of the drill-string system is defined by  $G_{cl}$  and shown in Figure 3.4. Using the linearized system (3.27) we can also investigate the closed-loop bit-mobility function. In Figure 3.12, the magnitude of the closed-loop bit-mobility of the system with the observer-based controller and the industrial controller (ST) are shown and compared with the open-loop bit-mobility as previous shown. The objective of the industrial controller is to damp the first resonance mode, which is also visible in the bit-mobility plot. However, higher flexibility modes are still present, which can be related to the fact that these undamped higher flexibility modes still cause stick-slip oscillations when the SoftTorque controller is applied. The proposed controller design strategy clearly achieves damping of multiple flexibility modes. From Figure 3.12, it can be seen that the first three modes are well-damped by the observer-based output-feedback controller, where these first three modes are the dominant flexibility modes as put forward by the open-loop bit-mobility. This confirms that, with the proposed controller design strategy, it is indeed possible to damp multiple flexibility modes.

### 3.7 Robustness of the closed-loop system

In the previous section, a simulation case-study is shown of the closed-loop system consisting of the finite-element model for the drill-string and the observer-based output-feedback controller based on the reduced-order model. This simulation has been performed under “ideal” conditions, i.e. without disturbances and/or changing operating conditions in terms of desired angular velocity, increasing length of the drill-string and changing bit-rock interaction. In this section, simulation results are presented where these effects are taken into account. In Section 3.7.1, the minimal angular velocity that can be stabilized is investi-



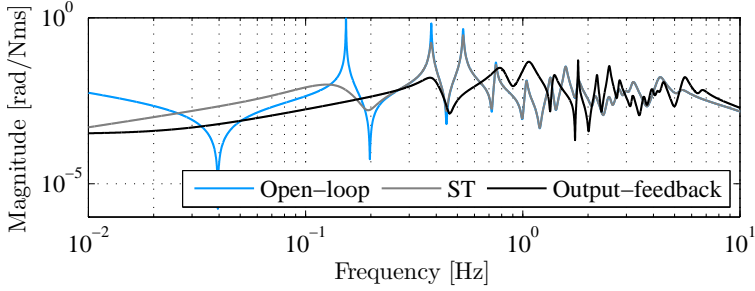


Figure 3.12: Closed-loop bit-mobility, i.e. the frequency response function from bit torque  $T_{bit}$  to bit velocity  $\omega_{bit}$  for the linearized system (3.27).

gated to analyze the improved operating envelope in terms of angular velocity of the observer-based output-feedback controller. In Section 3.7.2, a simulation study with a changed bit-rock interaction model is performed. In Section 3.7.3, sensor and actuator noise disturbances are taken into account and, finally, in Section 3.7.4, robustness with respect to changing length of the drill-string is investigated. All these results are obtained for a closed-loop system with the 18-DOF FEM model and the reduced-order controller with the gains given in (3.26).

### 3.7.1 Different operating velocity

The designed controller (Section 3.6) is synthesized for a desired angular velocity of 50 rpm. This controller is designed such that, on the one hand, the robustness with respect to the bit-rock interaction is improved and, on the other hand, the control action is limited, i.e. feasible for a typical top drive. This balance is achieved by tuning the sector bound  $k$  and the slope of the transformed nonlinearity  $\tilde{\varphi}_r$  around the desired setpoint (determined by  $\delta$ ). The resulting bounds  $\tilde{q}_{r,a1}$  and  $\tilde{q}_{r,b1}$ , for which the nonlinearity satisfies Assumptions 3.1 and 3.2, give an indication of the lower limits for the bit angular velocity for which stability can still be guaranteed; however, these bounds are typically conservative and hold for the reduced-order closed-loop system. These values indicate the region of attraction in terms of the bit angular velocity. However, from a practical point of view it is interesting to investigate the variation of the setpoint for which the drill-string system can be stabilized. For the nonlinear closed-loop system the (local) stability of different setpoints is investigated by linearization of the equilibrium (see Section 3.6.1). Due to the velocity-weakening effect in the bit-rock interaction, which has a destabilizing effect, lower angular velocities are more difficult to stabilize. That is, if the velocity is decreased, then the amount of negative damping increases and at a certain moment the con-

troller is not able to stabilize the desired velocity, indicated by a transition of the right-most eigenvalue from the left-half-plane (LHP) to the right-half-plane (RHP). This lower limit on the desired angular velocity for different controllers is indicated in Figure 3.13. For the industrial (SoftTorque) controller the lower limit is approximately 40 rpm, while the lower limit for the designed controller is slightly above 30 rpm. Once more, it has to be mentioned that these velocities indicate a theoretical lower limit and the lowest velocity for which stick-slip oscillations can be avoided will be higher. For example, we mention that with the SoftTorque controller in simulations stick-slip oscillations already appeared for a desired angular velocity of 50 rpm. For the startup scenario these velocities are also higher due the changing conditions and transient oscillations caused by a difference between the initial conditions and the equilibrium. To give an indication, the minimum velocity that can be stabilized in simulations using the startup procedure is approximately 41.5 rpm (and 51 rpm for the industrial controller).

In Figure 3.13, also a third controller is indicated ( $\omega_{min,lowrpm}$ ). This controller is designed without keeping in mind robustness and/or actuator limitations. For the 18-DOF model, a controller (based on the reduced-order model) can be designed that focuses on a large operating envelope in terms of angular velocity. This controller is obtained by decreasing the size  $k$  of the sector, resulting in less robustness with respect to the bit-rock interaction. As can be seen, the resulting lower bound for the angular velocity can not be decreased that much in this case. However, it shows that different controllers can be designed depending on the performance specifications for the drilling system.

### 3.7.2 Changing bit-rock interaction model

In practice, it is difficult to obtain an accurate model for the bit-rock interaction and additionally this bit-rock interaction is prone to changes during the drilling process due to changing formation characteristics and bit wear. Robustness with respect to uncertainty in the bit-rock interaction is key in practice and is obtained by enlarging the sector  $k$  for the bit-rock interaction in the controller synthesis. This means that the controller is robust as long as the nonlinearity (locally) satisfies the sector condition and satisfies the conditions stated in Assumptions 3.1 and 3.2. In this section, a simulation result is shown to illustrate the variations in the bit-rock interaction that the proposed controller can cope with.

Recall the nominal parameter values for the bit-rock interaction model, that is  $T_s = 7700$  Nm,  $T_d = 1700$  Nm and  $N_d = 5$  rpm. These values are used in the controller synthesis and are also used in the observer. So, during the simulation the observer always uses the nominal bit-rock interaction model, since this is the only model that is available in practice. Due to changing conditions the actual bit-rock interaction, acting on the plant, changes. In this simulation study both

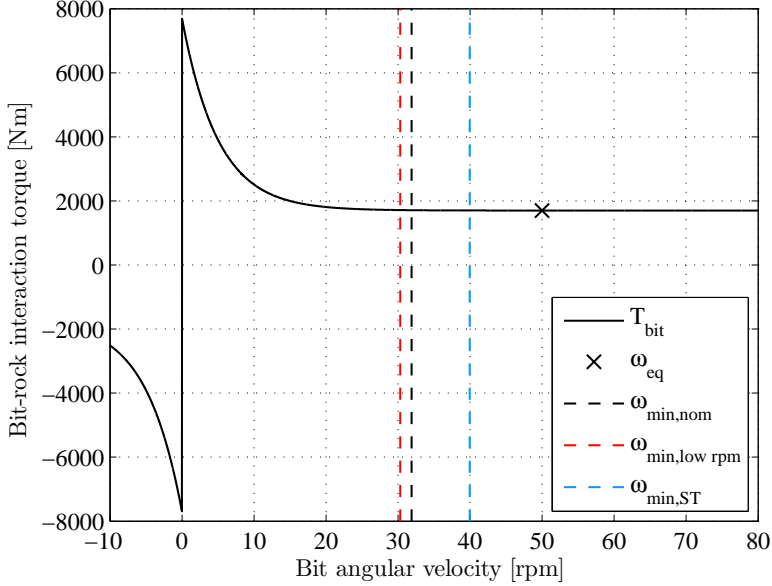


Figure 3.13: Lower limit of the desired angular velocity that can be stabilized for different controllers.

the torque level and the decrease rate of the bit-rock interaction is changed. First, the nominal level of the bit-rock interaction model is increased. In other words, both the static torque  $T_s$  and the dynamic torque  $T_d$  are increased. Also the decrease rate (related to  $N_d$ ) is adapted, by increasing  $N_d$ . This leads to a less severe velocity-weakening effect and therefore more negative damping at higher velocities. The parameters for the adapted bit-rock interaction model are given by  $T_s^c = T_s + 500$ ,  $T_d^c = T_d + 500$  and  $N_d^c = N_d + 1$ . The nominal and adapted bit-rock interaction model are shown in the left plot in Figure 3.14. The plot on the right-hand side shows the equivalent transformed representation of both bit-rock interaction models. It can be seen that both bit-rock interaction models (locally) satisfy the  $[0, k]$  sector condition. It has to be mentioned that the increase of the torque level is compensated by the feedforward torque, i.e. the plant uses a higher (constant) feedforward torque than the observer. This is a reasonable assumption from a practical point of view, because the amount of torque necessary to rotate the drill-string can be determined from measurements. Another possibility would be to compensate for this effect using integral action in the controller; however, this is not incorporated in the current controller design strategy.

The simulation result with the changed bit-rock interaction model is shown in Figure 3.15. It takes about 25 seconds before the states of the observer have

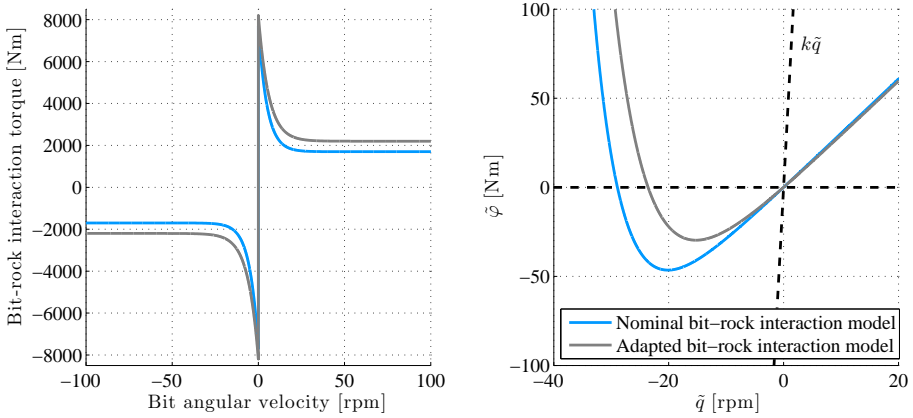


Figure 3.14: Nominal and adapted bit-rock interaction model, and a zoom plot of its equivalent transformed representations to indicate the sector bounds.

converged to the actual states. When the observer-based controller is switched on after 50 seconds the desired setpoint is stabilized and stick-slip oscillations have been mitigated. Again, a small mismatch between the actual bit-velocity and the reduced-order estimate can be recognized, which is caused by the reduction error. Moreover, the difference between the torque for the plant and the observer can be observed clearly in the bottom plot. As mentioned before, this difference is the (constant) difference between the actual feedforward torque and the observer feedforward torque which is based on the nominal bit-rock interaction. The necessary top drive torque as shown in the bottom plot shows only small oscillations and also the level of the required torque is feasible for typical top drives in practice. Due to the switch of the controllers at  $t = 50$  seconds a step in the required torque is present, but as can be seen also this only requires a relatively small change of the top drive torque.

Further studies have shown that we can increase the value of  $N_d$ , which determines the decrease rate of the bit-rock interaction model, to 6.17 rpm for the particular start scenario presented here. This increased value of  $N_d$  results in a more negative slope in the bit-rock interaction, i.e. more negative damping, around the desired operating velocity. Again, it has to be mentioned that the controller and observer are designed based on the original bit-rock interaction parameters. A controller specifically designed for a system with higher values for  $N_d$  would be able to deal with bit-rock interaction models with those parameter settings. In addition, the settings of the startup scenario are also of influence whether or not a controller fails to stabilize the desired setpoint.

To conclude, with the designed observer-based output-feedback controller the drill-string system can effectively deal with uncertainty in the bit-rock interac-

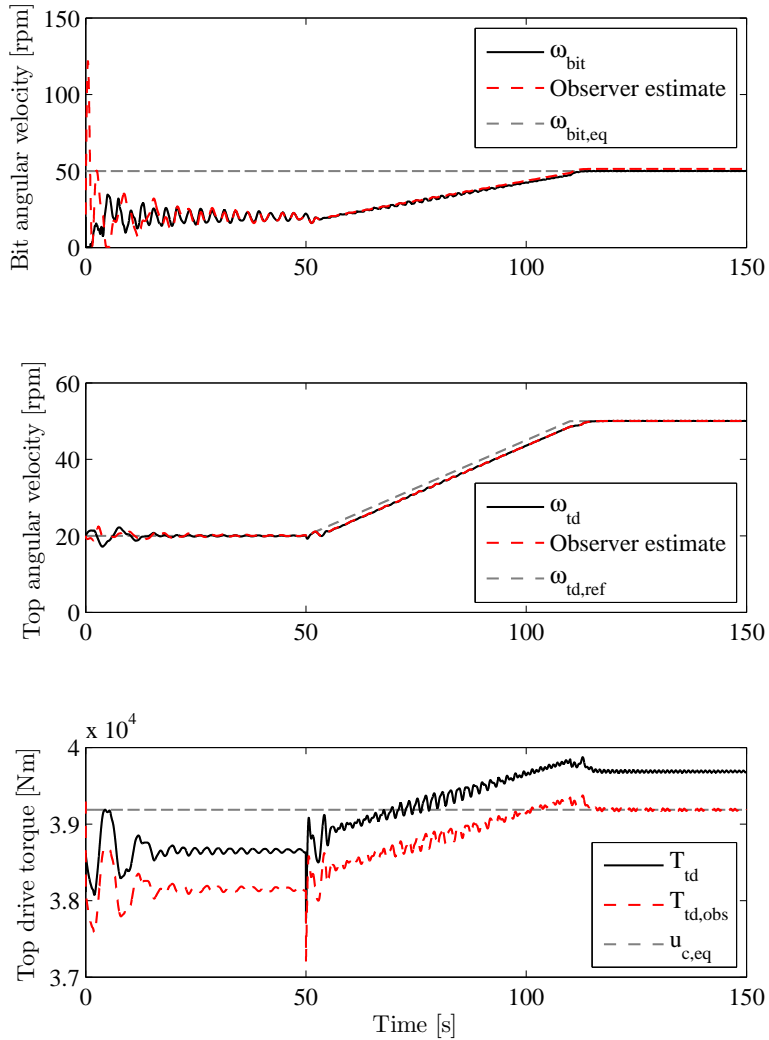


Figure 3.15: Simulation result of the closed-loop system with a changed bit-rock interaction for the plant model.

tion. More specifically, robustness with respect to uncertainty in the nominal level of the bit-rock interaction, as well as, in the slope of the nonlinearity, has been obtained. This is an important aspect from practical point of view because uncertainty in the bit-rock interaction is always present due to a changing lithology and/or changing conditions due to for example bit wear.

### 3.7.3 Sensor and actuator noise disturbances

The previous simulations are all performed under ideal conditions regarding sensors and actuators. In practice, the controller also has to deal with sensor and actuator noise. In this section, the robustness with respect to such noise perturbations is investigated and both sensor and actuator noise are taken into account. The noise disturbances are modelled as additive white noise signals. That is, the actual top drive torque  $T_{td}$  is given by  $T_{td} = u_t + d_{T_{td}}$  with  $u_t$  the output from the controller and  $d_{T_{td}}$  the disturbance. The measurement  $y_m$  is the actual top drive velocity plus sensor noise, i.e.  $y_m = y + n_{\omega_{td}}$ . The actuator noise on the top drive torque has a standard deviation of approximately 560 Nm, i.e. 1.5% of the nominal value, this means that the top drive torque varies between approximately 37.2 kNm and 41.1 kNm (nominal torque in equilibrium is  $u_c = 39.2$  kNm). The standard deviation of the sensor noise is also chosen to be approximately 1.5% of the nominal value, i.e. approximately 0.7 rpm, thus the measured top drive angular velocity varies between 47.5 rpm and 52.5 rpm.

A simulation of the system including measurement noise is shown in Figure 3.16. In this figure the actual top drive velocity  $\omega_{td}(= y)$  and control action  $u_t$  are shown. Compared to the previous simulation results, the response of the system is similar. A closer look at the states of the system of course shows some more oscillations caused by the sensor and actuator noise. An important observation is the difference in the control action from the industrial controller in the first 50 seconds compared to the control action from the observer-based controller. As can be seen in the bottom plot, the high-frequent disturbances are much more filtered by the observer-based controller compared to the industrial controller. This can be explained by the lack of a roll-off filter in the industrial controller, while the dynamics in the observer-controller combination do filter high-frequent oscillations.

### 3.7.4 Changing length of the drill-string

Another important aspect in the control of drilling systems is the change of length of the drill-string while drilling. Current controllers need to be re-tuned during the drilling operation and this re-tuning is prone to errors, resulting in wrong controller settings and possibly failing to mitigate stick-slip oscillations due to tuning errors. Additionally, the re-tuning process is time consuming and requires qualified staff to be present at the rig. Therefore, it is of practical

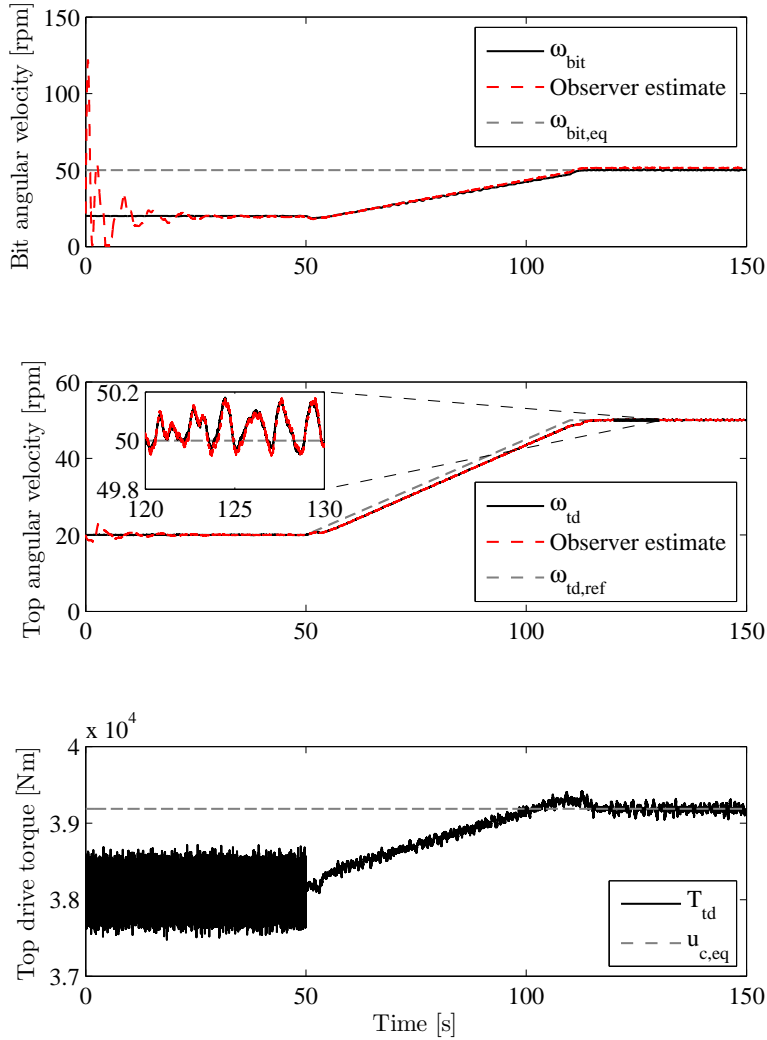


Figure 3.16: Simulation result of the closed-loop system with sensor and actuator noise, the peak-to-peak disturbances are approximately 10% of the nominal value of the disturbed signal.

importance to reduce the need for re-tuning due to length changes in the drill-string. In other words, the controller should be robust with respect to the increasing length of the drill-string. In this section, the plant model (3.8) is changed such that the dynamics of the plant correspond to a drill-string of different length. The controller remains the same and the observer is always based on the nominal reduced-order model (3.9).

In many drilling operations the drill-string is stopped to rotate to add a new pipe section. In this analysis, it is assumed that several new stands, of 3 drill pipes of 9 m length each, are added to the drill-string (i.e. 27 m of length is added to the drill-string with each stand). In practical situations, the current industrial controller needs to be re-tuned every stand, and sometimes even after one or two added drill pipes. The results of the analysis of the linearized closed-loop system with different lengths are shown in Figure 3.17. The real value of the right-most eigenvalue is shown as function of changing length compared to the nominal model. The right-most eigenvalue of the nominal model (indicated by 0 on the horizontal axis) lies in the LHP as shown in Section 3.6.1. When the length of the drill-string is decreased the right-most eigenvalue moves further into the LHP, while for an increase of length the right-most eigenvalue moves towards the imaginary axis. The same holds for the closed-loop system induced by the industrial controller (albeit more slowly). However, as mentioned before, the location of the eigenvalue is not the only important factor. Therefore, also the  $\mathcal{H}_\infty$ -norm<sup>1</sup> of the bit-mobility ( $G_{cl}$ ) is shown in Figure 3.17. Recall that the bit-mobility is related to the robustness with respect to the bit-rock interaction. The  $\mathcal{H}_\infty$ -norm of the closed-loop bit-mobility with the observer-based controller is approximately a factor 5 lower than the  $\mathcal{H}_\infty$ -norm of  $G_{cl}$  with the industrial controller, as was also visible in the bit-mobility plot (Figure 3.12) for the nominal case. The minor change of the  $\mathcal{H}_\infty$ -norm of the bit-mobility of the system with the observer-based controller due to a change in drill-string length and the fact that the right-most eigenvalue is still in the LHP indicates that the controller is probably able to stabilize the desired equilibrium. To confirm this conjecture, a simulation result of the closed-loop system with a plant model that is 135 m ( $15 \times 9$  m) longer than the nominal model (with a total length of 6249 m) is shown in Figure 3.18.

Compared to previous simulation results, the response of the closed-loop system with a plant model representing a drill-string with different length shows more transient oscillations. Moreover, the frequency of these oscillations is somewhat different; compare for example the oscillations at the bit during the first 50 seconds in Figure 3.15 with the oscillations in Figure 3.18. This is due to the fact that the eigenfrequencies of the drill-string system have changed due to the added length, because the stiffness and inertia of the upper part of the drill-string has changed. Another observation (see zoom plot in Figure 3.18) is that the state estimates of the reduced-order observer do not exactly match the

<sup>1</sup>The  $\mathcal{H}_\infty$ -norm of a transfer function  $H(s)$  is given by  $\|H(s)\|_\infty := \sup_{\omega \in \mathbb{R}} (H(j\omega))$ .



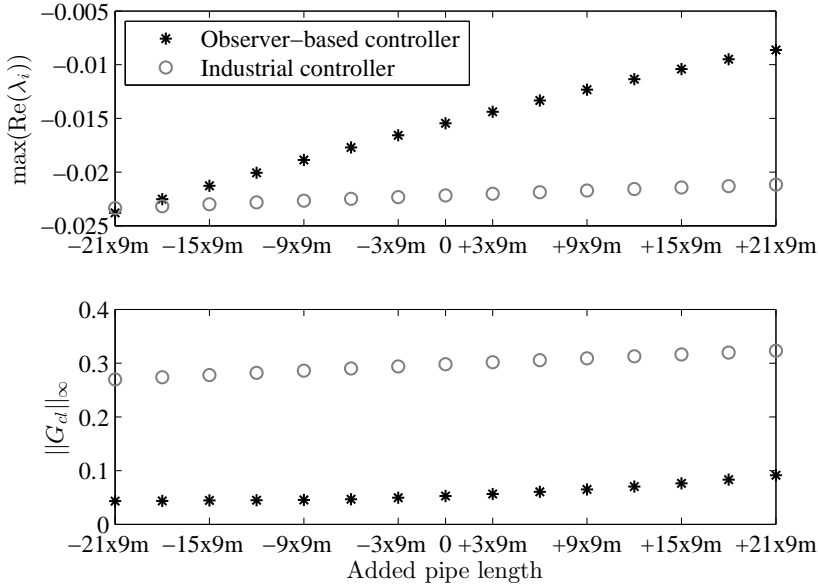


Figure 3.17: Location of the right-most eigenvalue of the closed-loop system and  $\mathcal{H}_\infty$ -norm of the bit-mobility as function of added pipe length to the drill-string.

states of the drilling system. This is caused by the mismatch between the plant model and the model used by the observer. However, as shown in the simulation, the state estimate is still sufficiently accurate for the controller to stabilize the desired equilibrium under the applied operating conditions.

The right-most eigenvalue has been determined for more drill-string configurations than shown in Figure 3.17. When 45 pipe sections of 9 m are added to the drill-string the right-most eigenvalue moves into the RHP, indicating that the linearized closed-loop system is unstable. Simulations with different plant models show that in practice the controller is able to stabilize the desired set-point for a drill-string model with a maximum of 39 pipe sections (i.e. 351 m) added to the nominal model. This is due to the fact that the eigenvalues only give information about the local stability of the closed-loop, while for the nonlinear closed-loop system also robustness with respect to uncertainties (especially related to the bit-rock interaction) is important. It can be concluded that a significant increase in robustness with respect to increasing drill-string length is obtained compared to the industrial controller.

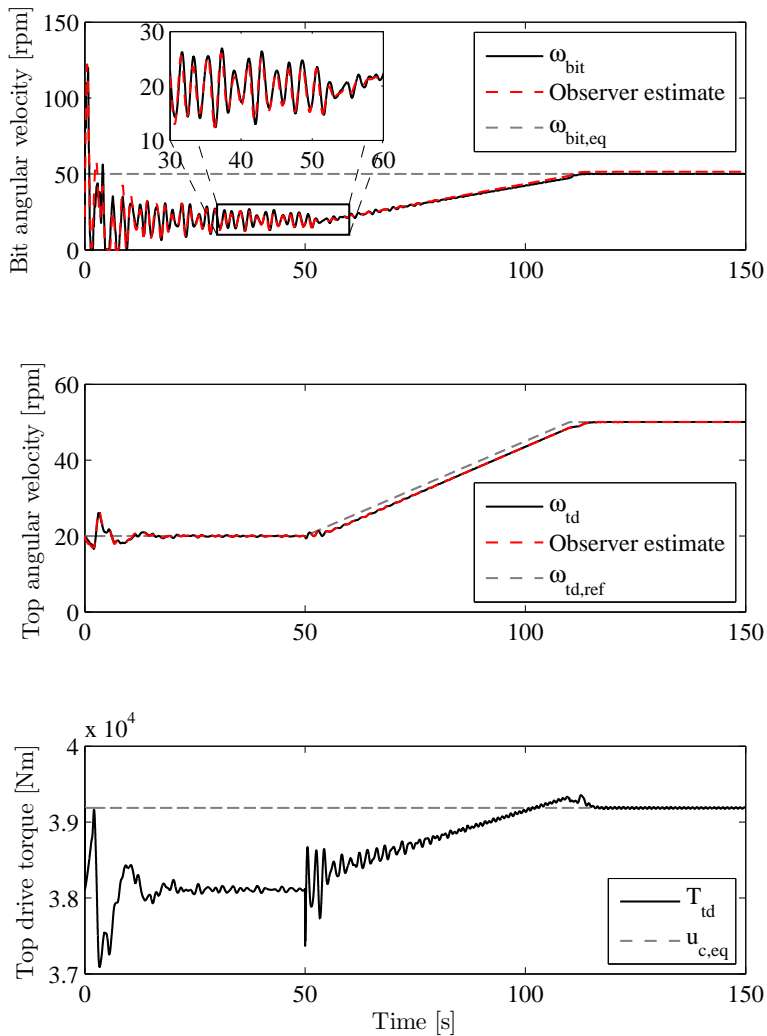


Figure 3.18: Simulation result of the closed-loop system and a drill-string model with increased length ( $15 \times 9$  m added drill pipe).

## 3.8 Discussion

In this work, a nonlinear observer-based output-feedback control strategy is proposed to eliminate torsional stick-slip vibrations in drilling systems. Particular benefits of the proposed approach with respect to existing controllers are, firstly, the fact that a realistic multi-modal model of the drill-string dynamics is taken into account, secondly, that severe velocity-weakening (and uncertainty) in the bit-rock interaction is taken into account, thirdly, that only surface measurements are employed. Additionally, a guarantee for (local) asymptotic stability of the closed-loop reduced-order system is given for bit-rock interaction laws lying within a certain sector (which is beneficial as the bit-rock interaction is subject to uncertainty in practice). To support controller synthesis, a reduced-order model is used, based on a high-fidelity finite-element model for the drill-string dynamics. The reduced-order model is constructed such that it captures the dominant dynamics (flexibility modes) of the original system. Simulation studies show that the controller design strategy successfully eliminates stick-slip oscillations when applied to a realistic drill-string model in representative drilling scenarios for which an industrial SoftTorque controller is unable to do so.

Robustness of the closed-loop drill-string system with respect to several practical aspects is investigated by means of simulation studies. These studies show that the closed-loop system with the proposed controller can effectively deal with sensor and actuator noise, is able to operate for different angular velocity setpoints and is robust with respect to changes in the bit-rock interaction and increasing length of the drill-string. Under all the imposed operating conditions the controller is able to stabilize the desired angular velocity and therefore stick-slip vibrations are eliminated. These results show that a significant increase in the operating envelope can be achieved by using the proposed controller design methodology compared to currently used industrial controllers.

# Design of a linear robust output-feedback controller

---

## 4.1 Introduction

Efficiency, reliability, and safety are important aspects in the drilling of deep wells for the exploration and production of oil, gas, mineral resources, and geothermal energy. Deep and curved borehole geometries need to be drilled to reach hydrocarbon reservoirs and extract these natural resources. Drill-strings of several kilometers in length are used to transmit the axial force and torque necessary to drill the rock formations. These drill-string systems are known to exhibit different types of self-excited vibrations, which decrease the drilling efficiency, accelerate bit wear, and may cause drill-string failure due to fatigue. The focus of this chapter is on the aspect of mitigation of torsional stick-slip vibrations by developing a design approach for robust linear output-feedback controllers.

Modelling of the torsional dynamics of the drill-string is an important step towards the control of torsional vibrations. Most controller designs presented in literature rely on one- or two degree-of-freedom (DOF) models for the torsional dynamics only, see e.g. [19, 51, 103, 115]. The resisting torque-on-bit (TOB) as a result of the interaction torques at the bit-rock interface is typically modelled as a frictional contact with a velocity-weakening effect, i.e., a decrease in the resisting torque for increasing velocity. Although experiments using single cutters to identify the bit-rock interaction law [22] do not reveal such a velocity-weakening effect, analysis of models that take the coupled axial and torsional dynamics into account show that such coupling effectively leads to a velocity-weakening

effect in the TOB [93]. This motivates a modelling-for-control approach involving the torsional dynamics only and incorporating a velocity-weakening bit-rock interaction law. In contrast to other studies (see e.g. [19, 40, 51, 53, 103]), however, we use a multi-modal model of the torsional dynamics as field observations have revealed that multiple torsional resonance modes play a role in the onset of stick-slip oscillations [82, 96]. In this work, a finite-element method (FEM) representation of the drill-string is used to model the drill-string dynamics. A different modelling approach is taken in [34, 37], where infinite-dimensional models, i.e. formulated in terms of partial differential equations, are considered. Using the same approach as a basis, models in terms of delay-differential equations are derived in [4, 9, 10, 99]. Recent results as presented in e.g. [10, 30] show that these representations of the drill-string can also be used for controller design. However, these methods require assumptions on the bit-rock interaction and/or trivialize the BHA as a single inertia. Discretizations of such infinite-dimensional models (see [62]) result in a lumped parameter model, based on a finite-element representation of the drill-string dynamics; this is the approach also taken in this chapter. Summarizing, in order to adopt a model-based controller design strategy, we use a FEM model of the drill-string dynamics involving the torsional dynamics only and with a velocity-weakening bit-rock interaction law.

Controllers for drilling systems aim at drill-string rotation at a constant angular velocity and the mitigation of torsional (stick-slip) vibrations. Moreover, the following control specifications are important. First, only surface measurements can be used for feedback, because down-hole measurements for real-time control purposes are not available in practice, due to limitations on the sampling rate, time delay of the measurements, and/or the high costs involved. Second, the controller should be able to cope with dynamics related to multiple torsional flexibility modes. Third, robustness with respect to uncertainty in the bit-rock interaction has to be guaranteed and, fourth, control performance specifications, related to e.g. measurement noise sensitivity and actuator constraints, need to be taken into account in the control design.

A well-known control method that uses both torque feedback and (top drive) velocity feedback to damp the first torsional mode, is the *Soft Torque Rotary system* [40]. The same objective is set in [51], which uses a PI-controller to damp the first resonance mode based on feedback of the top drive velocity only. Other control methods, including torsional rectification [115], observer-based output-feedback [19, 25, 122], feedback linearization [1], impedance matching [30], adaptive output-feedback for wave PDE [10], backstepping control [97], sliding mode control [81], model predictive control [52], weight-on-bit (WOB) control [12] and robust control [53, 103] have been developed and are documented in literature.

Although important steps have been made in the above works, an approach that satisfies all mentioned requirements has not yet been developed. A robust control approach, as proposed in [53, 103], is particularly suitable for this

problem since robustness with respect to uncertainty of the system dynamics and control performance specifications can be taken into account in the control design in addition to guaranteeing internal stability of the closed-loop system. For drill-string models focusing on torsional dynamics, the nonlinear bit-rock interaction model is often difficult to determine and is therefore considered as such an uncertain factor. In [103], an  $\mathcal{H}_\infty$  controller synthesis method is used to design a controller for a 2-DOF drill-string model. Moreover, it is assumed that the twist in the drill-string can be measured, i.e. knowledge about the angular position of the bit is assumed to be known. In [53], the  $\mu$ -synthesis technique through a DK-iteration procedure is used to obtain less conservative bounds on the uncertainty and obtain robustness with respect to the nonlinear bit-rock interaction. The used model is a similar 2-DOF model and also in this case down-hole measurements (to assess the twist of the drill-string) are used. As mentioned before, multiple torsional flexibility modes are important in the onset of stick-slip vibrations, whereas the 2-DOF models employed in [103] and [53], only take the first flexibility mode into account and rely on down-hole measurements. In this chapter, we propose a robust controller design technique on the basis of a finite-element method drill-string model which relies only on surface measurements.

The main contribution of this chapter is the design of a robust output-feedback controller methodology to eliminate stick-slip vibrations with the following advantages over existing controllers: 1) usage of surface measurements only, 2) application of the controller to multi-modal drill-string models while guaranteeing local stability of the desired setpoint, 3) optimization of the robustness with respect to uncertainty in the bit-rock interaction and, 4) integration of control performance specifications in the design approach. Preliminary results of this controller design strategy applied to a 4-DOF drill-string model have been presented in [120]. In this chapter, the controller methodology is applied to a 18-DOF finite-element method representation of a real drilling system. Additionally, the robustness of the closed-loop system is investigated in model-based case studies. The following robustness aspects are key in the scope of practical applications, and are extensively studied in this chapter: robustness with respect to changes in the bit-rock interaction characteristic, increasing length of the drill-string, different desired angular velocities (i.e. increased operating envelope), and sensor and actuator noise. Furthermore, a comparison between the proposed controller design strategy and the observer-based output-feedback controller design strategy presented in Chapter 3 will be made.

This chapter is organized as follows. In Section 4.2, the drill-string model based on a finite-element model of a real-life drilling rig is introduced. Subsequently, in Section 4.3 the control problem is formulated. Next, in Section 4.4 the design of an output-feedback controller based on skewed- $\mu$  DK-iteration is proposed and the controller synthesis by weighting filter design is treated in Section 4.5. In Section 4.6, simulation results illustrating the effectiveness of

the proposed approach are presented and compared with the results obtained using an industrial controller (SoftTorque [51]). Moreover, a comparison with the observer-based output-feedback controller design methodology developed in Chapter 3 is made. Next, in Section 4.7 the robustness of the controller is investigated by means of several simulation studies involving realistic drilling scenarios, for example increasing length of the drill-string and disturbances due to sensor and actuator noise. Finally, the results are summarized in Section 4.8.

## 4.2 Drill-string dynamics model

A finite-element method (FEM) model of a realistic drilling system is used as basis for controller design in this chapter. The model is based on an offshore jack-up drilling rig to reach reservoir sections at depths of >6000 m. The rig is equipped with an AC top drive and fitted with a modern SoftTorque system [64]. When drilling those deep wells, stick-slip vibrations have been observed in the field for this drilling system, as shown in Figure 2.2 [39]. This motivates the use of this drill-string model as basis for the development of a novel controller design methodology.

The finite-element method is used to construct a multi-modal torsional drill-string model (with 18 elements). The element at the top is a rotational inertia to model the top drive inertia, the subsequent elements are equivalent pipe sections based on the dimensions and material properties of the drill-string. The resulting model can be written as

$$M\ddot{\theta} + D\dot{\theta} + K_t\theta_d = S_w T_w(\dot{\theta}) + S_b T_{bit}(\dot{\theta}_1) + S_t T_{td} \quad (4.1)$$

with the coordinates  $\theta \in \mathbb{R}^m$  with  $m = 18$ , the top drive motor torque input  $T_{td} \in \mathbb{R}$  being the control input, the bit-rock interaction torque  $T_{bit} \in \mathbb{R}$  and the interaction torques  $T_w \in \mathbb{R}^{m-1}$  between the borehole and the drill-string acting on the nodes of the FEM model. The coordinates  $\theta$  represent the angular displacements of the nodes of the finite-element representation. Next, we define the difference in angular position between adjacent nodes as follows;  $\theta_d := [\theta_1 - \theta_2 \ \theta_2 - \theta_3 \ \cdots \ \theta_{17} - \theta_{18}]^\top$ . In (4.1), the mass, damping and “stiffness” matrices are, respectively, given by  $M \in \mathbb{R}^{m \times m}$ ,  $D \in \mathbb{R}^{m \times m}$  and  $K_t \in \mathbb{R}^{m \times m-1}$ , the matrices  $S_w \in \mathbb{R}^{m \times m-1}$ ,  $S_b \in \mathbb{R}^{m \times 1}$  and  $S_t \in \mathbb{R}^{m \times 1}$  represent the generalized force directions of the interaction torques, the bit torque and the input torque, respectively. The coordinates  $\theta$  are chosen such that the first element ( $\theta_1$ ) describes the rotation of the bit and the last element ( $\theta_{18}$ ) the rotation of the top drive at surface. The interaction between the borehole and the drill-string is modelled as Coulomb friction, that is

$$T_{w,i} \in T_i \text{Sign}(\dot{\theta}_i), \quad \text{for } i = 2, \dots, 18, \quad (4.2)$$

with  $T_i$  representing the amount of friction at each element and the set-valued sign function defined as

$$\text{Sign}(y) \triangleq \begin{cases} -1, & y < 0 \\ [-1, 1], & y = 0 \\ 1, & y > 0. \end{cases} \quad (4.3)$$

The bit-rock interaction model, including the velocity-weakening effect, is given by

$$T_{bit}(\dot{\theta}_1) \in \text{Sign}(\dot{\theta}_1) \left( T_d + (T_s - T_d) e^{-v_d |\dot{\theta}_1|} \right) \quad (4.4)$$

with  $T_s$  the static torque,  $T_d$  the dynamic torque and  $v_d := \frac{30}{N_d \pi}$  indicating the decrease from static to dynamic torque. For this model, the parameters are tuned such that a match between the simulation results and the (surface) field data is obtained. The parameter values are given by  $T_s = 7700$  Nm,  $T_d = 1700$  Nm,  $N_d = 5$  rpm, the resulting bit-rock interaction model is shown Figure 3.1. The drill-string-borehole interaction torques  $T_{w,i}(\theta_i)$ ,  $i = 2, \dots, 18$  are defined by  $\phi(q_2) := [T_{w,2}(\dot{\theta}_2) \cdots T_{w,18}(\dot{\theta}_{18})]^\top$  with  $q_2 := [\dot{\theta}_2 \cdots \dot{\theta}_{18}]^\top$  and the interaction torque at the bit-rock interface is written as  $\varphi(q) := T_{bit}(\dot{\theta}_1)$ . The resulting equations of motion are written in first-order state-space form:

$$\begin{aligned} \dot{x} &= Ax + Gv + G_2 v_2 + Bu_t \\ q &= Hx \\ q_2 &= H_2 x \\ y &= Cx \\ v &\in -\varphi(q) \\ v_2 &\in -\phi(q_2). \end{aligned} \quad (4.5)$$

Herein,  $x := [\theta_d \ \dot{\theta}]^\top \in \mathbb{R}^{35}$  is the state, note that only relative positions are taken into account, such that the 18-DOF system is described with only 35 state variables. Moreover,  $u_t := T_{td} \in \mathbb{R}$  is the control input and,  $y := [\omega_{td} \ T_{pipe}]^\top \in \mathbb{R}^2$  is the measured output. The top drive velocity and bit velocity are defined as  $\omega_{td} := \dot{\theta}_{18}$  and  $\omega_{bit} := \dot{\theta}_1$ , respectively. The available measurements are the top drive velocity  $\omega_{td}$  and the pipe torque  $T_{pipe}$ , which is defined as the torque in the drill-string directly below the top drive (sometimes also referred to as saver sub torque).

One of the relevant frequency response functions of the linear part of the dynamics (4.5) is shown in Figure 4.1. This frequency response function is called the bit-mobility, as it describes the transfer from bit torque to bit velocity. The bit-mobility gives an indication of the dominant resonance modes in the onset of stick-slip vibrations. Namely, it is the input-output dynamics represented by the bit-mobility which, in ‘closed-loop’ with the nonlinear bit-rock interaction law, that is responsible for the presence (or not) of torsional instabilities and stick-slip vibrations. Therefore, damping of the resonance modes in the bit-mobility plays an important role in the controller design methodology in Section 4.4.



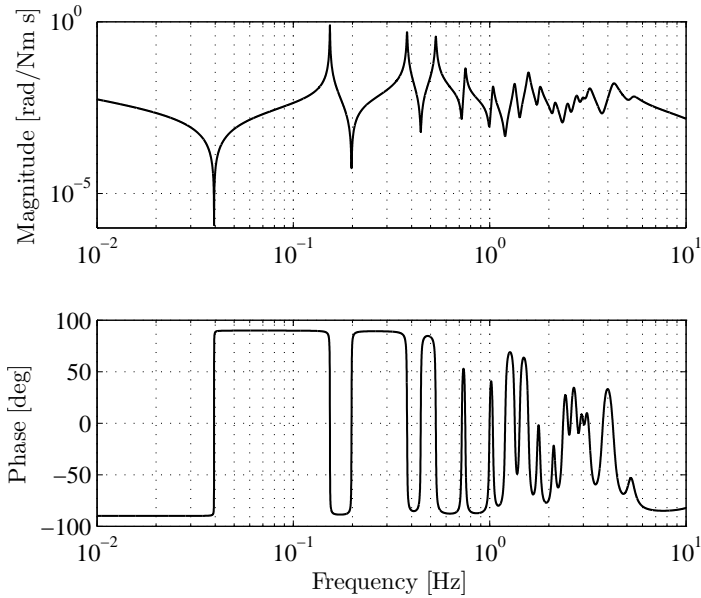


Figure 4.1: Frequency response function of the 18-DOF model from bit torque  $T_{bit}$  to bit velocity  $\omega_{bit}$ , i.e. bit-mobility.

### 4.3 Control problem formulation

In Section 4.3.1, we formulate the control problem and specify the controller objectives. Additionally, in Section 4.3.2 we apply a loop transformation to the model in (4.5) to render it amenable for controller design in Section 4.4.

#### 4.3.1 Controller objectives

The desired operation of the drill-string system is a constant angular velocity  $\omega_{eq}$  for the entire drill-string. So, the objective is to regulate the nonlinear drill-string system to this setpoint by means of an output-feedback controller. The available measurements for the controller are the top drive angular velocity  $\omega_{td}$  and the pipe torque  $T_{pipe}$ , which implies that only surface measurements are employed. The system can be controlled by the top drive torque  $T_{td}$ . As briefly mentioned in the introduction, the controller should

1. locally stabilize the constant rotational velocity  $\omega_{eq}$  of the drill-string, therewith eliminating torsional (stick-slip) vibrations;
2. ensure robustness with respect to uncertainty in the nonlinear bit-rock interaction  $\varphi$ ;

3. guarantee the satisfaction of closed-loop performance specifications, in particular on measurement noise sensitivity, i.e., limitation of the amplification of measurement noise, and limitation of the control action such that top drive limitations can be satisfied;
4. guarantee robust stability and performance in the presence of multiple flexibility modes dominating the torsional dynamics.

### 4.3.2 Model reformulation

To facilitate controller synthesis, the drill-string dynamics (4.5) are rewritten in a specific form. The desired constant angular velocity  $\omega_{eq}$  can be associated with a desired equilibrium  $x_{eq}$  for the state of the system. To ensure that  $x_{eq}$  is indeed an equilibrium of the closed-loop system, the control input  $u_t = u_c + \tilde{u}$  is decomposed in a constant feedforward torque  $u_c$  (inducing  $x_{eq}$ ) and the feedback control input  $\tilde{u}$ . For the purpose of feedforward design, we assume that  $\omega_i > 0$ , for  $i = 2, \dots, 18$ ; then it follows from (4.2) that the resistive torques along the drill-string ( $\phi_i$ ) are constant. Hence  $\phi$  is constant and can be compensated for by  $u_c$ . The (constant) equilibrium  $x_{eq}$  and feedforward torque  $u_c$  can be obtained from the equilibrium equation of system (4.5):

$$Ax_{eq} - G\varphi(Hx_{eq}) - G_2\phi(H_2x_{eq}) + Bu_c \ni 0 \quad (4.6)$$

Next, let  $\xi := x - x_{eq}$ . Moreover, we apply a linear loop transformation such that the slope of a transformed nonlinearity  $\tilde{\varphi}(q)$  (associated to  $\varphi(q)$  through the loop transformation) is equal to zero at the desired equilibrium velocity, i.e.  $\left. \frac{\partial \tilde{\varphi}}{\partial q} \right|_{q=\omega_{eq}} = 0$ . This results in the following state-space representation of the transformed drill-string dynamics in perturbation coordinates:

$$\dot{\xi} = A_t \xi + B\tilde{u} + G\tilde{v} \quad (4.7a)$$

$$\tilde{q} = H\xi \quad (4.7b)$$

$$\tilde{y} = C\xi \quad (4.7c)$$

$$\tilde{v} \in -\tilde{\varphi}(\tilde{q}) \quad (4.7d)$$

with  $A_t := A + \delta GH$ ,  $\delta = -\left. \frac{\partial \varphi}{\partial q} \right|_{q=\omega_{eq}} > 0$ ,  $\tilde{y} := y - Cx_{eq}$ ,  $\tilde{q} := q - Hx_{eq}$ ,  $\tilde{\varphi}(\tilde{q}) := \varphi(\tilde{q} + Hx_{eq}) - \varphi(Hx_{eq}) + \delta\tilde{q}$  and  $\tilde{v} := v - v_{eq} - \delta\tilde{q}$ . The dynamics in (4.7) represents a Lur'e-type system, see Figure 4.2(a), with the linear dynamics  $G_{ol}$  ((4.7a) - (4.7c)), having inputs  $\tilde{u}$  and  $\tilde{v}$  and outputs  $\tilde{y}$  and  $\tilde{q}$ , and the nonlinearity  $\tilde{\varphi}$  in the feedback loop. The open-loop transfer function  $G_{ol}(s)$  is defined as

$$\begin{bmatrix} \tilde{q}(s) \\ \tilde{y}(s) \end{bmatrix} := G_{ol}(s) \begin{bmatrix} \tilde{v}(s) \\ \tilde{u}(s) \end{bmatrix} = \begin{bmatrix} g_{11}(s) & g_{12}(s) \\ g_{21}(s) & g_{22}(s) \end{bmatrix} \begin{bmatrix} \tilde{v}(s) \\ \tilde{u}(s) \end{bmatrix}. \quad (4.8)$$

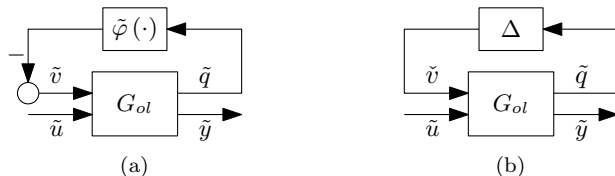


Figure 4.2: Block diagram of the system dynamics (4.7) in Lur'e type form (a) and the linear dynamics  $G_{ol}$  with (complex) model uncertainty  $\Delta$  (b).

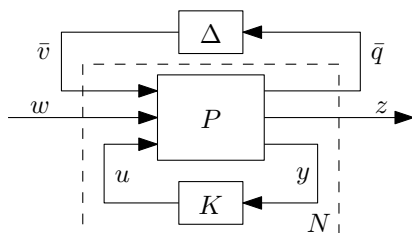


Figure 4.3: General control configuration with uncertainty block  $\Delta$ .

As a next step, we model the nonlinearity  $\tilde{\varphi}$  (Figure 4.2(a)) by an uncertainty  $\Delta$  (Figure 4.2(b)). This model formulation is used in the controller design approach developed in Section 4.4. Note that  $\tilde{\varphi}$  describes a nonlinear mapping from  $\tilde{q}$  to  $\tilde{v}$ , while the uncertainty  $\Delta$  is assumed to be a (complex) LTI uncertainty (with output  $\tilde{v}$ ). This means that, for example, stability of the closed-loop system with uncertainty  $\Delta$  does not directly imply stability for the closed-loop system with nonlinearity  $\tilde{\varphi}$ . Nevertheless, the model in Figure 4.2(b) is used as a basis for controller synthesis in the next section. Subsequently, the stability of the nonlinear closed-loop system is analyzed in detail in Section 4.4.4.

## 4.4 Controller design methodology

In this section, we present a robust control design approach based on skewed- $\mu$  DK-iteration. This technique combines several concepts from robust control theory to design a linear controller that achieves robust stability and performance of a system with model uncertainties [106].

Robust control methods focus on the design of controllers while system uncertainties are explicitly taken into account in the design. The general control configuration for a (LTI) plant  $P$  with an uncertainty  $\Delta$  and (LTI) controller  $K$  is shown in Figure 4.3, where  $y$  is the measured output,  $u$  the control output and  $w$  and  $z$  represent the exogenous inputs and outputs. This structure is similar

to the block diagram in Figure 4.2(b) with in addition the controller  $K$  and the performance inputs and outputs  $w$  and  $z$ , respectively. The system  $P$ , in Figure 4.3, can be described by

$$\begin{bmatrix} \bar{q} \\ z \\ y \end{bmatrix} = \begin{bmatrix} P_{11} & P_{12} & P_{13} \\ P_{21} & P_{22} & P_{23} \\ P_{31} & P_{32} & P_{33} \end{bmatrix} \begin{bmatrix} \bar{v} \\ w \\ u \end{bmatrix}. \quad (4.9)$$

The system  $N$  is defined as the lower linear fractional transformation (LFT) of the plant  $P$  with the controller  $K$ , that is

$$N := F_l(P, K) = \begin{bmatrix} P_{11} & P_{12} \\ P_{21} & P_{22} \end{bmatrix} + \begin{bmatrix} P_{13} \\ P_{23} \end{bmatrix} K (I - P_{33}K)^{-1} \begin{bmatrix} P_{31} & P_{32} \end{bmatrix}.$$

With the introduction of the controller  $K$  we can also introduce the closed-loop bit-mobility function. The closed-loop bit-mobility transfer function  $G_{cl}$  from input the  $\bar{v}$  to the output  $\bar{q}$ , of system (4.7) with controller  $K$ , is defined by

$$G_{cl} := g_{11} - g_{12}K(I + g_{22}K)^{-1}g_{21}. \quad (4.10)$$

As mentioned in Section 4.2 this bit-mobility plays an important role in the stability of the closed-loop system (see Section 4.4.4) and is therefore important in the controller design methodology.

#### 4.4.1 Nominal stability and performance

As mentioned in Section 4.3.1, the controller design aims at stability, performance, and robustness for the uncertainty  $\Delta$ . In this section, the focus is on the first two aspects. Robustness is considered in the next section. Hereto, consider the system without uncertainty given by

$$\begin{bmatrix} z \\ y \end{bmatrix} := P_{sub} \begin{bmatrix} w \\ u \end{bmatrix} = \begin{bmatrix} P_{22} & P_{23} \\ P_{32} & P_{33} \end{bmatrix} \begin{bmatrix} w \\ u \end{bmatrix} \quad (4.11)$$

and the lower LFT of  $P_{sub}$  with the controller  $K$ , that is,  $N_{22} := F_l(P_{sub}, K)$ .

Based on the system representation in Figure 4.2(b), the closed-loop system of the linear drill-string dynamics  $G_{ol}$  in feedback with the linear, dynamic controller  $K$  to be designed is shown in Figure 4.4. In this representation, additional inputs  $n$  and  $d$  are introduced, representing measurement noise and actuator noise, respectively. Define the unweighted inputs  $\underline{w} := [n \ d]^\top$  and unweighted outputs  $\underline{z} := [e \ u]^\top$  such that the closed-loop transfer functions between  $\underline{w}$  and  $\underline{z}$  equal the relevant sensitivity functions, as follows:

$$\begin{bmatrix} e \\ u \end{bmatrix} = - \begin{bmatrix} (I + g_{22}K)^{-1} & (I + g_{22}K)^{-1}g_{22} \\ K(I + g_{22}K)^{-1} & K(I + g_{22}K)^{-1}g_{22} \end{bmatrix} \begin{bmatrix} n \\ d \end{bmatrix}, \quad (4.12)$$

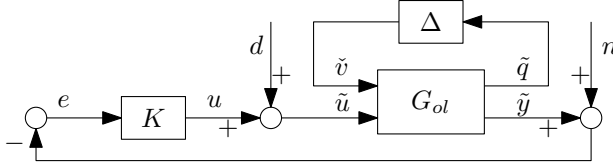


Figure 4.4: Linear drill-string dynamics  $G_{ol}$  in closed-loop with the controller  $K$  and including model uncertainty  $\Delta$ .

where  $g_{22}$  is the open-loop transfer function of the linear drill-string dynamics  $G_{ol}$ , from input  $\tilde{u}$  to output  $\tilde{y}$  as defined in (4.8). Performance specifications can now be introduced by the design of weighting functions for these sensitivity functions. For example, consider the sensitivity function  $S = (I + GK)^{-1}$  (for a SISO plant and controller,  $G$  and  $K$ , respectively) and the upper bound  $1/|w_P(s)|$  on this sensitivity function, where  $w_P(s)$  is the weighting filter to be specified. Then

$$|S(j\omega)| < 1/|w_P(j\omega)|, \forall \omega \Leftrightarrow |w_P(j\omega)S(j\omega)| < 1, \forall \omega.$$

In a general setting, the latter fact implies that the bound on the sensitivity can be written as a norm-bound on the product of the weighting filter and sensitivity function, i.e.  $\|w_P S\|_\infty < 1$ , where we used the definition of the  $\mathcal{H}_\infty$ -norm

$$\|H(s)\|_\infty := \sup_{\omega \in \mathbb{R}} \bar{\sigma}(H(j\omega)). \quad (4.13)$$

This is a key element in the design of a controller that guarantees nominal performance.

The concept nominal performance is defined as follows: for a system without uncertainty  $\Delta$  the closed-loop system  $N_{22} = F_l(P_{sub}, K)$  is internally stable and the  $\mathcal{H}_\infty$ -norm of this system (from  $w$  to  $z$ ) is smaller than 1, that is

$$\|N_{22}\|_\infty = \sup_{\omega} \bar{\sigma}(F_l(P_{sub}, K)) < 1. \quad (4.14)$$

This means that nominal performance can be achieved by solving the “standard”  $\mathcal{H}_\infty$  optimal control problem, where the aim is to find the internally stabilizing controller  $K$  which minimizes  $\|F_l(P_{sub}, K)\|_\infty$ . Internal stability of the closed-loop can be guaranteed by a proper choice of the inputs  $w$  and outputs  $z$ . As proved in [130, Section 5.3], by choosing  $w$  and  $z$  as the weighted version of  $\underline{w}$  and  $\underline{z}$ , the  $\mathcal{H}_\infty$  controller synthesis guarantees internal stability of the closed-loop system. Specification of the weighting filters is treated in more detail in the Section 4.4.2. Moreover, the system *with* uncertainty is addressed in the next section, leading to the concept of robust performance.

Summarizing, using the  $\mathcal{H}_\infty$  controller synthesis procedure we are able to design an internally stabilizing controller  $K$  which minimizes  $\|F_l(P, K)\|_\infty$ , hence

we achieve nominal performance for a system without uncertainty. However, we would like to mention that we are interested in a stabilizing controller for the system with uncertainty, therefore, the robust performance problem is discussed in the next section.

#### 4.4.2 Alternative robust performance

Robust performance means that the performance objective, addressed in Section 4.4.1, is achieved for all possible models in the uncertainty set [106]. In other words, in addition to internal stability and satisfying performance specifications for a nominal plant (as treated in Section 4.4.1), it is required that the closed-loop system is robust with respect to the uncertainty  $\Delta$ .

**Remark 4.1.** *Standard robust performance techniques aim at optimizing the performance for all possible plants in the uncertainty set. In contrast, we aim to optimize the robustness with respect to the uncertainty while still guaranteeing internal stability and satisfaction of given performance objectives. This is what we call ‘alternative robust performance’.*

Consider the system  $P$  in Figure 4.3, including the uncertainty block  $\Delta$ . The input-output pair  $\bar{v}$ ,  $\bar{q}$  is related to this uncertainty block and the (weighted) closed-loop transfer function  $N(s) = F_l(P, K)$  is given by

$$\begin{bmatrix} \bar{q} \\ w \end{bmatrix} = N \begin{bmatrix} \bar{v} \\ z \end{bmatrix} = F_l(P, K) \begin{bmatrix} \bar{v} \\ z \end{bmatrix}. \quad (4.15)$$

Robust stability is obtained by designing a controller  $K$  such that the system  $N$  is internally stable and the upper LFT,  $F := F_u(N, \Delta)$ , is stable for all  $\Delta \in \mathbf{\Delta}$ . Herein, the uncertainty set is a norm-bounded subset of  $\mathcal{H}_\infty$ , i.e.,  $\mathbf{\Delta} = \{\Delta \in \mathcal{RH}_\infty \mid \|\Delta\|_\infty < 1\}$ .  $\mathcal{H}_\infty$  is a (closed) Banach space of matrix-valued functions that are bounded on the imaginary axis. The real rational subspace of  $\mathcal{H}_\infty$  is denoted by  $\mathcal{RH}_\infty$  which consists of all proper and real rational stable transfer matrices [130, Section 4.3]. The aim is to find a stabilizing controller that also meets certain performance specifications. Therefore, we use a similar approach as in [106, Section 8.10] and consider the fictitious ‘uncertainty’  $\Delta_P$ . The uncertainty  $\Delta_P$  is a complex unstructured uncertainty block which represents the  $\mathcal{H}_\infty$  performance specifications, as explained for the weighted sensitivity function in Section 4.4.1. Moreover, note that  $\Delta_P \in \mathbf{\Delta}_P$ , with  $\mathbf{\Delta}_P = \{\Delta_P \in \mathcal{RH}_\infty \mid \|\Delta_P\|_\infty < 1\}$ . The result given in [130, Theorem 11.8] states that a robust performance problem is equivalent to a robust stability problem with the augmented uncertainty

$$\hat{\Delta} = \begin{bmatrix} \Delta & 0 \\ 0 & \Delta_P \end{bmatrix} \quad (4.16)$$

with  $\hat{\Delta}$  a block-diagonal matrix. In other words, both the performance specifications and uncertainty are taken into account in a similar fashion. Moreover  $\hat{\Delta}$  is the uncertainty set with the structure as given in (4.16) and any  $\Delta \in \mathbf{\Delta}$  and  $\Delta_P \in \mathbf{\Delta}_P$ . The robust performance condition can now be formulated as follows:

$$\mu_{\hat{\Delta}}(N(j\omega)) < 1, \quad \forall \omega, \quad (4.17)$$

where  $\mu_{\hat{\Delta}}$  is the structured singular value with respect to  $\hat{\Delta}$ . The structured singular value is defined as the real non-negative function

$$\mu_{\hat{\Delta}}(N) = \frac{1}{\bar{k}_m}, \quad \bar{k}_m = \min \left\{ k_m \mid \det \left( I - k_m N \hat{\Delta} \right) = 0 \right\} \quad (4.18)$$

with complex matrix  $N$  and block-diagonal uncertainty  $\hat{\Delta}$ .

To optimize the robustness with respect to the uncertainty  $\Delta$  (i.e. part of  $\hat{\Delta}$  in (4.16)), the skewed structured singular value  $\mu^s$  can be used. The skewed structured singular value is used if some uncertainty blocks in  $\hat{\Delta}$  are kept fixed ( $\Delta_P$  in this case) to investigate how large another source of uncertainty ( $\Delta$  in this case) can be before robust stability/performance cannot be guaranteed anymore. In this case, we aim to optimize the robustness of the closed-loop system with respect to uncertainty  $\Delta$  in the bit-rock interaction. Thus we aim to obtain the largest possible uncertainty set  $\Delta$ , given a fixed  $\Delta_P$  (i.e. fixed performance specifications). Hereto, we introduce the matrix  $K_m^s := \text{diag}(k_m^s, I)$  and the skewed structured singular value  $\mu_{\hat{\Delta}}^s(N)$  can then be defined as

$$\mu_{\hat{\Delta}}^s(N) = \frac{1}{\bar{k}_m^s}, \quad \bar{k}_m^s = \min \left\{ k_m^s \mid \det \left( I - K_m^s N \hat{\Delta} \right) = 0 \right\}. \quad (4.19)$$

Thus, the robust performance condition (4.17), with additional scaling (through  $K_m^s$ ) in terms of the skewed structured singular value, can be written as

$$\mu_{\hat{\Delta}}^s(N(j\omega)) < 1, \quad \forall \omega. \quad (4.20)$$

To support controller design satisfying particular performance specifications, weighting filters and scaling matrices are introduced in the loop in Figure 4.4, as shown in Figure 4.5. Those frequency-domain weighting filters allow us to specify the (inverse) maximum allowed magnitudes of the closed-loop transfer functions in (4.12). Moreover, the scaling matrices are introduced to improve the numerical conditioning of the problem and to tune the desired bandwidth. The (weighted) generalized plant  $P$  with input weighting filters  $V_i(s)$  and output weighting filters  $W_i(s)$ , with  $i \in \{1, 2, 3\}$ , and scaling matrices  $W_{sc}$  and  $V_{sc}$ , is specified by

$$\begin{bmatrix} \bar{q} \\ \bar{e} \\ \bar{u} \\ e \end{bmatrix} = \underbrace{\begin{bmatrix} W_1 & 0 & 0 & 0 \\ 0 & W_2 W_{sc} & 0 & 0 \\ 0 & 0 & W_3 & 0 \\ 0 & 0 & 0 & I_2 \end{bmatrix} P \begin{bmatrix} V_1 & 0 & 0 & 0 \\ 0 & V_{sc} V_2 & 0 & 0 \\ 0 & 0 & V_3 & 0 \\ 0 & 0 & 0 & 1 \end{bmatrix}}_P \begin{bmatrix} \bar{v} \\ \bar{n} \\ \bar{d} \\ u \end{bmatrix}$$

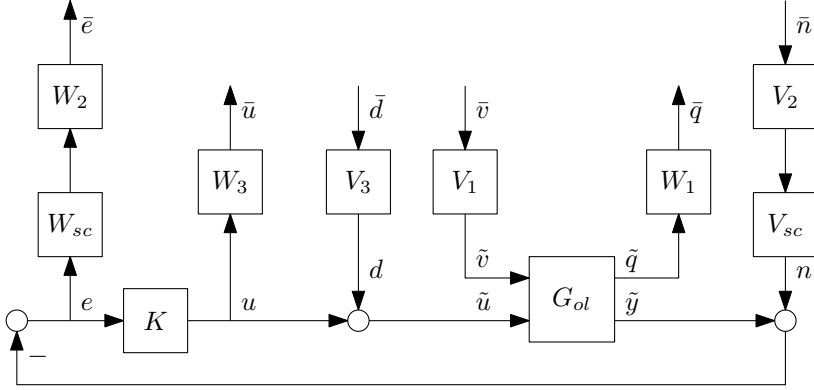


Figure 4.5: Closed-loop system with weighting filters and scaling matrices.

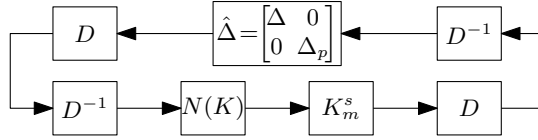


Figure 4.6: Block diagram of the implementation for the skewed- $\mu$  DK-iteration procedure.

Herein,  $\underline{P}(s)$  is the MIMO transfer function of the unweighted system  $\underline{P}$  with inputs  $[\tilde{v} \ n \ d \ u]^\top$  and outputs  $[\tilde{q} \ e \ u \ e]^\top$  with its state-space realization given by

$$\underline{P} \stackrel{s}{=} \left[ \begin{array}{c|cccc} A_t & G & 0 & B & B \\ \hline H & 0 & 0 & 0 & 0 \\ -C & 0 & -I & 0 & 0 \\ 0 & 0 & 0 & 0 & I \\ -C & 0 & -I & 0 & 0 \end{array} \right]. \quad (4.21)$$

In this section, we have introduced an alternative robust performance framework. To design a controller that minimizes the skewed structured singular value  $\mu_{\hat{\Delta}}^s$ , for the purpose of obtaining robust performance, a procedure to synthesize such controller, known as the DK-iteration procedure, is treated in Section 4.4.3.

### 4.4.3 Skewed- $\mu$ DK-iteration

This section focuses on the synthesis of a controller that minimizes a skewed structured singular value  $\mu_{\hat{\Delta}}^s$  to obtain closed-loop robust performance. The so-called skewed- $\mu$  DK-iteration procedure is used to synthesize a controller.

The first step in such DK-iteration procedure is the introduction of  $D$ -scaling



matrices. This scaling uses the fact that  $\hat{\Delta}$  is structured and is such that stability is not affected. Hence, the inputs and outputs to  $\hat{\Delta}$  and  $N$  are scaled by inserting the matrices  $D$  and  $D^{-1}$  on both sides as shown in Figure 4.6. Clearly, this has no effect on stability. Using such scaling, generally enables to find potentially tighter robust stability/performance conditions. Therefore, we define a block-diagonal scaling matrix  $D := \text{diag}(d_1, d_2 I)$  with scalars  $d_i$ ,  $i = 1, 2$ . Note that with the chosen form of  $D$ , it holds that  $\Delta = d_1 \Delta d_1^{-1}$  and  $\Delta_P = d_2 I \Delta_P d_2^{-1} I$ ; that is, we have  $\hat{\Delta} = D \hat{\Delta} D^{-1}$ . Moreover,  $N(s)$  is stable by design of the controller  $K$  and we assume that  $\hat{\Delta}(s)$  is also stable. Then, an upper bound for the skewed structured singular value can be obtained as follows:

$$\mu_{\Delta}^s(N(j\omega)) \leq \min_{D(\omega) \in \mathcal{D}} \bar{\sigma}(D(\omega) K_m^s N(j\omega) D(\omega)^{-1}), \quad (4.22)$$

where  $\mathcal{D}$  is the set of (frequency-dependent) block-diagonal matrices  $D(\omega)$  whose structure is compatible to that of  $\hat{\Delta}$ , i.e.  $\hat{\Delta} D = D \hat{\Delta}$  (see [106] for more details). Using the upper bound in (4.22), the robust performance condition (4.20), can be replaced by the (potentially) stricter condition

$$\min_{D(\omega) \in \mathcal{D}} \bar{\sigma}(D(\omega) K_m^s N(j\omega) D(\omega)^{-1}) < 1, \quad \forall \omega. \quad (4.23)$$

This condition is the basis for the skewed- $\mu$  DK-iteration procedure.

The skewed- $\mu$  DK-iteration procedure aims at designing a controller that minimizes the peak value over frequency of the upper bound on the skewed structured singular value, i.e. a controller  $K$  should be designed by solving the following optimization problem:

$$\min_K \left( \min_D \|DK_m^s N(K) D^{-1}\|_{\infty} \right). \quad (4.24)$$

Here, the original scaling matrix  $D(\omega)$  is replaced by a stable minimum-phase transfer function fit  $D(s)$  of  $D(\omega)$ . The dependency of the closed-loop transfer function  $N$  on the controller  $K$  is indicated by  $N(K)$ . In DK-iterations, a  $\mu$ -analysis ( $D$ -step) and  $\mathcal{H}_{\infty}$ -optimization ( $K$ -step) are solved alternately (see [84]). In other words, the skewed- $\mu$  DK-iteration procedure alternates between minimizing (4.24) with respect to either  $K$  or  $D$  (while holding the other fixed) and recursively updating  $k_m^s$  during the  $D$ -step. This procedure can be summarized as follows:

1.  $K$ -step: Synthesize an  $\mathcal{H}_{\infty}$ -controller  $K(s)$  for the scaled problem  $\min_K \|DK_m^s N(K) D^{-1}\|_{\infty}$  with fixed  $D(s)$  and  $k_m^s$ .
2.  $D$ -step: Find  $D(\omega)$  to optimize at each frequency  $\min_{D(\omega) \in \mathcal{D}} \bar{\sigma}(D(\omega) K_m^s N(K) D(\omega)^{-1})$ , for fixed  $K(s)$  and  $k_m^s$ . Moreover, if  $\|DK_m^s N(K) D^{-1}\|_{\infty} \neq 1$ , update  $k_m^s$  recursively using  $k_m^s = \frac{1}{\|DK_m^s N(K) D^{-1}\|_{\infty}} \tilde{k}_m^s$  with  $\tilde{k}_m^s$  the previous value of  $k_m^s$ . Continue this iterative procedure until  $\|DK_m^s N(K) D^{-1}\|_{\infty} = 1$ .

3. Fit the magnitude of each element of  $D(\omega)$  to a stable, minimum-phase transfer function  $D(s)$  and go back to step 1.

A fundamental problem with the DK-iteration procedure is the fact that it may converge to a local optimum. This is a result of the fact that although each of the minimization steps are convex, the overall optimization problem is not. However, as is also claimed in [106, Section 8.12.1], the algorithm performs well in practice.

#### 4.4.4 Closed-loop stability analysis

The main purpose of the controller is to stabilize the equilibrium  $\xi = 0$  of the nonlinear system (4.7). Let us assume a controller  $K$  has been designed that meets the performance specifications and is robust with respect to the uncertainty  $\Delta$ . Hence, the designed controller guarantees stability for the *linear* closed-loop system  $N(s)$  and achieves robustness with respect to the specified uncertainty  $\Delta$ . In this section, the stability of the *nonlinear* closed-loop system is investigated. Hereto, we define a symmetric sector condition on the nonlinearity  $\tilde{\varphi}$ , such that for any (locally Lipschitz) nonlinearity within this sector asymptotic stability of the origin of the closed-loop system can be guaranteed.

We use the circle criterion [54, Theorem 7.1] to determine a (symmetric) sector on the nonlinearity  $\tilde{\varphi}$  for which robust stability can be guaranteed. Consider the closed-loop bit-mobility (4.10). Moreover, consider a symmetric sector condition on the nonlinearity, i.e.  $\tilde{\varphi} \in [-\gamma, \gamma]$  for  $\gamma > 0$ . According to the circle criterion, the nonlinear system is absolutely stable (i.e.  $\xi = 0$  is asymptotically stable for any  $\tilde{\varphi} \in [-\gamma, \gamma]$ ) if

$$H(s) = (1 + \gamma G_{cl}(s))(1 - \gamma G_{cl}(s))^{-1}, \quad (4.25)$$

is strictly positive real. Applying Lemma 6.1 in [54], a scalar transfer function  $H(s)$  is strictly positive real if the following conditions are satisfied:

1.  $H(s)$  is Hurwitz;
2.  $\operatorname{Re} [H(j\omega)] = \operatorname{Re} \left[ \frac{1 + \gamma G_{cl}(j\omega)}{1 - \gamma G_{cl}(j\omega)} \right] > 0, \quad \forall \omega \in \mathbb{R};$
3.  $H(\infty) > 0$ .

For the symmetric sector, the condition on  $H(s)$  being Hurwitz is equivalent to  $G_{cl}(s)$  being Hurwitz. The closed-loop transfer function  $G_{cl}(s)$  of the feedback interconnection is Hurwitz by the design of the stabilizing controller  $K$ . Moreover,  $G_{cl}$  is strictly proper, therefore  $H(\infty) = 1$ , such that the third condition is satisfied. The second condition is equivalent to the condition:

$$\|G_{cl}(j\omega)\|_{\infty} < \frac{1}{\gamma}. \quad (4.26)$$

Hence, the  $\mathcal{H}_\infty$ -norm of the closed-loop bit-mobility  $G_{cl}$  gives an upper bound on the sector that the nonlinearity  $\tilde{\varphi}$  should comply with, for the system to be absolutely stable. With the DK-iteration procedure, presented in Section 4.4.3, a controller  $K$  can be designed such that  $\|G_{cl}\|_\infty$  is minimized. In other words, the robustness with respect to uncertainty in the bit-rock interaction is optimized. Note that for this aim at maximum robustness with respect to uncertainty in the bit-rock interaction the alternative robust performance technique (see Section 4.4.2) is necessary. Because standard robust performance techniques aim at optimizing the performance for all possible plants in a given uncertainty set. While we aim to optimize the robustness with respect to uncertainty, satisfying a set of given performance objectives.

In the following section, the settings for the controller synthesis (i.e. tuning of the weighting filters) are explained and the designed controller is presented.

## 4.5 Controller synthesis

Weighting filter design is key in satisfying the performance specifications related to, e.g., measurement noise sensitivity and actuator limitations. Moreover, achieving specific design targets such as the inclusion of integral action and high-frequency roll-off can be achieved by absorbing these filters in the loop, see [73]. High-frequency roll-off reduces measurement noise amplification. Also, integral action is desired from a practical point of view, e.g., in case of a mismatch between the (model-based) feedforward torque  $u_c$  and the actual required feedforward torque due to uncertainty in the model for the bit-rock interaction and uncertainty in the model for the drill-string borehole interaction. In that case, integral action will compensate for this mismatch to obtain the desired setpoint.

For the design of a controller for the drill-string model (4.5), the following objectives are set:

- Integral action below 0.1 Hz, i.e. the controller should have an integrator with a zero at 0.1 Hz;
- First-order roll-off at 6 Hz, so for frequencies above 6 Hz the controller reduces the amplification of disturbances;
- Cross-over frequency of the open-loop transfer function  $KG_{ol}$  (at the plant input) at 0.7 Hz, i.e. above the third eigenfrequency of the drill-string system (see Figure 4.1);
- Plant output scaling, i.e. scale the plant output  $y = [\omega_{td} \ T_{pipe}]^\top$  such that the components of the weighted plant output  $\bar{y}$  are in the same order of magnitude.

These objectives are obtained by specific choices for several settings of the weighting filters. The specific choice for these weighting filters will be discussed in the remainder of this section.

### 4.5.1 Weighting filter design

First, we apply plant scaling by using the scaling matrices  $W_{sc}$  and  $V_{sc}$ . This scaling is applied to compensate for the different order of magnitude of the two plant outputs  $\omega_{td}$  and  $T_{pipe}$ . This is important for a system with multiple outputs in a norm-based controller synthesis method such as skewed- $\mu$  DK-iteration. When the plant outputs are not scaled and the outputs differ in order of magnitude, one off-diagonal term in the closed-loop sensitivity function will be large and the other small. In the synthesis, it is then possible that the emphasis is on reducing the large off-diagonal element at the expense of other elements. The plant scaling matrices  $W_{sc}$  and  $V_{sc}$  are tuned to compensate for this effect. The matrices are given by

$$W_{sc} = \begin{bmatrix} w_{sc1} & 0 \\ 0 & w_{sc2} \end{bmatrix}, \quad V_{sc} = W_{sc}^{-1}$$

with  $w_{sc1} = 10$  and  $w_{sc2} = 0.01$ .

The filters  $V_i(s)$  and  $W_i(s)$  are so-called performance filters and used to tune the performance related properties of the closed-loop system. The filters  $V_1(s)$  and  $W_1(s)$  can be used to tune the closed-loop bit-mobility ( $G_{cl}$ ). Ideally, the bit-mobility should be damped as much as possible (as follows from the stability analysis in Section 4.4.4). However, this typically results in high control action. To deal with this trade-off, the weighting filter  $V_1(s)$  has two notch filters and is defined as follows:

$$\begin{aligned} V_1 &= v_1 W_{notch,1} W_{notch,2} \\ &= v_1 \frac{\frac{1}{(2\pi f_{1,1})^2} s^2 + \frac{2b_{1,1}}{2\pi f_{1,1}} s + 1}{(2\pi f_{1,2})^2 s^2 + \frac{2b_{1,2}}{2\pi f_{1,2}} s + 1} \frac{\frac{1}{(2\pi f_{2,1})^2} s^2 + \frac{2b_{2,1}}{2\pi f_{2,1}} s + 1}{(2\pi f_{2,2})^2 s^2 + \frac{2b_{2,2}}{2\pi f_{2,2}} s + 1} \end{aligned} \quad (4.27)$$

with  $f_{i,j}$  ( $j = 1, 2$ ) the frequencies of the notch filters  $W_{notch,i}(s)$  ( $i = 1, 2$ ) and  $b_{i,1}$  and  $b_{i,2}$  parameters to tune the depth of the notch filter. The output weighting filter  $W_1(s)$  is set to  $W_1 = 1$ , since tuning of  $V_1(s)$  only suffices to specify the desired bound on the bit-mobility.

The remaining weighting filters are the filters to tune the closed-loop performance transfer functions in (4.12). Let us first focus on the input weighting filters  $V_2(s)$  and  $V_3(s)$ . The filter  $V_2(s)$  is given by

$$V_2 = \begin{bmatrix} v_{21} & 0 \\ 0 & v_{22} \end{bmatrix} \quad (4.28)$$

with  $v_{21}$  and  $v_{22}$  static gains. These gains, as well as static gains in other weighting filters, are used to scale the weighting filters. Scaling is necessary to

obtain a feasible controller design with respect to the performance uncertainty  $\Delta_P(s)$  and changing the gains allows for the synthesis of different controllers. The input weighting filter  $V_3(s)$  is set as

$$V_3(s) = v_3 \|g_{co}\|^{-1} \frac{1}{w_{sc1}}, \quad (4.29)$$

where  $v_3$  is a static gain and  $g_{co} := g_{22,1}(j2\pi f_{co})$ , i.e. the sub plant gain, related to input  $\tilde{u}$  and output  $\tilde{y}_1 = \omega_{td} - \omega_{eq}$ , at the target cross-over frequency  $f_{co}$ . This gain is chosen to obtain a cross-over frequency of the open-loop transfer function  $KG_{ol}$  at 0.7 Hz as specified. This cross-over frequency is chosen to achieve damping of the dominant resonance modes.

The output weighting filters  $W_2(s)$  and  $W_3(s)$  are also used to tune the closed-loop transfer functions, but in addition, these filters are also used to meet the first two controller objectives, i.e. to include integral action and first-order roll-off. The controller  $K_t(s)$  to be designed has two inputs and a single output (due to the two measured signals of the plant), i.e.  $K_t(s) = [K_{\omega_{td}}(s) \ K_{T_{pipe}}(s)]$ . The controller aims at stabilizing the desired angular velocity setpoint. Hence, an integrator should be specified in the top drive angular velocity control loop. Note that it is not possible (and not necessary) to include an integrator in both control loops  $K_{\omega_{td}}(s)$  and  $K_{T_{pipe}}(s)$ . An integrator would force the sensitivity function to zero for  $s = 0$ ; however this is not possible for both sensitivity functions, due to the fact that we are dealing with a non-square plant. In other words, there is only one control signal that can eliminate the steady-state error for one of the two measurements. However, forcing  $\omega_{td}$  to its equilibrium value also results in  $T_{pipe}$  converging to its equilibrium. So, by only requiring integral action in the control loop related to  $\omega_{td}$ , the output weighting filter  $W_2(s)$  is given by

$$W_2(s) = \begin{bmatrix} W_I(s) & 0 \\ 0 & w_{22} \end{bmatrix} = \begin{bmatrix} P_I \frac{s+2\pi f_I}{s} & 0 \\ 0 & w_{22} \end{bmatrix} \quad (4.30)$$

with  $W_I(s)$  to obtain an integral action in  $K_{\omega_{td}}(s)$  and  $w_{22}$  a static gain. To obtain high-frequency roll-off, a roll-off filter is included in the output filter  $W_3(s)$ , hence

$$W_3(s) = w_3 w_{sc1} \|g_{co}\| W_R^{-1} \quad (4.31)$$

with  $w_3$  a static gain,  $W_R = \frac{2\pi f_R}{s+2\pi f_R}$  the roll-off filter with roll-off frequency  $f_R$ .

The weighting filters  $W_2(s)$  and  $W_3(s)$  are unstable and non-proper weighting filters, respectively. Therefore, these filters are not applicable in the  $\mathcal{H}_\infty$ -controller synthesis. To circumvent this limitation and still obtain a controller that includes integral action and high-frequency roll-off, we add filters in the loop [73]. We require high-frequency roll-off on both input signals (top drive velocity and pipe torque) of the controller and integral action on the top drive velocity. To do so, the actual plant that is used in the controller synthesis

Table 4.1: Parameter settings for the performance weighting filters that are equal for the designed high-gain and low-gain controller.

| Filter / setting     | Parameters   |
|----------------------|--|
| $W_I$                | $f_I = 0.1$ Hz $P_I = 0.1$   |
| $W_R$                | $f_R = 6$ Hz   |
| Cross-over frequency | $f_{co} = 0.7$ Hz  |
| $V_1$                | $v_1 = 100$<br>$b_{1,1} = 0.15$ $b_{1,2} = 1.2$<br>$f_{2,1} = 1.58$ Hz $f_{2,2} = 1.58$ Hz<br>$b_{2,1} = 0.05$ $b_{2,2} = 0.1$ |
| $V_2$                | $v_{21} = 5$ $v_{22} = 1.4$  |
| $V_3$                | $v_3 = 2$  |
| $W_2$                | $w_{22} = 0.1$   |

algorithm is given by

$$G_t(s) = \text{diag}(1, W_I(s), 1) G_{ol}(s) \text{diag}(1, W_R(s)) \quad (4.32)$$

with  $W_R(s)$  and  $W_I(s)$  the roll-off and integrator filters, respectively. The resulting controller  $K(s)$  from the DK-iteration procedure, treated in Section 4.4.3, for this plant  $G_t$ , has no integrator and roll-off properties. However, the actual controller (for the plant  $G_{ol}$ ) can be calculated as follows:

$$K_t(s) = W_R(s) K(s) \text{diag}(W_I(s), 1), \quad (4.33)$$

which does include the desirable integrator and roll-off properties.

### 4.5.2 Controller synthesis results

In this section, two different controllers will be synthesized based on the skewed- $\mu$  DK-iteration procedure and the proposed weighting filters from the previous section. Of course, it is possible to change all weighting filters to obtain a different controller; however, the weighting filters in Section 4.5.1 have been chosen such that the controller objectives can be met and tuning of the parameters already allows to synthesize different controllers. The two controllers mainly differ in the allowed control action and will be referred to as a *high-gain* (hg) controller and *low-gain* (lg) controller. The extra allowed control action for the high-gain controller is used to suppress the bit-mobility even more compared to the low-gain controller. In Table 4.1 the parameters of the weighting filters that are equal for both controllers are summarized. The parameters that are

Table 4.2: Parameter settings for the performance weighting filters that are not equal for the designed high-gain and low-gain controller.

| Filter | Parameters           |                       |
|--------|----------------------|-----------------------|
|        | High-gain controller | Low-gain controller   |
| $V_1$  | $f_{1,1} = 0.53$ Hz  | $f_{1,1} = 0.48$ Hz   |
|        | $f_{1,2} = 0.35$ Hz  | $f_{1,2} = 0.31$ Hz   |
| $W_3$  | $w_3 = \frac{1}{7}$  | $w_3 = \frac{1}{3.1}$ |

changed for the two different controllers are given in Table 4.2. The settings for the first notch filter in  $V_1(s)$  are different and the gain  $w_3$  is used to allow for less (or more) control action. By decreasing the gain  $w_3$ , the allowed magnitude of the control sensitivities is increased, i.e. allowing for more control action and therefore higher controller gains. The notch filter in  $V_1(s)$  is used to allow for a higher bit-mobility in specific frequency ranges. Note that a so-called skewed notch filter is used in the weighting filter for both controllers to tune the level of bit-mobility suppression for frequencies below and above the frequency of the notch, i.e. allow for less suppression for high frequencies.

Performing the DK-iteration procedure for the drill-string system with the weighting filters as specified above, results in the controller  $K_t(s) = [K_{\omega_{td}}(s), K_{T_{pipe}}(s)]$ , as shown in Figure 4.7 for both the high-gain and the low-gain controller. From this figure, the integral action in the controller,  $K_{\omega_{td}}(s)$ , that uses the top drive angular velocity can be clearly recognized. Moreover, the first-order roll-off is present in both controllers. It can also be seen that the designed controllers are active in the frequency range of the torsional resonance modes of the drill-string system (see Figure 4.1), which is not the case for the Soft-Torque controller shown in the same figure. This industrial controller, which only uses top drive velocity measurements, is a properly tuned active damping system (i.e. PI-control of the angular velocity) which aims at damping the first torsional mode of the drill-string dynamics. A comparison with this controller by means of a simulation is presented in Section 4.6.

The closed-loop bit-mobility for the different controllers is shown in Figure 4.8 and also compared to the bit-mobility with the industrial controller, indicated by  $ST$ . Moreover, the bounds, specified by the weighting filter  $V_1$ , for the controller synthesis are indicated by the dashed lines. It can be seen that the high-gain controller suppresses the bit-mobility the most, but also with the low-gain controller a significant decrease of the peak value of the bit-mobility is achieved compared to the industrial controller. Let us now determine the  $\mathcal{H}_\infty$ -

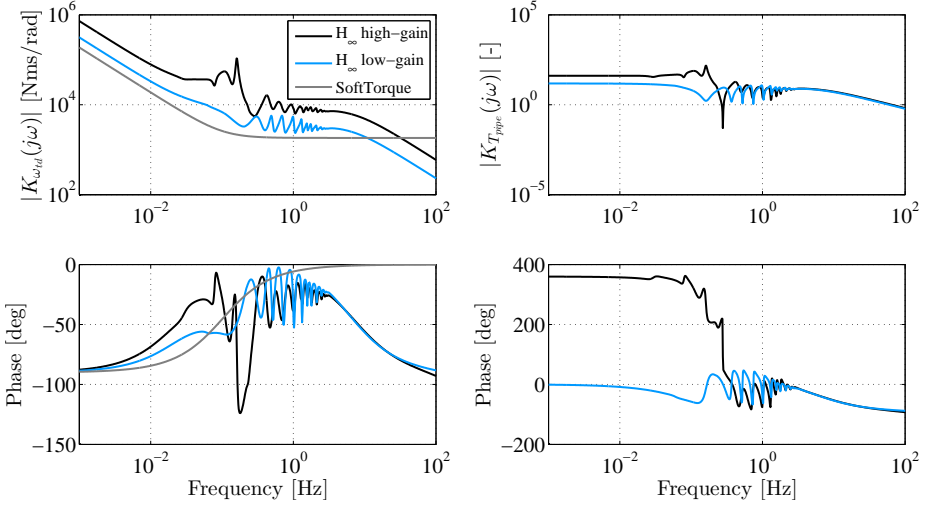


Figure 4.7: Designed linear dynamic controllers for the drill-string system, left plot is the controller which uses the top drive angular velocity, the controller in the right plot is based on the pipe torque measurement.

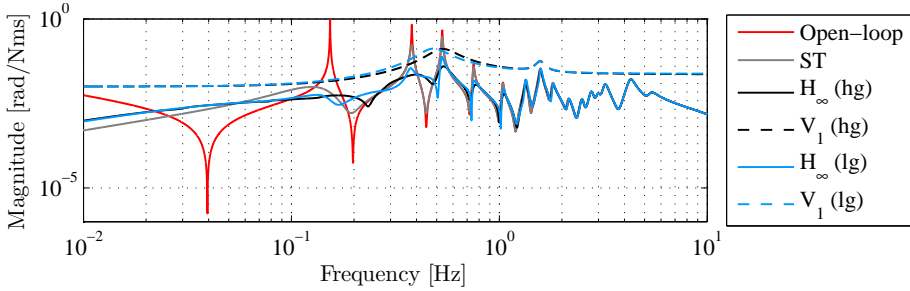


Figure 4.8: Closed-loop bit-mobility, i.e. the frequency response function from bit torque  $T_{bit}$  to bit velocity  $\omega_{bit}$ .

norm for the closed-loop system  $G_{cl}^{hg}(s)$  with the high-gain controller:

$$\left\| G_{cl}^{hg}(s) \right\|_{\infty} = \sup_{\omega} \left| G_{cl}^{hg}(j\omega) \right| = 0.039. \quad (4.34)$$

For comparison, for the low-gain controller the  $\mathcal{H}_{\infty}$ -norm is equal to  $\left\| G_{cl}^{lg}(s) \right\|_{\infty} = 0.074$  and for the industrial controller  $\left\| G_{cl}^{ST}(s) \right\|_{\infty} = 0.298$ . Hence, with the high-gain controller the peak value of the bit-mobility has been decreased with almost a factor 8. It can also be seen in Figure 4.8 that multiple modes of the



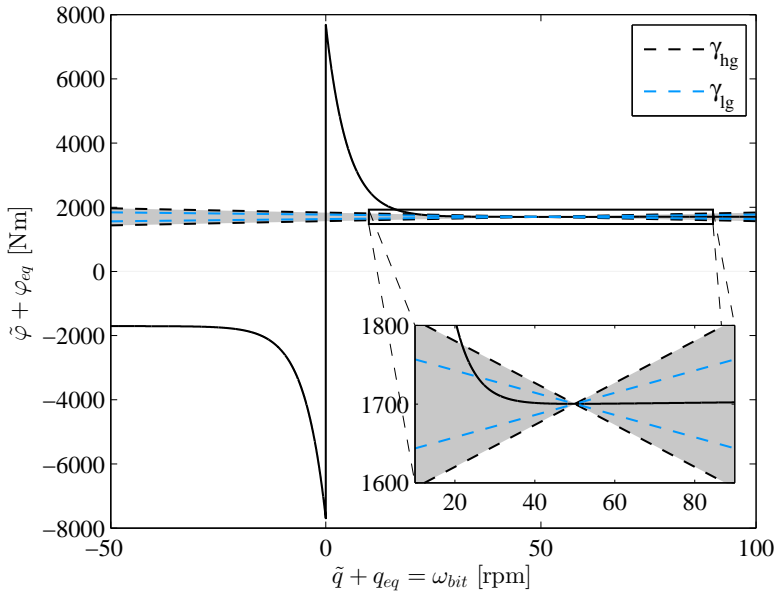


Figure 4.9: Transformed bit-rock interaction model  $\tilde{\varphi}(\tilde{q})$  and maximal sector condition for the high-gain and low-gain controllers.

bit-mobility are damped by the controllers obtained with the proposed controller design strategy, while with the SoftTorque controller only significant damping of the first torsional mode is achieved.

According to (4.26), the sector (for  $\tilde{\varphi}$ ) for which stability can now be guaranteed is equal to  $[-\gamma_{hg}, \gamma_{hg}]$  with  $\gamma_{hg} = 1/0.039 = 25.46$  (for the high-gain controller). In Figure 4.9, the nonlinearity  $\tilde{\varphi} + \varphi_{eq}$  is shown, including the sector  $[-\gamma_{hg}, \gamma_{hg}]$  (and  $[-\gamma_{lg}, \gamma_{lg}]$  for reference). From this figure, it can be seen that the closed-loop nonlinear system is locally absolutely stable, as long as the bit angular velocity is larger than (approximately) 22 rpm (because  $\tilde{q} + Hx_{eq} = \omega_{bit}$ ). The region of attraction (in terms of the bit angular velocity) is slightly smaller for the low-gain controller because  $\gamma_{lg} < \gamma_{hg}$ . To conclude, with the designed controllers, robustness with respect to uncertainty in the bit-rock interaction is achieved for a substantial variation in the bit velocity.

## 4.6 Simulation results

In this section, the controllers designed in Section 4.5 are applied to the drill-string model presented in Section 4.2. First, we present a simulation result of the drill-string system in closed-loop with an existing industrial controller (based on [51]). For the simulations, we introduce a so-called startup scenario,

which is based on practical startup procedures for drilling rigs. Herein, the drill-string is first accelerated to a low constant rotational velocity, starting from zero angular velocity for the whole drill-string, with the bit above the formation (off bottom). Subsequently, the angular velocity and weight-on-bit (WOB) are gradually increased to the desired operating conditions. The increase in WOB is modelled as a scaling of the bit-rock interaction torque. Assume that the WOB is scaled according to the following profile:

$$\alpha(t) = \begin{cases} 0, & t_0 \leq t \leq t_1 \\ \frac{t-t_1}{t_2-t_1}, & t_1 < t < t_2 \\ 1, & t \geq t_2 \end{cases} \quad (4.35)$$

with  $t_1 = 50$  and  $t_2 = 110$  in this case. Then, the bit-rock interaction model is scaled by using this scaling factor  $\alpha(t)$ , hence:

$$T_{bit}(t) = \text{Sign}(\omega_{bit}) \left( T_{ini} + \alpha(t) \left( T_d - T_{ini} + (T_s - T_d) e^{-\frac{30}{N_d \pi} |\omega_{bit}|} \right) \right) \quad (4.36)$$

where  $T_{ini}$  is the amount of resisting torque that is still present at the bit-rock interface, even when the bit is off bottom (e.g. due to drilling mud and interactions with the bore hole). For WOB = 0 (off bottom) there is no velocity-weakening in the TOB. The startup scenario comprises the following steps:

1. Turn on the controller and start with WOB = 0, such that there is no velocity-weakening effect in the bit-rock interaction model and operate at relatively low velocity (starting from initial zero velocity for the whole drill-string) to build up torque in drill-string to overcome static torques due to drag in the time window  $0 < t < 50$  s;
2. Slowly increase the reference angular velocity until the desired operating velocity ( $\omega_{eq}$ ) is reached (in the time window  $50 \leq t < 110$  s). At the same time, slowly increase the WOB and finally obtain the nominal operating condition in the angular velocity and WOB.

A simulation result of the drill-string model (4.5) in feedback with the industrial controller, shown in Figure 4.7, is shown in Figure 4.10. In the plot in the middle, the top drive velocity ( $\omega_{td}$ ) is shown along with the reference velocity  $\omega_{td,ref}$  that starts at a velocity of 20 rpm and is gradually increased to the desired equilibrium velocity,  $\omega_{eq}$ , of 50 rpm. From the bit response, in the top plot, we can clearly recognize stick-slip oscillations. The increasing amplitude of the oscillations in the top drive velocity and top drive torque (bottom plot) demonstrates that these vibrations arise when the WOB is increased ( $50 \leq t < 110$  s), i.e., when due to scaling of the TOB the velocity-weakening effect starts affecting the dynamics.

Simulation results of the designed controllers in Figure 4.7 are shown in Figure 4.11. The same startup scenario and initial conditions, as in Figure 4.10,

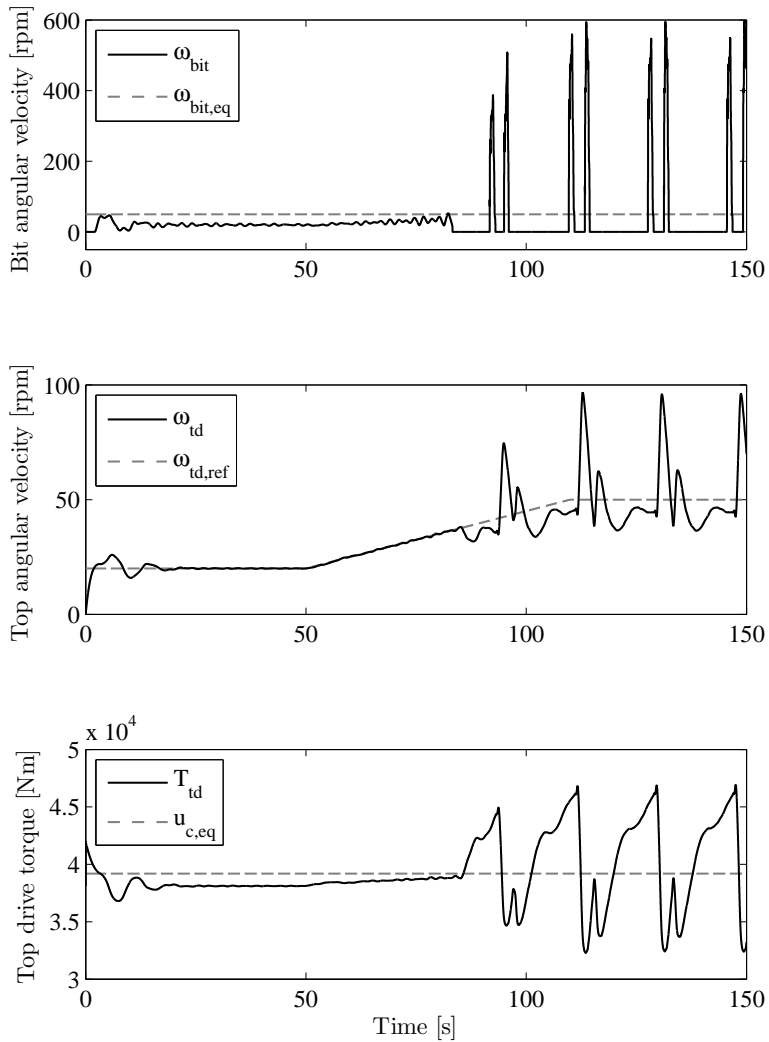


Figure 4.10: Simulation result of the drill-string model with an existing industrial (SoftTorque) controller in the startup scenario.

are used for these simulations. The simulation results show that the top drive and bit angular velocity converge to their setpoint and stick-slip vibrations are avoided. The controllers are able to stabilize the desired setpoint, because damping of multiple flexibility modes is achieved and robustness with respect to the bit-rock interaction is taken into account in the design. The difference between the low-gain and the high-gain is particularly visible in the top drive torque; the high-gain controller acts more aggressively in response to the initial error, resulting in more control action (see zoom plot). Consequently, this results in transient oscillations with a larger amplitude in the angular velocity of the drill-string, as can be seen in both the top drive velocity and the bit velocity. On the other hand, the amplitude of the oscillations decays faster for the high-gain controller compared to the low-gain controller, in particular at the bit, which is a result of increased bit-mobility suppression obtained by the high-gain controller.

The simulation results of the controllers designed with the skewed- $\mu$  DK-iteration technique show that the desired setpoint of the drill-string system is stabilized. Moreover, it is shown that the high-gain controller indeed obtains an increased suppression of the oscillations at the bit compared to the low-gain controller at the expense of increased control action. The simulation results in this section are performed under nominal conditions. In Section 4.7, robustness with respect to different operating velocities, sensor and actuator noise, changing bit-rock interaction and increased drill-string length are investigated. First, a comparison study will be performed in the next section. The observer-based output-feedback controller design methodology (see Chapter 3) and the linear  $\mathcal{H}_\infty$ -based controller design method presented in this chapter are compared with each other.

#### 4.6.1 Comparison with the observer-based output-feedback controller design strategy

The controller objectives for the  $\mathcal{H}_\infty$ -based controller are summarized in Section 4.3.1. The observer-based controller design strategy is also designed to (locally) stabilize the constant rotational velocity of drill-string systems with multiple dominant torsional flexibility modes, while ensuring robustness with respect to uncertainty in the bit-rock interaction, using surface measurements only. It has been shown that both controllers are able to stabilize the desired angular velocity of the drill-string and that stick-slip oscillations have been eliminated. However, the latter controller design methodology does not guarantee the satisfaction of closed-loop performance specifications on for example measurement noise sensitivity and the limitation of control action. The performance of this nonlinear controller in terms of these specifications can only be analyzed a posteriori (i.e. after designing the controller). Moreover, the  $\mathcal{H}_\infty$  controller design approach has some additional advantages. First, specific design targets such

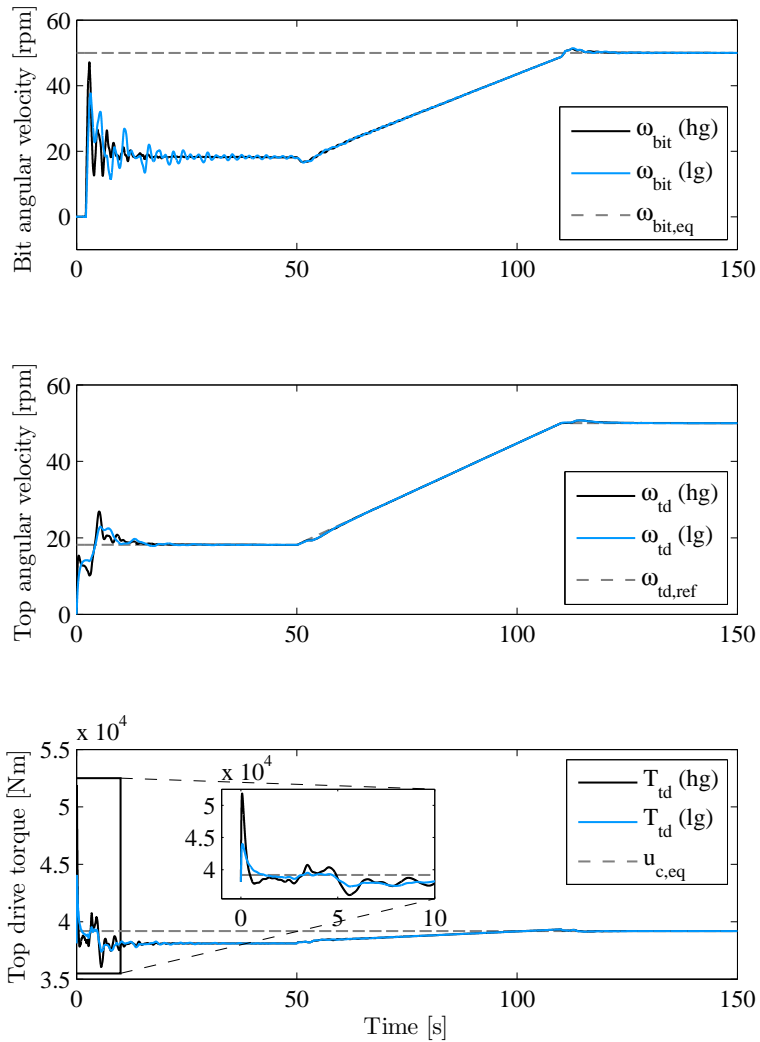


Figure 4.11: Simulation result of the drill-string model with the designed output-feedback controllers in the startup scenario.

as the inclusion of integral action and high-frequency roll-off can be achieved by absorbing specific filters in the controller design. Second, the pipe torque measurement can be easily adopted as additional measurement in order to increase the robustness of the controller, i.e. more information is available for feedback due to the use of an additional sensor. This can be beneficial because the third torsional flexibility mode is almost unobservable in the top drive angular velocity. Third, the observer-based controller approach needs a model of the nonlinear bit-rock interaction in the observer. It has been shown that the observer-based controller is robust with respect to changes in the bit-rock interaction; the  $\mathcal{H}_\infty$ -based controller does not need a model at all. Last, the  $\mathcal{H}_\infty$  controller can be switched on immediately, while in the observer-based approach the observer needs time to estimate the states of the system and in that initial period another controller (that does not use the estimated states) is necessary.

A simulation result of the 18-DOF drill-string model in closed-loop with the high-gain  $\mathcal{H}_\infty$  controller and an observer-based output-feedback controller as designed in Chapter 3 is shown in Figure 4.12. Both simulations are performed under the same operating conditions in the startup scenario and with equal initial conditions (i.e. zero angular velocity of the entire drill-string). For readability of the plots, the state estimates of the observer in the observer-based controller are not shown. A particular difference between the two controllers, clearly visible in Figure 4.12, is the fact that the  $\mathcal{H}_\infty$  controller is switched on immediately, while in the simulation with the observer-based controller an industrial PI-controller is used in the first 50 seconds. Therefore, the  $\mathcal{H}_\infty$  controller is able to damp the transient oscillations in the bit angular velocity while these oscillations are not as well damped with the PI-controller. This can also be seen in the top drive torque, which clearly acts at higher frequencies for the  $\mathcal{H}_\infty$  controller. At  $t = 50$  s, when the observer-based output-feedback controller is switched on, a step in the control action is visible (see zoom plot) due to the switch in the controller. Also in the control action of the  $\mathcal{H}_\infty$  controller some oscillations are present due to the fact that at the same time the velocity and WOB start to increase.

## 4.7 Robustness of the closed-loop system

As already stated in the controller objectives in Section 4.3.1, robustness of the closed-loop system is an important objective of the proposed controller design strategy. Several aspects regarding the robustness of the closed-loop drill-string system are investigated in this section. In Section 4.7.1, robustness with respect to different operating velocities is investigated and, in Section 4.7.2, robustness with respect to uncertainty in the bit-rock interaction is investigated. Next, in Section 4.7.3 the performance of the drill-string system in the presence of sensor and actuator noise is investigated and, in Section 4.7.4, the influence of the increasing length of the drill-string while drilling is examined.

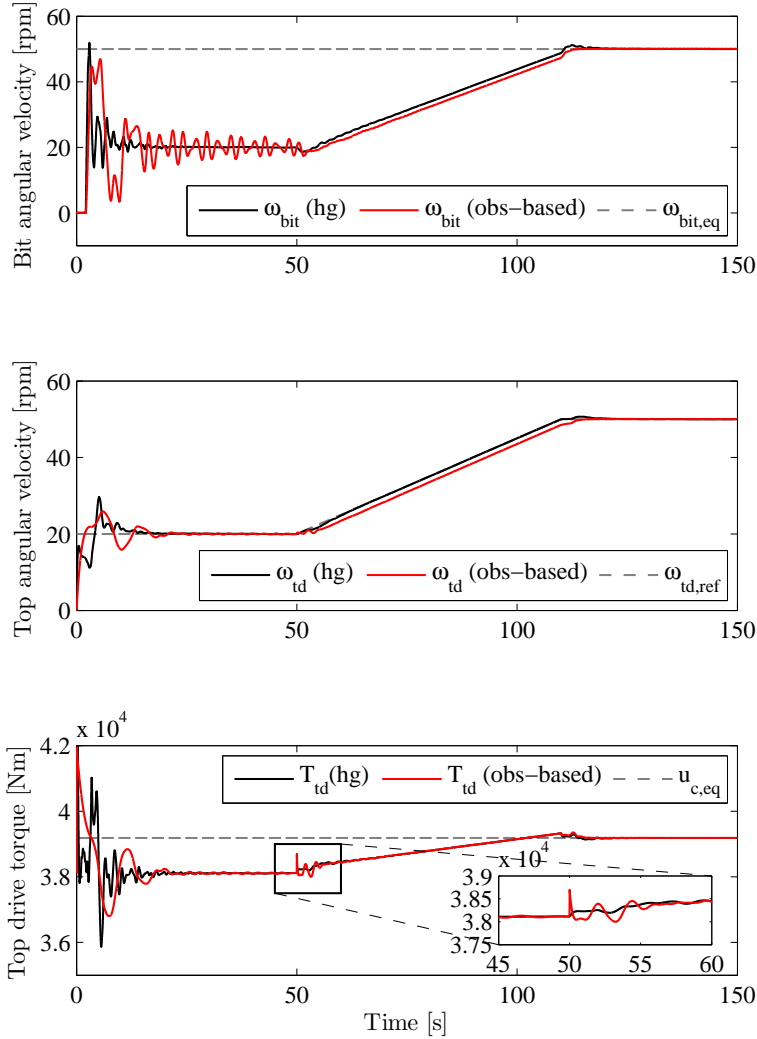


Figure 4.12: Simulation result of the drill-string model with the designed high-gain output-feedback controller compared with the observer-based output-feedback controller in the startup scenario.

Note that the simulation results in this section mainly involve results of the drill-string system in closed-loop with the high-gain  $\mathcal{H}_\infty$ -controller. The same simulations have also been performed with the low-gain controller and it has been observed that the results are very similar. Only in case there is a significant difference between the two controllers' performance, results of both controllers are discussed.

### 4.7.1 Different operating velocity

The controller design methodology in Section 4.4 is applied to the system in perturbation coordinates and therefore designed to stabilize the desired equilibrium velocity  $\omega_{eq}$ . However, in practice it is not desirable to have a controller that is only applicable at a single angular velocity. Therefore, the operating envelope in terms of velocity for the designed controller is investigated. In Figure 4.9 the lower limit of the bit-angular velocity based on the sector bounds of the nonlinear stability analysis is indicated. However, this lower limit for the bit velocity does not give full information about the region of attraction for the other states of the system, e.g. a lower limit for the angular velocity of the entire drill-string. In this section, we investigate the closed-loop poles of  $G_{cl}$  for different equilibrium velocities  $\omega_{eq}$ , that is the pole locations of the (transformed) linear drill-string system in closed-loop with the designed  $\mathcal{H}_\infty$ -controllers. Due to the destabilizing effect of the velocity-weakening effect in the bit-rock interaction, the (linear) closed-loop system will become unstable below a certain equilibrium velocity. This velocity gives a lower bound of the angular velocity that can be stabilized with the designed controller. In Figure 4.13, the lower limit of the angular velocity for the low-gain and high-gain controller is given ( $\omega_{min,lg}$  and  $\omega_{min,hg}$ , respectively) and compared with the lower limit for the industrial controller ( $\omega_{min,ST}$ ). The numerical values of these limits are summarized in Table 4.3. As can be seen, the lower limit of the angular velocity that can still be stabilized is decreased from approximately 40 rpm for the industrial controller to 33 and 30 rpm for the low-gain and high-gain  $\mathcal{H}_\infty$  controller, respectively. Moreover, it shows that the increased bit-mobility suppression of the high-gain controller also results in a lower angular velocity for the entire drill-string that can be stabilized. It has to be noted that these values are determined based on the location of the closed-loop poles of the (transformed) linear drill-string system and therefore only give information about the local asymptotic stability of the desired equilibrium point. Due to this reason the angular velocity that can be stabilized in practice is probably higher. The latter fact is also indicated by the simulations using the industrial controller (see Figure 4.10) that show that this controller is unable to stabilize the desired velocity of 50 rpm under the imposed operating conditions while the theoretical lower limit concerning local asymptotic stability is approximately 40 rpm.

To investigate the applicability of the  $\mathcal{H}_\infty$ -controllers at lower angular ve-



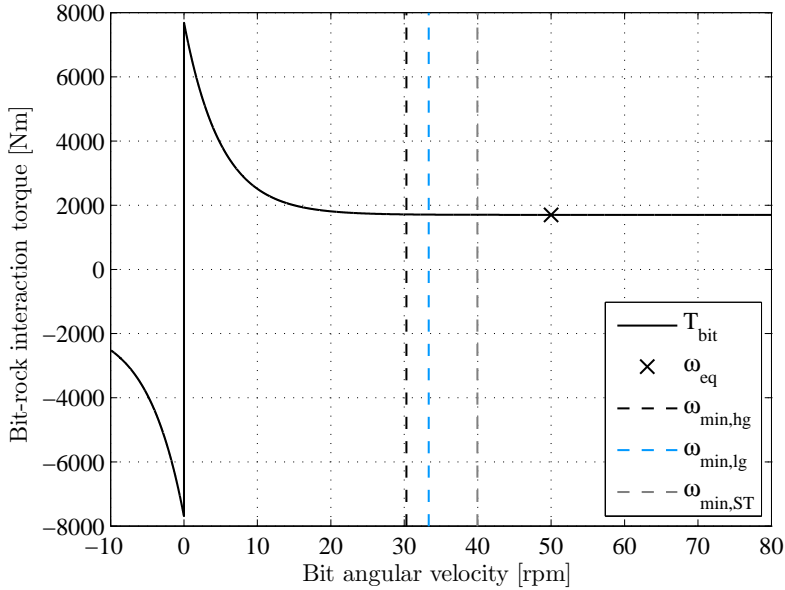


Figure 4.13: Lower limit of the desired angular velocity that can be (locally) stabilized for different controllers.

Table 4.3: Lower limit of the desired angular velocity that can be stabilized for different controller based on the closed-loop poles of the drill-string system.

| Controller | Lower limit $\omega_{eq}$ [rpm] |
|------------|---------------------------------|
| High-gain  | 30.3                            |
| Low-gain   | 33.3                            |
| SoftTorque | 40.0                            |

locities, simulations with the startup scenario and a desired angular velocity of 35 rpm have been performed. The results are shown in Figure 4.14, the first 50 seconds are equal to the simulation results shown in Figure 4.11 as the initial conditions and starting velocity (20 rpm) are the same. In the time period from 50 to 110 seconds the WOB and angular velocity are again increased, but in this case with a desired end velocity of 35 rpm. Both the low-gain and high-gain controller are able to stabilize the desired setpoint of 35 rpm (under the imposed operating conditions), however the response of the system shows more oscillatory behavior compared to the simulations in Figure 4.11. For the low-gain

controller these oscillations result from not fully damped transient oscillations in the first 50 seconds, which grow when the operating conditions change (for  $50 \leq t < 110$ s). However, as can be seen in the top drive torque the controller acts on these vibrations and eventually the vibrations are damped. The oscillations are also caused by the changing operating conditions at  $t = 50$ . Especially, the second-order reference profile for the angular velocity, and therefore a step in acceleration, cause some transient oscillations. This can particularly be seen in the response of the drill-string system in closed-loop with the high-gain controller. The same simulation as shown in Figure 4.14, is shown in Figure 4.15 for the high-gain controller and focusing on the time period from 40 to 150 seconds. The transient oscillations are clearly visible in the response after  $t = 50$ . In the same figure, the result of another simulation is shown (indicated by the red lines), where instead of a second-order reference profile, a third-order reference profile is used for the change in velocity and WOB. Up to  $t = 50$  the response of the system is exactly the same, but in the period between 50 and 110 seconds the operating conditions are changed in a much smoother way using the third-order reference signal compared to the second-order reference signal. As a result, the transient oscillations have disappeared and the controller stabilizes the desired setpoint of the drill-string system. This simulation shows that the design of a suitable reference signal, in addition to the controller design, can improve the performance of the closed-loop drill-string system. Another possibility to, potentially even further, improve the performance is the design of additional (mass) feedforward terms. By the design of feedforward the control action is also based on the a priori known reference signal, instead of feedback (i.e. measurements) only. The use of additional feedforward is not investigated here, but serves as a recommendation for cases where the performance of the system is not sufficient.

To summarize, the analysis in this section shows that with the controllers designed using the controller design methodology proposed in Section 4.4 a significant increase in the operating envelope in terms of angular velocity can be achieved.

### 4.7.2 Changing bit-rock interaction model

Robustness with respect to uncertainty in the bit-rock interaction is an important property of the closed-loop system from a practical point of view, first of all because it is difficult to obtain an accurate model of the bit-rock interaction. Another reason is the fact that the bit-rock interaction is prone to changes during the drilling process, for example, due to bit wear and changes in the formation. Therefore, one of the controller objectives (Section 4.3.1) is to obtain robustness with respect to uncertainty in the bit-rock interaction. In Figure 4.9, the sector condition on the bit-rock interaction has already been visualized. This sector conditions states that the desired equilibrium point is (locally) absolutely stable

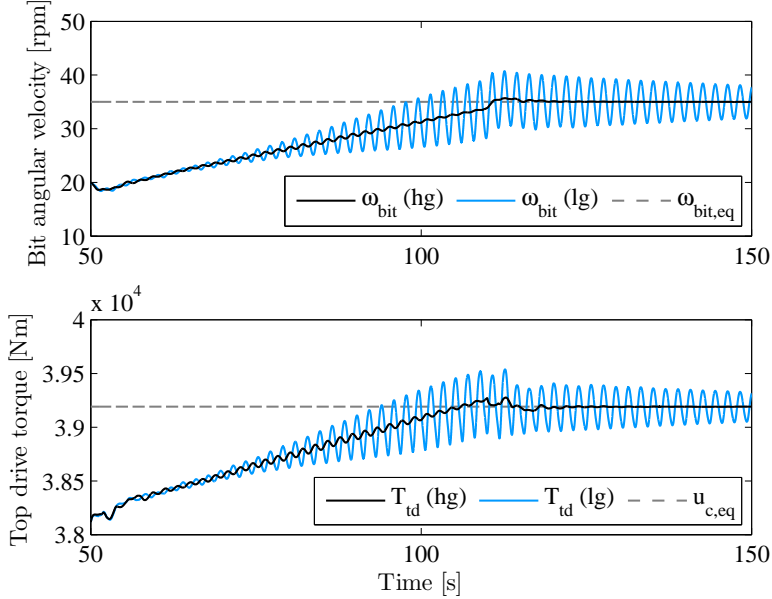


Figure 4.14: Simulation result of the drill-string model in the startup scenario with the designed output-feedback controllers and a desired angular velocity of 35 rpm.

for any bit-rock interaction within the sector, i.e. the grey area in Figure 4.9 for the high-gain controller. In this section, we present a simulation result of the drill-string system in closed-loop with the designed high-gain controller to illustrate the robustness with respect to changes in the bit-rock interaction.

Recall the nominal parameter values for the bit-rock interaction model, that is  $T_s = 7700$  Nm,  $T_d = 1700$  Nm and  $N_d = 5$  rpm, which are used for the controller synthesis. In this simulation study, both the torque level and the decrease rate of the bit-rock interaction is changed. First, the nominal level of the bit-rock interaction model is increased. In other words, both the static torque  $T_s$  and the dynamic torque  $T_d$  are increased. Also the decrease rate (related to  $N_d$ ) is adapted, by increasing  $N_d$ . This leads to a less severe velocity-weakening effect at low velocities and therefore more negative damping at higher velocities. The parameters for the adapted bit-rock interaction model are given by  $T_s^c = T_s + 200$ ,  $T_d^c = T_d + 200$  and  $N_d^c = N_d + 1$ . The value of  $N_d$  is chosen such that the bit-rock interaction still locally satisfies the sector condition. The simulation is started with the same settings as the simulation results shown before, subsequently the WOB and angular velocity are changed according to the startup scenario to obtain the desired angular velocity of 50 rpm and the nominal bit-rock interaction model. At  $t = 130$  s, the bit-rock interaction model is suddenly changed to the

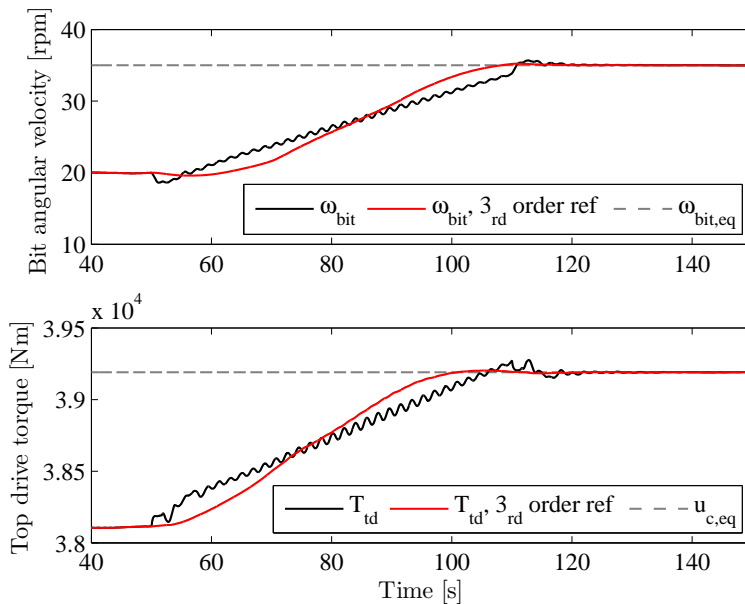


Figure 4.15: Simulation result of the drill-string model in the startup scenario with the high-gain controller and a desired angular velocity of 35 rpm, comparison between second and third-order reference signal.

adapted parameter settings. As can be seen from the response in Figure 4.16 the change in bit-rock interaction causes some oscillations in the states of the drill-string system. However, the oscillations are damped and the velocity of both the top drive and the bit converge to the desired angular velocity. In the zoom plot of the top drive torque it can be seen that the top drive torque converges to a new equilibrium value which is slightly higher than the original equilibrium. A closer look at the new equilibrium value shows that it exactly compensates for the added 200 Nm in torque of the adapted bit-rock interaction model. This illustrates the effect of the integral action in the controller; without integral action the controller does not compensate for a steady-state offset in the controlled states. However, with the designed controller, integral action is included in the top drive velocity part ( $K_{\omega_{td}}$ ) of the controller such that the desired velocity is stabilized, resulting in a new equilibrium value for the top drive torque.

### 4.7.3 Sensor and actuator noise disturbances

Another aspect that the drilling system has to deal with in practice is the presence of sensor and actuator noise. In this section, the robustness with respect to

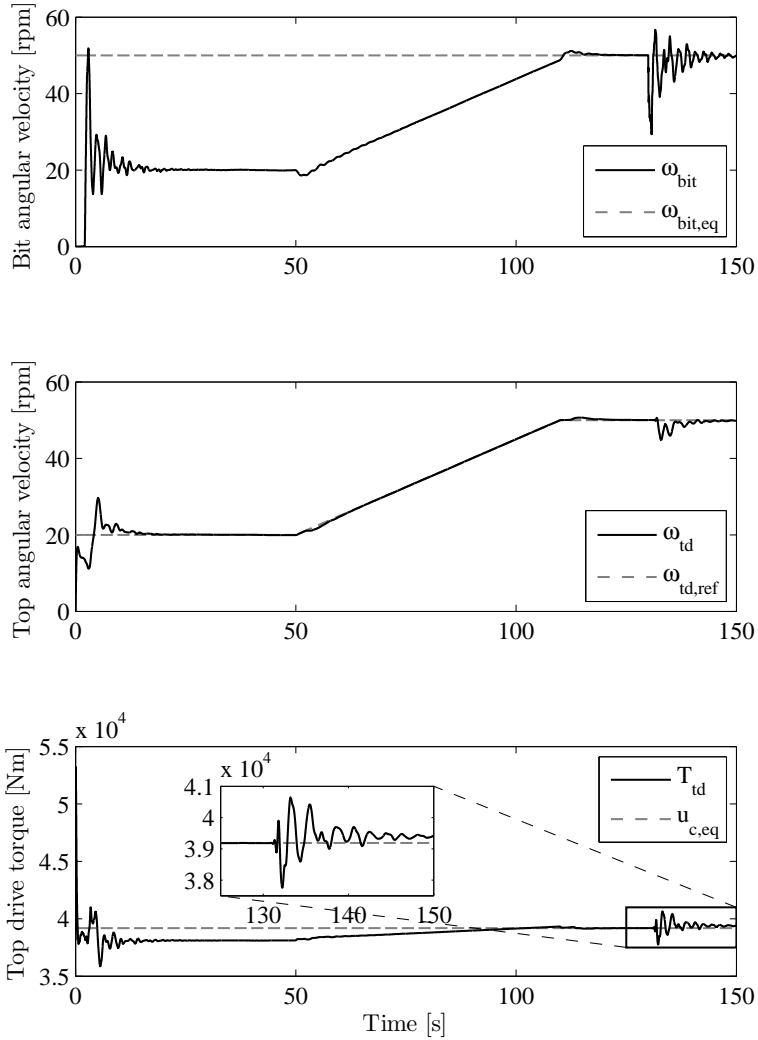


Figure 4.16: Simulation result of the drill-string model in the startup scenario with the high-gain controller and a change in the bit-rock interaction at  $t = 130$  s.

noise is investigated and both sensor and actuator noise are taken into account. The noise disturbances are modelled as additive white noise signals. That is, the actual top drive torque  $T_{td}$  is given by  $T_{td} = u_t + d_{T_{td}}$  with  $u_t$  the output from the controller and  $d_{T_{td}}$  the disturbance. The measurement  $y_m$  is the actual state plus sensor noise, i.e.  $y_m = y + n$ . The actuator noise on the top drive torque has a standard deviation of approximately 560 Nm, i.e. 1.5% of the nominal value, this means that the top drive torque varies between approximately 37.2 kNm and 41.1 kNm (nominal torque in equilibrium is  $u_c = 39.2$  kNm). Due to sensor noise both the top drive velocity and pipe torque measurement are perturbed. The standard deviation of the sensor noise is also chosen to be approximately 1.5% of the nominal value, i.e. approximately 0.7 rpm for the top drive velocity and approximately 520 Nm for the pipe torque. The measured top drive angular velocity varies between 47.5 rpm and 52.5 rpm and the pipe torque measurement between approximately 38.0 kNm and 34.4 kNm (i.e. peak-to-peak the disturbances are approximately 10% of the nominal value).

A simulation of the system including measurement noise is shown in Figure 4.17. In this figure, the actual top drive velocity  $\omega_{td}$ , pipe torque  $T_{pipe}$  and control action  $u_t$  are shown. Compared to the previous simulation results, the response of the system is similar. A closer study of the states of the system of course shows some more oscillations caused by sensor and actuator noise. Due to these disturbances, the states of the system will always show some oscillations, however compared to the noise levels of 5% in amplitude the effect on the states is limited. For example the actual top drive velocity only varies between approximately 49.7 and 50.3 rpm. This relatively low measurement noise sensitivity is mainly obtained by the required roll-off filter in the controller. This roll-off filter reduces the effect of (high-frequency) disturbances and the fact that such filter can be included in the controller is an important advantage of the proposed controller design methodology. Most importantly, the simulation result shows that the controller is able to stabilize the desired velocity and mitigate stick-slip vibrations even in the presence of sensor and actuator noise.

#### 4.7.4 Changing length of the drill-string

During the drilling process the drill-string is gradually lengthened as the well gets deeper. Current controllers need to be re-tuned during the drilling operation and this re-tuning is prone to errors, resulting in wrong controller settings and possibly failing of the stick-slip mitigation due to tuning errors. Additionally, the re-tuning process is time consuming and requires qualified staff to be present at the rig. Therefore, the amount of tuning occurrences should be minimized. In other words, the controller should be robust with respect to the increasing length of the drill-string. In this section, the plant model (4.5) is changed such that the dynamics of the plant correspond to a drill-string of different length.

In practice, to add a new pipe section, the drill-string is stopped and a stand

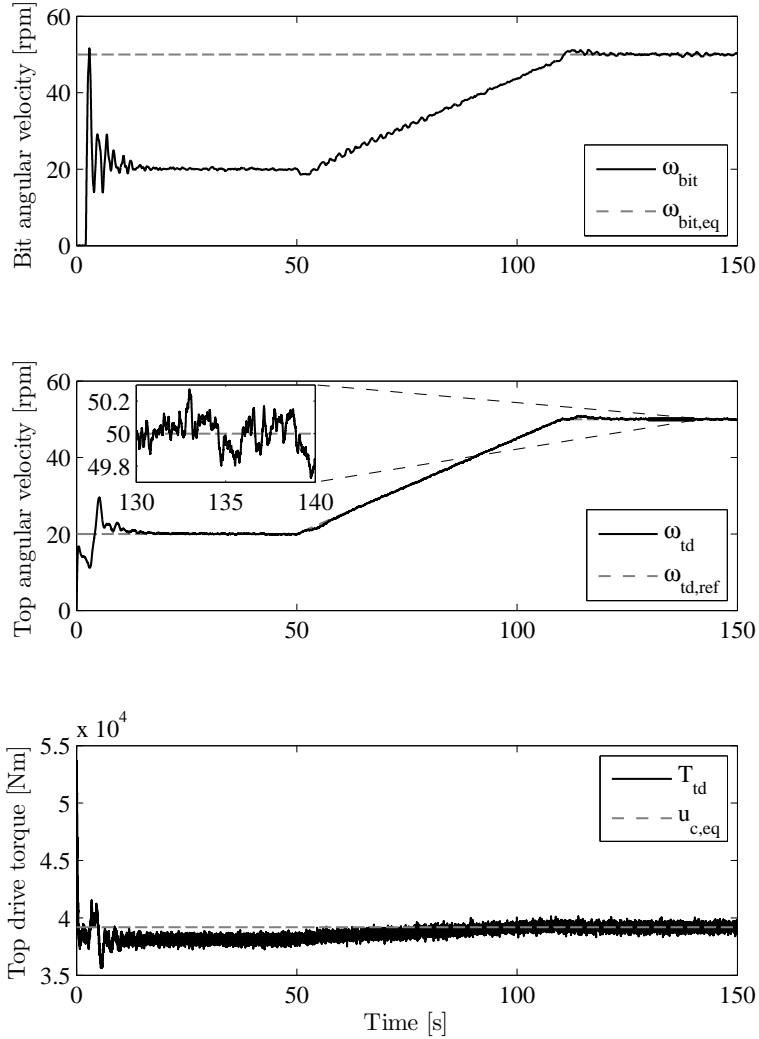


Figure 4.17: Simulation result of the drill-string model in the startup scenario in closed-loop with the high-gain controller, disturbed with sensor and actuator noise, the amplitude of the noise signals is approximately 5% of the nominal value of the disturbed signal.

of one or multiple drill pipes is connected to the drill-string. In this analysis it is assumed that a new stand of 3 drill pipes is added to the drill-string (i.e. 27 m of length is added to the drill-string). In practical situations, the current industrial controller needs to be re-tuned every stand, and sometimes even after one or two added drill pipes. The pole locations of the closed-loop system, consisting of a changed plant model and a controller designed for the nominal drill-string, are investigated for different controllers. The results of this analysis are shown in Figure 4.18 for both the low-gain and the high-gain  $\mathcal{H}_\infty$ -controller and compared with the industrial controller. The real value of the right-most pole is shown as function of changing length compared to the nominal model. The right-most pole of the nominal model (indicated by 0) lies in the LHP for all three controllers. When the length of the drill-string is decreased the right-most pole moves further into the LHP, while for an increase of length the right-most pole moves towards the imaginary axis. The same holds for the closed loop with the industrial controller. The closed-loop system controlled with the low-gain controller even has an unstable equilibrium in case 15 or more pipe sections are added to the drill-string. This follows from the fact that in these cases the right-most pole moves into the RHP, as can be seen in Figure 4.18.

As mentioned before, the location of the eigenvalue is not the only important factor, as local asymptotic stability does not imply that no stick-slip vibrations occur. Clearly, SoftTorque locally asymptotically stabilizes the system, but stick-slip oscillations still occur. Therefore, the  $\mathcal{H}_\infty$ -norm of the bit-mobility ( $G_{cl}$ ) is also shown. The  $\mathcal{H}_\infty$ -norm of the closed-loop bit-mobility with the  $\mathcal{H}_\infty$ -controllers is approximately a factor 4 to 8 lower than the  $\mathcal{H}_\infty$ -norm of  $G_{cl}$  with the industrial controller (see also Figure 4.8 for the nominal case). This indicates that the  $\mathcal{H}_\infty$ -controllers have significantly more robustness with respect to bit-rock interaction variations than the industrial controller and are therefore able to stabilize the desired setpoint (and avoid stick-slip vibrations) as shown in the previous simulations, while the industrial controller is unable to do so.

Changing the length of the drill-string with a few pipe sections does not have a large effect on the pole locations and  $\mathcal{H}_\infty$ -norm as can be seen in Figure 4.18. However, when 15 or more pipe sections are added to the drill-string the system controlled with the low-gain controller has an unstable equilibrium point, i.e. the right-most pole lies in the RHP. Simulation results indeed show that the controller is unable to stabilize the desired setpoint in these cases. For a drill-string system with 15 or more pipe sections added to the drill-string the  $\mathcal{H}_\infty$ -norm of the system controlled with the low-gain controller seems to vary, this is caused by the fact that peak values at other frequencies become dominant in the bit-mobility. To be more precise, generally speaking the third mode (around  $f_3 = 0.53$  Hz) is dominant in the bit-mobility, as can also be seen in Figure 4.8 for the nominal model. However, for the case with  $15 \times 9$  m drill pipe added to the drill-string a peak around the fifth eigenmode (at approximately 1.03 Hz) is dominant and when  $21 \times 9$  m drill pipe is added to the drill-string a peak around



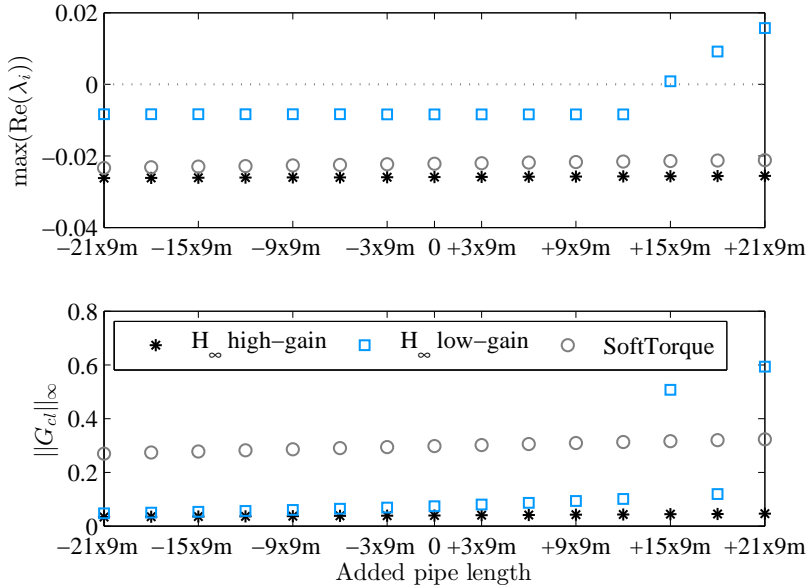


Figure 4.18: Location of the right-most pole of the closed-loop system and  $\mathcal{H}_\infty$ -norm of the bit-mobility as function of added pipe length to the drill-string.

the fourth eigenmode (at approximately 0.74 Hz) is present. This shows that due to the changing dynamics of the drill-string caused by the changing length of the drill-string some peaks in the bit-mobility arise due to a mismatch in frequencies at which the controller tries to damp certain modes. In these cases it is even possible that certain modes are amplified instead of damped, resulting in higher peaks in the bit-mobility at these frequencies compared to the open-loop case.

For the high-gain controller, on the other hand, the right-most pole is still in the LHP and the  $\mathcal{H}_\infty$ -norm is only slightly increased when the length of the drill-string is increased. A simulation result of a plant model that is 189 m ( $21 \times 9$  m) longer than the nominal model (which has a total length of 6249 m) and controlled with the high-gain  $\mathcal{H}_\infty$ -controller, is shown in Figure 4.19. This simulation confirms that the desired equilibrium is indeed stable with this controller. This means that this controller is able to stabilize the desired setpoint of drill-string systems for a large variation in length of the drill-string. It can be concluded that a significant increase in robustness with respect to increasing drill-string length is obtained compared to the industrial controller.

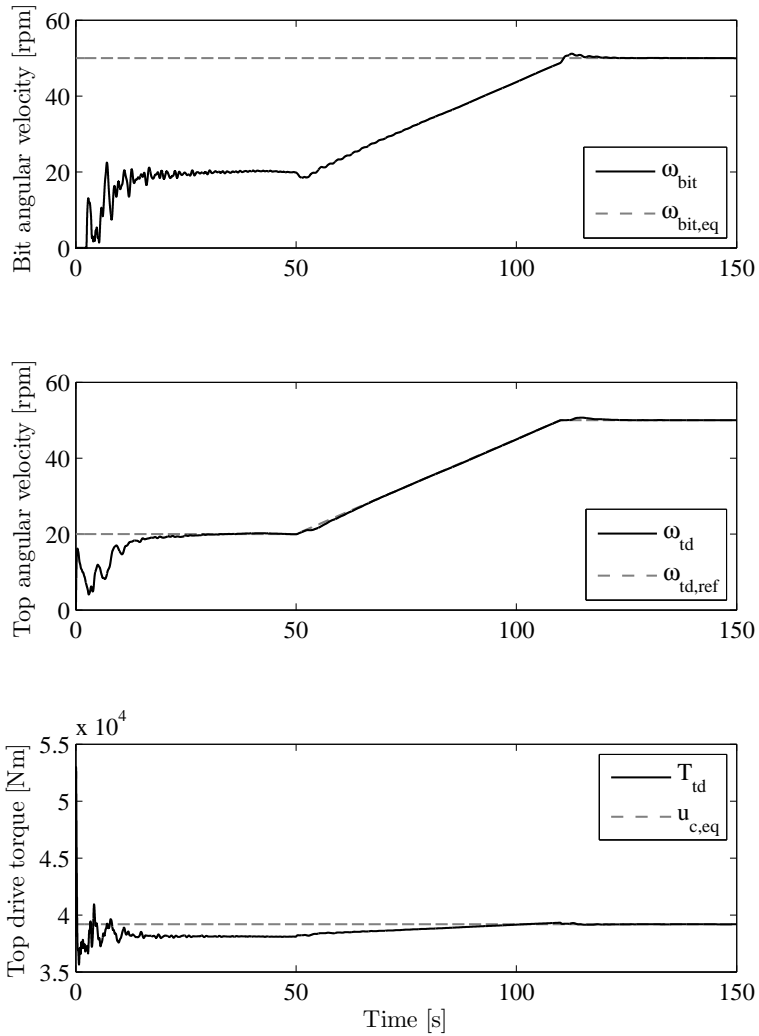


Figure 4.19: Simulation result of the drill-string model in the startup scenario with the high-gain controller and a drill-string model with increased length ( $21 \times 9$  m added drill pipe).

## 4.8 Summary

In this chapter, a synthesis strategy for controllers aiming at the mitigation of torsional stick-slip oscillations in drilling systems is proposed. The controller design is based on skewed- $\mu$  DK-iteration, and offers several benefits over existing controllers. First, the designed controller is applicable to a multi-modal drill-string model while guaranteeing (local) stability of the desired operating point. Second, the controller is optimized to have robustness with respect to uncertainty in the bit-rock interaction. Third, performance specifications regarding measurement noise sensitivity and actuator limitation are integrated in the controller design. Fourth, the controller uses only surface measurements, which is a requirement from practical point of view. Simulation results of the proposed controller applied to the 18-DOF drill-string model show that the stick-slip oscillations are eliminated, while a simulation of an existing industrial controller, under the same conditions, shows stick-slip vibrations. Stability of the nonlinear closed-loop system is also investigated and conditions on the bit-rock interaction, in terms of a sector bound, for which the desired equilibrium is locally asymptotically stable, have been derived.

From a practical point of view, several robustness aspects have been investigated. An important property of the proposed controller design strategy is that the controllers can be tuned based on both robustness and performance specifications. The robustness of the designed controllers is investigated by means of several simulation studies. A significant increase in the operating envelope of the drill-string system is achieved, both in terms of angular velocity and increasing length of the drill-string. Moreover, the proposed controller can effectively deal with sensor and actuator noise due to the fact that a roll-off filter can be easily incorporated in the controller. Another aspect that is investigated is robustness with respect to uncertainty in the bit-rock interaction. Simulation results have shown that a sudden change in the bit-rock interaction can be dealt with and the integral action in the controller enables to compensate for a steady-state offset in the desired angular velocity.

Summarizing, it can be concluded that the proposed controller can effectively deal with practical drilling conditions and it outperforms currently used industrial controllers in terms of the operating envelope for which stick-slip oscillations can be eliminated.

# Design of an experimental drill-string setup

---

## 5.1 Introduction

In this chapter, the design of an experimental drill-string system is presented. This system is designed to represent the dominant dynamics of an oil-field drill-string system that exhibits torsional vibrations while drilling at certain depths. With the development and use of such an experimental drill-string system an improved understanding on the dynamical phenomena that occur while drilling can be obtained. Moreover, this system is used as an experimental benchmark system for the implementation of the controllers designed in Chapters 3 and 4.

The motivation for the development of an experimental drill-string system is twofold. First, such an experimental drilling system can help in understanding the dynamical phenomena that play a role in the onset of torsional stick-slip vibrations. Second and most importantly, the experimental setup can be used for the experimental validation of the proposed controller design strategies and serve as an intermediate step towards field implementation of the controllers on a real rig. The latter is often not directly possible due to the high costs involved in testing on a real rig and the uncertainty and disturbances present in real-life drilling. Moreover, using the experimental setup, controllers can be extensively tested in different scenarios to validate the robustness of the controller design strategies, before implementing the controller on a real rig.

Because of the high costs involved in testing on a real rig, experimental setups to represent the drilling dynamics used for multiple purposes can be found in literature and some examples are mentioned here (see [85] for a more comprehensive overview). In [77], an experimental 2-DOF drill-string system is used

for the analysis of friction-induced stick-slip limit cycles. The same setup is used in [19] for experimental validation of an observer-based output-feedback controller. In [56], an experimental setup is developed that can emulate various excitation mechanisms of the drill-string, including stick-slip, well-borehole contact, and drilling fluid interaction. The aforementioned test rigs both use brake systems to implement bit-rock interaction laws. A different approach is taken in [60], in which an experimental setup to explore stick-slip phenomena is used that involves real cutting using a bit. In [119], an experimental setup is used to investigate whirling effects in drilling systems and it involves both torsional and lateral dynamics. Another example of the experimental validation of a controller design approach for torsional vibrations in drilling systems can be found in [72]. Also for the testing of down-hole tools experimental setups are used as a stepping stone towards implementation of the technique. For example, experimental results of the Resonance Enhanced Drilling (RED) technology are presented in [124] and in [91] an experimental setup to investigate the Anti Stick-slip Tool (AST) is shown.

The need for a new setup stems from the fact that the controllers proposed in this thesis focus on the robustness with respect to multiple dominant torsional flexibility modes in the drill-string dynamics. To investigate this robustness it is important that the experimental setup represents such a drilling system with multiple dominant flexibility modes (in contrast to e.g. [77, 119] where setups with a single flexibility mode are considered). Moreover, existing setups often use mechanical brakes (see e.g. [77]) to model the bit-rock interaction. With these systems it is difficult to implement different bit-rock interaction models. In this work, a motor is used to generate the resisting torque at the bit-rock interface such that different types of bit-rock interaction models can be implemented.

The outline of this chapter is as follows. In Section 5.2, the model of the experimental drill-string setup is discussed and the steps that are taken to develop this model based on a model of a realistic drilling system. Next, in Section 5.3 the design of the setup is presented and the different components are discussed in more detail. Finally, a summary is given in Section 5.4.

## 5.2 Modelling of the dynamics of the drill-string setup

A finite-element method (FEM) model of a realistic drilling system is used as basis for the design of the experimental drill-string setup. The model is based on an offshore jack-up drilling rig to reach reservoir sections at depths of  $>6000$  m. The rig is equipped with an AC top drive and fitted with a modern SoftTorque system [64]. When drilling those deep wells, stick-slip vibrations have been observed in the field for this drilling system. This motivates the use of this drill-string model as basis for the development of the lab-scale drill-string setup. A

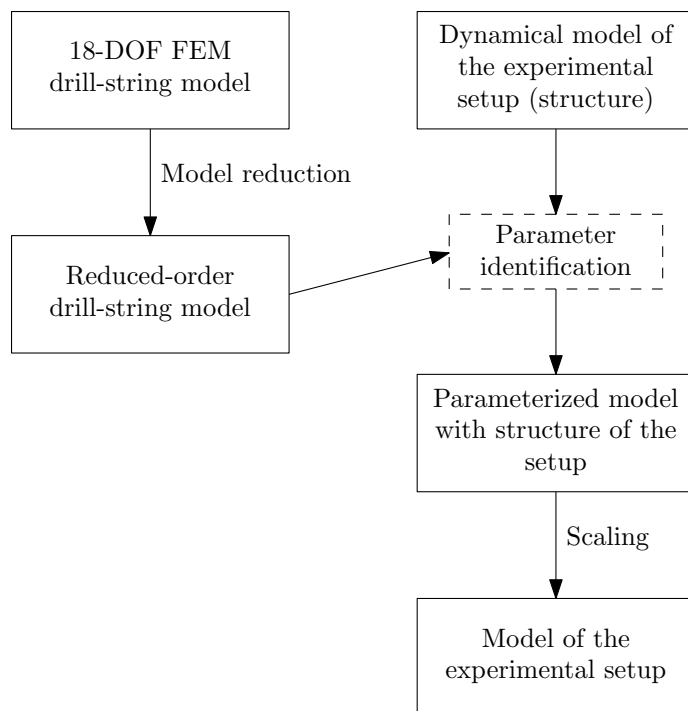


Figure 5.1: Overview of the different steps in developing a model to be used as a basis for the design of the experimental setup.

detailed description of the FEM model is given in Section 2.3. Here, the focus is on the steps that are taken to develop a model of the experimental setup based on this 18-DOF FEM model. These steps are summarized in Figure 5.1 and are discussed in more detail in the following sections. In Section 5.2.1, the model reduction strategy that is used to obtain a reduced-order drill-string model is discussed. Next, the model of the experimental setup is explained in more detail in Section 5.2.2 and the identification approach to obtain the parameters for this model based on the reduced-order model is given in Section 5.2.3. Since it is impossible to scale down an oil-field drill-string to a lab-scale setup that still exhibits the main (torsional) dynamics we aim to study, we propose a model with 4 rotating discs, coupled with (steel) strings as shown in Figure 5.2. It is important to mention that the proposed model of the experimental setup has a specific structure due to the mechanical elements (i.e. inertias and springs) that are used in the setup resulting in a lumped parameter model, while on the other hand the reduced-order drill-string model does not have such specific structure. The identified parameters of the obtained model are still in the same order of

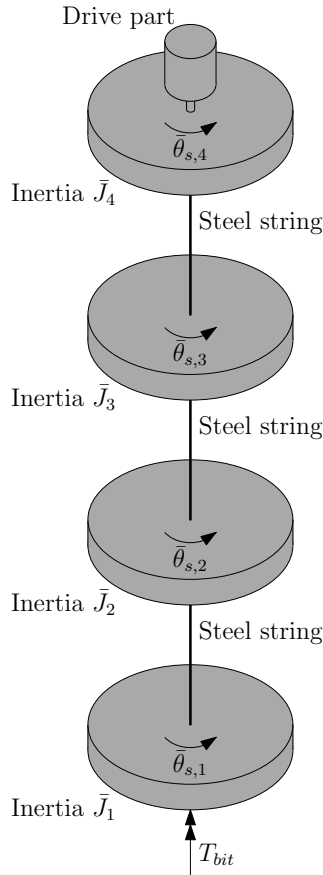


Figure 5.2: Schematic representation of a model with four discs.

magnitude as the original drill-string model (e.g. inertia and stiffness properties of the system as a whole are still in the same order of magnitude and are hence not (yet) scaled). As a consequence, the representative torsional velocity and torque levels of the setup match those of a real drill-string system. Therefore, as a next step the parameters are scaled to obtain suitable torque levels and velocities for a lab-scale drill-string setup, but also to obtain feasible inertias and stiffnesses for the lab-scale system. This scaling procedure is discussed in Section 5.2.4.

### 5.2.1 Reduced-order model

The FEM model presented in Section 2.3 has 18 degrees of freedom. For the design of the setup we rely on a reduced-order model. The purpose of this reduced-order model is to approximate the higher-order FEM model with a reduced number of states, while still preserving the key dynamic system properties. As mentioned before, models with multiple flexibility modes (i.e. with more than 2-DOF) are considered, because field observations have revealed that also higher flexibility modes of the drill-string play a role in the onset of stick-slip vibrations [82]. As mentioned in Section 2.3.1, the first three resonance modes, with resonance frequencies at  $f_1 \approx 0.15$ ,  $f_2 \approx 0.38$  and  $f_3 \approx 0.53$  Hz, are dominant in the drill-string dynamics (see Figures 2.8-2.9). Therefore, a drill-string model with at least 4 degrees of freedom is considered to enable accurately capturing those first three modes and the rigid body mode by the reduced-order model.

For the design of the experimental setup we would like to accurately approximate the torsional flexibility modes of the drill-string system associated with the lowest resonance frequencies. Therefore, an eigenmode based reduction strategy is used, also known as the mode displacement method (see e.g. [36]). Recall the equation of motion for the 18-DOF drill-string system (2.1), that is

$$M\ddot{\theta} + D\dot{\theta} + K_t\theta_d = S_w T_w(\dot{\theta}) + S_b T_{bit}(\dot{\theta}_1) + S_t T_{td}. \quad (5.1)$$

Now let us consider the undamped (and unforced) drill-string system and in addition consider the stiffness in terms of the absolute positions  $\theta = [\theta_1 \cdots \theta_m]^\top$  instead of the difference in angular position  $\theta_d$ , hence

$$M\ddot{\theta} + K\theta = 0. \quad (5.2)$$

Then, the mode displacement method is based on the free vibration modes of these structural dynamics. This leads to the following generalized eigenvalue problem:

$$[K - \lambda_i^2 M] v_i = 0, \quad (5.3)$$

where  $v_i$  is the mode shape vector corresponding to the eigenfrequency  $\lambda_i$ , with  $i \in [1, \dots, m]$ . The resulting eigenfrequencies are grouped in ascending order, i.e.  $\lambda_1 \leq \lambda_2 \leq \dots \leq \lambda_m$  and the corresponding eigenmodes  $v_1, v_2, \dots, v_m$  are collected in the square ( $m \times m$ ) modal matrix

$$V = [v_1 \ v_2 \ \cdots \ v_m]. \quad (5.4)$$

Using this matrix, we employ the following coordinate transformation to modal coordinates  $\eta$ :

$$\theta = V\eta. \quad (5.5)$$

The general idea of the expansion procedure is to keep the first  $m_r < m$  eigenvectors, that correspond to the lowest eigenfrequencies in the reduced-order model.



Hereto, consider the following transformation matrix

$$T = [v_1 \ v_2 \ \cdots \ v_{m_r}]. \quad (5.6)$$

Using this transformation matrix, (5.5) can be rewritten as

$$\theta = [T \ U] \begin{bmatrix} \theta_r \\ \eta_2 \end{bmatrix} = T\theta_r + U\eta_2 \quad (5.7)$$

where  $U$  contains the truncated eigenmodes, that is the eigencolumns  $m_r + 1$  to  $m$  and  $\eta_2$  contains the states that correspond to these modes; the coordinates preserved in the reduced-order model are defined by  $\theta_r$ . Using (5.1) and (5.7) and projecting the resulting equations of motion on the expansion basis  $T$  results in the following reduced-order dynamics:

$$M_r \ddot{\theta}_r + D_r \dot{\theta}_r + K_r \theta_r = T^\top S_w T_w (\dot{\theta}) + T^\top S_b T_{bit} (\dot{\theta}_1) + T^\top S_t T_{td} \quad (5.8)$$

with  $M_r = T^\top M T \in \mathbb{R}^{m_r \times m_r}$ ,  $D_r = T^\top D T \in \mathbb{R}^{m_r \times m_r}$ ,  $K_r = T^\top K T \in \mathbb{R}^{m_r \times m_r}$  and  $\tilde{\theta} := T\theta_r \in \mathbb{R}^m$  is the estimated (full-order) state based on the reduced-order estimates. We can not expect  $\tilde{\theta}$  to be equal to the original states  $\theta$ , since in the reduction step a part of the original dynamics (related to  $\eta_2$ ) is omitted.

In this work, the case with  $m_r = 4$  is considered, that is we take the rigid body mode and three torsional flexibility modes into account. The relevant frequency response functions of the (linear) drill-string dynamics are shown in Figures 5.3-5.5. These frequency response functions describe the (linear) drill-string dynamics from the relevant inputs (top drive torque and bit-rock interaction torque) to the angular velocity outputs at the top drive and bit, i.e. respectively  $\omega_{td}$  and  $\omega_{bit}$ . As can be seen, the first three eigenmodes are indeed accurately matched by the reduced-order model.

## 5.2.2 Dynamical model of the experimental setup

In this section, the model that is used for the design of the experimental setup, as shown in Figure 5.2, is discussed in more detail. For the model, we will not restrict ourselves to connections between adjacent discs only, but take potential connections between all the discs into account. This is schematically shown in Figure 5.6, where  $k_{ij}$  and  $d_{ij}$  ( $i, j = 1, \dots, 4$ ) are the stiffness and damping factors between the discs, respectively. The coordinates  $\bar{\theta}_s = [\bar{\theta}_{s,1} \ \cdots \ \bar{\theta}_{s,4}]^\top$  represent the angular displacements of the discs. The equations of motion of the system are given by:

$$\bar{M}_s \ddot{\bar{\theta}}_s + \bar{D}_s \dot{\bar{\theta}}_s + \bar{K}_s \bar{\theta}_s = S_{ws} T_{ws} (\dot{\bar{\theta}}_s) + S_{bs} T_{bit} (\dot{\bar{\theta}}_{s,1}) + S_{ts} T_{td} \quad (5.9)$$

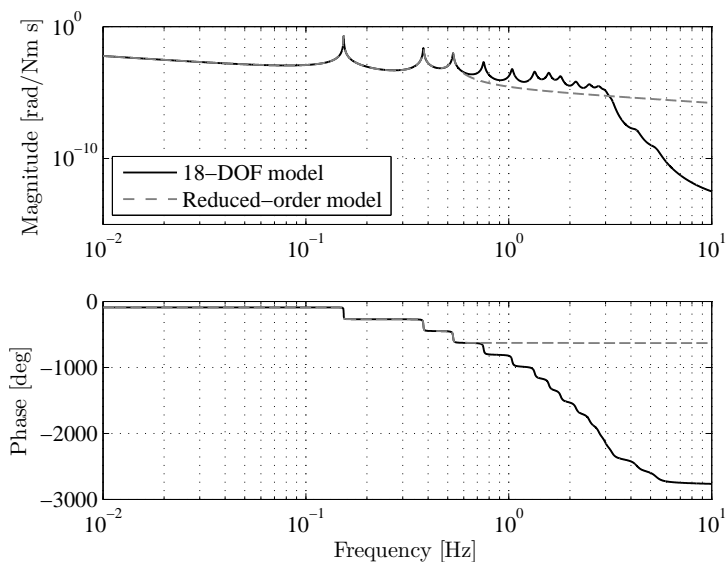


Figure 5.3: Frequency response function of the 18-DOF model and the reduced-order model (based on the mode displacement method) from input torque  $T_{td}$  to bit velocity  $\omega_{bit}$ .

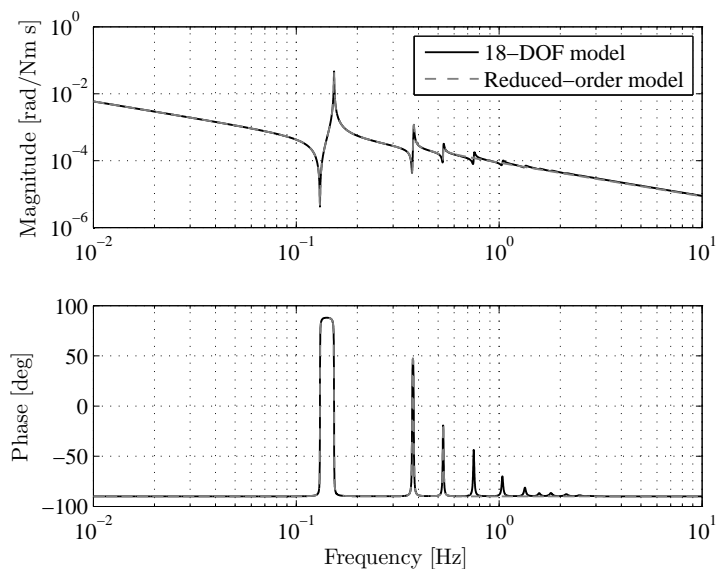


Figure 5.4: Frequency response function of the 18-DOF model and the reduced-order model (based on the mode displacement method) from input torque  $T_{td}$  to top drive velocity  $\omega_{td}$ .

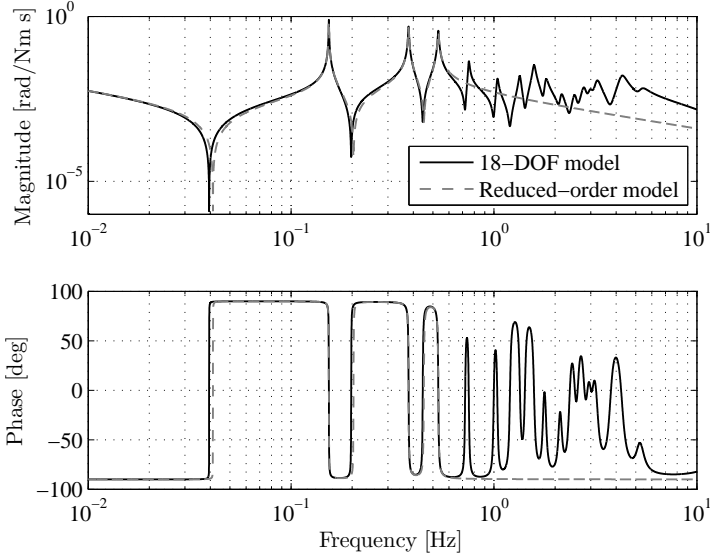


Figure 5.5: Frequency response function of the 18-DOF model and the reduced-order model (based on the mode displacement method) from bit torque  $T_{bit}$  to bit velocity  $\omega_{bit}$ , i.e. bit-mobility.

with

$$\bar{M}_s = \begin{bmatrix} \bar{J}_1 & 0 & 0 & 0 \\ 0 & \bar{J}_2 & 0 & 0 \\ 0 & 0 & \bar{J}_3 & 0 \\ 0 & 0 & 0 & \bar{J}_4 \end{bmatrix} \quad (5.10)$$

$$\bar{D}_s = \begin{bmatrix} \bar{d}_{12} + \bar{d}_{13} + \bar{d}_{14} & -\bar{d}_{12} & -\bar{d}_{13} & -\bar{d}_{14} \\ -\bar{d}_{12} & \bar{d}_{12} + \bar{d}_{23} + \bar{d}_{24} & -\bar{d}_{23} & -\bar{d}_{24} \\ -\bar{d}_{13} & -\bar{d}_{23} & \bar{d}_{13} + \bar{d}_{23} + \bar{d}_{34} & -\bar{d}_{34} \\ -\bar{d}_{14} & -\bar{d}_{24} & -\bar{d}_{34} & \bar{d}_{14} + \bar{d}_{24} + \bar{d}_{34} \end{bmatrix} \quad (5.11)$$

$$\bar{K}_s = \begin{bmatrix} \bar{k}_{12} + \bar{k}_{13} + \bar{k}_{14} & -\bar{k}_{12} & -\bar{k}_{13} & -\bar{k}_{14} \\ -\bar{k}_{12} & \bar{k}_{12} + \bar{k}_{23} + \bar{k}_{24} & -\bar{k}_{23} & -\bar{k}_{24} \\ -\bar{k}_{13} & -\bar{k}_{23} & \bar{k}_{13} + \bar{k}_{23} + \bar{k}_{34} & -\bar{k}_{34} \\ -\bar{k}_{14} & -\bar{k}_{24} & -\bar{k}_{34} & \bar{k}_{14} + \bar{k}_{24} + \bar{k}_{34} \end{bmatrix} \quad (5.12)$$

$$S_{ws} = \begin{bmatrix} 0 & 0 & 0 \\ 1 & 0 & 0 \\ 0 & 1 & 0 \\ 0 & 0 & 1 \end{bmatrix}, \quad S_{bs} = \begin{bmatrix} 1 \\ 0 \\ 0 \\ 0 \end{bmatrix}, \quad S_{ts} = \begin{bmatrix} 0 \\ 0 \\ 0 \\ 1 \end{bmatrix} \quad (5.13)$$

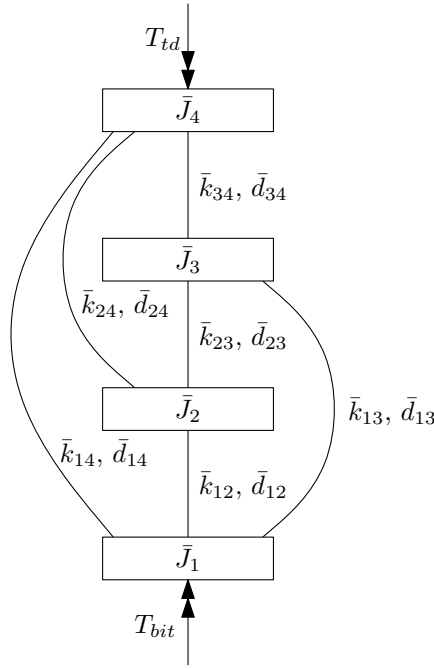


Figure 5.6: Schematic model showing all the connections between the discs.

and the resistive torques at discs 2,3 and 4 to model the borehole drill-string interaction are given by  $T_{ws}$ .

### 5.2.3 Parameter identification

The next step is to determine the parameters of the 4-DOF model of the experimental setup based on the reduced-order model presented in Section 5.2.1. First, the inertias of the 4 discs are determined. The total inertia of the 4-disc setup is chosen to be equal to the total inertia of the original 18-DOF model. In addition, we require the inertia of the upper disc ( $\bar{J}_4$ ) to be equal to the inertia of the top drive, such that the upper disc actually represents the top drive. Doing so, the torque in the string below disc 4 represents the pipe torque that is used as measurement in the linear robust controller approach (Chapter 4). The inertia of the bottom disc ( $\bar{J}_1$ ) is determined based on the “high”-frequency behavior (i.e. above the eigenfrequencies) of the reduced-order model. In other words, the inertia of the bottom disc is chosen such that the bit-mobility of the setup model matches the bit-mobility of the reduced-order model at high frequencies. The

remaining part of the total inertia is equally distributed over the two remaining discs. The remaining parameters, i.e. damping and stiffness parameters, are determined using an optimization approach. The objective of the optimization procedure is to find the model parameters such that the difference in the complex plane between the frequency response function of the reduced-order model and the model of the setup is minimized over all frequencies in the frequency range of interest. Hence, we seek to solve the following optimization problem:

$$\min_{p \in [\underline{p}, \bar{p}]} J(p), \quad (5.14)$$

where  $p := [\bar{k}_{12} \bar{k}_{23} \bar{k}_{34} \bar{k}_{13} \bar{k}_{14} \bar{k}_{24} \bar{d}_{12} \bar{d}_{23} \bar{d}_{34} \bar{d}_{13} \bar{d}_{14} \bar{d}_{24}]$  are the parameters of the setup to be determined,  $\underline{p}$  and  $\bar{p}$  a lower and upper bound for the parameters and the objective function  $J(p)$  is given by

$$J(p) = \sum_{\omega_l} w(j\omega) \left( |W(j\omega)H_r^{T_{td}\omega_{bit}}(j\omega) - W(j\omega)H_s^{T_{td}\omega_{bit}}(j\omega)|^2 \right) \quad (5.15)$$

with  $H_r^{T_{td}\omega_{bit}}$  and  $H_s^{T_{td}\omega_{bit}}$  the frequency response functions from top drive torque input to bit velocity output of the reduced-order model and the setup model, respectively. The frequency response function from top drive torque input to bit velocity output is chosen for the parameter identification because it captures the relevant dynamics of the drilling system that should be represented in the setup. Note that  $H_s^{T_{td}\omega_{bit}}$  depends on the parameters  $p$ . The frequency grid  $\omega_l$  is a discrete grid of frequencies between 0.05 and 6 Hz, because that is the relevant frequency range of the reduced-order drill-string dynamics (see Figure 5.3). The frequency-dependent weighting filter  $W(j\omega)$  is chosen to be

$$W(j\omega) = J_{tot}j\omega, \quad (5.16)$$

to compensate for the negative slope of the frequency response function from top drive torque input to bit velocity output. The (scalar) multiplication factor  $w(j\omega)$  in (5.15) is used to give extra weighting in specific frequency ranges. This multiplication factor is equal to 1.5 for  $0.14 < f < 0.165$  (i.e. around the first resonance frequency), equal to 2 for  $0.5 < f < 0.57$  (i.e. around the third resonance frequency) and equal to 1 for all other frequencies.

The results of the fitting procedure are shown in Figures 5.7-5.9. In these figures, the same frequency response functions are shown as in Figures 5.3-5.5, however, now with the addition of the frequency response functions associated with the setup model with the identified parameters. Note that these parameters are still in the same order of magnitude as for the original drill-string model. For example, the inertia of the upper disc is equal to the inertia of a real top drive (i.e. approximately 1800 kgm<sup>2</sup>) and a driving torque at the top drive is typically in the order of 40 kNm. These settings and especially the high torque levels are infeasible for a lab-scale setup. Therefore, scaling of the parameters

in order to obtain feasible dimensions for the lab-scale setup is discussed in Section 5.2.4. It turned out that it is not possible to fit the reduced-order model of the original drill-string with model of the setup exactly. This is mainly caused by the fact that in the finite-element model (and therefore also in the reduced-order model) the mass properties of the drill-string are distributed along the drill-string, whereas the model of the setup is based on a lumped mass approach (i.e. multiple discs). This is particularly visible in Figure 5.7: due to the lumped inertias of the setup model the slope of the magnitude of the FRF decreases with 2 (on a loglog-scale) after each resonance peak and the phase decreases with 180 degree (due to the 2 poles associated with the resonance). However, the FRF's of the 18-DOF and reduced-order model do not show this behavior, this is caused by zeros of these models that are in the right-half-plane of the complex plane (i.e. non-minimum phase). Nevertheless, a satisfactory match of the dominant resonances is achieved and, moreover, simulation results of the setup model (see Figure 5.10) confirm that the response of the setup model is in good correspondence to the response of the reduced-order model and the original 18-DOF FEM model. In Figure 5.10, the response of the 18-DOF drill-string model (as already shown in Figure 2.14) is compared with the response of the 4-DOF setup model. In both simulations, the system is controlled with a SoftTorque controller (see (3.22) and the parameters  $c_t = 1829$  and  $k_t = 1177$ ) and the desired angular velocity is equal to 50 rpm. As can be seen, the response of the setup model is very similar to the response of the original FEM model. This illustrates that the dominant dynamics of the original 18-DOF model is captured by the 4-DOF setup model.

### 5.2.4 Scaling of the drill-string model

An identified set of parameters for the experimental setup has been obtained in the previous section. However, these parameters are based on a full-scale drilling rig and, as mentioned before, such parameter values are infeasible for a lab-scale experimental setup. To obtain feasible parameter values for the experimental setup, a scaling of the variables and parameters is in order, while retaining the resonance frequencies of the drill-string system. Therefore, two scaling factors are introduced:  $c_1$  is used to scale the torque level and  $c_2$  to scale the states of the system. The states are scaled according to:

$$\theta_s = \frac{1}{c_2} \bar{\theta}_s \quad (5.17)$$

and the equations of motion are pre-multiplied with a factor  $\frac{1}{c_1}$  to scale the torque level. This results in the following (scaled) equations of motion given by:

$$M_s \ddot{\theta}_s + D_s \dot{\theta}_s + K_s \theta_s = S_{ws} \hat{T}_{ws}(\dot{\theta}_s) + S_{bs} \hat{T}_{bit}(\dot{\theta}_{s,1}) + S_{ts} \hat{T}_{td} \quad (5.18)$$

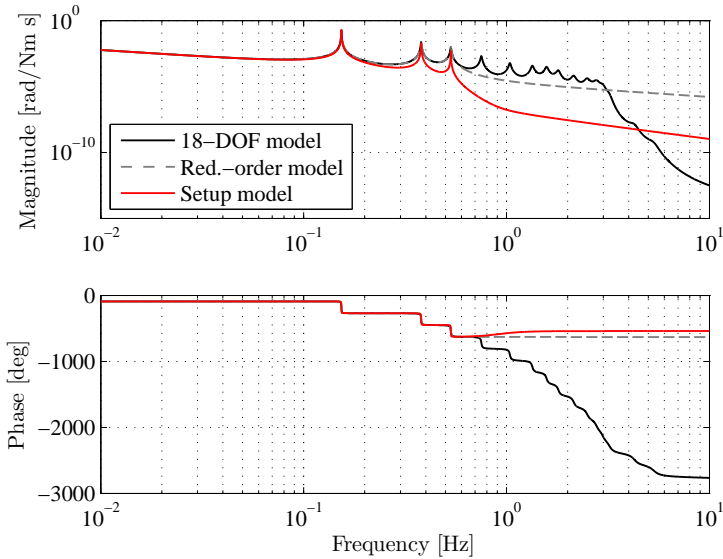


Figure 5.7: Frequency response function of the 18-DOF model, the reduced-order model and the setup model with the identified parameters from input torque  $T_{td}$  to bit velocity  $\omega_{bit}$ .

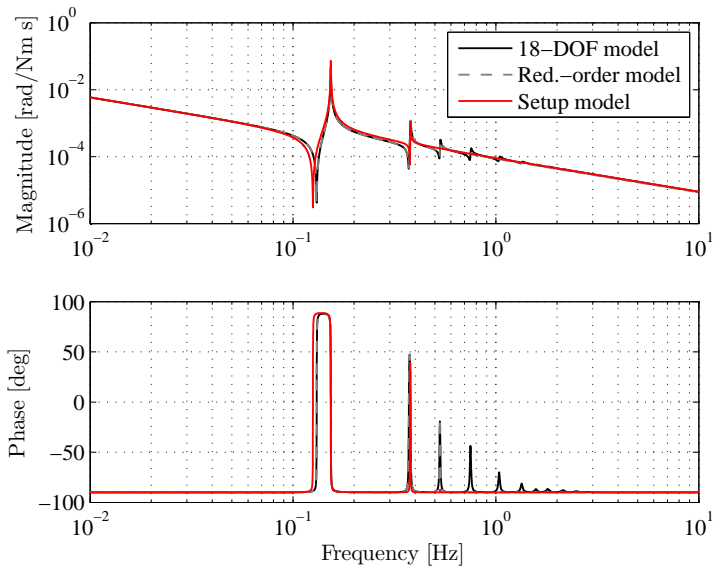


Figure 5.8: Frequency response function of the 18-DOF, the reduced-order model and the setup model with the identified parameters from input torque  $T_{td}$  to top drive velocity  $\omega_{td}$ .

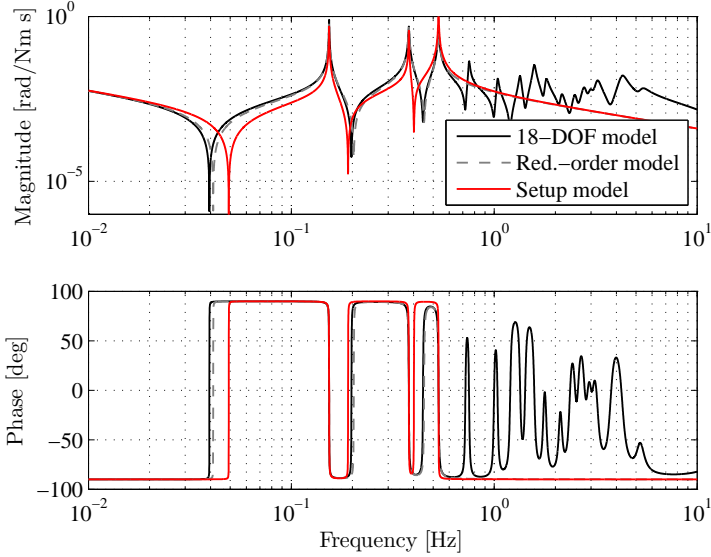


Figure 5.9: Frequency response function of the 18-DOF, the reduced-order model and the setup model with the identified parameters from bit torque  $T_{bit}$  to bit velocity  $\omega_{bit}$ , i.e. bit-mobility.

with  $M_s := \frac{c_2}{c_1} \bar{M}_s$ ,  $D_s := \frac{c_2}{c_1} \bar{D}_s$ ,  $K_s := \frac{c_2}{c_1} \bar{K}_s$ ,  $\hat{T}_{ws} := \frac{1}{c_1} T_{ws}$ ,  $\hat{T}_{bit} := \frac{1}{c_1} T_{bit}$  and  $\hat{T}_{td} := \frac{1}{c_1} T_{td}$ . The scaled bit-rock interaction torque  $\hat{T}_{bit}$  is given by the following scaled law:

$$\hat{T}_{bit}(\hat{\theta}_{s,1}) \in \text{Sign} \left( \hat{\theta}_{s,1} \right) \left( \hat{T}_d + \left( \hat{T}_s - \hat{T}_d \right) e^{(-30|\hat{\theta}_{s,1}|)/(\hat{N}_d \pi)} \right) \quad (5.19)$$

with  $\hat{T}_d = \frac{1}{c_1} T_d$ ,  $\hat{T}_s = \frac{1}{c_1} T_s$  and  $\hat{N}_d = \frac{1}{c_2} N_d$  and the scaled drill-string borehole interaction torques can be written as

$$\hat{T}_{ws,i} \in \hat{T}_{s,i} \text{Sign} \left( \hat{\theta}_{s,i} \right), \quad \text{for } i = 2, \dots, m, \quad (5.20)$$

where  $\hat{T}_{s,i} = \frac{1}{c_1} T_{s,i}$ . The scaling factors are determined to be  $c_1 = 6250$  and  $c_2 = 10$ . This scaling is chosen to, first, obtain feasible torque levels for typical motors that can be used in lab-scale systems (mainly influenced by  $c_1$ ) and, second, to achieve angular position differences between adjacent discs that are sufficiently small to avoid plastic deformation of the steel strings between those discs. The latter aspect of course also depends on the length and diameter of the strings, which need to have feasible dimensions. The scaled parameters are summarized in Table 5.1, the scaled parameters regarding the interaction torques are given in Table 5.2. As can be seen, for example the static torque  $T_s$ , which is



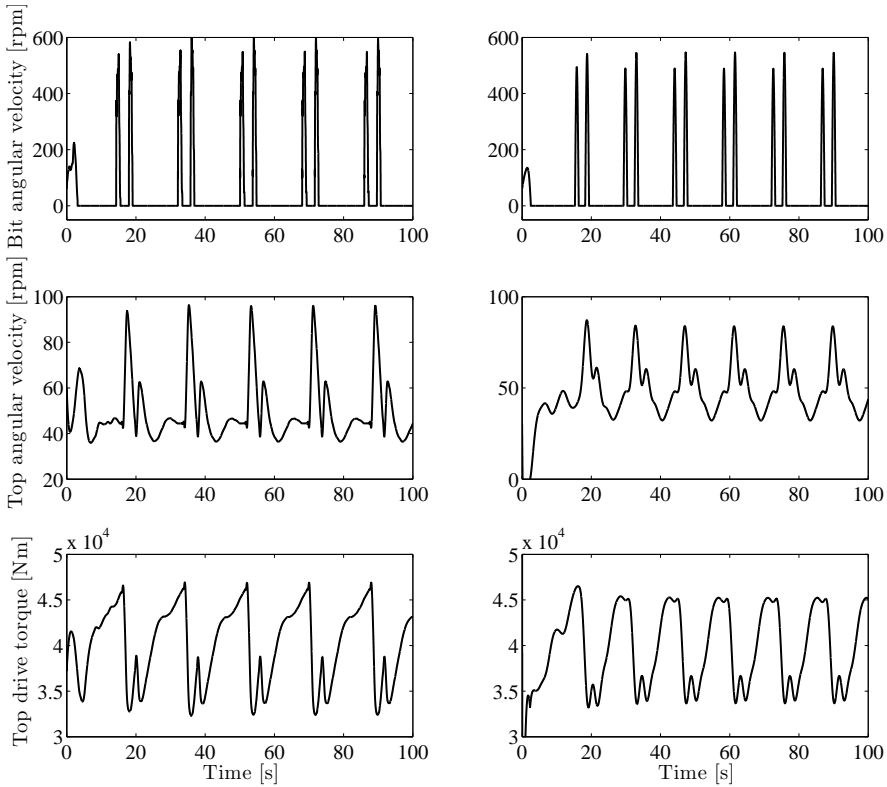


Figure 5.10: Simulation result of the 18-DOF drill-string model (left-hand side) compared with a simulation result of the 4-DOF model of the experimental setup (right-hand side).

equal to 7700 Nm for the original system is equal to  $7700/6250 = 1.232$  Nm for the lab-scale system. The top drive torque is in the order of 40 kNm for the full scale system, whereas this is scaled to approximately 6.4 Nm for the setup and since the states are scaled with a factor 10, a desired angular velocity of 50 rpm in practice is equal to a desired angular velocity of 5 rpm on the setup. Note that only the torque levels and states are scaled, while there is no time-scaling applied. This means that the resonance frequencies of the system have not been changed.

By applying the described scaling, the model of the experimental drill-string setup is scaled to feasible dimensions to design a lab-scale setup. With the method described in this section, a set of prescribed model parameters is obtained for the design of the setup. The setup design is discussed in more detail in the next section.

Table 5.1: Parameters of the setup model.

| Symbol | Value<br>[kgm <sup>2</sup> ] | Symbol   | Value<br>[Nm/rad] | Symbol   | Value<br>[Nms/rad] |
|--------|------------------------------|----------|-------------------|----------|--------------------|
| $J_1$  | 0.064                        | $k_{12}$ | 0.630             | $d_{12}$ | 0                  |
| $J_2$  | 0.708                        | $k_{23}$ | 1.799             | $d_{23}$ | 0.0018             |
| $J_3$  | 0.708                        | $k_{34}$ | 1.097             | $d_{34}$ | 0.0024             |
| $J_4$  | 2.845                        | $k_{13}$ | 0                 | $d_{13}$ | 0                  |
|        |                              | $k_{14}$ | 0                 | $d_{14}$ | 0.0005             |
|        |                              | $k_{24}$ | 0                 | $d_{24}$ | 0                  |

Table 5.2: Parameters of the scaled bit-rock interaction model and drill-string borehole interaction torques.

| Symbol      | Value     | Symbol          | Value    |
|-------------|-----------|-----------------|----------|
| $\hat{T}_s$ | 1.232 Nm  | $\hat{T}_{s,2}$ | 2.297 Nm |
| $\hat{T}_d$ | 0.272 Nm  | $\hat{T}_{s,3}$ | 3.038 Nm |
| $\hat{N}_d$ | 0.5 rad/s | $\hat{T}_{s,4}$ | 0.662 Nm |

### 5.3 The experimental drill-string setup

The experimental setup is designed to be adjustable and modular. In particular, it is designed such that it should be possible to change the inertia of the discs, the stiffness of the strings and, by using a hardware-in-the-loop approach, also other parameters such as damping can be adjusted. With this hardware-in-the-loop approach, additional dynamics is emulated in software and implemented using the motors driving the discs. In addition, the setup is designed such that it is possible to investigate a system with additional flexibility modes by adding an extra disc to the setup. A schematic overview of the setup is shown in Figure 5.11. The mechanical and electrical design of the setup is developed by Hittech Multin BV, Shell and TU/e in a collaborative effort.

Let us now discuss the design of the setup in more detail. The total setup is 5 m tall and has a footprint of  $1 \times 1$  m. As can be seen in Figure 5.11(a), the setup has 4 disc platforms to support the 4 discs of the model (see Figures 5.11(b) and 5.11(c), note that the bottom disc platform is slightly different, which is explained in more detail later). These discs are interconnected by steel strings to represent the torsional stiffness of the drill-string system and each disc is equipped with a motor. For the top disc, this motor is used to drive the system and to apply the desired control action. At the bottom disc the motor is used to emulate the desired bit-rock interaction and at the intermediate discs the drill-string borehole interaction torques are implemented using these motors. In addition, these motors are used to emulate the hardware-in-the-loop compo-

nents, such as damping torque associated with the damping constant  $d_{14}$ , and to compensate for undesired effects, such as friction and cogging in the motors. Each of the motors is equipped with an encoder and the setup contains three torque sensors to measure the torques in the interconnecting strings. Furthermore, a DS1103 controller board from dSPACE [28] is used as real-time control and data acquisition platform. A picture of the lab-scale drill-string system is shown in Figure 5.12.

The three upper disc platforms are identical and equipped with Georgii Kobold KTY-F torque motors [35]. These are flat direct-drive brushless DC motors with a maximum torque of 26 Nm and a maximum angular velocity of 250 rpm. To actuate and control these motors, Siep & Meyer SD2S motor amplifiers [105] are used and to measure the angular position of the discs built-in 19 bit Heidenhain ECI 119 inductive encoders [45] are used. These encoders use an excitation coil to produce a magnetic flux and induce a current via the magnetic field in the receiving coils. Rotating the disc changes the magnetic field, which is measured by the receiving coils [101]. The 19 bit encoder signal is converted in the motor amplifiers to a 15 bit quadrature signal that is used by the dSPACE system to determine the angular position of the discs. The angular velocities of the discs are determined by numerical differentiation of the angular positions measured by the encoders. The discs have a inertia of approximately  $0.350 \text{ kgm}^2$ , including the inertia of the motor. By adding additional masses at a certain radius on the discs, the inertia of the discs can be adjusted (in steps of approximately  $0.05 \text{ kgm}^2$ ) to obtain the desired inertia as specified in Table 5.1.

The bottom disc platform is shown in Figure 5.13 and is different from the other platforms. This difference has two main reasons; first, the specified inertia of the bottom disc is much lower compared to the inertias of the other discs and, second, to accurately implement the desired bit-rock interaction law it is important that this disc has a low static friction. To realize these two aspects, a disc with a smaller diameter and a different type of motor is used. The installed motor is a brushed DC motor from Printed Motor Works (type: GN16RE) [89] with a maximum torque of 2.55 Nm and a maximum angular velocity of 3000 rpm. The static friction in this motor is approximately 0.05 Nm which is sufficiently lower than the dynamic torque level  $\hat{T}_d$  to be implemented (see Table 5.2). In addition, a 16 bit Sick DFS60A incremental encoder [104] is used together with a Copley Controls Xenus Plus motor amplifier (type: XTL-230-40) [17]. The bottom disc has an inertia of approximately  $0.03 \text{ kgm}^2$  and can be adjusted in steps of approximately  $0.01 \text{ kgm}^2$  to achieve the prescribed inertia.

To represent the torsional stiffness of the drill-string model, steel strings with a specific length and diameter are used. The length and diameter are chosen such that the prescribed stiffnesses (see Table 5.1) are achieved while keeping in mind typical differences in angular position of adjacent discs such that the strings are not plastically deformed. The specified damping factors are obtained by implementing the damping using the motors (i.e. in a hardware-in-the-loop

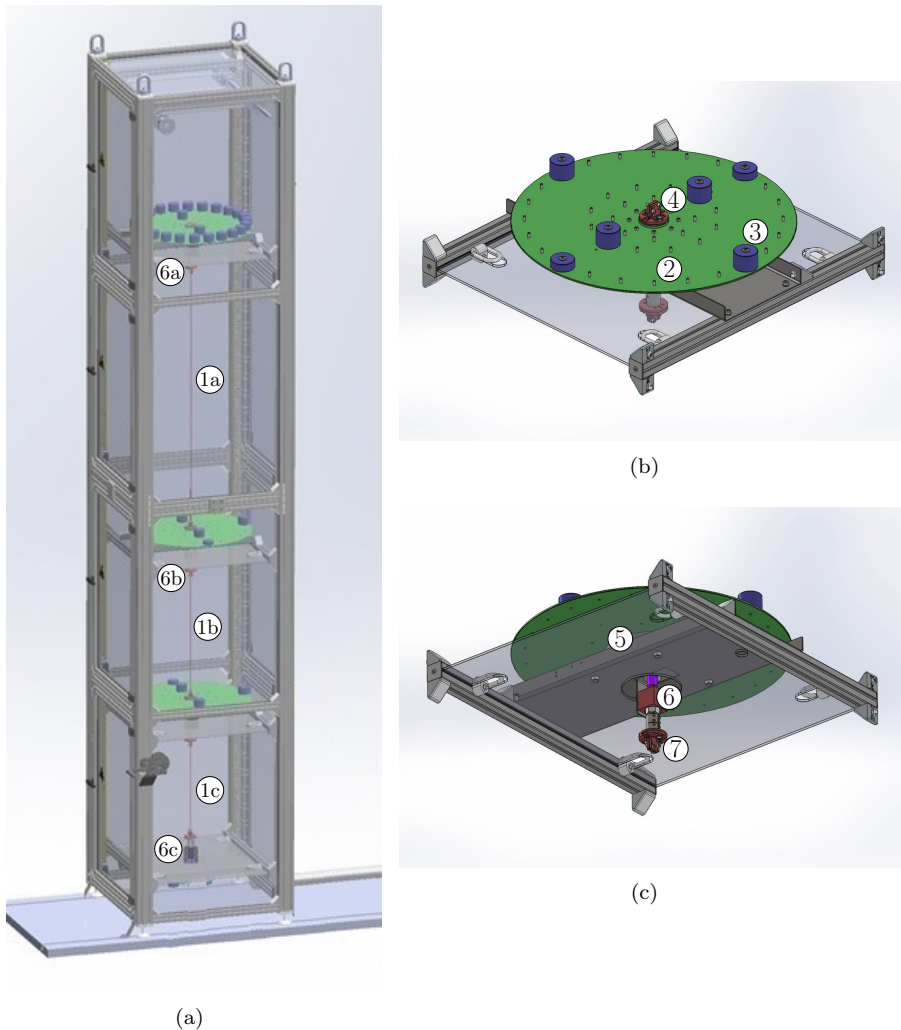


*Figure 5.11:* Schematic representation of the experimental drill-string setup. (a) is an overview of the setup, (b) is a top view on one of the disc platforms, (c) is a bottom view of one of the disc platforms. Different parts are numbered as follows; 1: (steel) strings between the different discs, 2: disc (representing inertia), 3: additional masses to change the inertia of the disc, 4: upward connection for the string, 5: flat hollow shaft torque motor (embedded in the frame), 6: torque sensors, 7: downward connection for the string.



Figure 5.12: The experimental drill-string setup.

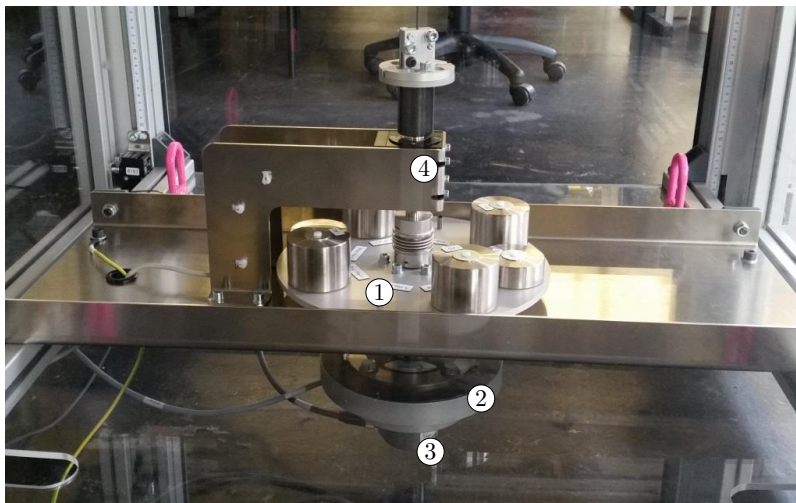


Figure 5.13: Bottom disc platform, with 1: the disc with additional weights, 2: the motor, 3: the encoder, 4: the torque sensor.

fashion) based on the measured difference in angular velocity of the discs, while compensating for the material damping that is already present in the strings.

The setup is also equipped with three PCM TQ-RT2A-25NM torque sensors [87]. These sensors can measure up to 25 Nm with an accuracy of  $\pm 0.2\%$ . The torque sensors are placed below the upper two discs and just above the bottom disc, as indicated in Figure 5.11(a) with 6a-c. The torque sensor below the top drive disc will be used for the pipe torque measurement.

From the foregoing description of the experimental setup it becomes clear that the setup is equipped with multiple sensors, i.e. encoders in all the discs to measure the angular position (and determine the angular velocity) and three torque sensors to measure the torques in the steel strings between the discs. However, the control design strategies presented in Chapters 3 and 4 only require surface measurements. The extra sensors, which are not required for the proposed control strategies, are important for multiple reasons. Firstly, these sensors are used for parameter identification and validation of the setup dynamics. Secondly, these sensors can be used for analyses of the obtained experimental results. Thirdly, although this is not directly practically relevant, these sensors can also be used for feedback in the controllers. For example, to validate the state-feedback control strategy of Chapter 3, which requires measurements of all the states of the system, or in order to investigate the effect of additional measurements for the output-feedback controllers.

## 5.4 Summary

In this chapter, the design of the experimental setup is discussed. First, a model of the experimental setup, based on the 18-DOF FEM drill-string model, is presented. The 4-DOF setup model is designed such that it represents the dominant dynamics of the dynamics of an oil-field drill-string system that exhibits torsional vibrations while drilling at certain depths. The model of the experimental drill-string setup is scaled (i.e. states and torque levels are scaled) to feasible dimensions in support of the design of the lab-scale setup. With this scaling, the time-scales of the system have not been changed, such that the resonance frequencies are equal to the resonance frequencies of the original model. Finally, the mechanical and electrical design of the designed setup is presented in detail.

# Experimental results: identification and controller implementation

---

## 6.1 Introduction

The design of the experimental drill-string setup and its realization are presented in Chapter 5. In this chapter, the dynamical properties of the setup are identified and the implementation and validation of the controllers designed in Chapters 3 and 4 are presented. As mentioned in the previous chapter, the experimental setup can be used for the experimental validation of the proposed controller design strategies and serves as an intermediate step towards field implementation of the controllers on a real rig. In the scope of this PhD research preliminary experimental results are presented, indicating the potential of the setup for controller validation for drill-string systems and the potential of the controllers developed in this thesis. To fully utilize the possibilities of the developed experimental setup additional experiments can be performed. Future research can, for example, focus on comprehensive robustness analyses of the control strategies.

Before using the drill-string setup for the experimental validation of the designed controllers, the dynamical properties of the setup have to be identified. In addition, the implementation of the additional dynamics (i.e. damping between non-adjacent discs) and interaction torques (i.e. bit-rock interaction and drill-string borehole interaction) is presented. These additional dynamics are emulated in software (through so-called hardware-in-the-loop) and implemented using the motors coupled to the discs in the setup. During the parameter iden-



tification, it has appeared that the setup contains some undesired dynamical effects such as cogging and viscous friction in the motors. These effects have to be compensated for the setup to work properly and the design and implementation of the compensation of such undesired dynamics is also discussed in this chapter. After the parameter identification, the dynamical behavior of the total setup is compared with the resulting quantitative model of the setup based on the identified parameters. For more details about the parameter identification, emulation of additional dynamics and model validation the reader is referred to [27].

Three different controller design strategies are experimentally validated on the setup. First, the industrial SoftTorque controller is implemented and the results are compared with the expected behavior of the closed-loop system based on simulations and field results. Second, the implementation of a state-feedback controller and observer-based output-feedback controller, based on the design methodology presented in Chapter 3 is discussed and experimental results of the state-feedback controller (therewith using measurements of all states of the system) are presented. Third, an  $\mathcal{H}_\infty$ -based controller as proposed in Chapter 4 has been implemented and tested experimentally.

This chapter is organized as follows. In Section 6.2, the compensation of undesirable motor dynamics and the parameter identification is discussed. Next, in Section 6.3 the implementation of the additional dynamics and interaction torques is presented. Subsequently, the experimental validation of the different controllers is presented in Section 6.4. Finally, the results are summarized in Section 6.5.

## 6.2 Parameter identification and compensation

In order to analyze the dynamics of the experimental setup, we need to estimate the parameters of the setup model (5.9). Moreover, the model-based controller design approaches presented in Chapters 3 and 4 need a model of the drill-string setup to synthesize controllers for the experimental setup. Therefore, the performed parameter identification is discussed in more detail in this section. However, first the compensation of undesirable motor dynamics effects, such as cogging and (viscous) friction in the motor, is presented.

### 6.2.1 Compensation of motor dynamics

Let us first focus on the cogging effect in the motors. Cogging is an electromagnetic effect that occurs in brushless permanent magnet motors, such as the brushless DC motors used in the experimental setup. Due to this cogging effect, the output torque of the motor varies while actuated with a constant input current. This is caused by the fact that the magnets on the rotor are more strongly attracted to the cores (poles) of the motor than to the space in between

the cores, resulting in a higher torque if the magnet is near a pole than when the magnet is in between poles [41]. The cogging torque is position dependent and its periodicity per revolution depends on the number of magnetic poles and the number of teeth on the stator. The motor at the lower disc is a brushed DC motor and therefore only the motors at the three upper discs suffer from the cogging effect.

Compensation of the cogging effect is achieved by generating a position dependent torque that is added to the desired torque in order to compensate for the cogging effect. To identify this cogging mapping, the motor is actuated to rotate at a low constant angular velocity; however, due to the cogging effect variations in the velocity will occur. A high-bandwidth motion controller is designed to suppress these fluctuations by means of feedback and the generated control action gives the torque that is necessary to compensate for the cogging effect. The averaged position-dependent mapping of this control torque (as a function of rotational position of the motor) over 37 full rotations is used and a mapping of the compensation torque between 0 and 360 degrees (i.e. a full rotation) is therewith generated. The resulting mapping for the three motors is shown in Figure 6.1 (more details about the cogging compensation can be found in [27]). Since the motors have 21 pole pairs we recognize 21 periods over one revolution in the compensation torque. Applying this compensation torque mitigates the velocity variations due to the cogging effect. In all following experiments, the compensation torques are implemented to compensate for cogging.

Let us now consider the friction effects in the motors. To identify the friction in the motors, experiments are performed at 18 different angular velocities in the range of 0-30 rpm. Again, by using a high-bandwidth motion controller, the discs are actuated to rotate at the desired angular velocity. The average torque needed to achieve these velocities is determined (neglecting transient effects) and these averaged torques are indicated by the dots in Figure 6.2. Since the motors are controlled to rotate at a constant velocity these torques indicate the amount of torque necessary to overcome the amount of friction for that particular angular velocity. As can be seen in this figure, the amount of friction in disc 1 is much lower than the amount of friction in the other discs. Based on the measurements in Figure 6.2, it is assumed that the friction in the discs can be approximated by a Coulomb friction model with viscous friction of the form

$$T_{f,i} = F_{c,i} \text{Sign}(\dot{\theta}_{s,i}) + F_{v,i} \dot{\theta}_{s,i} \quad (6.1)$$

with  $\dot{\theta}_{s,i}$  the angular velocity of disc  $i$ ,  $F_{c,i}$  and  $F_{v,i}$  the Coulomb and viscous friction coefficients, respectively. As one might note, the results for motors 2, 3 and 4 also show a small velocity-weakening effect at low velocities. Since this is only a small effect and the motors are mainly used to operate at angular velocities between 5 and 15 rpm, this effect is neglected here. A least square fit of the friction models (6.1) is made and the resulting parameter values are summarized in Table 6.1 for each disc. The fitted friction models are also plotted (solid

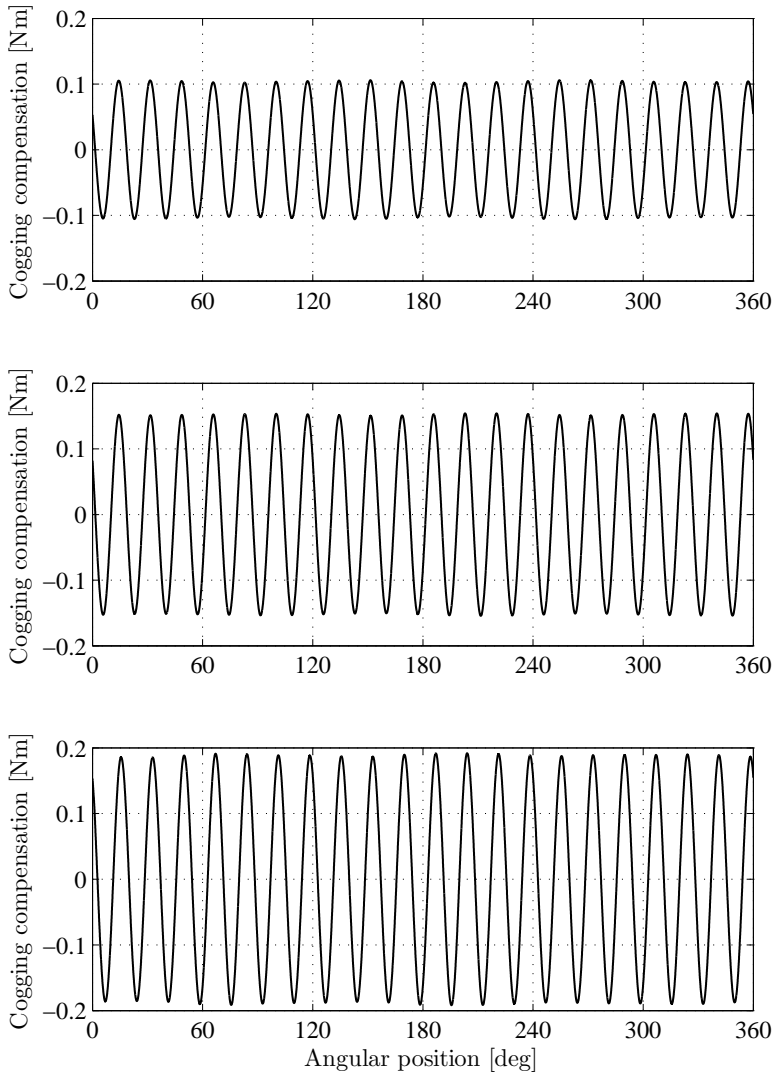


Figure 6.1: Mapping of the input torque as function of (angular) position to compensate for the cogging effect for motors 2, 3 and 4.

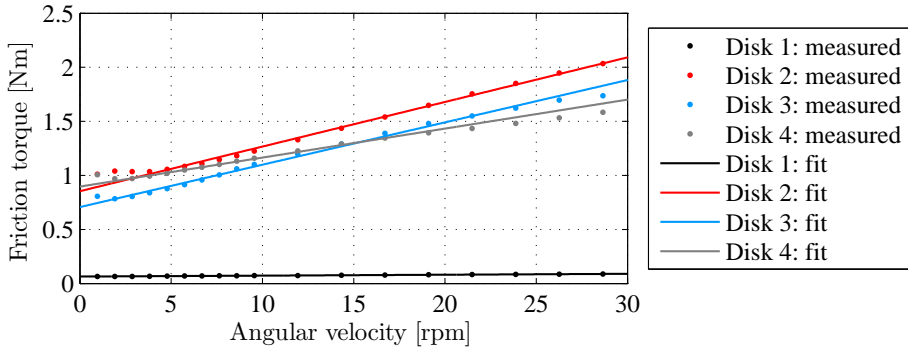


Figure 6.2: Measured and fitted torque as function of angular velocity of all motors to identify the motor friction.

Table 6.1: Determined parameter values for the friction models of the different motors.

| Motor | $F_{c,i}$<br>[Nm] | $F_{v,i}$<br>[Nms/rad] |
|-------|-------------------|------------------------|
| 1     | 0.064             | 0.008                  |
| 2     | 0.854             | 0.394                  |
| 3     | 0.707             | 0.374                  |
| 4     | 0.897             | 0.256                  |

lines) in Figure 6.2. Similar to the compensation for the cogging effects, these identified friction terms are used in the following experiments to compensate for these effects. However, it has to be noted that in the implementation the compensation of the viscous friction at disc 1 is chosen to be 0.004 Nms/rad. This is done because  $F_{v,1} = 0.008$  in Table 6.1 is a relatively small value and hence overcompensation of the viscous friction is likely and would result in undesirable (unstable) behavior. In addition, the velocity measurement (based on the encoder readings) is not perfect, due to e.g. sampling, numerical differentiation and delay, which can worsen the effects due to overcompensation. Therefore, a slightly lower value for the viscous friction compensation is used for disc 1.

### 6.2.2 Identification of the setup parameters

Parameter identification is important for model validation of the experimental setup. In other words, we aim to assess whether the dynamics of the designed experimental setup matches with that of the desired model of the experimental setup as presented in Section 5.2.4. Additionally, an accurate model of the experimental drill-string setup is important to synthesize controllers for the setup

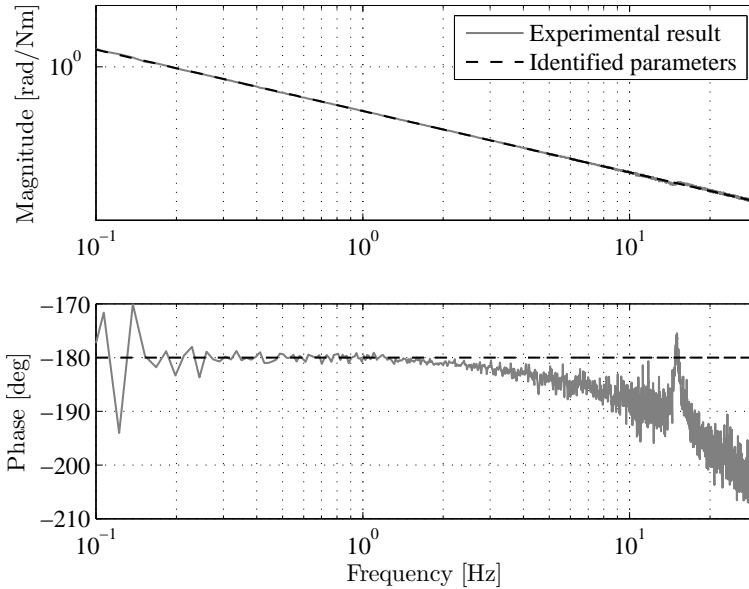


Figure 6.3: Measured frequency response function of disc 3 and the model of a single inertia determined using a fitting procedure.

using the model-based controller design methodologies developed in Chapters 3 and 4. In this section, the main aspects of the parameter identification are discussed, a detailed description of the parameter identification can be found in [27].

The parameters of the model for the experimental setup are determined using independent experiments (at least as much as possible). In other words, different experiments have been performed, each targeting to determine a single parameter. First, the inertias of the separate discs are determined. Subsequently, the interconnecting strings between two adjacent discs are connected to determine the stiffness and damping of the steel string, independently. The parameters of the model are determined by measuring a frequency response function (FRF) of (a part of) the setup and fitting a model of that specific part (e.g. a single inertia to determine the inertia of a disc) to the measured FRF to determine the parameters.

Consider the measured frequency response function of a single disc in Figure 6.3 from motor input to encoder position output, obtained by closed-loop measurements with a sample frequency of 1 kHz. In this figure, the frequency response function of disc 3 is shown as an example, the procedure to determine the inertias of the other discs is similar. To determine the inertia of the disc, a model of a single inertia is fitted on the measured data. The transfer function

Table 6.2: Identified inertias of the discs of the experimental setup.

| Symbol | Value [kgm <sup>2</sup> ] |
|--------|---------------------------|
| $J_1$  | 0.062                     |
| $J_2$  | 0.713                     |
| $J_3$  | 0.703                     |
| $J_4$  | 2.852                     |

of the model for the inertia of disc 3 is given by

$$H_3(s) = \frac{1}{J_3 s^2}, \quad s \in \mathbb{C}, \quad (6.2)$$

with  $J_3$  the inertia of disc 3 to be determined. A similar optimization procedure as presented in Section 5.2.3 is used to determine the inertia. Hence, the objective of the optimization procedure is to find the inertia of the disc such that the difference in the complex plane between the measured frequency response function ( $H_3^{exp}(j\omega)$ ) and the model ( $H_3(j\omega)$ ) is minimized over all discrete frequencies  $\omega$  in the frequency range of interest  $\omega_l$ . Hence  $J_3$  is found by solving the optimization problem below:

$$\min_{J_3 \in [\underline{J}_3, \bar{J}_3]} \sum_{\omega_l} \left( |C(j\omega)W(j\omega)H_3^{exp}(j\omega) - C(j\omega)W(j\omega)H_3(j\omega)|^2 \right) \quad (6.3)$$

with  $\underline{J}_3$  and  $\bar{J}_3$  a lower and upper bound for the inertia of disc 3. The transfer function of the filter  $W(s)$  is chosen to be

$$W(s) = J_3 s^2, \quad (6.4)$$

to compensate for the negative slope of the frequency response function from torque input to angular position output. The additional weighting filter  $C(j\omega)$  is the coherence of the (measured) process sensitivity, such that measurement points with a high coherence (i.e. close to 1) are more important than measurement points with a low coherence. Note that the measured frequency response function of the disc is based on a (closed-loop) measurement of the sensitivity and the process sensitivity. The identified inertias of the discs of the setup are summarized in Table 6.2. Comparing these values with the prescribed model parameters in Table 5.1, shows that the obtained inertias for the setup match well with the prescribed values.

Let us now focus on the stiffness and (material) damping of the interconnecting strings. To determine the stiffness and damping of a single string, the string is connected between two discs. This experiment is repeated twice to determine the stiffness and damping of the three interconnecting strings. The procedure is discussed on the basis of the string between disc 2 and 3, while for

the other strings only the results are presented. For the fitting procedure, the so-called collocated plant is considered (i.e. measurement and actuation at the same disc), while the non-collocated plant (i.e. measurement and actuation at different discs) is only used to verify the results but not taken into account in the fitting procedure. Again, the frequency response functions are measured and shown in Figures 6.4 and 6.5. In Figure 6.4, the (measured) frequency response from torque input at disc 3 to angular position output at disc 3 (collocated) is shown and Figure 6.5 shows the frequency response from torque input at disc 3 and angular position output at disc 2 (non-collocated). The transfer function of the collocated plant of the 2-DOF system is given by

$$H_{33}(s) = \frac{J_2 s^2 + d_{23} s + k_{23}}{J_3 J_2 s^4 + d_{23} (J_2 + J_3) s^3 + k_{23} (J_3 + J_2) s^2}, \quad (6.5)$$

with  $k_{23}$  and  $d_{23}$  the stiffness and damping to be determined, respectively. Note that the inertias  $J_2$  and  $J_3$  are assumed to be known, based on the experiments with the single discs. A similar objective function as in (6.3) is used and the weighting filter  $W(s)$  to compensate for the negative slope of the frequency response function from torque input to angular position output is given by

$$W(s) = s^2. \quad (6.6)$$

The resulting model of the 2-DOF system with the estimated parameters  $k_{23}$  and  $d_{23}$  is shown in Figures 6.4 and 6.5. As can be seen, the model with the identified parameters matches well with the measured frequency response functions.

These frequency response functions are measured with the interaction torques ( $\hat{T}_{ws}$  and  $\hat{T}_{bit}$ ) applied on the discs. It turned out that the stiffness characteristic of the strings is not perfectly linear, therefore the stiffness of the strings depends on the loading conditions. By already applying the interaction torques, the stiffness of the strings is determined in the relevant operating range (i.e. difference in angular position of the discs) for typical experiments. The obtained model parameters are summarized in Table 6.3, comparing these results with the prescribed values for the setup design (see Table 5.1); a difference up to approximately 10% can be observed. This results in a mismatch between the prescribed model and the dynamics of the setup. This means for example that the resonance frequencies are slightly shifted for the setup compared to the prescribed model. Therefore, the controller synthesis in Section 6.4 is based on a model of the setup with the identified parameters. The identified damping values deviate even more from their prescribed values. This was to be expected because the prescribed damping values are very low. Moreover, the steel strings are designed based on the stiffness properties, therewith the material damping is a result of the chosen material, length and diameter of the string.

For the purpose of full model validation, the frequency response functions of the full setup are shown in Figures 6.6 and 6.7. The bit-mobility is discussed in

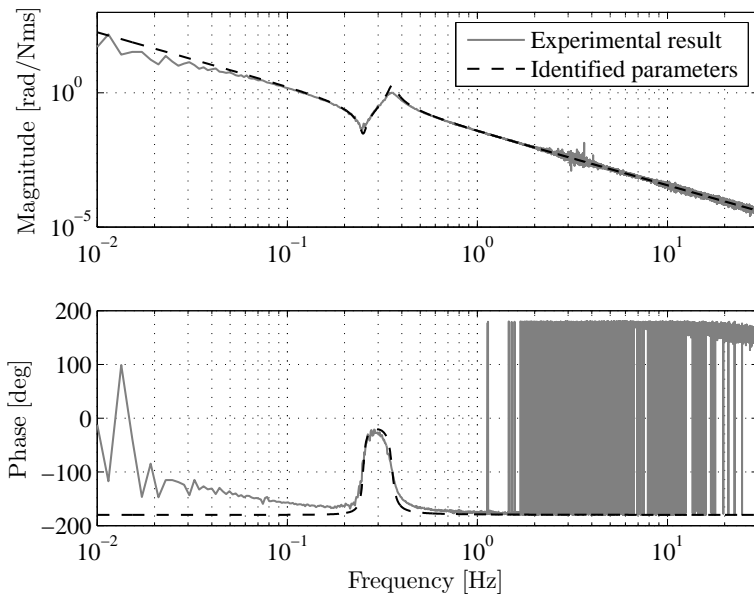


Figure 6.4: Measured frequency response function from torque input at disc 3 to angular position output at disc 3 and the model with the parameters determined using a fitting procedure.

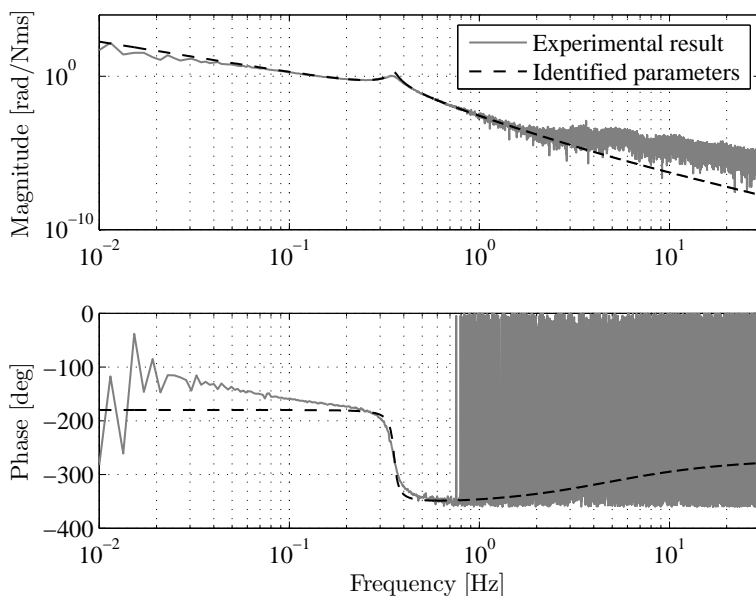


Figure 6.5: Measured frequency response function from torque input at disc 3 and angular position output at disc 2 and the model based on the identified parameters.



Table 6.3: Identified stiffness and damping parameters of the interconnecting strings of the experimental setup.

| Symbol   | Value [Nm/rad] | Symbol   | Value [Nms/rad] |
|----------|----------------|----------|-----------------|
| $k_{12}$ | 0.578          | $d_{12}$ | 0.006           |
| $k_{23}$ | 1.767          | $d_{23}$ | 0.06            |
| $k_{34}$ | 1.081          | $d_{34}$ | 0.019           |

more detail in Section 6.4. In Figure 6.6, the frequency response function from top drive torque input to top drive velocity output of the experimental setup and the model based on the identified parameters is shown (the identified parameters are based on the previous experiments and summarized in Tables 6.2 and 6.3). The match between the measured frequency response function and the model with identified parameters is good. However, as can be seen from this plot, the second and especially the third mode are hardly visible in this frequency response function (both in the measured FRF and the model). This might lead to observability problems for the controller design strategies, this issue is discussed more extensively in Section 6.4. The frequency response function from top drive torque input to bit velocity output is shown in Figure 6.7. The resonance frequencies are well estimated, although the lower resonance peaks indicate that there might be too much damping in the model. However, it has to be mentioned that the coherence of the process sensitivity (which is used to determine the plant FRF from  $T_{td}$  to  $\omega_{bit}$ ) indicates that the measurement is only reliable in the frequency range between 0.05 and 0.3 Hz. This might also be the reason for the mismatch in the slope of the FRF at higher frequencies.

Summarizing, the parameters for the setup have been estimated in this section. These parameters are determined using independent experiments. The measured frequency response functions of the setup match well with the frequency response functions of the model based on the identified parameters. However, it turned out that it is difficult to obtain a good estimate of the damping coefficients. Especially for the second and third resonance mode, these values might be relatively high compared to the actual damping in the system, as indicated by the difference in the resonance peaks in Figures 6.6 and 6.7.

### 6.3 Emulation of additional dynamics

In the previous section, the parameters of the setup model have been determined. These parameters involve the properties of the mechanical components of the drill-string setup. As mentioned before, the interaction torques, modelling the bit-rock interaction and drill-string borehole interaction, and damping terms between non-adjacent discs are implemented using the motors at the discs. The emulation of these additional dynamics is presented in this section.

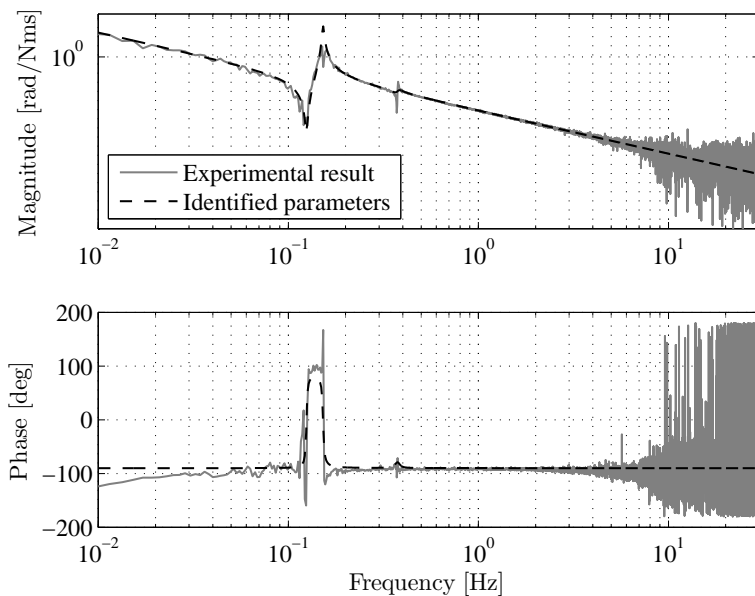


Figure 6.6: Frequency response function of the experimental setup and the model based on the identified parameters from input torque  $T_{td}$  to top drive velocity  $\omega_{td}$ .

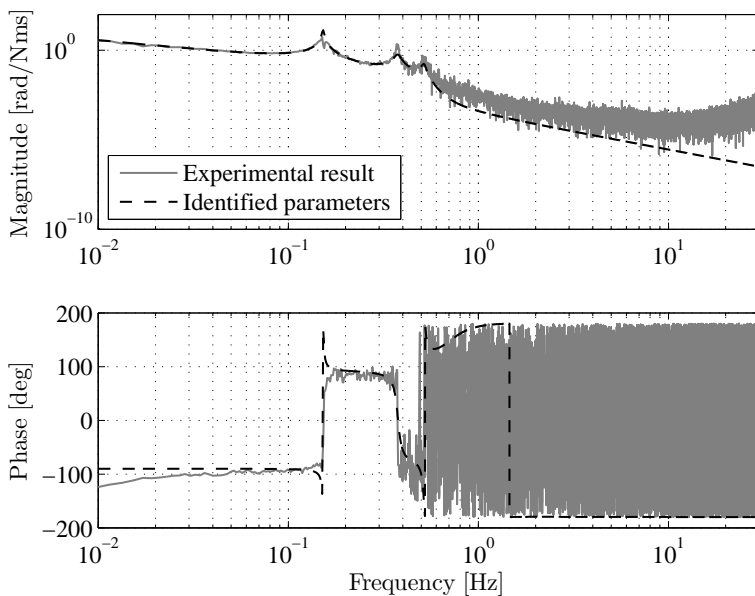


Figure 6.7: Frequency response function of the experimental setup and the model based on the identified parameters from input torque  $T_{td}$  to bit velocity  $\omega_{bit}$ .

Table 6.4: Identified Coulomb friction  $F_{c,i}$  and interaction torques  $\hat{T}_{s,i}$  to be implemented of discs 2, 3 and 4.

| Disc | $F_{c,i}$ [Nm] | $\hat{T}_{s,i}$ [Nm] |
|------|----------------|----------------------|
| 2    | 0.854          | 2.298                |
| 3    | 0.707          | 3.038                |
| 4    | 0.897          | 0.662                |

### 6.3.1 Drill-string borehole interaction torques

First, the implementation of the drill-string borehole interaction torques is discussed. These interaction torques act on disc 2, 3 and 4 of the experimental setup and are modelled as (set-valued) Coulomb friction models. The model of the drill-string borehole interaction torques to be implemented is given in (5.20) and the parameter values for  $\hat{T}_{s,i}$ , with  $i = 2, 3, 4$ , are given in Table 5.2. For the implementation of these Coulomb friction laws we make use of the Coulomb friction that is already present in the discs as identified in Section 6.2.1. The values of the identified Coulomb friction in the motors and the interaction torques to be implemented are summarized in Table 6.4. For disc 2 and 3 the interaction torques to be implemented are higher than the friction in the motors, in these cases the emulated friction torque is given by

$$\hat{T}_{s,i}^{emu} = -\text{sign}(\dot{\theta}_i) \left( \hat{T}_{s,i} - 2F_{c,i} \right) - F_{c,i}, \quad \text{for } i = 2, 3. \quad (6.7)$$

with  $F_{c,i}$  the identified Coulomb friction coefficients (see Section 6.2.1) and the sign function defined by

$$\text{sign}(y) \triangleq \begin{cases} -1, & y < 0 \\ 0, & y = 0 \\ 1, & y > 0. \end{cases} \quad (6.8)$$

Using this approach the amplitude of the chattering (associated with the implementation of such discontinuous torque law) around zero velocity is minimized. Note that due to measurement noise the velocity measurement will always fluctuate between positive and negative values when the disc is standing still. This implementation is possible because we assume that the discs are not rotating with negative angular velocities. The implementation is also visualized in Figure 6.8. The plot on the left shows the Coulomb friction present in the motor (in this case for disc 3). In the second plot the emulated friction model (6.7) is shown and the right-most plot shows the achieved friction on the disc (i.e. the emulated friction plus the friction in the motor) compared with the prescribed model for the interaction torque (as given in (5.20)). As can be seen, there is a mismatch between the model and the implemented interaction torque model

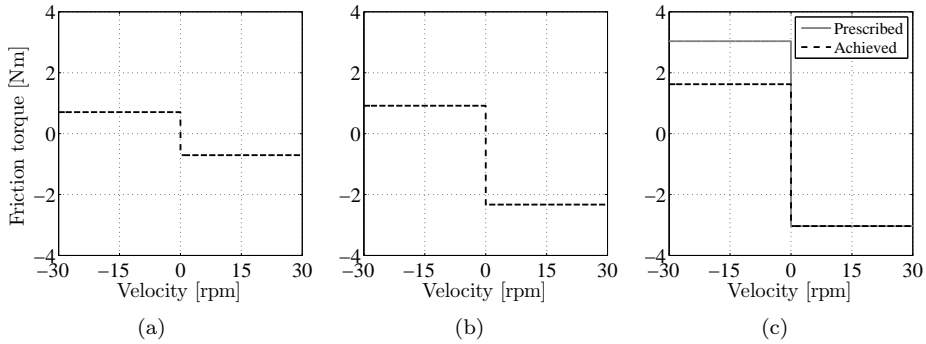


Figure 6.8: Implementation method for drill-string borehole interaction torques. (a) shows the Coulomb friction present in the motor, (b) shows the emulated friction model (6.7) and (c) shows the total achieved friction on the disc compared with the prescribed model (5.20).

for negative velocities, so the implementation is not valid for negative angular velocities.

The implementation of the Coulomb friction law for disc 4 is slightly different, because there the Coulomb friction level in the motor is higher than the interaction torque to be implemented. To emulate the drill-string borehole interaction torque the motor has to provide torque in positive direction to overcome the static friction in the motor, this is achieved by

$$\hat{T}_{s,4}^{emu} = F_{c,4} - T_{s,4}. \quad (6.9)$$

Also in this case a mismatch between the prescribed model and the emulated model at negative velocities is present, however, again it is assumed that the disc will only rotate with positive angular velocity.

A measurement of the obtained drill-string borehole interaction torques at the setup is shown in Figure 6.9. Experiments at several (positive) angular velocities have been performed for the discs without any friction compensation and interaction torque emulation and with the compensation for (viscous) friction and the emulated drill-string borehole interaction torques. As can be seen in this figure, the achieved friction models (i.e. with emulation) match well with the desired drill-string borehole interaction torques at the different discs. It has to be mentioned again that with this implementation the emulation of the drill-string borehole interaction torques is not accurate for negative angular velocities.

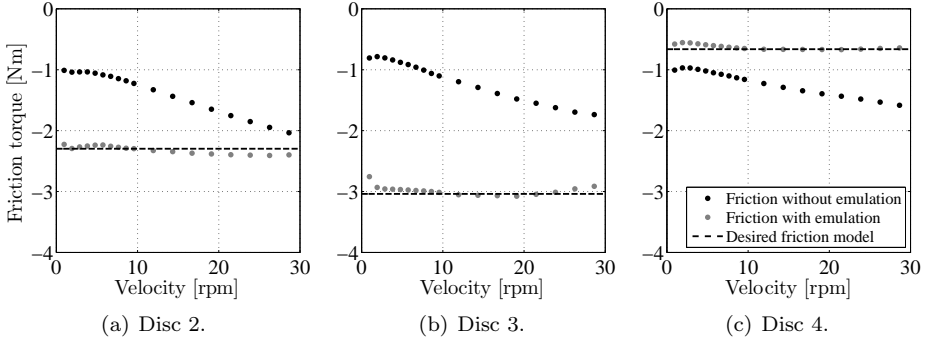


Figure 6.9: Measurements of the obtained drill-string borehole interaction torques.

### 6.3.2 Bit-rock interaction torque

The implementation of the bit-rock interaction torque (5.19) is a bit more involved. This is mainly due to the fact that we would like to accurately implement the set-valued nature of the bit-rock interaction model when the bit angular velocity is equal to zero. This is important because one of the main objectives for the experimental setup is to investigate torsional stick-slip behavior. For the other discs this was less important because simulation results have revealed that these discs rarely come to a complete stop (i.e. are sticking). In the implementation of the bit-rock interaction it is again assumed that the bit is not moving with negative angular velocity. That is, due to implementation issues and measurement noise negative velocities can be obtained, however, the bit-rock interaction model is only accurately implemented for non-negative angular velocities.

Recall the bit-rock interaction model (5.19) to be implemented, that is

$$\hat{T}_{bit}(\dot{\theta}_{s,1}) \in \text{Sign}(\dot{\theta}_{s,1}) \left( \hat{T}_d + \left( \hat{T}_s - \hat{T}_d \right) e^{(-30|\dot{\theta}_{s,1}|)/(\hat{N}_d\pi)} \right). \quad (6.10)$$

For the implementation of this bit-rock interaction model, we first define a bound  $\epsilon$  on the bit angular velocity. For measured angular velocities higher than this bound  $\epsilon$ , the bit-rock interaction is implemented according to (6.10). For measured velocities smaller than this bound, a feedback controller is used to stabilize the zero velocity setpoint (i.e it is assumed that the bit is in stick). This implementation is not trivial for several reasons. First, measurement noise on the angular velocity measurement has to be taken into account, i.e. we have to prevent chattering due to measurement noise. Second, the control action should not exceed the maximum static torque  $\hat{T}_s$ . Third, a feedforward torque based on the torque sensor at the bottom disc is used to improve the performance of

the position controller used when the angular velocity is smaller than the bound  $\epsilon$ . Therefore, the implementation of the emulated bit-rock interaction torque is given by

$$\hat{T}_{bit}^{emu} = \begin{cases} T_{ts} + T_c(\theta_{s,1}), & \text{if } \delta_k = 0 \\ -\left(\hat{T}_d + \left(\hat{T}_s - \hat{T}_d\right) e^{(-30|\dot{\theta}_{s,1}|)/(\hat{N}_d\pi)}\right), & \text{if } \delta_k = 1 \end{cases} \quad (6.11)$$

where  $T_{ts}$  is the feedforward torque based on the torque sensor,  $T_c$  is the control action of a position controller to stabilize the current angular position (i.e. zero velocity) and the variable  $\delta^k \in \{0, 1\}$  is used to switch between the position controller and implementation of the bit-rock interaction law. This variable  $\delta^k$  is determined at every (discrete) time-step  $k$  according to

$$\delta^k = \begin{cases} 1, & \text{if } \delta^{k-1} = 0 \wedge \left(\dot{\theta}_{s,1}^{k-1} > \epsilon \wedge T_c^{k-1} \geq T_s\right) \\ 0, & \text{if } \delta^{k-1} = 0 \wedge \left(\dot{\theta}_{s,1}^{k-1} \leq \epsilon \vee |T_c^{k-1}| < T_s\right) \\ 1, & \text{if } \delta^{k-1} = 1 \wedge \left(\dot{\theta}_{s,1}^{k-1} > \epsilon \vee \dot{\theta}_{s,1}^{k-500} \leq 3\epsilon\right) \\ 0, & \text{if } \delta^{k-1} = 1 \wedge \left(\dot{\theta}_{s,1}^{k-1} \leq \epsilon \wedge \dot{\theta}_{s,1}^{k-500} > 3\epsilon\right) \end{cases}. \quad (6.12)$$

Switching from the position controller ( $\delta^k = 0$ ) to direct implementation of the bit-rock interaction law ( $\delta^k = 1$ ) occurs if the angular velocity of the bit is higher than the bound  $\epsilon$  and the torque delivered by the controller is sufficient to overcome the static friction. The switch from direct implementation of the bit-rock interaction ( $\delta^k = 1$ ) to the position controller ( $\delta^k = 0$ ) occurs if the measured angular velocity is smaller than the bound  $\epsilon$ . To reduce the effect of chattering, this switch (from  $\delta^{k-1} = 1$  to  $\delta^k = 0$ ) is only possible if, in addition, the bit angular velocity was larger than  $3\epsilon$  at a time instant 0.5 s (i.e. 500 time-steps) earlier. This means that a slip to stick transition is only possible if the bit velocity was sufficiently high (i.e. the bit was in slip) 0.5 s earlier. This period of 0.5 s is chosen such that it is sufficiently larger than the period of transient oscillations in the stick to slip transition and smaller than the typical slipping period. The position controller is a lead filter with a first-order low-pass filter with a cut-off frequency of 30 Hz. The lead filter is given by

$$T_c(s) = 15 \frac{10s + 40}{s + 40}. \quad (6.13)$$

This implementation of the bit-rock interaction model is tested with a 2-DOF system. The upper disc is driven by a velocity controller to stabilize a constant angular velocity of 0.3 rad/s and, at the bottom disc the bit-rock interaction model is implemented. The response of the bottom disc and the implemented bit-rock interaction torque is shown in Figure 6.10. The bit angular velocity clearly shows a stick-slip limit cycle and also the torque profile of the implemented bit-rock interaction looks similar to the profile obtained by simulations

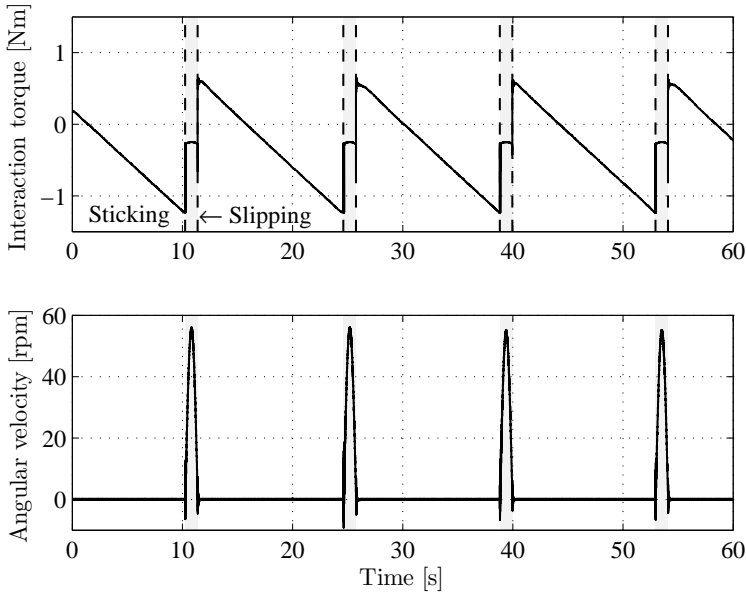


Figure 6.10: Stick-slip experiment with two discs to test the bit-rock interaction implementation.

using the set-valued mapping (6.10). In Figure 6.11, the implemented bit-rock interaction torque is plotted as function of the angular velocity. For positive angular velocities, the implemented torques are on top of the prescribed friction model, except for the cloud of points above 0.5 Nm. These points correspond to transient effects of the position controller to stabilize the zero angular velocity (i.e. sticking). In other words, in the transition from slip to stick. The points with negative angular velocities and maximum resisting torque (i.e. -1.23 Nm) correspond to the oscillations in the transition from stick to slip. In other words, when the velocity is changing from zero (in stick) to positive values (in slip). The implemented bit-rock interaction model is thus only accurate for non-negative angular velocities, which suffices for to accurately represent the desired drill-string dynamics.

### 6.3.3 Additional damping term

Finally, let us discuss the implementation of the additional damping term, to model the damper between disc 1 and 4. In the mechanical setup, of course, only damping (and stiffness) between adjacent discs is possible. However, in the designed model for the setup, we would also like to include a damper between disc 1 and 4 and possibly other damping or stiffness terms. This damping term

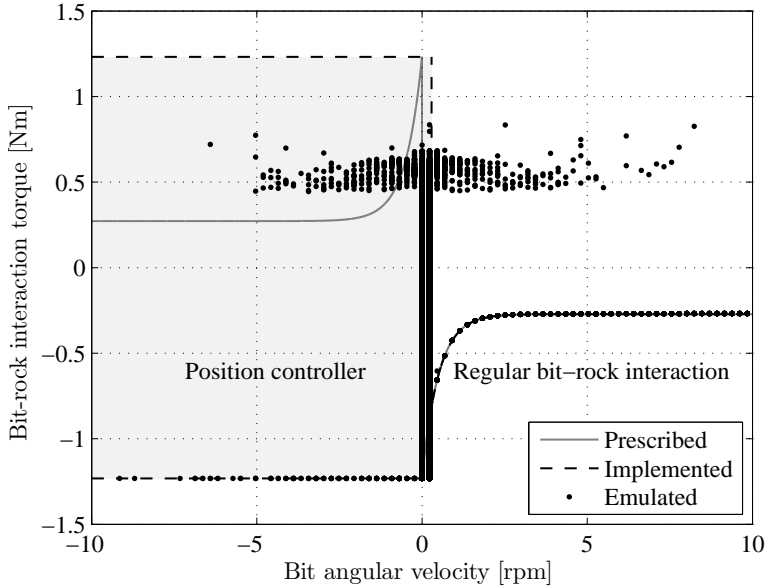


Figure 6.11: Implemented bit-rock interaction law.

is implemented based on the measured angular velocities of disc 1 and 4. The implementation is straightforward and given by

$$T_{d_{14}}^{emu} = \pm d_{14} \left( \dot{\theta}_{s,4} - \dot{\theta}_{s,1} \right), \quad (6.14)$$

where the negative component corresponds to the torque implemented on disc 4 and the positive component to the torque implemented on disc 1. For implementation reasons  $d_{14}$  is chosen to be  $d_{14} = 0.0020$  instead of 0.0005 as specified in Table 5.1.

## 6.4 Experimental controller validation

In the previous sections, the parameters of the model for the experimental setup are identified and the implementation of the additional dynamics, such as e.g. the bit-rock interaction torque, is presented. In this section, the implementation and experimental results of different controller design strategies are presented. First, a startup scenario for the experiments on the drill-string setup is discussed in Section 6.4.1. Next, in Section 6.4.2, the implementation of the SoftTorque controller is discussed and an experimental result of this industrial controller applied to the setup is shown. In Section 6.4.3, the implementation of a state-feedback controller, based on the design methodology in Chapter 3, is given and



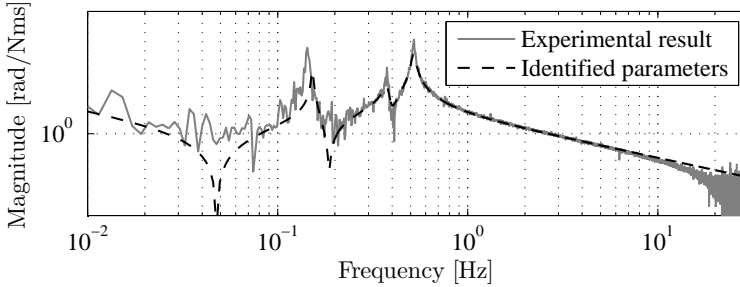


Figure 6.12: Open-loop bit-mobility of the setup, i.e. the frequency response function from bit torque  $T_{bit}$  to bit velocity  $\omega_{bit}$ .

corresponding experimental results are shown. In Section 6.4.4, the implementation of the observer-based output-feedback controller is discussed. Finally, in Section 6.4.5 the implementation and experimental results are discussed for the linear robust output-feedback controller as presented in Chapter 4.

Before going into detail on the implementation of the controllers and the experimental results, let us consider the (open-loop) bit-mobility of the experimental drill-string setup. As we have seen throughout this thesis, the bit-mobility plays an important role in the onset of stick-slip vibrations. The open-loop bit-mobility of the setup is shown in Figure 6.12. In the same figure, the bit-mobility of the setup model based on the identified parameters is shown. As can be seen, the first and third resonance mode are very well captured by the model, however, the second flexibility mode is more damped in the model compared to the actual bit-mobility of the setup. As mentioned before, this is again a consequence of the fact that it is hard to accurately identify the damping parameters.

The controllers designed in Section 6.4.3 and 6.4.5 are based on the model of the experimental setup using the identified parameters. The mismatch between the model (based on the identified parameters) and the setup is taken into account as model uncertainty. In other words, the designed controllers (based on the model) are implemented and their performance is analyzed based on the response of the setup. Because of this mismatch between the setup and the model, experimentally validating the controllers on the setup also gives an indication of the robustness of the designed (model-based) controllers with respect to these kind of model uncertainties.

### 6.4.1 Startup scenario for experiments

The startup scenario as presented in Chapters 3 and 4 for the simulations is adapted here for the experiments. This adaptation is necessary for different reasons: first, every experiment starts from standstill and the angular velocity has to be increased gradually to the desired reference velocity to avoid tran-

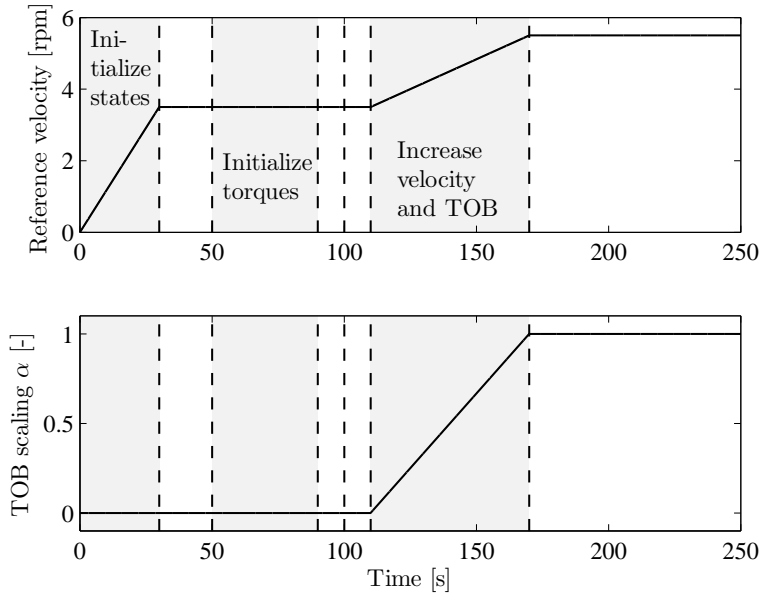


Figure 6.13: Reference velocity and TOB scaling of the startup scenario for the experimental setup, the selected controller is applied for  $t > 100$  s.

sient oscillations, second, the friction in the motors is prone to changes due to temperature, humidity etc., therefore an initialization procedure is developed to identify these friction levels in an online fashion. For the experiments with the state-feedback controller an additional adaptation is implemented. That is, the desired controller is switched on 10 seconds before starting to increase the angular velocity and the torque-on-bit. Doing so, transient oscillations that are caused by the switch between controllers can be damped and do not interfere with oscillations due to changing torque-on-bit and reference velocity. This is only applicable for the experiments with the state-feedback controller; in the experiments with the SoftTorque controller and the  $\mathcal{H}_\infty$ -controller it is not necessary to switch between controllers.

The startup scenario for the experiments is visualized in Figure 6.13. The reference angular velocity of the upper discs is shown in the upper plot and the scaling of the TOB, indicated by  $\alpha$  is shown in the bottom plot. The timing of the transitions in the startup scenario is indicative and might be different in the various experiments. However, the sequence of steps is similar for all experiments. The steps can be summarized as follows:

1. Start with zero initial velocities (i.e. the discs are not moving) and linearly increase the reference angular velocity from zero to 3.5 rpm in the period

between  $t = 0$  and  $t = 30$  s. At the same time increase the feedforward torque ( $T_{ff}$ ) to its nominal value. In the experiments with the state-feedback controller, a properly tuned SoftTorque controller is used in the first part of the startup scenario;

2. Between  $t = 50$  and  $t = 90$  s, adapt the drill-string borehole interaction torques to obtain the desired values, based on the torque sensor readings, in order to compensate for possibly changed friction characteristics;
3. If applicable, at  $t = 100$  s, switch from the SoftTorque controller to the state-feedback controller;
4. Gradually increase the reference angular velocity until the desired operating velocity ( $\omega_{eq}$ ) is reached (in the time window  $110 \leq t < 170$  s). At the same time, slowly change the TOB (see e.g. (4.36)) to emulate that the bit bites the formation and finally obtain the nominal operating condition in both the angular velocity and the TOB.

Note that, the implemented top drive torque  $\hat{T}_{td}$  on the drill-string setup is composed of a feedforward torque  $T_{ff}$  and a feedback part  $T_{fb}$ , that is

$$\hat{T}_{td} = T_{ff} + T_{fb}, \quad (6.15)$$

where the feedback torque depends on the chosen control strategy.

### 6.4.2 SoftTorque controller

The SoftTorque controller is a controller for drill-string systems, widely used in industry. This controller aims at damping of the first torsional flexibility mode of the drill-string system. This active damping system is a PI-controller, based on the error  $e_y$  between the measured top drive velocity  $y = \omega_{td}$  and the reference angular velocity  $\omega_{td,ref}$ , i.e.  $e_y := \omega_{td,ref} - \omega_{td}$ . The controller is given by the transfer function

$$T_{fb}(s) = \left( c_t + \frac{k_t}{s} \right) e_y(s) \quad (6.16)$$

with  $c_t = 2.93$  and  $k_t = 1.87$  tuned such that damping of the first torsional flexibility mode of the setup is obtained. In Figure 6.14, the closed-loop bit-mobility of the drill-string setup with the SoftTorque controller is shown. It is clearly visible that the first torsional mode is damped using the SoftTorque controller, but the amplitude of the second and third mode are similar in the open-loop and closed-loop case, illustrating a key deficiency of the SoftTorque controller.

An experimental result of the closed-loop drill-string system with SoftTorque controller is shown in Figure 6.15. In the response of the bit angular velocity, stick-slip oscillations can be observed. The onset of these oscillations starts when

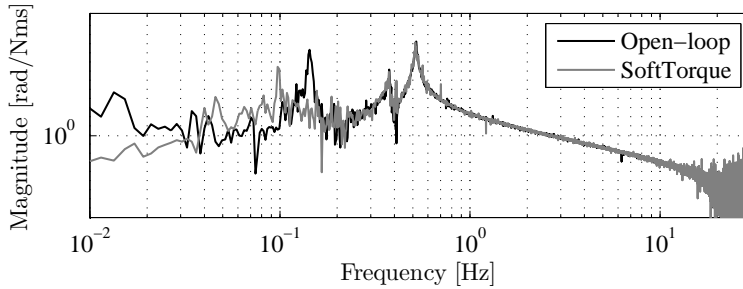


Figure 6.14: Bit-mobility of the setup with SoftTorque controller.

the reference angular velocity and scaling factor  $\alpha$  (to emulate an increase of the WOB) are started to increase around  $t = 100$  s. This shows experimentally that the SoftTorque controller is indeed not able to avoid stick-slip oscillations for the setup.

In Figure 6.15, the filtered and unfiltered response of the system are shown. The filtered response of the system is compared with a simulation result of the model of the setup with the identified parameters. The results are shown side-by-side in Figure 6.16. To allow for a clear comparison, a shift of the time axis has been applied for the experimental results. As can be seen from this figure, the response of the experimental setup is very similar to the response of the simulation results. The only difference is the somewhat shorter sticking period in the simulation results between two successive groups of two slipping periods (i.e. the long sticking period). This result further illustrates that the setup is able to accurately emulate the nonlinear drill-string dynamics to be investigated.

### 6.4.3 State-feedback controller

In this section, a state-feedback controller based on the controller design methodology in Chapter 3 is implemented on the experimental drill-string setup. For this state-feedback controller, it is assumed that all the states of the system can be measured, which is of course not feasible in practice. However, the state-feedback controller is a stepping stone towards implementation of observer-based output-feedback controller and as mentioned in Chapter 5 the setup has the sensors available to measure all the states of the system.

Let us first write the system (5.18) in first-order state-space form. Similar to the state-space representations of the different models in Chapters 3 and 4 the states are chosen such that the state of the system is independent of the absolute position, that is

$$x_s = [\theta_{s,1} - \theta_{s,2} \quad \dot{\theta}_{s,1} \quad \dot{\theta}_{s,2} \quad \theta_{s,2} - \theta_{s,3} \quad \dot{\theta}_{s,3} \quad \theta_{s,3} - \theta_{s,4} \quad \dot{\theta}_{s,4}]^\top. \quad (6.17)$$

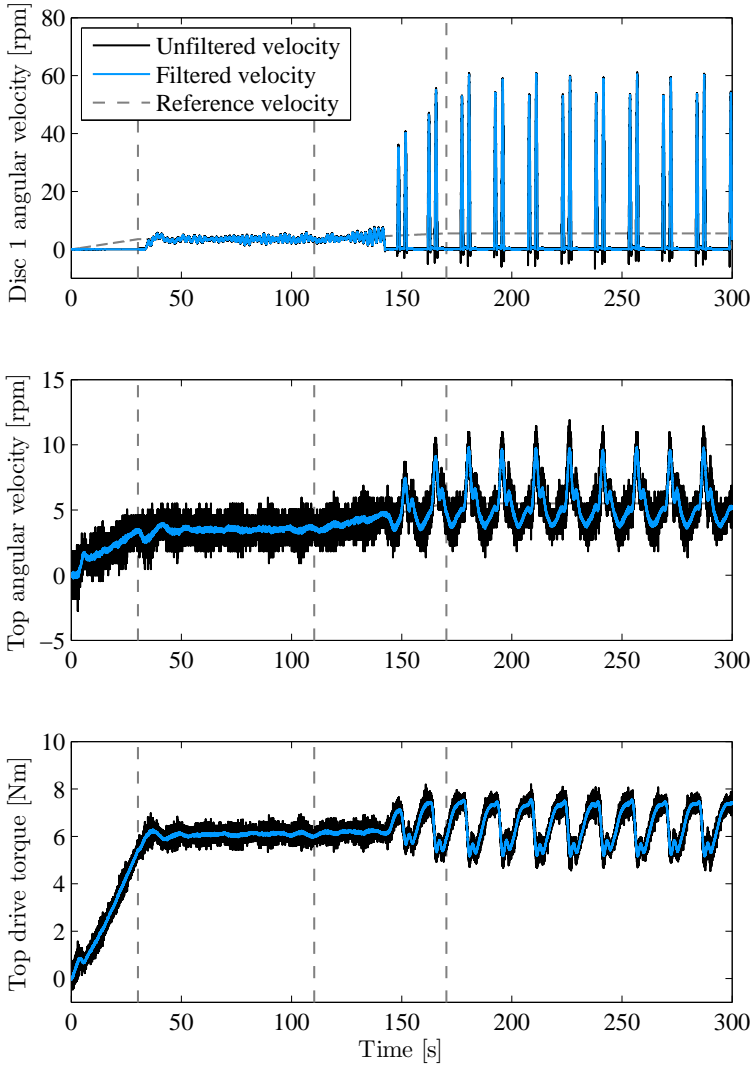


Figure 6.15: Experimental result of the drill-string setup with the Soft-Torque controller in the startup scenario.

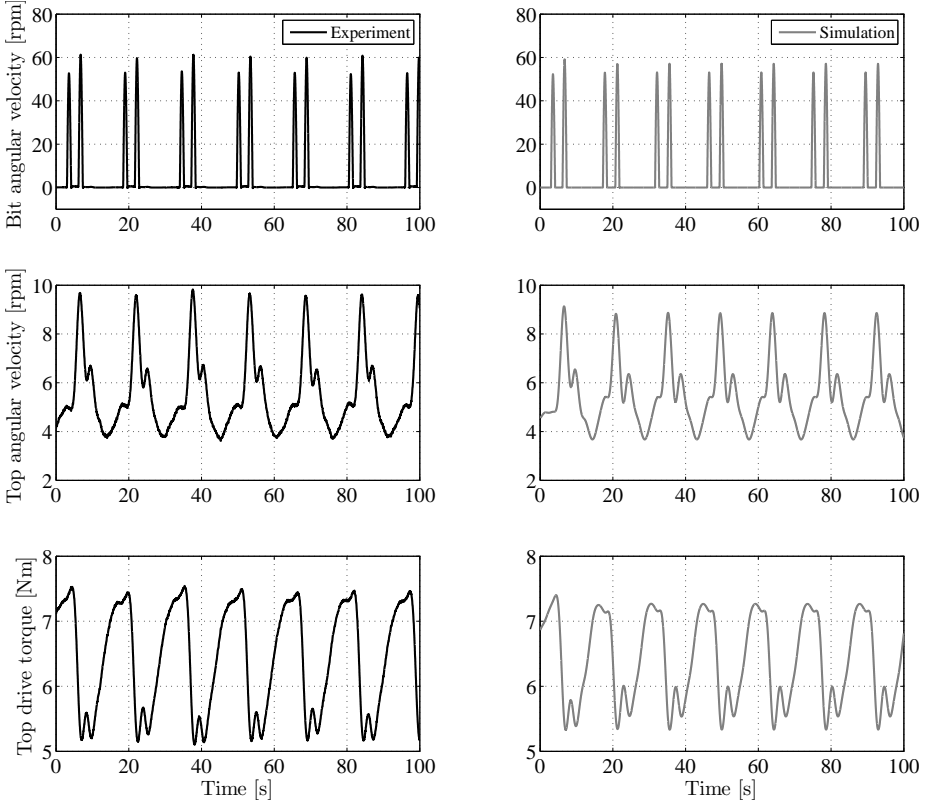


Figure 6.16: Comparison between the experimental result and simulation result of the drill-string model with the SoftTorque controller.

The resulting equations of motion are written in first-order state-space form:

$$\begin{aligned}
 \dot{x}_s &= A_s x_s + G_s v_s + G_{s,2} v_{s,2} + B_s \hat{T}_{td} \\
 q_s &= H_s x_s \\
 q_{s,2} &= H_{s,2} x_s \\
 v_s &\in -\varphi_s(q_s) \\
 v_{s,2} &\in -\phi_s(q_{s,2}),
 \end{aligned} \tag{6.18}$$

where  $q_s := \dot{\theta}_{s,1}$ ,  $q_{s,2} := [\dot{\theta}_{s,2} \ \dot{\theta}_{s,3} \ \dot{\theta}_{s,4}]^\top$ , are the angular velocity arguments of the set-valued nonlinearities  $\varphi_s := \hat{T}_{bit}$  and  $\phi_s := \hat{T}_{ws}$ , respectively. The bit-rock interaction torque is given by  $v_s$  and the drill-string borehole interaction torques are given by  $v_{s,2}$  and  $\hat{T}_{td} \in \mathbb{R}$  is the control input. The matrices  $A_s$ ,  $B_s$ ,  $G_s$ ,

$G_{s,2}$ ,  $H_s$  and  $H_{s,2}$  in (6.18), with appropriate dimensions are given by

$$A_s = \begin{bmatrix} 0 & 1 & -1 & 0 & 0 & 0 & 0 \\ -\sum_{j=2}^4 k_{1j} & -\sum_{j=2}^4 d_{1j} & \frac{d_{12}}{J_1} & \frac{-k_{13}-k_{14}}{J_1} & \frac{d_{13}}{J_1} & \frac{-k_{14}}{J_1} & \frac{d_{14}}{J_1} \\ \frac{k_{12}}{J_2} & \frac{d_{12}}{J_2} & \frac{-d_{12}-d_{23}-d_{24}}{J_2} & \frac{-k_{23}-k_{24}}{J_2} & \frac{d_{23}}{J_2} & \frac{-k_{24}}{J_2} & \frac{d_{24}}{J_2} \\ 0 & 0 & 1 & 0 & -1 & 0 & 0 \\ \frac{k_{13}}{J_3} & \frac{d_{13}}{J_3} & \frac{d_{23}}{J_3} & \frac{k_{23}+k_{13}}{J_3} & \frac{-d_{13}-d_{23}-d_{34}}{J_3} & \frac{-k_{34}}{J_3} & \frac{d_{34}}{J_3} \\ 0 & 0 & 0 & 0 & 1 & 0 & -1 \\ \frac{k_{14}}{J_4} & \frac{d_{14}}{J_4} & \frac{d_{24}}{J_4} & \frac{k_{24}+k_{14}}{J_4} & \frac{d_{34}}{J_4} & \frac{\sum_{j=1}^3 k_{j4}}{J_4} & -\frac{\sum_{j=1}^3 d_{j4}}{J_4} \end{bmatrix},$$

$$B_s = \begin{bmatrix} 0 \\ 0 \\ 0 \\ 0 \\ 0 \\ 0 \\ \frac{1}{J_4} \end{bmatrix}, \quad G_s = \begin{bmatrix} 0 \\ \frac{1}{J_4} \\ 0 \\ 0 \\ 0 \\ 0 \\ 0 \end{bmatrix}, \quad G_{s,2} = \begin{bmatrix} 0 & 0 & 0 \\ 0 & 0 & 0 \\ \frac{1}{J_2} & 0 & 0 \\ 0 & 0 & 0 \\ 0 & \frac{1}{J_3} & 0 \\ 0 & 0 & 0 \\ 0 & 0 & \frac{1}{J_4} \end{bmatrix},$$

$$H_s = [0 \ 1 \ 0 \ 0 \ 0 \ 0 \ 0], \quad H_{s,2} = \begin{bmatrix} 0 & 0 & 1 & 0 & 0 & 0 \\ 0 & 0 & 0 & 0 & 1 & 0 \\ 0 & 0 & 0 & 0 & 0 & 1 \end{bmatrix}.$$

The state-feedback controller, as discussed in Section 3.4.1, for this system is defined as

$$T_{fb} = K(x_s - x_{s,eq}) \quad (6.19)$$

with  $x_{s,eq}$  the desired equilibrium of the drill-string setup, associated with a desired constant angular velocity  $\omega_{eq} > 0$ . The controller gains  $K$  are designed according to the conditions given in Theorem 3.1. The results are obtained by using SeDuMi 1.3 [111], a linear matrix inequality (LMI) solver and the YALMIP interface [71]. The designed controller gains are given by

$$K = [15.22 \ -5.342 \ 6.507 \ -16.47 \ -3.160 \ 18.00 \ -7.761].$$

The measured closed-loop bit-mobility function is shown in Figure 6.17. The result is compared with the open-loop bit-mobility and it can be seen that all three flexibility modes are damped by the state-feedback controller. This illustrates that the state-feedback controller can indeed effectively deal with multiple torsional flexibility modes, also in this experimental setting.

Let us investigate the response of the drill-string system controlled by the state-feedback controller. The experimental result is shown in Figure 6.18, where

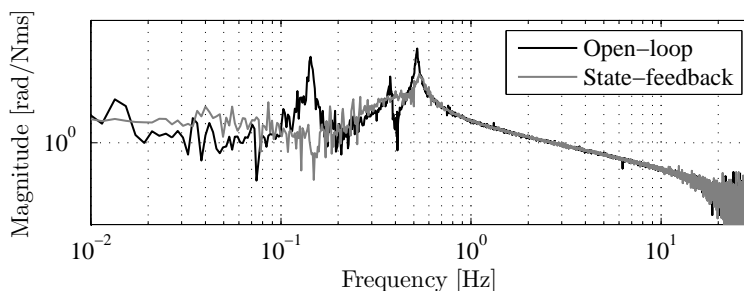


Figure 6.17: Bit-mobility of the setup with state-feedback controller.

the startup scenario is used as explained in Section 6.4.1. So, in the first 100 s, the system is controlled by the SoftTorque controller and the results are indeed similar to the response of the setup shown in Figure 6.15. As can be seen, the amplitude of the control action increases when the state-feedback controller is switched on. In addition, the state-feedback controller acts at a higher frequencies to suppress vibrations in the drill-string setup, as can be observed from the oscillations in the control signal, which have higher frequencies. The difference in suppression of vibrations can be clearly observed by comparing the bit response between 90 and 100 s (when SoftTorque is applied) with the response between 100 and 110 s (when the state-feedback controller is applied). The operating conditions in terms of bit-rock interaction are similar in these two periods, that is, there is no velocity-weakening effect in the bit-rock interaction yet. As can be seen, the bit angular velocity fluctuates between approximately 2 and 5 rpm (the desired reference velocity is 3.5 rpm) when the SoftTorque controller is applied. After switching to the state-feedback controller, the amplitude of the oscillations has been reduced and the bit angular velocity varies between approximately 3 and 4.5 rpm. Thus indeed the state-feedback controller is able to reduce the amplitude of the fluctuations in the angular velocity at the bit. Most importantly is of course the question whether the state-feedback controller is also able to mitigate the stick-slip vibrations. The experimental results with the SoftTorque controller (see Figure 6.15) showed that when the WOB and the angular velocity are increased, stick-slip oscillations appeared at the bit. The response of the bit angular velocity of the system with the state-feedback controller, as shown in the upper plot in Figure 6.18, shows that the bit angular converges to a constant angular velocity and only small oscillations (due to disturbances in the setup) are present. In other words, the state-feedback controller is able to mitigate the stick-slip vibrations at the experimental setup. One might have noted that the angular velocities of the bit and the top drive do not converge to the reference angular velocities, but are slightly higher (approximately 6 instead of 5.5 rpm). This is caused by a mismatch between the applied feedforward torque and the torque that is necessary to overcome the interaction torques at the discs. The



state-feedback controller does not have integral action to compensate for this steady-state mismatch and therefore an angular velocity slightly higher than the reference velocity is obtained. In this case, the feedforward torque should be decreased to obtain the desired angular velocity.

Summarizing, the designed state-feedback controller is able to mitigate stick-slip vibrations in the experimental drill-string setup, in a realistic startup scenario in which SoftTorque could not mitigate stick-slip oscillations. This controller uses measurements of all the states in the system which is not feasible in practice. Therefore, an observer has to be designed to estimate the states of the setup based on surface measurements only.

#### 6.4.4 Observer-based output-feedback controller

As mentioned before, the state-feedback controller uses measurements of all the states of the system, which is not feasible in practice. Therefore, the controller design methodology presented in Chapter 3 also included the design of an observer to determine an estimate of the states based on surface measurements only. Such an observer is also designed for the experimental setup and this observer is also applied to the setup. However, implementation of the observer in order to only use surface measurements with the observer-based output-feedback controller turned out to be difficult. The current problems with the observer-based output-feedback controller are discussed in this section.

After implementation of a suitably designed observer for the drill-string setup, it turned out that the state estimates obtained by the observer are not sufficiently accurate to be used in the observer-based output-feedback controller. Two aspects play an important role in the mismatch of the observer estimates. First, even after compensating for the cogging effect in the motors a residual disturbance dependent on the angular velocity of the disc is present. The frequency of the disturbance is related to a frequency 7 times higher than the rotational frequency of the disc, however, it is not possible to determine a position-dependent compensation for this disturbance. Since the frequency of this disturbance is close to the eigenfrequencies of the drill-string system for typical desired angular velocities, the observer acts on this frequency resulting in a mismatch of the state estimates. Second, oscillations with a frequency of approximately 0.55 Hz are present in the estimated states of the observer. It turned out that this frequency is related to one of the poles of the observer. Due to this closed-loop pole the observer is sensitive for disturbances at this frequency. Therefore, it also results in a mismatch between the estimated states of the observer compared to the actual states of the system. This second aspect might be solved by re-tuning the observer, however, as already mentioned in Section 3.5 it is difficult to tune the observer (and controller) gains because these are the result of the LMI conditions in Theorems 3.1 and 3.2. Since, the obtained solution is probably not unique. It might be possible to add additional constraints to the conditions for

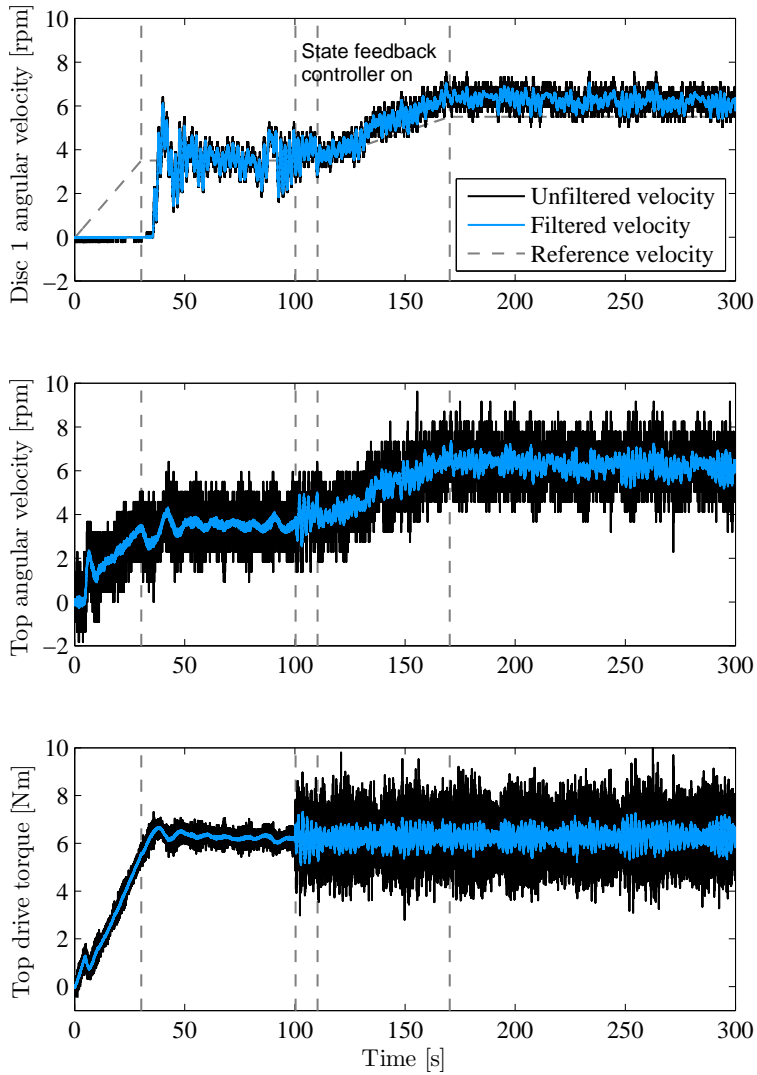


Figure 6.18: Experimental result of the drill-string setup with the designed state-feedback controller in the startup scenario.

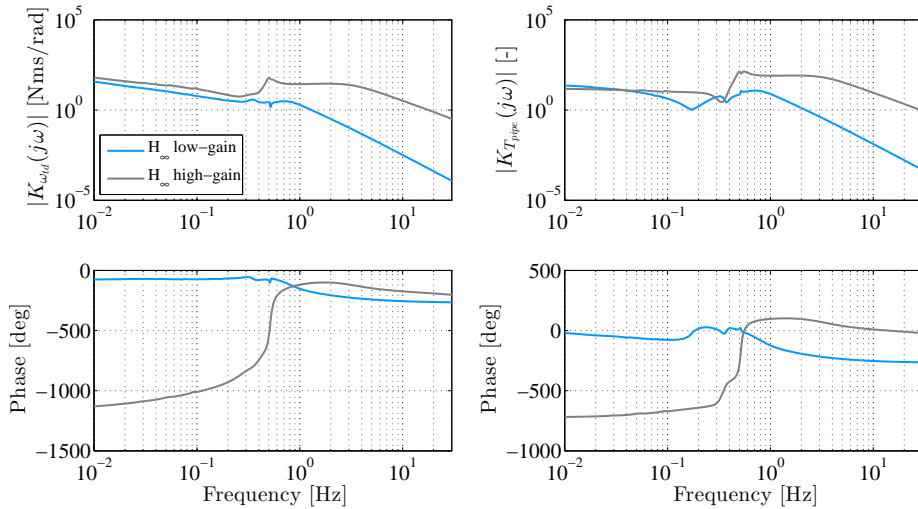


Figure 6.19: Designed linear dynamic controllers for the experimental drill-string setup, left plot is the controller which uses the top drive angular velocity, the controller in the right plot is based on the pipe torque measurement.

the observer gains, however, this has not been further investigated yet.

Further investigation of the above mentioned problems might result in a properly working observer for the experimental setup such that only surface measurements can be employed for the observer-based output-feedback controller.

#### 6.4.5 $\mathcal{H}_\infty$ -based output-feedback controller

The linear robust output-feedback controller design methodology, presented in Chapter 4, is also used to design a controller for the experimental drill-string setup. The results of the drill-string setup in closed-loop with the  $\mathcal{H}_\infty$ -based controller are presented in this section.

The designed linear, dynamic output-feedback controller for the experimental setup is shown in Figure 6.19. Actually, two controllers have been designed by different choices for the weighting filters similar to the design choices made in Section 4.5. These controllers only use the measured top drive angular velocity  $\omega_{td}$  and the pipe torque measurement  $T_{pipe}$ . In the experimental setup, the pipe torque measurement is based on the torque sensor reading just below the upper disc, compensated for the additional damping term between disc 1 and 4. As can be seen in the figure, both the high-gain and the low-gain controller have a second-order roll-off filter and the integral action in the controller  $K_{\omega_{td}}(s)$ , that uses the top drive angular velocity, can be clearly recognized.

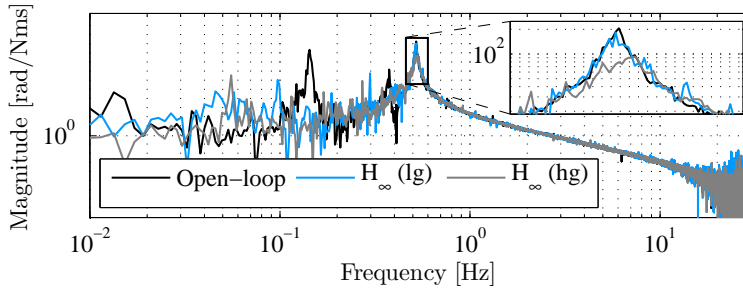


Figure 6.20: Bit-mobility of the setup with two different  $\mathcal{H}_\infty$ -controllers.

The resulting measured bit-mobilities are shown in Figure 6.20. It can be seen that the designed controllers suppress the first and second flexibility mode in the bit-mobility. However, the third mode is only slightly damped using these controllers. Clearly, the high-gain controller ( $\mathcal{H}_\infty$  (hg)) achieves more damping of the third mode than the low-gain controller ( $\mathcal{H}_\infty$  (lg)). The limited amount of damping of this mode is caused by the fact that it is difficult to synthesize a controller that suppresses the third flexibility mode and at the same time satisfies the performance specifications regarding measurement noise sensitivity. The sensitivity with respect to measurement noise plays an important role in the design of controllers for the experimental setup, because the level of noise (especially on the top drive angular velocity) is relatively high. In addition, as we have seen in Figures 6.6 and 6.7, the third mode is almost unobservable in the measured frequency response functions of the setup. Therefore, it is difficult to suppress the third torsional flexibility mode. To obtain controllers with improved suppression of the third flexibility mode, it might be possible to design controllers based on improved tuning of the weighting filters. Nevertheless, the designed controllers are applied to the experimental setup and the response of the setup is investigated.

The measured response is shown in Figure 6.21. First, the low-gain  $\mathcal{H}_\infty$ -controller is used and after approximately 210 s we switch to the high-gain controller. This switch is not necessary and the desired setpoint can also be stabilized using the low-gain controller only. However, the high-gain controller has improved robustness properties (due to the improved damping of the third mode) which can be beneficial. By only using the high-gain controller in the startup scenario it is not possible to stabilize the desired setpoint. A closer look at the experimental results with the  $\mathcal{H}_\infty$ -controllers shows that the low-gain controller is able to stabilize the desired setpoint of 5.5 rpm with limited control action (i.e. at least the controller acts less aggressively compared to the state-feedback controller and the high-gain  $\mathcal{H}_\infty$ -controller). The oscillations in the bit angular velocity are still relatively large in amplitude; however, the oscillations are sufficiently damped to mitigate stick-slip vibrations. In addition,

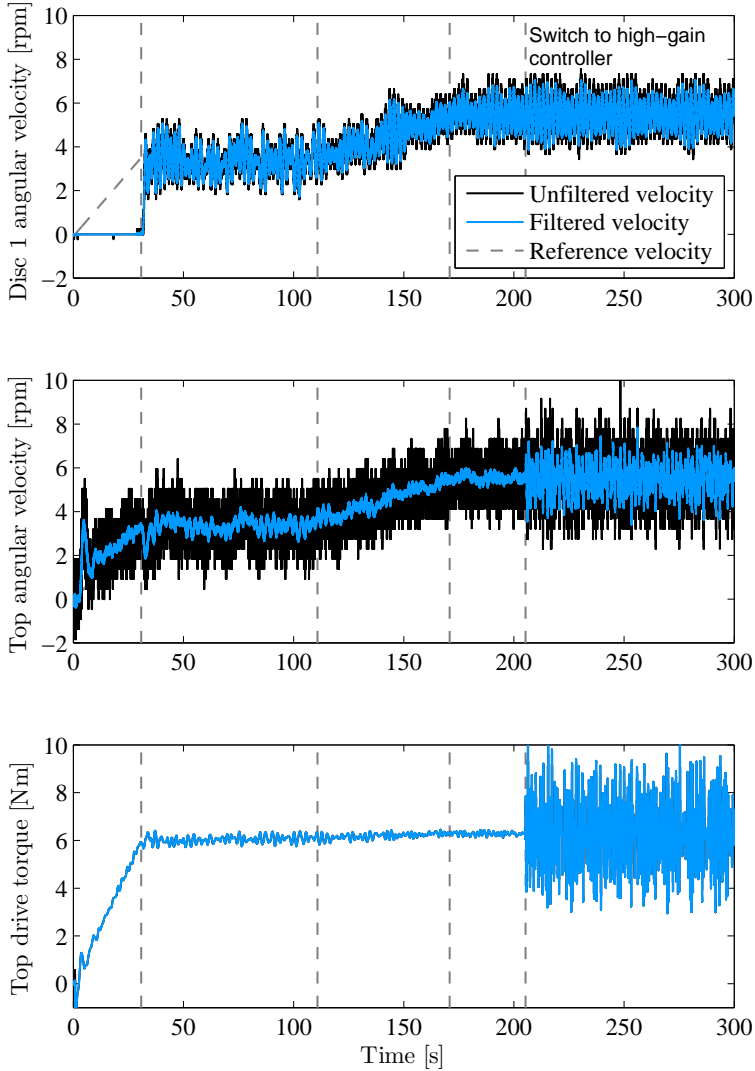


Figure 6.21: Experimental result of the drill-string setup with the designed  $\mathcal{H}_\infty$ -controllers in the startup scenario, after approximately 210 s the controller is switched to a high-gain  $\mathcal{H}_\infty$ -controller.

it has to be noted that due to the presence of the roll-off filters in the controller, high-frequent (measurement) noise is not amplified by the controller, such that possible oscillations caused by such disturbances are avoided. The high-gain controller clearly uses more control action, also resulting in more oscillations in the top drive angular velocity. However, it also slightly reducing the amplitude of the oscillations at the bit. Moreover, as mentioned before, with this controller the robustness with respect to disturbances at the bit is improved.

Summarizing, with the designed  $\mathcal{H}_\infty$ -controllers it is possible to stabilize a desired angular velocity of 5.5 rpm and to avoid stick-slip oscillations in a realistic scenario in which SoftTorque could not avoid stick-slip oscillations. However, it would be worth to investigate possible improvements of the controllers (by retuning the weighting filters) to improve performance. This can probably be obtained by designing a controller that results in more suppression of the third flexibility mode in the bit-mobility. However, the controller still has to satisfy the performance specifications regarding measurement noise sensitivity due to the relatively high level of measurement noise in the setup.

## 6.5 Summary

In this chapter, the first results obtained with the designed experimental drill-string system are presented. The first part of this chapter focused on the identification of the parameters for the setup, compensation of undesirable dynamics and the emulation of additional dynamics. The resulting model of the experimental setup based on the identified parameters is presented. This model is used for analysis of the setup dynamics and as a basis for the (model-based) controller design strategies. Validation of the model of the experimental setup showed that the setup has more damping than the prescribed design of the setup in Chapter 5. In addition, it turned out that it is difficult to determine the damping parameters. This results in a small mismatch between the model of the experimental setup and the dynamics of the setup. Implementation of the (nonlinear) drill-string borehole and bit-rock interaction torques is presented and it is shown that with the implementation of the bit-rock interaction the setup is able to accurately reproduce stick-slip vibrations. A comparison between the response of the experimental setup and the response of the drill-string model in simulations has evidenced that the setup is able to emulate the drill-string dynamics to be investigated.

In the second part of this chapter, the focus is on the implementation and validation of the controllers on the experimental setup. First, the industrial SoftTorque controller is implemented on the setup. Experimental results showed that this controller is unable to stabilize the desired angular velocity of 5.5 rpm (corresponding to 55 rpm for a real drilling system). The response of the experimental setup is compared to the response of the drill-string model in simulations and it was shown that these responses match well. This illustrates once more that the

setup is able to accurately emulate the drill-string dynamics to be investigated.

Second, a state-feedback controller is implemented. This controller uses measurements of all the states of the system. To rely on surface measurements only, an observer has to be used, but this observer has not been successfully implemented yet. The measured closed-loop bit-mobility of the system with the state-feedback controller shows that this controller is able to damp all three torsional flexibility modes. Moreover, the response of the system also shows that this controller can successfully stabilize the desired angular velocity of 5.5 rpm and therewith mitigate stick-slip vibrations.

Third, a linear robust output-feedback controller is implemented on the setup. Two controllers have been designed which are experimentally tested. These controllers only use surface measurements and damping of the flexibility modes in the bit-mobility can be achieved. However, damping of the third flexibility mode is rather limited. It turned out that it is difficult to achieve a high level of damping of this mode while still satisfying the performance specifications on measurement noise sensitivity to reduce measurement noise amplification. Due to the significant amount of measurement noise, especially in the top drive velocity measurement, the sensitivity with respect to measurement noise is important in order to mitigate stick-slip vibrations. An experimental result of the controllers applied to the drill-string setup shows that this controller is able to stabilize a desired angular velocity of 5.5 rpm and thus mitigates stick-slip oscillations for this setpoint. To improve the performance of the controllers, future research should focus on improving the designed controllers based on re-tuning of the weighting filters.

# Modelling and analysis of drilling systems for the assessment of a down-hole anti stick-slip tool<sup>1</sup>

---

## 7.1 Introduction

The continuous search for oil, gas, mineral resources and geo-thermal energy is moving the drilling industry into new, unknown environments. To reach these unconventional reservoir sections, deep and curved borehole geometries need to be drilled. The tendency towards drilling slimmer and deeper wells requires drill-strings of several kilometers in length to transmit the axial force and torque necessary to drill the rock formations. These long and slender drill-string systems makes drilling systems susceptible to self-excited vibrations. These vibrations might lead to whirling, bit bouncing and (torsional) stick-slip [50, 57, 110, 114]. Here, the focus is on axial and torsional vibrations and their interaction. Torsional stick-slip vibrations occur when the bit is stalled (due to certain operating conditions) and the top drive system at surface is still driving the system. When enough energy has accumulated, the bit is suddenly released and starts rotating at very high velocities; subsequently, the bit slows down and can stall again. The resulting stick-slip limit cycles decrease the drilling efficiency and are detrimental to the bit, (down-hole) drilling components and the drill pipes. Therefore, mitigation of these vibrations is an important topic in the drilling industry. In this chapter, the coupled axial and torsional dynamics are modelled and analyzed for the assessment of a down-hole tool developed to mitigate stick-slip vibrations and to improve the rate-of-penetration.

---

<sup>1</sup>The notation in this chapter is different from the notation used in the rest of this thesis.



The analysis of torsional stick-slip vibrations often relies on models that account for the torsional dynamics only, see e.g. [4, 10, 13, 19, 61, 77, 114]. In these models, it is usually assumed that the resisting torque at the bit-rock interface can be modelled as a frictional contact with a velocity-weakening effect as reported in [11, 115]. Due to this velocity-weakening effect the bit-rock interaction acts as negative damping at the bit which destabilizes the drill-string dynamics leading to the onset of torsional stick-slip vibrations. However, experiments using single cutters to identify the bit-rock interaction [22] do not reveal such a velocity-weakening effect. In fact, modelling of the coupled axial and torsional dynamics, as initiated in [93], shows that the velocity-weakening effect is a consequence of the drill-string dynamics in interaction with the bit-rock interface law, rather than an intrinsic property of the bit-rock interface.

These two insights have led to modelling the torsional and axial dynamics of drilling systems coupled via a rate-independent bit-rock interaction model presented in [22, 23]. Both lumped-parameter models of the coupled axial-torsional dynamics (see e.g. [6, 21, 79, 93]) and infinite-dimensional models, i.e. formulated in terms of partial differential equations [37], are considered. In this chapter, we take a low-dimensional lumped-parameter modelling approach, motivated by the work in [37] in which it is shown that low-dimensional models can capture the essential drill-string dynamics relevant to coupled axial-torsional stick-slip oscillations. However, in contrast to many other studies, we model the bit-rock interaction as a combined cutting and frictional boundary condition as proposed in [93] and analyzed first in [38].

As mentioned before, torsional stick-slip vibrations can be harmful for drilling components and the drill-string itself and lead to a decrease of the drilling efficiency. Controller design methodologies to mitigate these torsional stick-slip vibrations have been investigated extensively, see e.g. [10, 19, 30, 40, 51, 53, 103, 120, 122] for controllers designed based on models of the torsional dynamics only, and [8] for two controller design methods based on a model of the coupled axial-torsional dynamics. An alternative solution strategy to mitigate stick-slip oscillations can be recognized in the use of a passive down-hole tool. In [129], a specialized roller reamer, designed to mitigate stick-slip vibrations, is presented. The tool is tested in the field and two offset wells have been compared, where a reduction of stick-slip vibrations and a decrease of drilling time has been achieved when the down-hole tool is used. Another down-hole tool is presented in [102]; this tool is referred to as the anti stick-slip tool (AST) (in early references also called Anti Stall Technology). This is a mechanical down-hole tool which aims to adjust the drilling torque automatically and therewith to reduce stick-slip oscillations and increase the drilling efficiency (rate-of-penetration (ROP)). Reported field results show that the tool indeed reduces the amount of vibration related failures and improves the drilling rate-of-penetration [90, 91]. This tool is investigated more extensively in this chapter. Therefore, the drill-string model presented in [6] is extended with a model of the tool to investigate its influence



Figure 7.1: Impression of the anti stick-slip tool (AST) placed in the drill-string near the bit [112].

on the drill-string dynamics. A schematic impression of the tool is shown in Figure 7.1 and its properties and the working principle are presented in Section 7.2.

The main objective of this work is to develop a modelling approach for a drill-string system including the anti stick-slip tool developed by Tomax (see [102]) and to perform analyses to investigate the working principle of the tool. In this context, the main contributions of this chapter are as follows. First, the drill-string model as in [6] is extended with a model of the anti stick-slip tool. Second, a simulation tool is developed to numerically obtain the response of the resulting nonlinear (non-smooth) drill-string model with state-dependent delay. Based on the simulation results, the dynamic behavior of the key variables of the drill-string system, such as the weight-on-bit (WOB), torque-on-bit (TOB) and (bit) angular and axial velocities of the system, can be investigated. Third, we perform dynamic analyses on the drill-string dynamics including the anti stick-slip tool

and compare the results with a benchmark model without the tool to assess the effectiveness of the tool in mitigating stick-slip vibrations and improving ROP. The analyses include a stability analysis based on a linearization approach for delay-differential equations with state-dependent delays as proposed by [42, 48]. In addition, a two time-scale analysis in the spirit of [6, 38] is performed, leading to a system with constant delay to investigate the apparent velocity-weakening effect in the TOB (being a key destabilizing factor for the torsional dynamics leading to stick-slip oscillations). Moreover, a (preliminary) study towards the effect of the AST on the rate-of-penetration (ROP) is performed based on averaging of the steady-state response of the simulation results of the nonlinear model. To the best of the author's knowledge, these results are the first attempt to model the drill-string dynamics including the anti stick-slip tool. At the end of this chapter, it is recommended to pursue a further study the modelling approach for drilling systems including the AST and some recommendations for future research are proposed. The fact that there is no drill-string model including the AST available yet also motivates the choice for the drill-string model with relatively low order. This has been done to decrease the implementation burden and to facilitate the analysis focusing on the working principle of the tool.

The outline of this chapter is as follows. First, the anti stick-slip tool is discussed in more detail and the claimed performance improvements based on field results of drilling systems including the anti stick-slip tool are presented. Then, the drill-string model including the AST is introduced in Section 7.3. The resulting nonlinear drill-string model with state-dependent delay is used for a simulation study in Section 7.4. Subsequently, in Section 7.5 the drill-string dynamics are analyzed based on a linearization approach and a two time-scale analysis. These analysis studies give some more insights in the claimed performance properties of a drill-string system including AST. Finally, the main results of this work are discussed in Section 7.6 and some recommendations for future research are discussed in Section 7.7.

## 7.2 Anti stick-slip tool

The anti stick-slip tool (AST) is a patented [43] mechanical down-hole solution placed in the lower part of the drill-string. According to [102], the working principle of the tool can be described as follows: *“The principle of the anti stick-slip tool (AST) is to provide active down-hole control of the rock-cutting process by diverting energy from the drilling process and using it to prevent dynamic forces from reaching destructive levels and thereby preserving the drill-string components as well as optimizing rock-cutting efficiency”*. Under normal, stable conditions, the tool will transfer torque and weight to the bit as a passive part of the bottom hole assembly (BHA). However, if the bit becomes unstable (starts exhibiting vibrations), the AST will intervene to regulate the bit's depth-of-cut

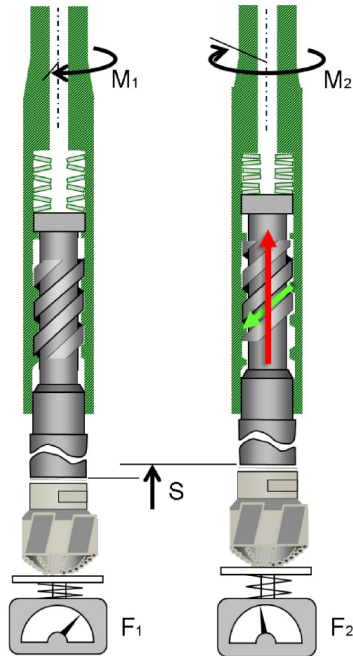


Figure 7.2: Anti Stick-slip Tool (AST). An abrupt increase in torque ( $M_2$ ) will cause a telescopic contraction ( $S$ ) to off-load the weight from the cutters ( $F_2$ ) [2].

(DOC) by manipulating the weight-on-bit (WOB).

The tool mainly consists of two tool bodies connected to each other with a helical spline and an internal pre-loaded spring, see Figures 7.1 and 7.2. Its working principle can be shortly summarized as follows: any abrupt change in torque, such as a torque spike from the cutters hanging on a hard stringer will cause a telescopic contraction of the tool along an internal helix. This contraction instantaneously reduces the weight on the cutters and consequently the depth-of-cut. The contraction continues until the depth-of-cut is reduced sufficiently (thereby reducing the torque-on-bit) for rotation to continue. An internal spring in the tool will gradually re-apply the initial weight and the tool will repeat the process as needed [91].

Test results as presented in [102] and field results as reported in [2, 58, 90, 91] revealed two main benefits of the anti stick-slip tool:

- Implementation of the anti stick-slip tool in the BHA can result in mitigation of (torsional) stick-slip oscillations;
- Incorporation of the AST results in a higher drilling efficiency compared

to offset wells, especially resulting in an increase of the surface rate-of-penetration for similar operating conditions regarding the weight-on-bit.

Overall, the AST is claimed to enable drilling highly mixed and laminated formations with less risk of severe vibrations and down-hole equipment failures [90]. In addition, it is claimed to open up ways to drill hard formations with aggressive polycrystalline diamond compact (PDC) bits to maximize drilling efficiency in terms of increased penetration rates and PDC durability [2].

Despite the above evidence based on field data, a fundamental physics-based explanation for these effects is lacking to this date. Therefore, the above claims are investigated in this research using a model-based approach.

### 7.3 Modelling of the drill-string dynamics

In this section, the model of the drill-string dynamics including AST is presented. First, in Section 7.3.1 a short overview is given of a benchmark model that describes the coupling of the axial and torsional dynamics, excluding the tool. This model is based on the work presented in [6]. Next, in Section 7.3.2 the anti stick-slip tool is modelled, resulting in an extended drill-string model, including the AST. In Section 7.3.3, a model reformulation is given to obtain a dimensionless model of the drill-string dynamics which is used for the simulations and analyses in Sections 7.4 and 7.5, respectively.

#### 7.3.1 Modelling of the benchmark drill-string dynamics

In Figure 7.3, a schematic illustration of a (vertical) drilling system is shown. Such a drilling system consists of a drilling rig on the surface, where the drill-string is driven by a so-called top drive. The drill-string consists of drill pipes and can be several kilometers in length; the bottom part consists of heavier-weight drill pipe known as the bottom hole assembly (BHA). The BHA also contains down-hole tools (e.g. down-hole motors, stabilizers and measurement while drilling (MWD) tools) and the drill bit at its end.

A model of a drill-string system is schematically depicted in Figure 7.4(a). Here, the top drive is not modelled and it is assumed that it exhibits a constant rotational and vertical velocity,  $\Omega_0$  and  $V_0$ , respectively. Therefore, the boundary conditions at the top of the drill-string are both prescribed angular and axial displacement. The bottom hole assembly with axial and angular position  $U$  and  $\Phi$ , respectively, is modelled as a discrete mass  $M$  with inertia  $I$  and represents the first modal inertia of the combined drill-string and bottom hole assembly. The drill-string is modelled as a spring with torsional stiffness  $C$  and axial stiffness  $K$ . The viscous friction parameter  $D$  characterizes viscous friction along the drill-string and BHA, leading to the equations of motion characterizing the drill-string

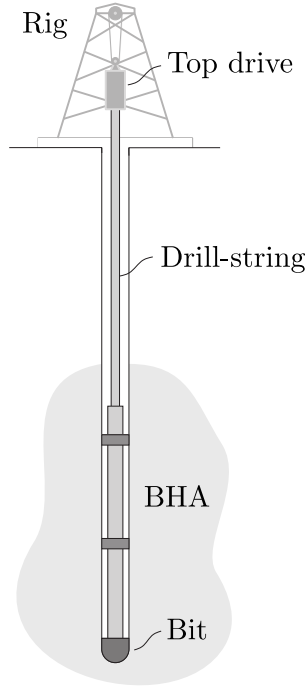


Figure 7.3: Schematic illustration of a drilling system for a vertical bore-hole configuration [8].

dynamics as follows:

$$M\ddot{U} + D\dot{U} + K(U - V_0 t) = -W^c - W^f, \quad (7.1)$$

$$I\ddot{\Phi} + C(\Phi - \Omega_0 t) = -T^c - T^f. \quad (7.2)$$

in which  $W^i$  and  $T^i$  ( $i \in \{c, f\}$ ) denote the force and torque on the drill bit as a result of the bit-rock interaction, respectively. The force and torque both consists of a cutting and friction component, denoted by superscripts  $c$  and  $f$ , respectively, i.e.  $W := W^c + W^f$  and  $T := T^c + T^f$ . The cutting process takes place on the cutting face of the blades with the cutters on the drill bit and describes the removal of rock, whereas the friction component is caused by the contact between the underside of the blades (called the wearflat) and the well bottom. Following [22, 93], these processes are modelled by

$$W^c = na\zeta\varepsilon d, \quad W^f = nal\bar{\sigma} \frac{1 + \text{sign}(\dot{U})}{2}, \quad (7.3)$$

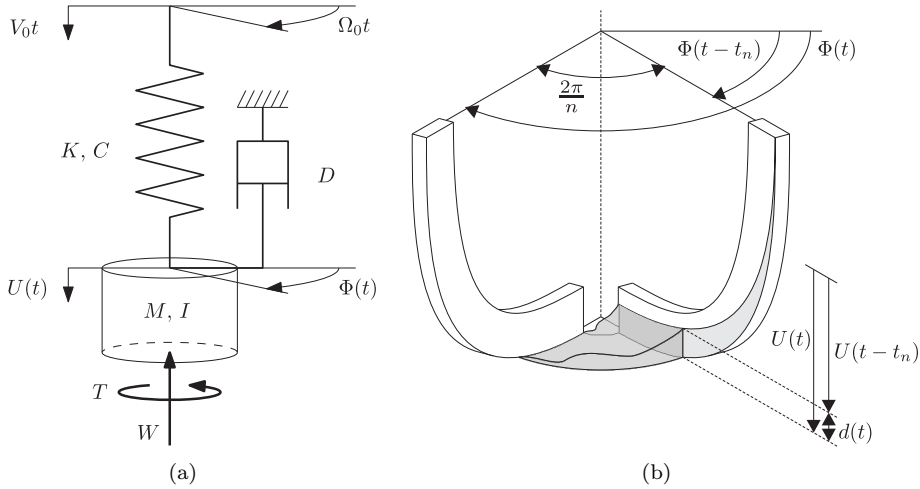


Figure 7.4: (a) Schematic model of a drill-string [6]. (b) Bottom hole profile between two successive blades of cutters [92].

$$T^c = \frac{1}{2}na^2\varepsilon d, \quad T^f = \frac{1}{2}na^2\xi\mu\bar{\sigma} \frac{1 + \text{sign}(\dot{U})}{2} \quad (7.4)$$

with  $n$  the number of blades on the drill bit with radius  $a$ . The cutting process is characterized by the intrinsic specific energy  $\varepsilon$ , which gives the required energy to destroy a unit volume of rock, and the orientation of the cutting face of the cutters on the bit, represented by  $\zeta$ . The frictional process takes place at the bit-rock interface at the underside of the blades, known as the wearflat, with length  $l$ . The bit-rock contact at the wearflats is described by the contact stress, which is constant (and equal to  $\bar{\sigma}$ ) when the bit moves downwards into the rock. The geometry of the bit-rock contact indicates that the wearflat is no longer in contact with the rock when the bit moves upwards. This is modelled using the sign-function in  $W^f$ , see (7.3). A frictional process at the wearflat relates this contact force  $W^f$  to the frictional torque  $T^f$  via the friction coefficient  $\mu$  and the parameter  $\xi$ , which characterizes the spatial distribution of the wearflats. Finally, the cutting forces are proportional to the depth-of-cut (DOC)  $d$ , which is in general not constant. Specifically, the DOC depends on the axial position of the cutter with respect to the rock surface, as generated by the previous blade some timelapse  $t_n$  ago. This is schematically depicted in Figure 7.4(b). Hence, the depth-of-cut, describing the height of material in front of a single blade, can be written as

$$d(t) = U(t) - U(t - t_n(t)). \quad (7.5)$$

The delay  $t_n$  itself is time-dependent (actually state-dependent) and denotes the

time interval in which the bit rotates  $2\pi/n$  rad, which is the angle between two successive blades of cutters on the bit:

$$\int_{t-t_n(t)}^t \frac{d\Phi(s)}{ds} ds = \Phi(t) - \Phi(t - t_n(t)) = \frac{2\pi}{n}. \quad (7.6)$$

In the calculation of the depth-of-cut and the delay it is assumed that the drill bit moves down in a perfectly vertical well. Lateral motions of the drill bit (i.e. bit whirl) are not considered.

In the remainder of this chapter, the model (7.1)-(7.6) presented in this section is referred to as the benchmark model, as this model is used as a benchmark to compare with the model including the AST presented in the next section.

### 7.3.2 Modelling of the drill-string dynamics including anti stick-slip tool

An impression of the anti stick-slip tool (AST) is given in Figure 7.5(a); the tool comprises relatively few components. It mainly consists of two tool bodies connected to each other with a helical spline and an internal pre-loaded spring. The principle of the AST is that a torsional load with sufficient magnitude to overcome the loading in the compressed spring will make the upper tool part with internal helical spline rotate onto the mating lower part. When the upper and lower parts screw together in this manner, the tool telescopically contracts and the drill-string becomes shorter [102]. In this section, the model presented in Section 7.3.1 is extended by including a model of the down-hole AST.

A schematic representation of the drill-string model including AST is shown in Figure 7.5(b). As can be seen in this figure, the BHA is separated in two parts, the first part is modelled as a discrete mass  $M$  with inertia  $I$  and again represents the first modal inertia of the combined drill-string and bottom hole assembly (as far as the part above the tool is concerned) and the second part represents the part of the BHA below the AST, modelled as mass  $M_b$  with inertia  $I_b$ . The coordinates of the system are given by

$$q = [U \ U_b \ \Phi \ \Phi_b]^\top. \quad (7.7)$$

with  $U$  the axial position of the BHA (above the AST-tool),  $\Phi$  the angular position of the BHA (above the AST-tool),  $U_b$  the axial position of the bit (i.e. below the tool) and  $\Phi_b$  the angular position of the bit. The forces  $W$  and torques  $T$  now depend on the axial position and velocity and angular position of the bit, as can be seen in Figure 7.5(b). To model the AST-tool, an additional axial spring  $K_b$  and axial damper  $D_b$  are introduced and a kinematic constraint is introduced that describes the coupling between the axial and torsional displacement, due to the helical spline in the tool. The related holonomic constraint equation follows



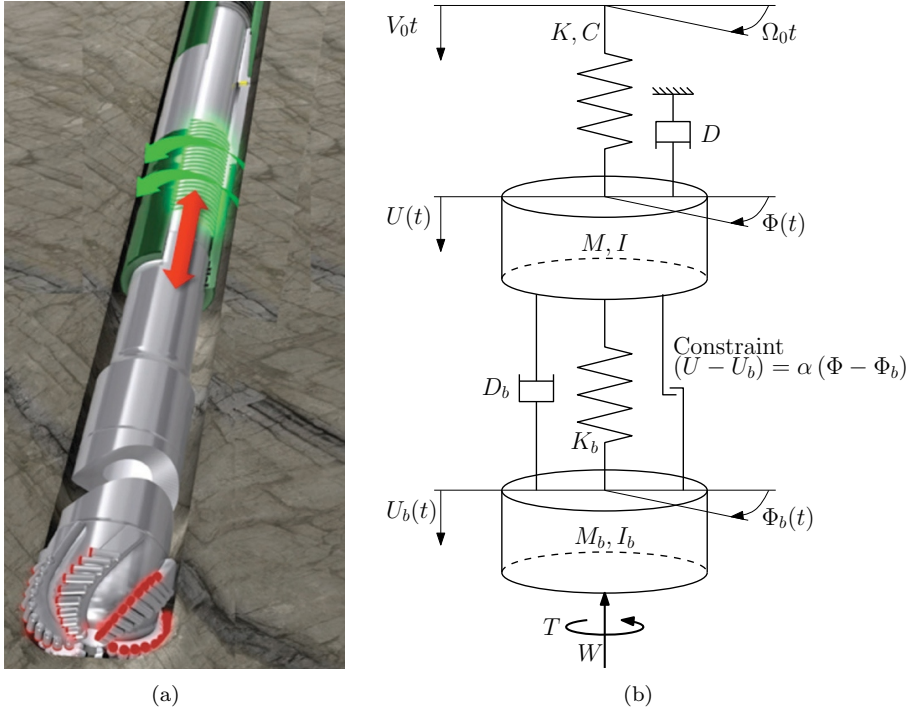


Figure 7.5: (a) Impression of the working principle of the anti stick-slip tool (AST) [46]. (b) Schematic model of a drill-string including anti stick-slip tool (AST).

from the relation between the lead  $p$ , lead angle  $\beta$  and the pitch radius  $r$  and is given by:

$$U - U_b = \frac{p}{2\pi r} (\Phi r - \Phi_b r) = \frac{p}{2\pi} (\Phi - \Phi_b) =: \alpha (\Phi - \Phi_b). \quad (7.8)$$

A Lagrangian approach for systems with constraints is used to derive the equations of motion for this system (see Appendix D.1), resulting in the equations of motions given by:

$$\begin{aligned} M\ddot{U} + D\dot{U} + D_b(\dot{U} - \dot{U}_b) + K(U - V_0 t) + K_b(U - U_b) &= -\lambda \\ M_b\ddot{U}_b - D_b(\dot{U} - \dot{U}_b) - K_b(U - U_b) &= -W^c - W^f + \lambda \\ I\ddot{\Phi} + C(\Phi - \Omega_0 t) &= \alpha\lambda \\ I_b\ddot{\Phi}_b &= -T^c - T^f - \alpha\lambda \end{aligned} \quad (7.9)$$

with the kinematic constraint that is described by (7.8):

$$U - U_b = \alpha (\Phi - \Phi_b). \quad (7.10)$$

The holonomic constraint equation is used to derive an explicit expression for the Lagrange multiplier  $\lambda$ ; subsequently the degree of freedom related to  $\Phi$  can be eliminated. The expressions for the force, torque, depth of cut and time-dependent delay are similar to (7.3)-(7.5), for the benchmark model. The difference is that the displacements and velocities that play a role in this respect now appear as  $U_b$ ,  $\Phi_b$  and  $\dot{U}_b$ ,  $\dot{\Phi}_b$ , respectively. The resulting equations of motion in the independent coordinates  $U$ ,  $U_b$  and  $\Phi_b$  are given by:

$$\begin{aligned} \left(M + \frac{I}{\alpha^2}\right) \ddot{U} - \frac{I}{\alpha^2} \ddot{U}_b + \frac{I}{\alpha} \ddot{\Phi}_b + D\dot{U} + D_b(\dot{U} - \dot{U}_b) + K(U - V_0 t) + \\ K_b(U - U_b) + \frac{C}{\alpha^2}(U - U_b) + \frac{C}{\alpha}(\Phi_b - \Omega_0 t) = 0, \end{aligned} \quad (7.11)$$

$$\begin{aligned} -\frac{I}{\alpha^2} \ddot{U} + \left(M_b + \frac{I}{\alpha^2}\right) \ddot{U}_b - \frac{I}{\alpha} \ddot{\Phi}_b - D_b(\dot{U} - \dot{U}_b) - \\ K_b(U - U_b) - \frac{C}{\alpha^2}(U - U_b) - \frac{C}{\alpha}(\Phi_b - \Omega_0 t) = \\ -na\zeta\varepsilon(U_b(t) - U_b(t - t_n(t))) - nal\bar{\sigma} \frac{1 + \text{sign}(\dot{U}_b)}{2}, \end{aligned} \quad (7.12)$$

$$\begin{aligned} \frac{I}{\alpha} \ddot{U} - \frac{I}{\alpha} \ddot{U}_b + (I_b + I) \ddot{\Phi}_b + \frac{C}{\alpha}(U - U_b) + C(\Phi_b - \Omega_0 t) = \\ -\frac{1}{2}na^2\varepsilon(U_b(t) - U_b(t - t_n(t))) - \frac{1}{2}na^2\xi\mu l\bar{\sigma} \frac{1 + \text{sign}(\dot{U}_b)}{2}. \end{aligned} \quad (7.13)$$

The time delay equation for the model with AST is as follows:

$$\int_{t-t_n(t)}^t \frac{d\Phi_b(s)}{ds} ds = \Phi_b(t) - \Phi_b(t - t_n(t)) = \frac{2\pi}{n}. \quad (7.14)$$

This model can be used for the analysis of the AST. First, in the next section the model is transformed into a dimensionless form to reduce the number of parameters and to facilitate numerical simulation.

### 7.3.3 Model reformulation

The equations of motion (7.11)-(7.14) are scaled to reduce the number of parameters and, in addition, perturbation coordinates are introduced to describe the equations of motion around the nominal solution (corresponding to a constant

rotational speed and constant rate-of-penetration, thereby reflecting nominal drilling conditions). Introduce the characteristic time and length as:

$$t_* = \sqrt{\frac{I}{C}}, \quad L_* = \frac{2C}{\varepsilon a^2}.$$

Typically,  $t_* \sim 1$  s and  $L_* \sim 1$  mm. These characteristic parameters are used for the coordinate transformation

$$u(\tau) = \frac{U - U_0}{L_*}, \quad u_b(\tau) = \frac{U_b - U_{b0}}{L_*}, \quad \varphi_b(\tau) = \Phi_b - \Phi_{b0}, \quad (7.15)$$

where  $u$ ,  $u_b$  and  $\varphi_b$  are functions of the dimensionless time

$$\tau = \frac{t}{t_*} \quad (7.16)$$

and represent the (scaled) relative axial ( $u$  and  $u_b$ ) and torsional ( $\varphi_b$ ) displacements. In (7.15),  $U_0(t)$ ,  $U_{b0}(t)$  and  $\Phi_{b0}(t)$  are the nominal solutions of (7.11)-(7.13), which are given by:

$$\begin{aligned} U_0 &= V_0 t - \frac{DV_0 + B}{K}, \\ U_{b0} &= V_0 t - \frac{DV_0}{K} - \frac{A}{\alpha K_b} - \frac{B(K + K_b)}{K_b K}, \\ \Phi_{b0} &= \Omega_0 t - \frac{A}{\alpha^2 K_b} - \frac{A}{C} - \frac{B}{\alpha K_b}, \end{aligned} \quad (7.17)$$

with  $A := \frac{1}{2}na^2\varepsilon V_0 t_{n0} + \frac{1}{2}na^2\xi\mu l\bar{\sigma}$  and  $B := na\zeta\varepsilon V_0 t_{n0} + nal\bar{\sigma}$ . These solutions correspond to a constant axial and torsional velocity  $V_0$  and  $\Omega_0$ , respectively, and also induce a constant delay  $t_{n0} = \frac{2\pi}{\Omega_0 n}$ . In dimensionless time, the time delay is given by  $\tau_n = \frac{t_n}{t_*}$  and the prescribed velocities at the surface in their dimensionless form are given by:

$$v_0 = \frac{V_0 t_*}{L_*}, \quad \omega_0 = \Omega_0 t_*. \quad (7.18)$$

In addition, a perturbation of the time delay with respect to the nominal time delay is introduced:

$$\hat{\tau}_n = \tau_n - \tau_{n0}, \quad (7.19)$$

where  $\tau_{n0} = \frac{t_{n0}}{t_*} = \frac{2\pi}{\omega_0 n}$ . The above scaling and introduction of perturbation coordinates leads to the following dimensionless model formulation:

$$\begin{aligned} (1 + \kappa)u'' - \kappa u_b'' + \nu \varphi_b'' + \gamma u' - \gamma_b(u_b' - u') + \eta^2 u + \\ \eta_b^2(u - u_b) + \kappa(u - u_b) + \nu \varphi_b = 0. \end{aligned} \quad (7.20)$$

$$\begin{aligned} -\kappa u'' + (m_* + \kappa)u_b'' - \nu \varphi_b'' + \gamma_b(u_b' - u') - \eta_b^2(u - u_b) - \\ \kappa(u - u_b) - \nu \varphi_b = n\psi(-u_b(\tau) + u_b(\tau - \tau_n) - v_0 \hat{\tau}_n + \lambda g(u_b')), \end{aligned} \quad (7.21)$$

Table 7.1: Parameters of the drill-string model including AST in dimensionless form (7.20)-(7.23).

| Parameter                   | Symbol  | Value |
|-----------------------------|---|-------|
| Drill-string design         | $\psi = \frac{\zeta \varepsilon a I}{M C_p}$        | 129.4 |
| Drill bit design            | $\beta = \zeta \mu \xi$                             | 0.36  |
| Wearflat friction           | $\lambda = \frac{a^2 l \bar{\sigma}}{2 \zeta C_p}$  | 5.6   |
| Scaled viscous friction     | $\eta = \sqrt{\frac{K_p I}{M C_p}}$                 | 1.59  |
| Scaled axial damping        | $\gamma = \frac{D}{M} \sqrt{\frac{I}{C_p}}$         | 0.86  |
| Scaled viscous friction AST | $\eta_b = \sqrt{\frac{K_{AST} I}{M C_p}}$           | 4.62  |
| Scaled axial damping AST    | $\gamma_b = \frac{D_{AST}}{M} \sqrt{\frac{I}{C_p}}$ | 0.18  |
| Mass ratio                  | $m_* = M_b / M$                                     | 0.080 |
| Inertia ratio               | $\iota = I_b / I$                                   | 0.082 |
| Scaled inertia              | $\kappa = \frac{I}{M \alpha^2}$                     | 0.94  |
| Scaled lead AST             | $\nu = \frac{\kappa \alpha}{L_*}$                   | 213.0 |

$$(1 + \iota) \varphi_b'' + \varphi_b + \frac{\kappa}{\nu} u'' - \frac{\kappa}{\nu} u_b'' + \frac{\kappa}{\nu} (u - u_b) \quad (7.22)$$

$$= n(-u_b(\tau) + u_b(\tau - \tau_n) - v_0 \hat{\tau}_n + \beta \lambda g(u_b')).$$

$$\varphi_b(\tau) - \varphi_b(\tau - \tau_n) + \omega_0 \hat{\tau}_n = 0. \quad (7.23)$$

where the prime  $(\cdot)'$  denotes differentiation with respect to the dimensionless time  $\tau$ . The dimensionless depth-of-cut is given by

$$\delta = u_b(\tau) - u_b(\tau - \tau_n) + v_0 \tau_n, \quad (7.24)$$

and perturbations with respect to the nominal depth-of-cut are defined as  $\hat{\delta} := \delta - \delta_0$  with  $\delta_0 = \frac{2\pi v_0}{n\omega_0} = v_0 \tau_{n0}$ . The parameters used in this dimensionless form are given in Table 7.1 (an overview of the model parameters based on a real drill-string configuration is given in Appendix D.2). The nonlinear function  $g(u_b')$  in (7.21) and (7.22) describes whether the wearflat is in contact with the rock ( $g = 0$ ) or not ( $g = 1$ ), where the discontinuity at  $u_b' = -v_0$  is represented by a convex set-valued map:

$$g(u_b') \in \frac{1 - \text{Sign}(u_b' + v_0)}{2} = \begin{cases} 0, & u_b' > -v_0 \\ [0, 1], & u_b' = -v_0 \\ 1, & u_b' < -v_0 \end{cases} \quad (7.25)$$

where  $\text{Sign}(\cdot)$  is the set-valued sign function. Hence the model (7.20)-(7.23) and the set-valued map (7.25) constitute a delay-differential inclusion with state-dependent delay, describing the drill-string dynamics in perturbation coordinates.

It has to be noted that the model (7.20)-(7.23) describes the dynamics for nonnegative depth-of-cut ( $d \geq 0$ , i.e.  $\delta \geq 0$ ) and positive angular velocity of the bit ( $\dot{\phi}_b > -\omega_0$ ). This means that the model loses validity when the depth-of-cut becomes negative due to severe axial vibrations, i.e. bit bouncing, or when the bit is sticking in torsional direction. Nonetheless, the model can be used to predict the onset of torsional vibrations which can lead to stick-slip. An approach for the inclusion of torsional stick in the model is given in [6] and this approach is also used for the simulation results in the next section.

## 7.4 Simulation results

In this section, both simulation results of the benchmark model (Section 7.3.1) and the drill-string model including AST (Section 7.3.2) are presented. For these simulations, we used a dedicated simulation environment that has been developed to numerically obtain the response of the non-smooth drill-string model with set-valued discontinuity and state-dependent delay. For the simulations, we used the models in perturbation coordinates as presented in Section 7.3.3 for the drill-string model with and without AST. However, the results are presented in the system coordinates  $q = [U \ U_b \ \Phi \ \Phi_b]^\top$  to support straightforward physical interpretation of the results. In Section 7.4.1, the results of the benchmark model are presented. These results are in agreement with the results in [6], except for some parameter changes. The simulation results of the model including the AST are presented in Section 7.4.2. In both sections, the results are presented for two different operating scenarios:

- A “low”-rpm case, where  $\Omega_0 = 50$  rpm,
- A “high”-rpm case, where  $\Omega_0 = 120$  rpm,

where the prescribed axial velocity is equal to  $V_0 = 20$  ft/hr for both scenarios. These two scenarios are chosen because these reflect nominal drilling operations and field observations showed that the AST performs better for high angular velocities, which can be investigated by comparing the results of the two scenarios.

In this section, both claims regarding the benefits of the tool as mentioned in Section 7.2 are investigated. The first claim, regarding mitigation of stick-slip vibrations by implementation of the AST in the BHA is investigated by simulation study in Section 7.4.2 and compared with simulation result of the benchmark model (see Section 7.4.1). The second claim, regarding the increased ROP when using the tool is investigated in Section 7.4.3 by determining the average WOB as function of axial velocity (ROP) based on the obtained simulation results.

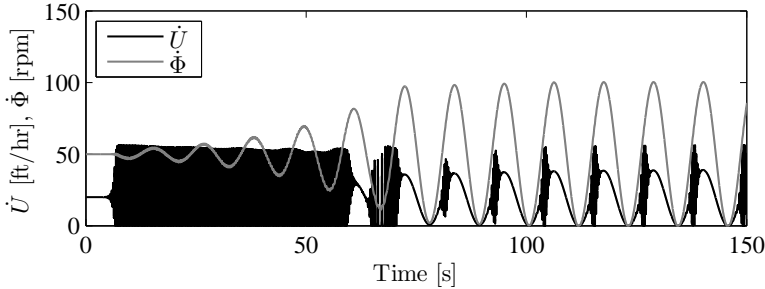


Figure 7.6: Simulation result of the benchmark model with a prescribed angular velocity of 50 rpm and axial velocity of 20 ft/hr.

#### 7.4.1 Simulation results of the benchmark model

The simulation result for the first operating scenario of the benchmark model is shown in Figure 7.6. The initial conditions of the system coordinates are chosen close to the desired setpoint. That is, small initial perturbations with respect to the nominal solution corresponding to a constant rotational velocity and constant ROP are employed. After some transient oscillations in approximately the first 80 seconds, the response converges to a limit cycle. The amplitude of the oscillations in the torsional velocity increase until the torsional velocity experiences a stick-slip limit cycle. In the model it is assumed that the rock underneath the bit cannot be indented, implying that the bit also sticks in axial direction when the bit sticks in torsional direction. Another observation that can be made is that the oscillations in the axial dynamics take place at a higher frequency compared to the torsional oscillations. This has also been observed in the analysis in [6].

From this simulation result, it can be concluded that the desired operating point of the drill-string model is unstable and that the response of both the torsional and axial velocity converges to a limit cycle. In Section 7.5, the stability of the desired setpoint is further investigated by means of a linearization of the drill-string dynamics around this nominal operating condition.

Let us now study the response of the benchmark model for the second operating scenario; herein, also oscillations can be recognized, see Figure 7.7. However, these are oscillations with a small amplitude around the desired operating velocities (note the scaling of the vertical axes). We observe, however, that the amplitude of the oscillations is slowly increasing. Increasing the simulation time span shows that eventually also for these operating conditions, the drill-string dynamics show stick-slip vibrations. Therefore, it can be concluded that also at these operating conditions the desired setpoint of the drill-string dynamics is unstable. This observation is in correspondence with the stability analysis in [21]. This stability analysis revealed a fast and a slow regime of instability

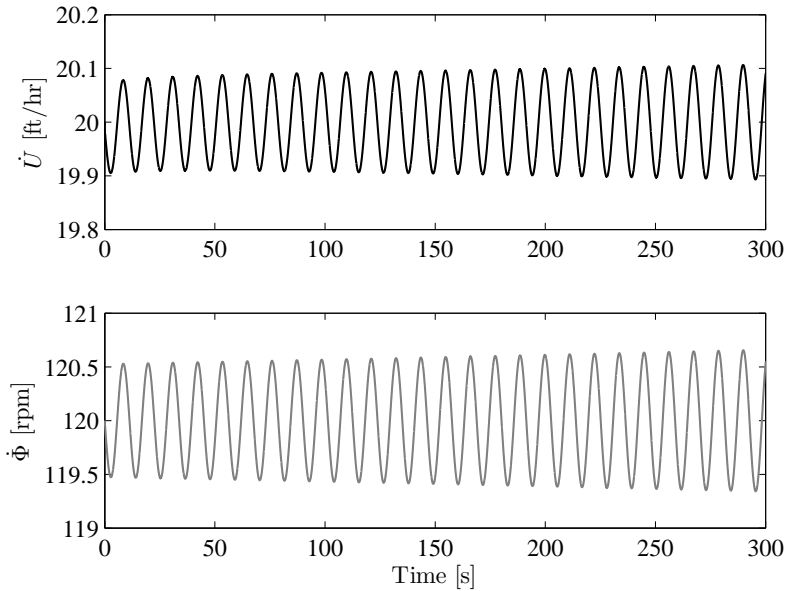


Figure 7.7: Simulation result of the benchmark model with a prescribed angular velocity of 120 rpm and axial velocity of 20 ft/hr.

depending on the nominal rotation speed, which is discussed in more detail in Section 7.5.1. Another observation that can be made is that the oscillations in the axial and torsional dynamics now occur at a similar time-scale.

#### 7.4.2 Simulation results of the model including anti stick-slip tool

Simulations of the drill-string model including AST have been performed under the same operating conditions as the simulations of the benchmark model and these results are presented in this section. First, the response of the system with a desired angular velocity of 50 rpm is shown in Figure 7.8. In this figure, the axial and torsional velocity of the bit, respectively  $U_b$  and  $\Phi_b$ , are shown. Compared to the response of the benchmark model the bit evolves faster towards a torsional stick-slip limit cycle. Contrary to the expectation that the tool is able to mitigate torsional stick-slip vibrations, this indicates that the growth rate of the torsional instability has increased. This might indicate that the desired angular velocity of 50 rpm is not within the working range of the AST. Moreover, it can be seen that the amplitude of the axial vibrations at the bit has increased, with peak values up to 5 times the amplitude of the axial vibrations in the simulation of the benchmark model. However, it also has to be mentioned that these

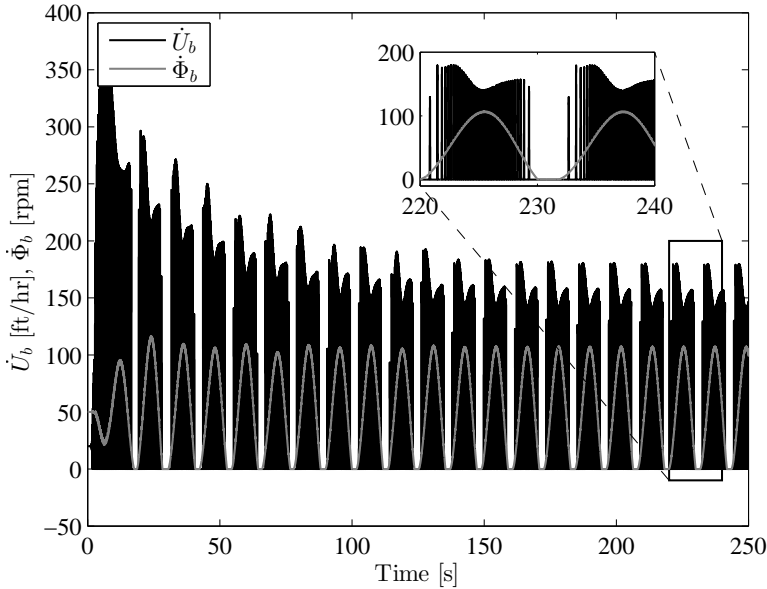


Figure 7.8: Simulation result of the drill-string model including AST with a prescribed angular velocity of 50 rpm and axial velocity of 20 ft/hr. Note that this is a simulation result of the drill-string model with AST as proposed in this thesis, it does not represent field results of a drilling system with AST.

results are obtained using simulations of the model proposed in Section 7.3.2. Improvements of the model and the model parameters might be necessary to obtain a better correspondence with field results.

The results of the second scenario for the drill-string system with AST are shown in Figure 7.9. The response of the axial and torsional velocity are shown for a simulation with a desired angular velocity of 120 rpm. Also in this situation the torsional velocity converges to a stick-slip limit cycle; similar as for the benchmark model it takes more time to reach this limit cycle behavior, compared to the 50 rpm scenario. However, also in this case the growth rate of the oscillations is larger for the system with tool compared to the benchmark model. Furthermore, the axial vibrations are lower in amplitude for the 120 rpm case compared to the 50 rpm case.

Let us now investigate if we can draw conclusions about the working principle of the tool based on these simulation results. A possible explanation for the working principle of the tool is given in [102]. Increasing bit torque from the rock-cutter interface will cause the AST to contract, offloading the weight-on-bit and reducing the depth-of-cut. The tool will then extend and reapply weight to



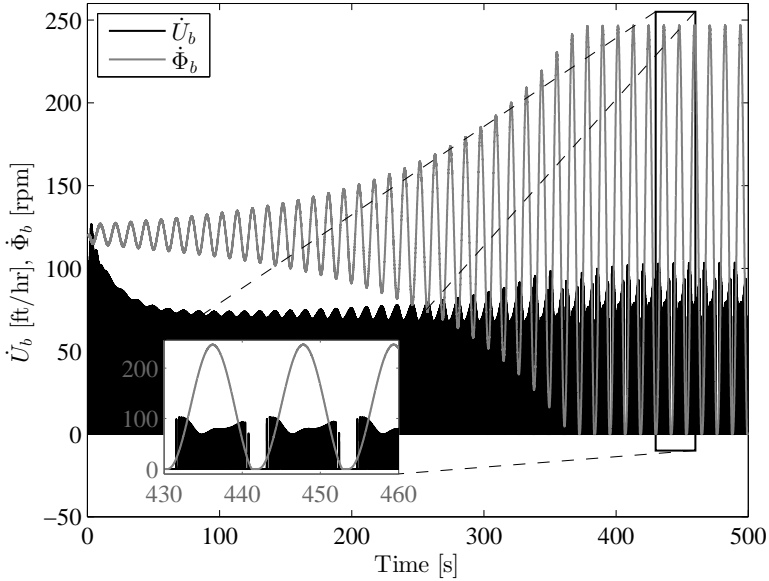


Figure 7.9: Simulation result of the drill-string model including AST with a prescribed angular velocity of 120 rpm and axial velocity of 20 ft/hr. Note that this is a simulation result of the drill-string model with AST as proposed in this thesis, it does not represent field results of a drilling system with AST.

deliver a steady load. To investigate this claim, the torque-on-bit, actual tool stroke and depth-of-cut are shown in Figure 7.10 for the 120 rpm case. Note that the stroke of the tool is indicated by  $U_b - U$ ; this means that an unloaded axial spring in the tool corresponds to a value of zero and a negative value for  $U_b - U$  corresponds to indentation of the tool. As can be seen in the second plot in Figure 7.10, the spring is always indented during operation to transfer the nominal weight and torque to the bit. In addition, it can be observed that the actual movement of the tool is approximately 2 cm. This corresponds to the limited contraction of the tool as reported in [2]. From the response of the system, we can see that when the bit is in torsional stick, i.e. depth-of-cut is constant, (for example between  $t \approx 441$  and  $t \approx 443$ ) the AST contracts further. At the same time, the WOB reduces; however, at the end of the sticking period (when the tool still contracts) the WOB increases again and a similar pattern holds for the TOB. This increase is caused by an increase in the friction force (torque) as the cutting force (torque) is constant when the depth-of-cut is constant. Recall that the WOB and TOB depend on the depth-of-cut and sign of the axial bit velocity. So these simulation results do not directly match with the hypothesis that the tool contracts due to an increasing torque-on-bit

resulting in a decrease of the weight-on-bit.

Another observation that can be made is that the dominant frequency in the motion of the tool corresponds to the frequency of the torsional limit cycle, while only a small-amplitude oscillation related to the axial dynamics is visible in the stroke of the tool. Although the frequency of the tool movement corresponds to the frequency of the torsional dynamics, it has to be noted that there is a phase shift present between the tool movement and the angular velocity of the bit. So, again, these results only partially match with the claimed working principle of the tool.

It can be concluded that it is not possible to formulate a direct relation between the torque-on-bit, depth-of-cut and contraction of the AST, as the before mentioned hypothesis about the working principle of the tool suggests. Thus, the simulations do not illustrate the expected behavior of the drill-string system including AST. From field observations and experimental results it is known that the AST can mitigate torsional stick-slip vibrations and additionally increase the rate-of-penetration. In Section 7.5, we will further investigate the drill-string model including AST by means of linearization to investigate the stability properties in more detail and employ averaging to investigate the axial and torsional dynamics separately. These methods are used to further investigate of the claims regarding the working principle of the AST. In Section 7.4.3, the claim regarding the increased ROP is investigated by averaging the response of the system obtained by numerical simulation.

### 7.4.3 Investigation of the effect of the tool on the rate-of-penetration

As mentioned in Section 7.2, it is claimed that an increase of the rate-of-penetration can be achieved (for an equal hookload at the top of the drill-string) by using the tool in the drill-string. In other words, an increase of performance is achieved for the same axial (and torsional) boundary conditions at the surface. In the adopted model, the axial velocity at the top of the drill-string is prescribed; therefore, it is not possible to compare the response of the model including AST with the benchmark model for equal hookload settings. However, we can investigate the (averaged) weight-on-bit of the response of the (nonlinear) drill-string dynamics, i.e. (7.20)-(7.23), for various prescribed axial velocities. The (averaged) weight-on-bit as function of the (prescribed) axial velocity gives an indication of the drilling efficiency in terms of the amount of WOB necessary to obtain a certain rate-of-penetration. The same approach is taken for the benchmark model such that a comparison of the averaged WOB between the two models is possible.

The response of the drill-string model including AST is determined by numerical integration of the system dynamics in (7.20)-(7.23). Based on this response, the actual cutting force  $W^c$  and (frictional) contact force  $W^f$  can be deter-

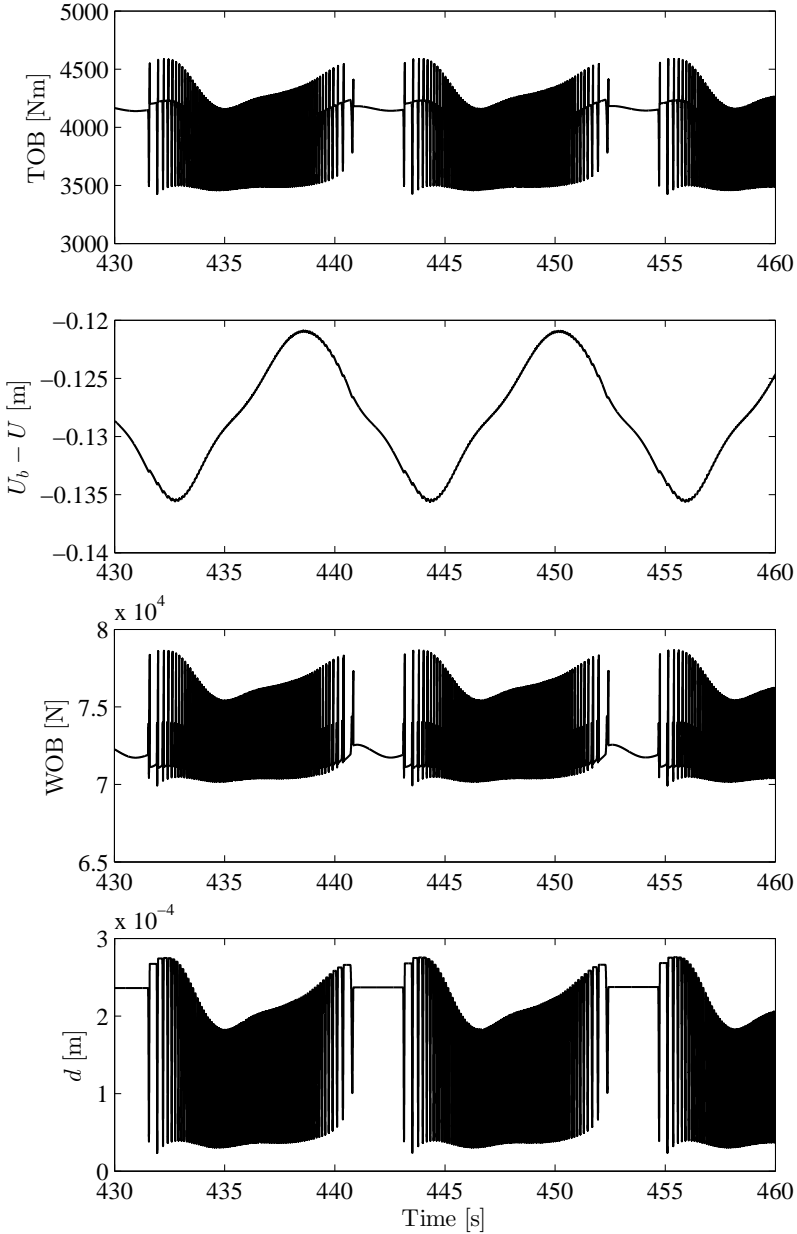


Figure 7.10: Simulation result of the drill-string model including AST with a prescribed angular velocity of 120 rpm and axial velocity of 20 ft/hr, zoom plot of the torque-on-bit (TOB), actual tool stroke ( $U_b - U$ ), weight-on-bit (WOB) and depth-of-cut ( $d$ ).

mined. When the system is in steady-state (i.e. related to stick-slip limit cycles for most parameter settings), the cutting force and frictional force are averaged over  $2 \cdot 10^6$  dimensionless time-steps (with a stepsize of  $1 \cdot 10^{-4}$ , i.e. approximately 350 s), resulting in an averaged value for these two components of the WOB. This time-span is sufficiently large as a single limit cycle takes approximately 10-15 s, see e.g. Figure 7.10. Note that these averaged values are based on a constant setting for the surface rate-of-penetration  $V_0$ ; this does, however, not imply a constant axial velocity at the bit as oscillations are present due to the drill-string dynamics. Of course, the average rate-of-penetration at the bit is equal to the prescribed axial velocity at surface. The results of the (averaged) total weight-on-bit for the model including AST, as well as for the benchmark model, are shown in Figure 7.11. This figure shows that the averaged WOB for the benchmark model is higher compared to the model including AST for an equal reference axial velocity and a prescribed angular velocity of 120 rpm. Or stated differently, to obtain the same rate-of-penetration a lower WOB is required for the system with tool. The results in Figure 7.11 can also be interpreted as follows as indicated by the dashed lines. For the same level of the averaged weight-on-bit, a significantly higher rate-of-penetration can be obtained for the system with the tool. For example, an averaged WOB of 73 kN results in an averaged rate-of-penetration of approximately 15.7 ft/hr for the benchmark model while a rate-of-penetration of approximately 23.8 ft/hr is achieved for the model including AST, which is an increase of more than 50%. Similar results have been obtained for a prescribed angular velocity of 50 rpm as can be seen in Figure D.1 in Appendix D.3. In this case the increase of the rate-of-penetration is even higher for the model with AST compared to the model without tool.

In Figure 7.12, a distinction is made between the contribution of the cutting force and the frictional force, for both models. Recall the expression for the friction force given in (7.42) and especially the set-valued nature of the discontinuity at  $\dot{U}_b = 0$  ( $\dot{U} = 0$  for the benchmark model). If we investigate more closely the (averaged) friction force  $\hat{W}^f$  of the benchmark model, it can be seen that for all axial velocities the friction force is equal to (or at least close to) its maximum value. Looking at the response of the friction force as function of time, it indeed turns out that the maximum friction force is always present; even when  $\dot{U} = 0$  (i.e. the bit is sticking in axial direction), the friction force is close to the maximum value. For the model including the AST, the averaged friction force are decreasing for increasing axial velocity. In addition, the averaged friction force is up to 10% (depending on  $V_0$ ) lower than the maximum value. The response of the friction force shows that during axial stick phases the friction force is decreased. This indicates that during axial stick the AST indeed contracts and therewith reduces the friction due to contact between the wearflat and the well bottom. Moreover, it turns out that the average cutting force has increased for the drill-string including AST compared to the benchmark model. The fact that the (average) amount of friction is decreased and the cut-

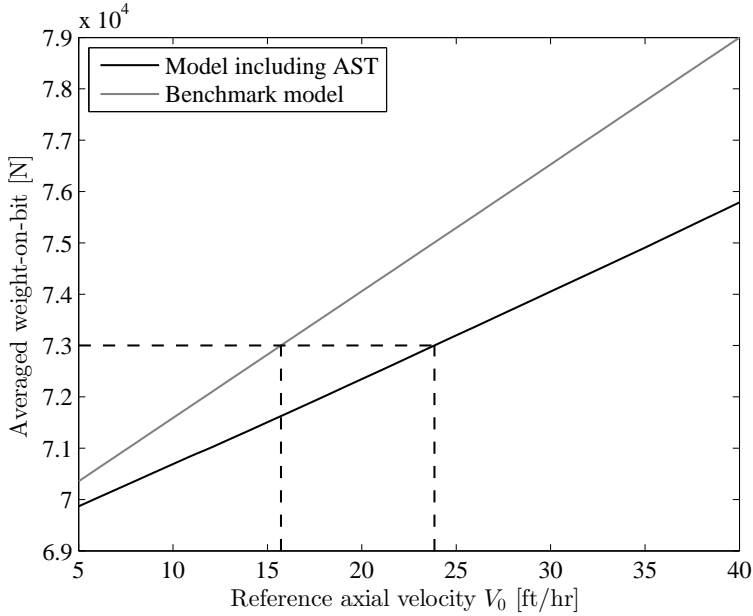


Figure 7.11: Averaged value of the total weight-on-bit as function of the prescribed axial velocity at the top of the drill-string with a prescribed rotational velocity of 120 rpm.

ting forces are increased indicates that the drilling efficiency is increased. This can be an explanation for the increased rate-of-penetration observed in the field when the AST is applied. Similar results have been obtained for a prescribed angular velocity of 50 rpm (see Figure D.2 in Appendix D.3). To further confirm these findings, some model adaptations are necessary to include hookload in the model as a boundary condition at surface instead of a prescribed axial velocity at surface.

## 7.5 Detailed analysis of the drill-string dynamics including anti stick-slip tool

In this section, the drill-string dynamics are analyzed in further detail to achieve better understanding of the behavior observed in the simulation results in Section 7.4. First, we use a linearization approach for systems with state-dependent delays, as proposed in [42,48], to study the stability of the nominal solution (constant ROP and RPM). Next, a two time-scale analysis is used to investigate the apparent velocity-weakening effect in the TOB as function of angular velocity

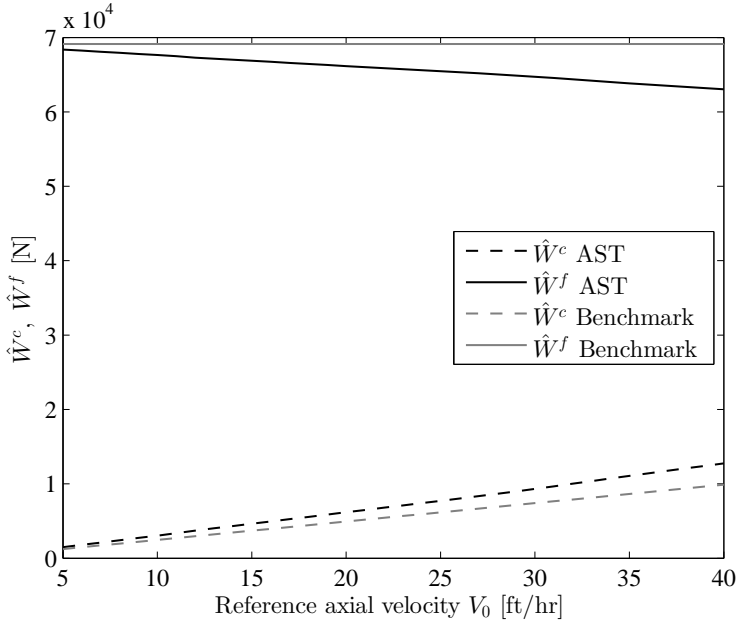


Figure 7.12: Averaged value of the cutting force  $\hat{W}^c$  and frictional contact force  $\hat{W}^f$  as result of averaging the response of drill-string dynamics and a prescribed rotational velocity of 120 rpm.

for the benchmark model and the model including AST. The latter is done as such velocity-weakening effect is a key destabilizing effect leading to torsional stick-slip limit cycling.

### 7.5.1 Linearization of the drill-string dynamics

The stability of the desired angular velocity (and ROP) of the drill-string dynamics is investigated in this section. For this stability analysis of the delay-differential equation, with state-dependent delay, an associated linear system is constructed. As stated in [42, 48], asymptotic stability of the nominal solution of this associated linearized system implies (local) asymptotic stability of the desired equilibrium of the original delay-differential equation. The linearized model is used to determine the poles of the system by means of a MATLAB tool for the computation of right-most characteristic roots of time-delay systems [125]. The right-most roots are determined for both the benchmark model and the drill-string model including the AST. In this section, only the derivation of the linearized system including AST is given, the linearization of the benchmark model can be obtained in a similar way.

Recall the drill-string dynamics of the system including AST in dimensionless form (7.20)-(7.22) and rewrite the model in the following form:

$$M\ddot{\hat{q}} = H, \quad (7.26)$$

where  $\hat{q} = [u \ u_b \ \varphi_b]^\top$  and

$$M := \begin{bmatrix} (1 + \kappa) & -\kappa & \nu \\ -\kappa & (m_* + \kappa) & -\nu \\ \frac{\kappa}{\nu} & -\frac{\kappa}{\nu} & (1 + \iota) \end{bmatrix} \quad (7.27)$$

and

$$H := \begin{bmatrix} -\gamma u' + \gamma_b (u'_b - u') - \eta^2 u - \eta_b^2 (u - u_b) - \kappa (u - u_b) - \nu \varphi_b \\ -\gamma_b (u'_b - u') + \eta_b^2 (u - u_b) + \kappa (u - u_b) + \nu \varphi_b + n\psi[-\hat{\delta} + \lambda g(u'_b)] \\ -\frac{\kappa}{\nu} (u - u_b) - \varphi_b + n[-\delta + \beta \lambda g(u'_b)] \end{bmatrix}. \quad (7.28)$$

By introduction of the state vector  $z := [u \ u_b \ \varphi_b \ u' \ u'_b \ \varphi'_b]^\top$ , the dynamics (7.26) can be written in first-order state-space form as

$$z'(\tau) = f(z(\tau), z(\tau - \tau_n(z_d)), \tau_n(z_d(\tau))), \quad (7.29)$$

where  $z_d(s) := z(\tau + s)$  with  $s \in [-\tau_n, 0]$  and

$$f = \begin{bmatrix} u' \\ u'_b \\ \varphi'_b \\ M^{-1}H \end{bmatrix}. \quad (7.30)$$

Here, the state-dependent delay (satisfying (7.23)) is governed by

$$z_3(\tau) - z_3(\tau - \tau_n) + \omega_0 \tau_n = \frac{2\pi}{n}. \quad (7.31)$$

For the linearization of the dynamics in (7.29), (7.31) around  $z = 0$ , the approach in [48] is followed. First, the state  $z$  is decomposed as follows:

$$z = \bar{z} + \tilde{z}, \quad (7.32)$$

where  $\bar{z}$  is the constant solution around which linearization is pursued and  $\tilde{z}$  is a perturbation with respect to  $\bar{z}$ . The linearized system associated to the dynamics in perturbation coordinates  $\tilde{z}$  is given as follows:

$$\begin{aligned} \tilde{z}' = D_1 f(\bar{z}, \bar{z}, \tau_n(\bar{z}_d)) \tilde{z}(\tau) + D_2 f(\bar{z}, \bar{z}, \tau_n(\bar{z}_d)) \tilde{z}(\tau - \tau_n(\bar{z})) + \\ D_3 f(\bar{z}, \bar{z}, \tau_n(\bar{z}_d)) D_{\tau_n}(\bar{z}_d) \tilde{z}_d(\tau) \end{aligned} \quad (7.33)$$

where  $D_i f$  denotes the derivative with respect to the  $i$ -th argument of  $f$  and  $D_{\tau_n}(z_d)$  denotes the Fréchet derivative of the time delay  $\tau_n$  with respect to

$z_d$ . Since the original model is already in perturbation coordinates, the desired constant solution is equal to  $\bar{z} = [0 \ 0 \ 0 \ 0 \ 0 \ 0]^\top$ . Note that  $\bar{z}_d = \bar{z}(\tau + s) = 0$  for all  $s \in [-\tau_n, 0]$  and  $\tau_n(\bar{z}) = \tau_n(\bar{z}_d) = \frac{2\pi}{n\omega_0} = \tau_{n0}$  which follows from (7.31). The derivatives  $D_1f$ ,  $D_2f$  and  $D_1fD_{\tau_n}\bar{z}_d$  are determined to be:

$$D_1f = \begin{bmatrix} I_3 & O_3 \\ O_3 & M^{-1} \end{bmatrix} \begin{bmatrix} 0 & 0 & 0 & 1 & 0 & 0 \\ 0 & 0 & 0 & 0 & 1 & 0 \\ 0 & 0 & 0 & 0 & 0 & 1 \\ (-\eta^2 - \eta_b^2 - \kappa) & (\eta_b^2 + \kappa) & -\nu & -(\gamma + \gamma_b) & \gamma_b & 0 \\ (\eta_b^2 + \kappa) & (-\eta_b^2 - \kappa - n\psi) & \nu & \gamma_b & -\gamma_b & 0 \\ -\frac{\kappa}{\nu} & \frac{\kappa}{\nu} - n & -1 & 0 & 0 & 0 \end{bmatrix}, \quad (7.34)$$

$$D_2f = \begin{bmatrix} I_3 & O_3 \\ O_3 & M^{-1} \end{bmatrix} \begin{bmatrix} 0 & 0 & 0 & 0 & 0 & 0 \\ 0 & 0 & 0 & 0 & 0 & 0 \\ 0 & 0 & 0 & 0 & 0 & 0 \\ 0 & 0 & 0 & 0 & 0 & 0 \\ 0 & n\psi & 0 & 0 & 0 & 0 \\ 0 & n & 0 & 0 & 0 & 0 \end{bmatrix}, \quad (7.35)$$

and

$$D_3fD_{\tau_n}(\bar{z}_d)\bar{z}_d = \begin{bmatrix} I_3 & O_3 \\ O_3 & M^{-1} \end{bmatrix} \begin{bmatrix} 0 \\ 0 \\ 0 \\ 0 \\ -n\psi v_0 \\ -nv_0 \end{bmatrix} \frac{1}{\omega_0} (\bar{z}_3(\tau - \tau_{n0}) - \bar{z}_3(\tau)). \quad (7.36)$$

Note that there is no term related to the nonlinear function  $g(u'_b)$  in the linearized model. This is due to the fact that when the function  $g(u'_b)$  is evaluated at the constant solution  $z = \bar{z}$  the partial derivative is equal to zero, because we assume  $v_0 > 0$ .

Substituting (7.34)-(7.36) in (7.33) yields the following linearized model with constant (nominal) delay  $\tau_{n0}$ :

$$\tilde{z}'(\tau) = A_0\tilde{z}(\tau) + A_1\tilde{z}(\tau - \tau_{n0}) \quad (7.37)$$

with

$$A_0 = \begin{bmatrix} I_3 & O_3 \\ O_3 & M^{-1} \end{bmatrix} \begin{bmatrix} 0 & 0 & 0 & 1 & 0 & 0 \\ 0 & 0 & 0 & 0 & 1 & 0 \\ 0 & 0 & 0 & 0 & 0 & 1 \\ (-\eta^2 - \eta_b^2 - \kappa) & (\eta_b^2 + \kappa) & -\nu & -(\gamma + \gamma_b) & \gamma_b & 0 \\ (\eta_b^2 + \kappa) & (-\eta_b^2 - \kappa - n\psi) & \nu + \frac{n\psi v_0}{\omega_0} & \gamma_b & -\gamma_b & 0 \\ -\frac{\kappa}{\nu} & \frac{\kappa}{\nu} - n & -1 + \frac{nv_0}{\omega_0} & 0 & 0 & 0 \end{bmatrix},$$



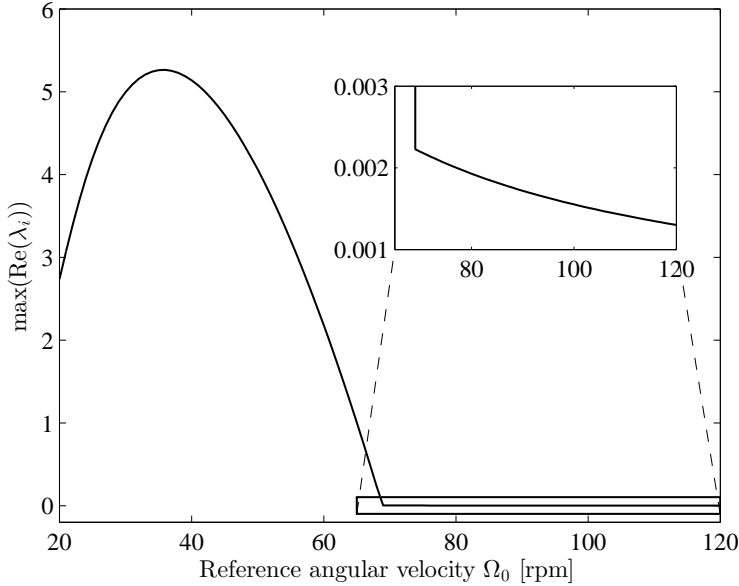


Figure 7.13: Location of the right-most eigenvalue of the benchmark model as function of angular velocity  $\Omega_0$  and a prescribed axial velocity of 20 ft/hr.

$$A_1 = \begin{bmatrix} I_3 & O_3 \\ O_3 & M^{-1} \end{bmatrix} \begin{bmatrix} 0 & 0 & 0 & 0 & 0 & 0 \\ 0 & 0 & 0 & 0 & 0 & 0 \\ 0 & 0 & 0 & 0 & 0 & 0 \\ 0 & 0 & 0 & 0 & 0 & 0 \\ 0 & n\psi & -\frac{n\psi v_0}{\omega_0} & 0 & 0 & 0 \\ 0 & n & -\frac{nv_0}{\omega_0} & 0 & 0 & 0 \end{bmatrix}.$$

The associated linearized drill-string model is used to determine the (local) stability of the desired equilibrium. The stability is analyzed through the poles of this linear system. Note that a delay-differential equation typically has an infinite number of poles [74]; however, (local) stability can be investigated by studying the location of the right-most pole. Therefore, a dedicated MATLAB tool is used [125]. The location of the right-most pole is investigated for a range of angular velocities for both the benchmark model and the model including AST; the results are shown in Figure 7.13 and Figure 7.14, respectively.

In Figure 7.13, it can be seen that the real part of the right-most eigenvalue is greater than zero, i.e.  $\max(\text{Re}(\lambda_i)) > 0$ , for the angular velocities of interest. In other words, the desired equilibrium of the benchmark model is unstable. As already mentioned in Section 7.4.1, a fast and slow regime of instability can be identified. For angular velocities  $\Omega_0 \geq 69$  rpm the right-most eigenvalue is close

to the imaginary axis, indicating an instability with a small growth rate. In [21], a stability analysis of the linearized coupled drill-string dynamics is performed. Note that the drill-string dynamics considered in this work is slightly different from the model in [21] (i.e. the model considered in this work also includes axial stiffness and damping). The stability analysis in [21] demonstrates the influence of the nominal rotation speed on the positions of the system poles. It is shown that the torsional poles remain close to the imaginary axis upon variation of the angular velocity, while the axial poles can move further away from this axis. The dominance of the axial or torsional poles defines two regimes of instability. Namely, the system exhibits slow divergence if the poles related to the torsional dynamics dominate and fast divergence if the poles mainly associated with the axial dynamics do. Moreover, a critical velocity  $\omega_c$ , which marks the transition between the two regimes, can be determined. This transition rotation speed can be approximated by

$$\omega_c = \sqrt{\frac{8\psi}{n}} \quad (7.38)$$

for the model as considered in [21]. The unscaled approximated transition velocity  $\Omega_c = \frac{\omega_c}{t_*}$  is equal to 70 rpm for the model parameters used in this thesis. Although the models are different, it turns out that the calculated transition velocity matches well with the transition velocity obtained graphically from Figure 7.13. Further investigation of the right-most root indeed confirms that for angular velocities smaller than 69 rpm the (initial) growth rate of the oscillations in the axial velocity  $u'$  correspond to the location of the right-most root. While for higher angular velocities (i.e.  $\Omega_0 \geq 69$  rpm) the growth rate of the oscillations in the torsional velocity  $\phi'$  correspond to the location of the right-most root.

The location of the right-most pole as function of the desired angular velocity for the drill-string model including AST is shown in Figure 7.14. As can be seen also for the model including AST, the right-most eigenvalue lies in the right-half-plane (RHP), indicating instability of the equilibrium corresponding to the desired angular velocity. Remarkable is the fact that the maximum value of the right-most eigenvalue is increasing for increasing angular velocities (apart from the typical stability lobes for time-delay systems observable in Figure 7.14), which is in contradiction with the hypothesis that the AST is most effective in terms of stick-slip mitigation for higher angular velocities. Moreover, again further investigating the right-most roots shows that these are related to the bit axial velocity  $u'_b$ . In other words, the right-most poles relate to an instability in the axial (bit) dynamics for angular velocities in a relevant range for drilling. This indicates that, in contrast to the results for the benchmark model, the dominant mode of instability is always related to the axial dynamics. The axial dynamics can still influence the torsional dynamics such that torsional stick-slip vibrations occur. However, for typical angular velocities the unstable response of the system is not dominated by the torsional dynamics.

To summarize, the linearization study confirms the behavior of the bench-

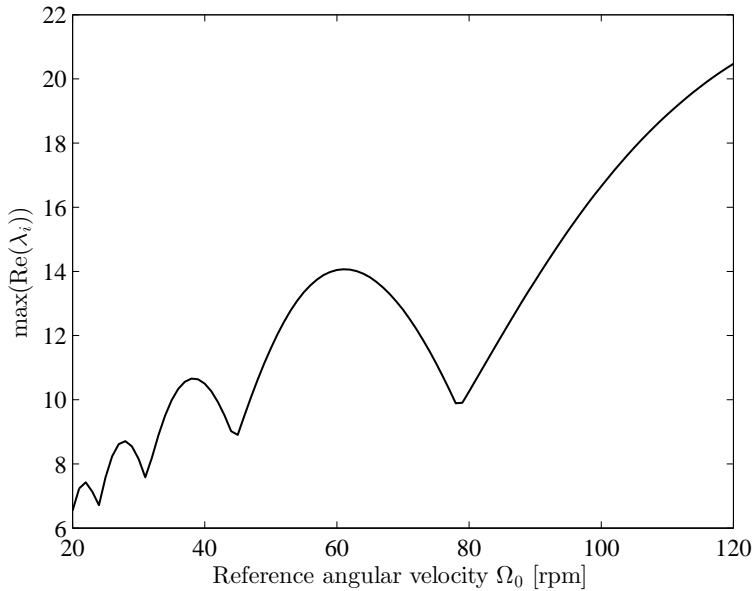


Figure 7.14: Location of the right-most eigenvalue of the drill-string model including AST as function of angular velocity  $\Omega_0$  and a prescribed axial velocity of 20 ft/hr.

mark model and the model including AST as observed in Section 7.4. For both the benchmark model and the drill-string model including AST, the equilibria corresponding to the desired angular velocities (and an prescribed axial velocity of 20 ft/hr) are unstable, as indicated by the fact that the right-most eigenvalue of the linearized system lies in the RHP for these operating conditions. Further investigation shows that these right-most eigenvalues of the benchmark model are related to an instability in the axial dynamics for low angular velocities and are related to an instability in the torsional dynamics when the angular velocity is above a certain threshold. For the model including the AST the right-most eigenvalues are related to an instability in the axial (bit) dynamics, for angular velocities in a relevant range for drilling.

### 7.5.2 Two time-scale analysis

The linearization-based analysis in the previous section indicates that the instability occurring at the fastest time-scale is related to the axial dynamics for both models. In [6, 38], it has been shown that for the benchmark model, the onset of torsional stick-slip vibrations is driven by the (unstable) axial dynamics. More specifically, the coupling between the axial and torsional dynamics effectively leads to a velocity-weakening effect of the torque-on-bit as function of angular

velocity, explaining the onset of torsional vibrations that might lead to torsional stick-slip. In this section, we adopt a similar analysis approach to investigate the effect of the AST on the TOB as a function of angular velocity. Again, the analysis is described for the model including AST and the analysis of the benchmark model is performed similarly.

As observed in the simulation results in Section 7.4, for a broad range of the parameter settings, the axial and torsional dynamics correspond to two different time-scales, i.e. the torsional dynamics typically evolves on a much slower time scale than the axial dynamics. This can be explained intuitively by the fact that the axial stiffness of the drill-string is much higher than the torsional stiffness of the drill-string. This also allows for the individual analysis of the axial dynamics (see also [38]), in which the slowly varying angular velocity can be considered constant. Here, a singular perturbation and averaging approach is taken. For the (approximative) analysis of the axial dynamics, the torsional velocity above the AST is assumed to be constant. Next, the response of the axial dynamics is averaged on the time scale of the torsional limit cycle.

Recall the equations of motion for the drill-string model including AST (7.9), with an extra Lagrange multiplier (related to the constant rotational velocity constraint following singular perturbation rationale), hence:

$$\begin{aligned} M\ddot{U} + D\dot{U} + K(U - V_0t) + K_b(U - U_b) &= -\lambda_1 \\ M_b\ddot{U}_b - K_b(U - U_b) &= -W^c - W^f + \lambda_1 \\ I\ddot{\Phi} + C(\Phi - \Omega_0t) &= \alpha\lambda_1 + \lambda_2 \\ I_b\ddot{\Phi}_b &= -T^c - T^f - \alpha\lambda_1 \end{aligned} \quad (7.39)$$

with the kinematic constraint that is described by (7.10) and the extra velocity constraint given by

$$\dot{\Phi} = \Omega_0 \quad (7.40)$$

and associated to the extra Lagrange multiplier  $\lambda_2$ . Rewriting the equations of motion and eliminating the constraint equations, results in the following (approximative) description of the axial dynamics in terms of the coordinates  $U$  and  $U_b$ :

$$\begin{aligned} M\ddot{U} + D\dot{U} - D_b(\dot{U}_b - \dot{U}) + K(U - V_0t) + K_b(U - U_b) &= \\ &= -\frac{1}{\alpha}(-T^c - T^f + \frac{I_b}{\alpha}(\ddot{U} - \ddot{U}_b)), \\ M_b\ddot{U}_b + D_b(\dot{U}_b - \dot{U}) - K_b(U - U_b) &= \\ &= -W^c - W^f + \frac{1}{\alpha}(-T^c - T^f + \frac{I_b}{\alpha}(\ddot{U} - \ddot{U}_b)), \end{aligned} \quad (7.41)$$

with

$$W^c = na\zeta\epsilon d, \quad W^f = nal\bar{\sigma} \frac{1 + \operatorname{sgn}(\dot{U}_b)}{2} \quad (7.42)$$

$$T^c = \frac{1}{2}na^2\varepsilon d, \quad T^f = \frac{1}{2}na^2\xi\mu l\bar{\sigma} \frac{1 + \operatorname{sgn}(\dot{U}_b)}{2} \quad (7.43)$$

where  $d = U_b(t) - U_b(t - t_n(t))$  and the state-dependent time delay equation is given by

$$\Omega_0 t_n + \frac{1}{\alpha} (U(t - t_n(t)) - U(t) + U_b(t) - U_b(t - t_n(t))) = \frac{2\pi}{n}. \quad (7.44)$$

Following the approach described in Section 7.3.3, this model is written in dimensionless form as:

$$\begin{aligned} (1 + \kappa_b)u'' - \kappa_b u_b'' + \gamma u' - \gamma_b(u_b' - u') + \eta^2 u + \eta_b^2(u - u_b) = \\ n\nu \left( \hat{\delta} - \beta \lambda g(u_b') \right), \\ (m_* + \kappa_b)u_b'' - \kappa_b u'' + \gamma_b(u_b' - u') - \eta_b^2(u - u_b) = \\ -n\psi \left( \hat{\delta} - \lambda g(u_b') \right) - n\nu \left( \hat{\delta} - \beta \lambda g(u_b') \right), \end{aligned} \quad (7.45)$$

where we introduced a new dimensionless parameter

$$\kappa_b := \frac{I_b}{M\alpha^2} \quad (7.46)$$

and the dimensionless time delay equation is given by

$$\omega_0 \hat{\tau}_n + \frac{\kappa}{\nu} (u(\tau - \tau_n) - u(\tau) + u_b(\tau) - u_b(\tau - \tau_n)) = 0. \quad (7.47)$$

The dimensionless equations of motion now only describe the axial dynamics for a constant rotational velocity above the tool. Note that the angular velocity at the bit can still vary due to the coupling between the axial and torsional dynamics in the tool and the fact that the constraint ( $\dot{\Phi} = \Omega_0$ ) only implies a constant angular velocity of the BHA above the tool. Based on simulations of (7.45), (7.47), the axial response can be averaged over 100 axial limit cycles. Using this averaged response, the averaged torque-on-bit can be determined. Doing so, for multiple prescribed (and constant) angular velocities  $\Omega_0$ , an averaged TOB can be computed as a function of angular velocity as shown in Figures 7.15 and 7.16 for the benchmark model and the model including AST, respectively.

The cutting torque and friction torque, that together form the total TOB, are depicted in Figure 7.15. From this figure, it is clear that the averaged cutting torque is subject to a velocity-weakening effect in the torque-on-bit, whereas the averaged (frictional) contact torques show a velocity-strengthening effect. As a result, the overall torque-on-bit shows a velocity-weakening effect, explaining the onset of torsional vibrations. This is in correspondence with the results of the previous works, see e.g. [6, 38]. Note that, for the benchmark model, the extra constraint of constant rotational velocity implies a constant time-delay  $\tau_n = \tau_{n0}$  because there is only one torsional degree-of-freedom that is now constrained.

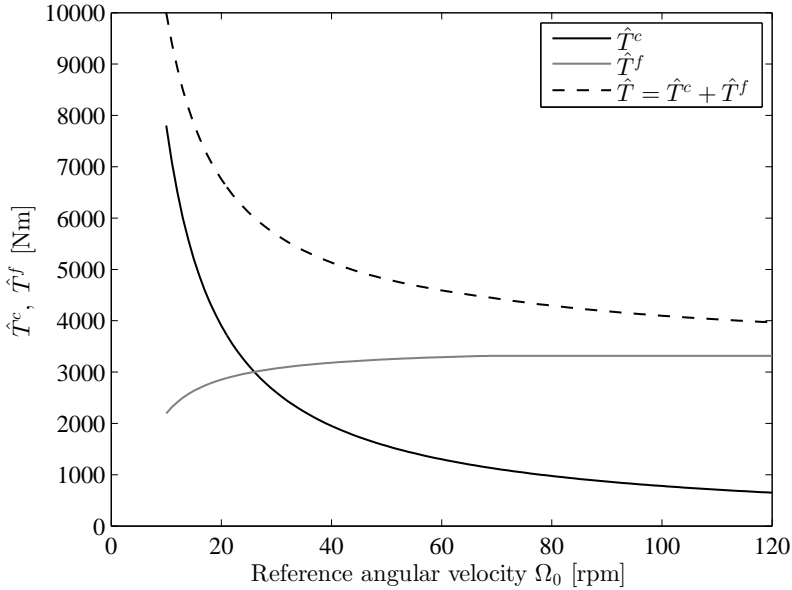


Figure 7.15: Averaged value of the cutting torque  $\hat{T}^c$  and frictional contact torque  $\hat{T}^f$  as result of averaging the response of benchmark model with constant angular velocity over 100 axial limit cycles and a prescribed axial velocity of 20 ft/hr.

As mentioned before, for the model including AST this is not the case due to the additional degree-of-freedom introduced by the tool. The drill-string model including AST with the additional constraint on the rotational velocity ((7.45), (7.47)) is used to determine the approximative response of the drill-string system. Based on this response, the averaged TOB is determined for a range of rotational velocities and the results are shown in Figure 7.16. For low angular velocities bit-bouncing occurred, which is not incorporated in the model, and these results are therefore excluded from the following analysis. In the figure, we observe a similar result as for the benchmark model, with a velocity-weakening effect in the cutting torque, a velocity-strengthening effect in the frictional contact torque and an overall velocity-weakening effect in the torque-on-bit. As mentioned before, the velocity-weakening effect has a destabilizing effect on the drill-string dynamics. Reducing this negative damping effect might have a stabilizing effect on the torsional dynamics. In Figure 7.17, the slope of the total TOB is shown for the benchmark model and the model including AST. From this figure, it can be seen that the negative damping effect is less severe for the model including AST, i.e. the slope of the TOB is smaller (closer to zero) compared to the benchmark model. This might indicate that the AST has a stabilizing effect

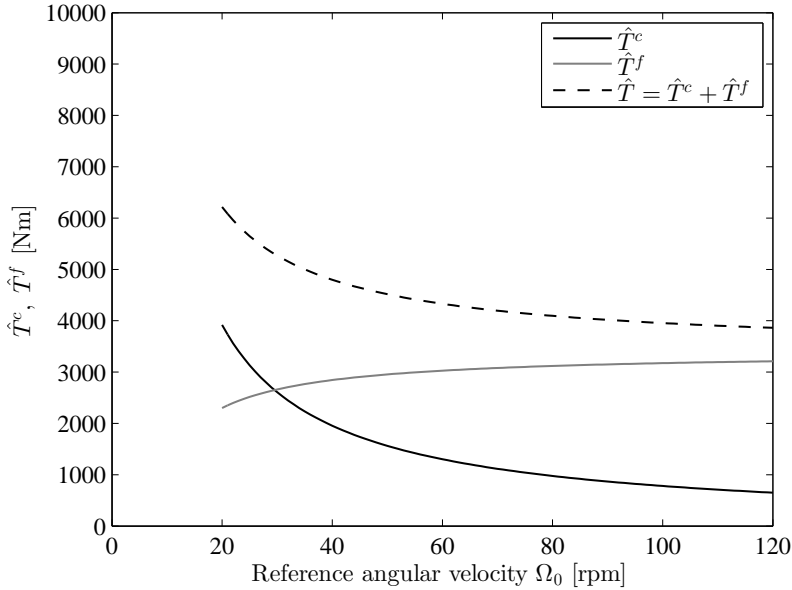


Figure 7.16: Averaged value of the cutting torque  $\hat{T}^c$  and frictional contact torque  $\hat{T}^f$  as result of averaging the response of (7.45), (7.47) (i.e. the model including AST) over 100 axial limit cycles and a prescribed axial velocity of 20 ft/hr.

on the torsional drill-string dynamics. However, for the used parameter values the equilibria corresponding to the range of desired angular velocities are still unstable, as also observed in the simulations in Section 7.4.

## 7.6 Discussion

In this chapter, the drill-string dynamics of a system including a down-hole tool for stick-slip mitigation is analyzed. Although field results have shown that the anti stick-slip tool (AST) can reduce the effect of (torsional) stick-slip vibrations and in addition increase the rate-of-penetration compared to offset wells, a fundamental physics-based explanation for these effects is lacking to this date. Therefore, the drill-string dynamics of a system with AST are investigated in this research using a model-based approach.

A drill-string model including the AST is derived by extending an existing model of the coupled axial-torsional dynamics with a model of the tool, resulting in a nonlinear (non-smooth) delay-differential equation with state-dependent delay. In a simulation study, the response of this model is compared with benchmark model of the drill-string dynamics without AST. The simulation results

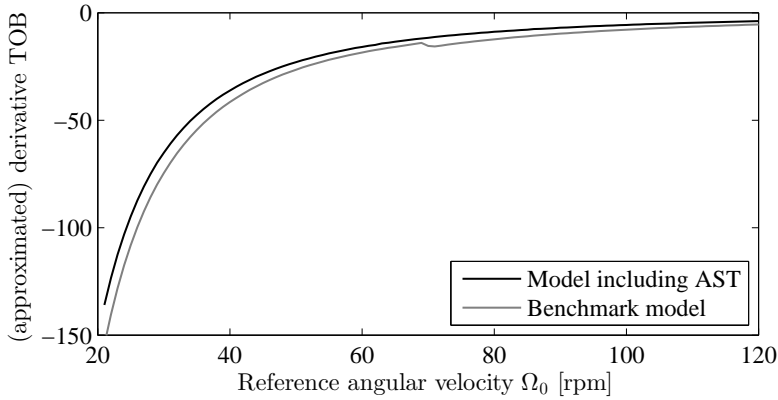


Figure 7.17: Slope of the averaged TOB as function of angular velocity for the benchmark model and the model including AST.

show an unstable response of the drill-string dynamics for both the benchmark model as the model with AST, resulting in (stick-slip) limit cycles. The unstable response of the drill-string dynamics is confirmed by a stability analysis of the associated linear system. Further investigation shows that the right-most eigenvalues of the benchmark model are related to an instability in the axial dynamics for low angular velocities and are related to an instability in the torsional dynamics when the angular velocity is above a certain threshold. For the model including the AST the dominant mode of instability is always related to the axial dynamics. In other words, for angular velocities in a relevant range for drilling the unstable response of the system including the AST is not dominated by the torsional dynamics.

Analysis based on time-scale separation in previous works revealed an apparent velocity-weakening effect in the TOB of the benchmark model. A similar two time-scale analysis is performed for the model including AST and, also for the drill-string model with AST, the TOB shows a velocity-weakening effect. However, the negative slope of the averaged torque-on-bit as function of angular velocity for the model including AST is smaller (i.e. closer to zero) compared to the benchmark model. This could indicate that the AST has a stabilizing effect on the dynamics, although the response of the system for the current parameter settings and operating conditions is still unstable.

The aforementioned analyses focused on the stability of the desired operating point of the drill-string dynamics. To investigate the claim regarding the increased ROP of the system including the AST, the (averaged) weight-on-bit of the response of the (nonlinear) drill-string dynamics is analyzed. It has been shown that the benchmark model requires a higher WOB to obtain the same ROP as the drill-string model including AST. Further investigation of the



WOB reveals that the (averaged) frictional forces are reduced for the model with tool, due to contraction of the tool during axial stick. At the same time the cutting forces are increased. These two observations indicate an increased drilling efficiency, resulting in a higher ROP. However, since the (surface) rate-of-penetration is prescribed in the current model, the increase in ROP for equal hookload at surface can only be investigated indirectly with the model at hand.

To conclude, a drill-string model including AST has been developed and the drill-string dynamics of this model have been investigated. Based on the results presented in this work, it is not possible to draw definitive conclusions about the working principle of the tool in terms of its effectiveness in mitigating stick-slip oscillations. However, some results indeed indicate that the AST has a stabilizing effect on the drill-string dynamics and in addition it increases the rate-of-penetration. To further investigate these claims, some model adaptations are proposed and the model should be validated based on field data.

## 7.7 Recommendations for future research

To further investigate the working principle of the tool, it is recommended to validate the simulation results of the model based on field measurements and possibly apply some model adaptations. It is important to determine the model parameters based on field data, in particular for the bit-rock related parameters. In that case, it would be possible to validate the drill-string model based on a representative field case. To do so, it would be valuable to have down-hole measurements of a test run with and without the AST.

Envisioned adaptations of the model are given below. First, by taking into account the top drive mass, the prescribed axial velocity at surface can be replaced by a prescribed force (hookload) boundary condition at surface. Doing so, the claim regarding the increased ROP can be investigated for equal hookload boundary conditions at surface. Second, using a drill-string model including multiple dynamical modes enables to investigate the effect of additional modes on both hypotheses regarding the tool. Related to the latter point, it is also worth investigating how to model could be adapted to model a drill-string in an inclined well. This is particularly important because field results have indicated that the AST might be less effective in (close to) vertical wells (see [102]).

# Conclusions and recommendations

---

## 8.1 Conclusions

In this thesis, the design and implementation of (control) strategies to eliminate (torsional) stick-slip oscillations in oil-field drill-string systems have been considered. The mitigation of stick-slip vibrations is of great practical interest because these vibrations reduce the drilling efficiency, resulting in a decrease of the rate-of-penetration. In addition, this type of vibrations results in excessive bit wear, may lead to damage of the drill pipes, and is detrimental for the tools in the bottom hole assembly.

The objective of this thesis (as stated in Section 1.2) is the development and analysis of (control) strategies to mitigate stick-slip vibrations in drilling systems. This main objective is subdivided in three research objectives. First, the development of controller design strategies for active feedback control of drilling systems with multiple dominant flexibility modes and severe velocity-weakening and uncertainty in the bit-rock interaction, second, the robustness analysis and validation on a lab-scale drill-string system of the proposed controller design methodologies, third, the modelling and analysis of a passive down-hole tool for the mitigation of stick-slip vibrations and rate-of-penetration increase.

The main contributions of this thesis addressing these objectives can be summarized in terms of contributions on modelling for control of torsional vibrations in drill-string systems, on novel controller design strategies for drill-string systems, on the realization of a lab-scale drill-string system, on the experimental validation of the proposed controllers, and on modelling and analysis of a down-hole anti stick-slip tool:

- *Modelling for control of torsional vibrations in drill-string systems:* field observations have revealed that multiple torsional flexibility modes play

a role in the onset of stick-slip vibrations, especially in deep and curved boreholes that are drilled nowadays. Therefore, a multi-modal model of the torsional dynamics, exhibiting the most dominant torsional flexibility modes and based on a finite-element method representation of a realistic drilling system, has been proposed as a basis for controller design in Chapter 2. The model is based on a jack-up drilling rig used to drill wells of over 6000 m. During operations, stick-slip vibrations have been observed for this rig while it is equipped with a modern SoftTorque system. This drill-string model is used as basis for the development of novel controller design methodologies;

- *Novel controller design strategies for drill-string systems:* two model-based output-feedback controller design methodologies have been presented in this thesis.

In Chapter 3, a novel nonlinear observer-based output-feedback control strategy mitigating torsional stick-slip vibrations has been developed. The particular benefits of the nonlinear observer-based output-feedback controller compared to existing controllers can be summarized as follows. First, it can effectively deal with (realistic) drill-string models with multiple dominant torsional flexibility modes, second, it is robust with respect to severe velocity-weakening (and uncertainty) in the bit-rock interaction and, third, it only employs surface measurements, which is important because down-hole measurements are not available in practice. Additionally, a guarantee for (local) asymptotic stability of the closed-loop reduced-order system is given for bit-rock interaction laws satisfying a certain sector condition, which is beneficial as the bit-rock interaction is subject to uncertainty in practice.

In Chapter 4, a novel linear robust output-feedback controller design approach to eliminate stick-slip vibrations has been developed. In addition to the controller objectives already mentioned for the nonlinear observer-based output-feedback controller, the linear robust output-feedback controller is, firstly, optimized to have robustness with respect to uncertainty in the bit-rock interaction and, secondly, closed-loop performance specifications regarding measurement noise sensitivity and actuator limitations are integrated in the controller design. The combination of robustness with respect to uncertainty in the bit-rock interaction and including closed-loop performance specifications in the controller design while guaranteeing (local) stability of the desired setpoint is an important improvement in the design of controllers to mitigate stick-slip vibrations in drilling systems. Through such design, also stability of the nonlinear closed-loop system with the robust output-feedback controller is obtained and conditions on the bit-rock interaction, in terms of a sector bound, for which the desired equilibrium is locally asymptotically stable, have been derived.

For both controllers, the robustness of the closed-loop system has been investigated in model-based case studies. The following robustness aspects are key in the scope of practical applications, and are extensively studied in this thesis: robustness with respect to changes in the bit-rock interaction characteristics, increasing length of the drill-string, different desired angular velocities (i.e. the operating envelope is investigated), and sensor- and actuator-induced disturbances.

- *Realization of a lab-scale drill-string system:* a lab-scale oil-field drill-string system has been designed and realized, based on the drill-string models developed. A detailed description of the design of the experimental setup is given in Chapter 5. The setup exhibits the essential dynamics of a real drilling system, and is designed to represent the dynamics of an oil-field drill-string system with multiple dominant torsional flexibility modes. A comparison of the response of the experimental setup with the response of the drill-string model in simulations has evidenced that the setup is able to emulate the drill-string dynamics to be investigated. Therefore, this setup can be used to experimentally validate the designed controllers presented in Chapters 3 and 4.
- *Experimental validation of controllers for drill-string systems:* the linear robust output-feedback control strategy of Chapter 4 and the state-feedback control strategy of Chapter 3 (using measurements of all the states) have been implemented on the lab-scale drill-string system. The controllers have been tested and both controllers successfully stabilize the desired angular velocity and therewith mitigate stick-slip vibrations on the experimental setup. Experimental validation of the designed controllers is an important intermediate step towards field implementation of the controllers on a real rig.
- *Modelling and analysis of passive tools for the mitigation of stick-slip vibrations and rate-of-penetration increase:* a modelling and analysis approach for a drill-string system including the anti stick-slip tool (AST) has been proposed in Chapter 7. A drill-string model including the anti stick-slip tool has been developed by extending an existing drill-string model of the coupled axial and torsional dynamics. The resulting nonlinear (non-smooth) drill-string model with state-dependent delay has been used to assess the effectiveness of the tool with respect to mitigation of stick-slip vibrations and increasing the rate-of-penetration. The analyses include a stability analysis based on a linearization approach for delay-differential equations with state-dependent delays and a two time-scale analysis. The effect of the AST on the rate-of-penetration has been investigated based on the simulation results of the nonlinear model.

Summarizing, two novel controller design methodologies to mitigate stick-slip

vibrations in drill-string systems have been introduced in this thesis. The designed controllers have several benefits compared to existing controllers. Namely, the controllers can effectively deal with (realistic) drill-string models with multiple dominant torsional flexibility modes, they are robust with respect to severe velocity-weakening (and uncertainty) in the bit-rock interaction and, they only employ surface measurements. In addition, for the linear robust output-feedback controller, closed-loop performance specifications are integrated in the controller design. The first step towards field implementation of the designed controllers has been taken by implementing the controllers on a lab-scale drill-string system, which exhibits the essential dynamics of a real drilling system. Moreover, a modelling and analysis approach for a drill-string system including a down-hole tool, for stick-slip mitigation and rate-of-penetration increase, has been developed. The model itself and the dynamic analyses of this model lay a foundation for a fundamental physics-based explanation for the working principle of such an anti stick-slip tool.

## 8.2 Recommendations

In this final section, recommendations for future research directions are given. First, two general recommendations for future research are presented. These recommendations involve possibilities for the drilling industry to enable further improvements of the drilling performance from a control point of view.

- In this thesis, the focus has been on the design of controllers to mitigate stick-slip vibrations using *surface* measurements only and drill-string systems with multiple dominant flexibility modes. The results in this work emphasize the importance of higher flexibility modes in the onset of stick-slip vibrations. On the other hand, it has also been shown that these higher modes are more difficult to observe in the available surface measurements. In that perspective, improvements in the controller designs can be obtained when additional (real-time) measurements can be employed for the purpose of feedback control. This does not necessarily mean measurements at the bit as these might be difficult to obtain in deep boreholes, but measurements along (the first part of) the drill-string could possibly already improve the results. The results of the state-feedback controller on the experimental setup can be seen as an example. Using measurements of all the states of the system this controller is able to stabilize the desired set-point. However, implementation of the controller in combination with the observer (and thus only using surface measurements) turns out to be more cumbersome. Additional measurements could improve the state estimates of the observer, which improves the performance of the controller design methodology;
- The model-based controller design methodologies developed in this thesis

require a model of the drill-string dynamics. A model of the drill-string can be obtained using finite-element method models of the drill-string configuration as employed in this thesis. However, accurate modelling of the bit-rock interaction requires detailed information about processes at the bit-rock interface. Also, for simulation and analysis purposes accurate models of the bit-rock interaction can be valuable. Down-hole measurements could improve these models and therewith improve the controllers to be designed and improve the reliability of model-based analyses. In particular, down-hole measurements (not necessarily real-time) of, for example, torque-on-bit and angular velocity, at a sufficiently high sample rate, are required to enable improvements of the models regarding the bit-rock interaction. In addition, accurate drill-string models and especially accurate models of the bit-rock interaction torque can be used for a proper stability analysis of controllers (also in case the controller does not necessarily need information about the bit-rock interaction).

In the scope of the nonlinear observer-based output-feedback controller, as introduced in Chapter 3, the following recommendations for future research directions are proposed:

- In order to facilitate the design and to decrease the implementation burden of the resulting observer-based output-feedback controller, model reduction is applied. With the employed balanced truncation model reduction technique, a reduced-order model, which captures the dominant modes, can be obtained. However, it turned out that a (small) steady-state mismatch is present between the outputs of the original system and the outputs of the reduced-order model. Using alternative reduction methods (e.g. balanced residualization) it might be possible to obtain a reduced-order model that eliminates this mismatch while still capturing the dominant flexibility modes. When this steady-state mismatch can be eliminated the nonlinear observer-based output-feedback controller can also employ additional measurements (such as the pipe torque measurement). As mentioned before, these additional measurements can improve the performance of the designed controller;
- Another aspect that can be interesting to investigate is the possibility to tune the controller and observer gains based on performance specifications as for example top drive limitations or measurement noise sensitivity. The design of the controller and observer gains is now solely determined by solving the linear matrix inequalities based on the derived stability conditions. Taking into account additional conditions and/or constraints on the control gains would enable the performance-based tuning of the controller and observer gains.

In the scope of the linear robust output-feedback controller, as introduced in Chapter 4, the following recommendations for future research directions are

proposed:

- The linear robust output-feedback control strategy allows to design a stabilizing controller for the drill-string system and optimizes the robustness with respect to uncertainty in the bit-rock interaction while still satisfying closed-loop performance specifications. However, in practice, not only the bit-rock interaction is subject to uncertainties. Also the (linear) drill-string dynamics can change, for example due to lengthening of the drill-string while drilling, or it is subject to model uncertainties, such as unmodelled dynamics. The employed robust control techniques also allow to incorporate such dynamic (i.e. frequency-dependent) uncertainties of the drill-string model in the controller design methodology. This enables to design controllers that are also robustly stable with respect to uncertainties in the drill-string model;
- The designed linear robust controllers have a relatively high order (up to approximately 80 internal states for the 18-DOF drill-string model). Implementation of these (high-order) controllers requires quite some computational power for implementation. In case the computational power is limited, controller order reduction techniques should be used to reduce the order of the controller;
- Tuning of the linear robust output-feedback controller is performed by tuning of the weighting filters in the frequency domain. These weighting filters specify bounds on specific closed-loop transfer functions. These closed-loop transfer functions are not directly related to specific drilling objectives, such as, operating envelope in terms of angular velocity or robustness with respect to uncertainty. To further facilitate tuning of the controllers, a systematic way to ‘translate’ drilling objectives to weighting filter design should be investigated.

A recommendation for future research regarding the experimental validation of the designed controllers is given below:

- Fully utilize the possibilities of the developed experimental setup. In the scope of this work, the designed controllers have been implemented on the experimental setup. The next step is to perform comprehensive robustness analyses on the experimental setup. In addition, for the observer-based output-feedback controller possibilities to improve the observer estimates need to be investigated in order to use surface measurements only. After this robustness study on the experimental setup, the possibilities for field implementation of the designed controller need to be explored.

The modelling and analysis approach for a drill-string system including the anti stick-slip tool, as considered in Chapter 7, leads to the following suggestions for future research directions:

- 
- The developed model for the drill-string dynamics including the anti stick-slip tool can be used to assess the effectiveness of the tool with respect to mitigation of stick-slip vibrations and rate-of-penetration increase. In further research, this model should be validated based on a representative field case. Moreover, (down-hole) field data can be used to determine the model parameters, in particular the bit-rock related parameters.
  - Two model adaptations are suggested to further improve the model. First, by taking into account the top drive mass, the prescribed axial velocity at surface can be replaced by a prescribed force (hookload) boundary condition at surface. This model adaptation would enable to further investigate the claim regarding the increased rate-of-penetration for equal hookload boundary conditions at surface. Second, employing a drill-string model including multiple dynamical modes enables to investigate the effect of additional modes on both hypotheses regarding the tool. Related to the latter point, it is also worth investigating how to model can be adapted to model a drill-string in an inclined well. This is particularly important because field results have indicated that the AST might be less effective in (close to) vertical wells.





## Appendix A

---

# Drill-string model settings

---

## A.1 FEM model drill-string configuration

The table below shows the drill-string configuration for the finite-element method model, schematically shown in Figure A.1. The original drill-string is represented by the equivalent pipe sections as shown in Table A.1.

Table A.1: Finite-element method drill-string configuration of the considered rig.

| #  | Top (Surface)      | OD     | ID     |                       | $\rho$ [ $\frac{\text{kg}}{\text{m}^3}$ ] | $G$ [ $\frac{\text{N}}{\text{m}^2}$ ] | $E$ [ $\frac{\text{N}}{\text{m}^2}$ ] |
|----|--------------------|--------|--------|-----------------------|---|---------------------------------------|---------------------------------------|
| 18 | Rotational inertia |        |        | 1778 kgm <sup>2</sup> |   |                                       |                                       |
| 17 | Pipe section       | 5.73 " | 4.80 " | 494.10 m              | 7850                                      | 6.09e <sup>10</sup>                   | 1.69e <sup>11</sup>                   |
| 16 | Pipe section       | 5.73 " | 4.80 " | 494.10 m              | 7850                                      | 6.09e <sup>10</sup>                   | 1.69e <sup>11</sup>                   |
| 15 | Pipe section       | 5.73 " | 4.80 " | 494.10 m              | 7850                                      | 6.09e <sup>10</sup>                   | 1.69e <sup>11</sup>                   |
| 14 | Pipe section       | 5.73 " | 4.80 " | 494.10 m              | 7850                                      | 6.09e <sup>10</sup>                   | 1.69e <sup>11</sup>                   |
| 13 | Pipe section       | 5.73 " | 4.80 " | 494.10 m              | 7850                                      | 6.09e <sup>10</sup>                   | 1.69e <sup>11</sup>                   |
| 12 | Pipe section       | 5.73 " | 4.80 " | 494.10 m              | 7850                                      | 6.09e <sup>10</sup>                   | 1.69e <sup>11</sup>                   |
| 11 | Pipe section       | 5.73 " | 4.80 " | 494.10 m              | 7850                                      | 6.09e <sup>10</sup>                   | 1.69e <sup>11</sup>                   |
| 10 | Pipe section       | 5.73 " | 4.80 " | 494.10 m              | 7850                                      | 6.09e <sup>10</sup>                   | 1.69e <sup>11</sup>                   |
| 9  | Pipe section       | 5.73 " | 4.80 " | 494.10 m              | 7850                                      | 6.09e <sup>10</sup>                   | 1.69e <sup>11</sup>                   |
| 8  | Pipe section       | 5.73 " | 4.80 " | 494.10 m              | 7850                                      | 6.09e <sup>10</sup>                   | 1.69e <sup>11</sup>                   |
| 7  | Pipe section       | 3.68 " | 2.69 " | 265.25 m              | 7850                                      | 6.63e <sup>10</sup>                   | 1.90e <sup>11</sup>                   |
| 6  | Pipe section       | 3.68 " | 2.69 " | 265.25 m              | 7850                                      | 6.63e <sup>10</sup>                   | 1.90e <sup>11</sup>                   |
| 5  | Pipe section       | 3.68 " | 2.69 " | 265.25 m              | 7850                                      | 6.63e <sup>10</sup>                   | 1.90e <sup>11</sup>                   |
| 4  | Pipe section       | 3.68 " | 2.69 " | 265.25 m              | 7850                                      | 6.63e <sup>10</sup>                   | 1.90e <sup>11</sup>                   |
| 3  | Pipe section       | 4.75 " | 2.21 " | 18.83 m               | 7850                                      | 7.95e <sup>10</sup>                   | 2.09e <sup>11</sup>                   |
| 2  | Pipe section       | 3.82 " | 2.40 " | 198.00 m              | 7850                                      | 6.35e <sup>10</sup>                   | 1.90e <sup>11</sup>                   |
| 1  | Pipe section       | 4.85 " | 2.68 " | 30.18 m               | 8232                                      | 7.18e <sup>10</sup>                   | 1.86e <sup>11</sup>                   |
|    | Bottom (Bit)       |        |        | =====                 |   |                                       |                                       |
|    | Total length       |        |        | 6249.00 m             |   |                                       |                                       |

The amount of friction torque at each element of the FEM model is given by  $T_i$ , for  $i = 2, \dots, 18$ . The parameter settings for the interaction torques between the borehole and the drill-string are given in Table A.2.

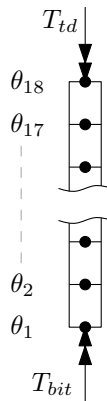


Figure A.1: Schematic representation of the 18-DOF finite-element method model.

Table A.2: Parameter settings for the amount of friction modelling the interaction between the borehole and the drill-string.

| Friction element | Amount of friction [Nm] |
|------------------|-------------------------|
| $T_2$            | 248.88                  |
| $T_3$            | 702.81                  |
| $T_4$            | 5.5957                  |
| $T_5$            | 589.17                  |
| $T_6$            | 606.11                  |
| $T_7$            | 609.98                  |
| $T_8$            | 664.86                  |
| $T_9$            | 3025.1                  |
| $T_{10}$         | 2512.4                  |
| $T_{11}$         | 2577.4                  |
| $T_{12}$         | 2812.7                  |
| $T_{13}$         | 3370.7                  |
| $T_{14}$         | 2867.8                  |
| $T_{15}$         | 3934.6                  |
| $T_{16}$         | 2181.2                  |
| $T_{17}$         | 6633.7                  |
| $T_{18}$         | 4142.2                  |



## Appendix B

---

# Proofs and technical results

---

### B.1 Proof of Theorem 3.1

We will provide a concise proof (employing the results in [19]) while focusing on the local aspect of Theorem 3.1. Consider the following LISS Lyapunov function candidate:

$$V(\xi_r) = V_1(\xi_r) + V_2(\tilde{q}_r) \quad (\text{B.1})$$

with  $\tilde{q}_r = H_r \xi_r$  and

$$V_1(\xi_r) = \frac{1}{2} \xi_r^\top P \xi_r, \quad P = P^\top > 0, \quad (\text{B.2})$$

$$V_2(\tilde{q}_r) = \gamma \int_0^{\tilde{q}_r} \tilde{\varphi}_r(\sigma) d\sigma. \quad (\text{B.3})$$

Note that  $V_2(\tilde{q}_r)$  is continuously differentiable on the domain  $\mathcal{S}_a \subset \mathbb{R}$  that contains  $\tilde{q}_r = 0$ . We will show that the function  $V$  satisfies the following bounds

$$\psi_1(\|\xi_r\|) \leq V(\xi_r) \leq \psi_2(\|\xi_r\|), \quad (\text{B.4})$$

where  $\psi_1$  and  $\psi_2$  are class  $\mathcal{K}_\infty$ -functions. To do so, note that  $V_2(\tilde{q}_r) \geq 0$ ,  $\forall \tilde{q}_r \in \mathcal{S}_a$  since  $\tilde{\varphi}_r$  belongs locally to  $[0, k]$ , with  $k > 0$ . Furthermore, we know that

$$\frac{1}{2} \lambda_{\min}(P) \|\xi_r\|^2 \leq V_1(\xi_r) \leq \frac{1}{2} \lambda_{\max}(P) \|\xi_r\|^2. \quad (\text{B.5})$$

Thus

$$V(\xi_r) \geq \psi_1(\|\xi_r\|) := \frac{1}{2} \lambda_{\min}(P) \|\xi_r\|^2. \quad (\text{B.6})$$

Using the sector condition (3.14), an upper bound for  $V_2$  can be derived:

$$\begin{aligned} V_2 &\leq \gamma \int_0^{|\tilde{q}_r|} |\tilde{\varphi}_r(\tilde{q}_r)| \, d\sigma \\ &\leq \gamma \int_0^{|\tilde{q}_r|} k\sigma \, d\sigma = \frac{\gamma k}{2} |\tilde{q}_r|^2 \\ &\leq \frac{\gamma k}{2} \|H_r\|^2 \|\xi_r\|^2. \end{aligned} \quad (\text{B.7})$$

Therefore,

$$V(\xi_r) \leq \psi_2(\|\xi_r\|) := \frac{1}{2} \lambda_{\max}(P) \|\xi_r\|^2 + \frac{\gamma k}{2} \|H_r\|^2 \|\xi_r\|^2. \quad (\text{B.8})$$

Moreover, it can be shown (see [19]) that there exists a  $\varepsilon > 0$  such that the time derivative of  $V$  along the trajectories satisfies

$$\dot{V} < -\psi_3(\|\xi_r\|) \quad \text{if } \|\xi_r\| \geq \chi(\|e\|) \quad (\text{B.9})$$

with the class  $\mathcal{K}_\infty$ -function  $\psi_3(\|\xi_r\|) := \frac{\varepsilon}{8} \|\xi_r\|^2$  and the following definition for the class  $\mathcal{K}$ -function  $\chi$ :

$$\chi(\|e\|) := \sqrt{\frac{4}{\varepsilon} \left( \left[ \lambda_{\max}(E) + \frac{2\eta_1^2}{\varepsilon} \right] \|e\|^2 \right)}$$

with  $E := \frac{1}{\varepsilon} K^\top B_r^\top P P B_r K$  and  $\eta_1 := k \left\| \check{Z}_r \right\| \|H_r\|$ . Consequently, we have proven that  $\dot{V}(\xi_r(t)) \leq -\frac{\varepsilon}{8} \|\xi_r(t)\|^2$  when  $\|\xi_r(t)\| \geq \chi(\|e(t)\|)$ , which means that  $V$  is an ISS Lyapunov function. According to [107] the existence of a continuously differentiable ISS Lyapunov function implies ISS. Given the fact that the sector condition on  $\tilde{\varphi}_r(\cdot)$  only holds locally, see Assumption 3.1, only local ISS can be concluded, where we can determine the bound on the initial condition  $\|\xi_{r,0}\| < c_1$  using the bounds on the Lyapunov function  $V$ . According to (3.1) we can write

$$\|\xi_r(t)\| \leq \rho(\|\xi_{r,0}\|, t) + \mu \left( \sup_{\tau \in [0, t]} \|e(\tau)\| \right), \quad \forall t \geq 0, \quad (\text{B.10})$$

with

$$\begin{aligned} \rho(\|\xi_{r,0}\|, t) &= \psi_1^{-1} \circ \nu(\psi_2(\|\xi_{r,0}\|), t) \\ \mu \left( \sup_{\tau \in [0, t]} \|e(\tau)\| \right) &= \psi_1^{-1} \circ \psi_2 \circ \chi \left( \sup_{\tau \in [0, t]} \|e(\tau)\| \right) \end{aligned}$$

and  $\nu$  a solution of the differential equation

$$\begin{aligned} \frac{d}{dt} (\nu(\|\xi_{r,0}\|, t)) &= -\psi_3 \circ \psi_2^{-1} (\nu(\|\xi_{r,0}\|, t)), \\ \nu(\|\xi_{r,0}\|, 0) &= \|\xi_{r,0}\|. \end{aligned} \quad (\text{B.11})$$

To guarantee the validity of the conditions on the nonlinearity in Assumption 3.1 it has to hold that  $\tilde{q}_r(t) \in \mathcal{S}_a \forall t \geq 0$ . Given the fact that  $\tilde{q}_r = H_r \xi_r$ , we have that  $\|\xi_r\| < \frac{\tilde{q}_{r,a,min}}{\|H_r\|}$  with  $\tilde{q}_{r,a,min} := \min(|\tilde{q}_{r,a1}|, |\tilde{q}_{r,a2}|)$ , implies that  $\tilde{q}_r \in \mathcal{S}_a$ . So, we require that

$$\|\xi_r(t)\| \leq \rho(\|\xi_{r,0}\|, t) + \mu \left( \sup_{\tau \in [0,t]} \|e(\tau)\| \right) \leq \frac{\tilde{q}_{r,a,min}}{\|H_r\|}, \quad \forall t > 0. \quad (\text{B.12})$$

To guarantee satisfaction of (B.12), we require the following combined condition on the initial condition and the input  $e(t)$ :

$$\bar{\rho}(\|\xi_{r,0}\|) + \mu \left( \sup_{\tau \in [0,t]} \|e(\tau)\| \right) \leq \frac{\tilde{q}_{r,a,min}}{\|H_r\|} \quad (\text{B.13})$$

with  $\bar{\rho}(r) := \rho(r, 0)$  a class  $\mathcal{K}$  function. By, for example choosing in Definition 3.1,  $c_1 = \bar{\rho}^{-1}(\alpha \frac{\tilde{q}_{r,a,min}}{\|H_r\|})$  and  $c_2 = \mu^{-1}((1 - \alpha) \frac{\tilde{q}_{r,a,min}}{\|H_r\|})$ , with  $\alpha \in (0, 1)$ , it can be shown that indeed system (3.13) is locally input-to-state stable.

## B.2 Proof of Theorem 3.2

We will provide a concise formulation of the proof, while referring to [26] and [44] for additional details on the proof. Here, we will mainly focus on aspects related to the local nature of the result in Theorem 3.2. Let  $P_o$  and  $Q_o$  be positive definite matrices such that  $P_o(A_{r,t} - LC_r) + (A_{r,t} - LC_r)P_o = -Q_o$  and  $G_r^\top P_o = H_r - NC_r$ , which is equivalent to the strict passivity of  $(A_{r,t} - LC_r, G_r, H_r - NC_r, 0)$ . To investigate the local asymptotic stability of the origin of the observer error dynamics (3.18), we consider the candidate Lyapunov function  $V_o(e) = \frac{1}{2}e^\top P_o e$ . Along solutions of (3.17), the derivative  $\dot{V}_o$  satisfies

$$\begin{aligned} \dot{V}_o &= -\frac{1}{2}e^\top Q_o e + e^\top (H_r - NC_r)^\top (\tilde{v}_r - \hat{v}_r) \\ &= -\frac{1}{2}e^\top Q_o e + (q_1 - q_2) (-\tilde{\varphi}_r(q_1) + \tilde{\varphi}_r(q_2)) \end{aligned} \quad (\text{B.14})$$

with  $q_1 := H_r \xi_r$ ,  $q_2 := (H_r - NC_r) \hat{\xi}_r + N \tilde{y}_r$ ,  $\tilde{v}_r \in -\tilde{\varphi}_r(q_1)$  and  $\hat{v}_r \in -\tilde{\varphi}_r(q_2)$ . Due to monotonicity of  $\tilde{\varphi}_r(\cdot)$  for all  $q_1 \in \mathcal{S}_b$  and  $q_2 \in \mathcal{S}_b$ , see Assumption 3.2, we can write  $e^\top (H_r - NC_r)^\top (\tilde{v}_r - \hat{v}_r) \leq 0$ , hence (B.14) yields

$$\dot{V}_o \leq -\frac{1}{2}e^\top Q_o e \leq -\frac{1}{2}\lambda_{\min}(Q_o) \|e\|^2, \quad (\text{B.15})$$

which implies local exponential stability, given the fact that Assumption 3.2 only holds locally. Furthermore, it holds that

$$\|e(t)\| \leq \left( \frac{\lambda_{\max}(P_o)}{\lambda_{\min}(P_o)} \right)^{\frac{1}{2}} \|e_0\| \exp \left( -\frac{\lambda_{\min}(Q_o)}{2\lambda_{\max}(P_o)} t \right) \quad (\text{B.16})$$



as long as  $q_1(t), q_2(t) \in \mathcal{S}_b$ . Let us investigate the bounds on  $\|\xi_r(t)\|$  and  $\|e(t)\|$  such that indeed  $q_1(t) \in \mathcal{S}_b$  and  $q_2(t) \in \mathcal{S}_b$  for all  $t \geq 0$ . First, given the fact that  $q_1 = H_r \xi_r$ , the requirement that  $|q_1| \leq \tilde{q}_{r,b,min}$  is satisfied if  $\|\xi_r\| \leq \frac{\tilde{q}_{r,b,min}}{\|H_r\|}$ . Second, given the fact that  $q_2 = (H_r - NC_r) \hat{\xi}_r + N\tilde{y}_r$  we rewrite the requirement  $|q_2| \leq \tilde{q}_{r,b,min}$  as

$$\begin{aligned} \left| (H_r - NC_r) \hat{\xi}_r + N\tilde{y}_r \right| &= \left| H_r (\xi_r - e) + NC_r (\xi_r - \hat{\xi}_r) \right| \\ &\leq \|H_r - NC_r\| \|e\| + \|H_r\| \|\xi_r\|. \end{aligned} \quad (\text{B.17})$$

Hence, we require that  $\|H_r - NC_r\| \|e\| + \|H_r\| \|\xi_r\| \leq \tilde{q}_{r,b,min}$ , which is satisfied if

$$\|\xi_r\| \leq \frac{\epsilon \tilde{q}_{r,b,min}}{\|H_r\|} \quad (\text{B.18})$$

$$\|e\| \leq \frac{(1 - \epsilon) \tilde{q}_{r,b,min}}{\|H_r - NC_r\|} \quad (\text{B.19})$$

for some  $\epsilon \in (0, 1)$ . Note that  $H_r - NC_r \neq 0$  due to the strict passivity of  $(A_{r,t} - LC_r, G_r, H_r - NC_r, 0)$ . Given (B.16), if

$$\|e_0\| \leq \frac{(1 - \epsilon) \tilde{q}_{r,b,min}}{\|H_r - NC_r\|} \left( \frac{\lambda_{max}(P_o)}{\lambda_{min}(P_o)} \right)^{-1/2}, \quad (\text{B.20})$$

inequality (B.19) is valid. Note that (B.20) is guaranteed by the assumptions on the initial conditions in the theorem and that (B.18) is also implied by the conditions in the theorem.

### B.3 Proof of Theorem 3.3

According to Theorem 3.1, we have to satisfy (B.13) to obtain local input-to-state stability (LISS) of (3.13) with respect to observer error  $e(t)$ . According to Theorem 3.2, for the system (3.18) to be locally exponentially stable conditions (B.18) and (B.19) have to be satisfied. The latter one is satisfied by restricting the initial conditions on the observer error as in (B.20). Moreover, (B.13) and (B.18) can be combined to

$$\bar{\rho}(\|\xi_{r,0}\|) + \mu \left( \sup_{\tau \in [0,t]} \|e(\tau)\| \right) \leq \min \left( \frac{\tilde{q}_{r,a,min}}{\|H_r\|}, \frac{\epsilon \tilde{q}_{r,b,min}}{\|H_r\|} \right).$$

Using (B.19) we can write

$$\bar{\rho}(\|\xi_{r,0}\|) + \mu \left( \frac{(1 - \epsilon) \tilde{q}_{r,b,min}}{\|H_r - NC_r\|} \right) \leq \min \left( \frac{\tilde{q}_{r,a,min}}{\|H_r\|}, \frac{\epsilon \tilde{q}_{r,b,min}}{\|H_r\|} \right)$$

which results in the requirement on the initial condition in  $\xi_r$ :

$$\bar{\rho}(\|\xi_{r,0}\|) \leq \min\left(\frac{\tilde{q}_{r,a,min}}{\|H_r\|}, \frac{\epsilon\tilde{q}_{r,b,min}}{\|H_r\|}\right) - \mu\left(\frac{(1-\epsilon)\tilde{q}_{r,b,min}}{\|H_r - NC_r\|}\right). \quad (\text{B.21})$$

The right-hand side of (B.21) can always be ensured to be positive, by taking  $\epsilon$  sufficiently close to 1, i.e. by taking  $\|e_0\|$  sufficiently small. Now, inequality (B.21) can always be guaranteed to be valid by taking  $\|\xi_{r,0}\|$  sufficiently small. So, indeed for sufficiently small  $\|\xi_{r,0}\|$  and  $\|e_0\|$ ,  $(\xi_r, e) = (0, 0)$  is an asymptotically stable equilibrium point of the interconnected system (3.13), (3.18); hence this equilibrium is locally asymptotically stable.



## Appendix C

---

# Time-stepping scheme for first-order systems

---

Time-stepping is a method for numerically simulating mechanical systems with unilateral constraints, as in this case the drill-string model with set-valued interaction torques along the drill-string and at the bit-rock interface. Moreau's time-stepping method as treated in [66] can be used for mechanical systems in second-order form. However, the reduced-order model in Section 3.2.1, and therefore also the observer dynamics in Section 3.4.2, are written in first-order form. Numerical simulation of the closed-loop drill-string system with the observer-based output-feedback controller is performed using a time-stepping algorithm. For the observer dynamics an adapted time-stepping algorithm is used that is suitable for systems in first-order form which is briefly described in this appendix. Here, the time-stepping algorithm is discussed in a rather concise manner.

Consider the following (nonlinear) system in first-order state-space form:

$$\begin{aligned} \dot{x} &= Ax + Bu + Gv \\ y &= Cx \\ q &= Hx \\ v &\in -\varphi(q) \end{aligned} \tag{C.1}$$

with state  $x$ , (control) input  $u$ , output  $y$ , and  $v$  and  $q$  the input and output related to the set-valued nonlinearity  $\varphi$ , respectively. For the application considered in this thesis, let us assume that we can split the nonlinearity  $\varphi$  in a smooth part and a non-smooth part, i.e.  $\varphi(q) = v_{sm}(q) + \lambda_T(q)$ , where the non-smooth part is a Coulomb (i.e. set-valued) friction law:

$$\lambda_T(q) \in T_s \text{Sign}(q). \tag{C.2}$$

In [68], it is shown that the Coulomb friction law in (C.2) can be rewritten using the following proximal point formulation:

$$\lambda_T = \text{prox}_{C_T}(\lambda_T - r q), \text{ with } C_T = \{\lambda_T | -T_s \leq \lambda_T \leq T_s\} \text{ and } r > 0. \quad (\text{C.3})$$

This proximal point function can easily be incorporated in the time-stepping algorithm using the following “min-max”-formulation:

$$\begin{aligned} \text{prox}_{[-T_s, T_s]}(z) &= \begin{cases} -T_s & \text{for } z \leq -T_s, \\ z & \text{for } -T_s < z < T_s, \\ T_s & \text{for } z \geq T_s, \end{cases} \\ &= \min(\max(-T_s, z), T_s). \end{aligned} \quad (\text{C.4})$$

This formulation will be used when implementing the time-stepping method.

Time-stepping uses a discretization using a fixed time-step and computes the solution while taking fixed time-steps forward in time (hence the name time-stepping). Note that at every discrete time-step  $k$  not only the state of the system is unknown but also the friction force  $\lambda_T$  is unknown. Therefore, the numerical integration procedure consists of two nested loops. The main loop involves the steps forward in time and the inner loop is used to solve a set of nonlinear algebraic equations to determine the unknowns  $x_E$  and  $\lambda_T$ . The set of nonlinear algebraic equations follows from the differential inclusion in (C.1) evaluated at a single time-step and is given by:

$$\begin{aligned} x_E &= x_A + (Ax_A + Bu + G(v_{sm}(q_E) + \lambda_T(q_E))) d_t \\ q_E &= Hx_E \end{aligned} \quad (\text{C.5})$$

with  $x_A$  the state at the beginning of the time-step,  $u$  the given (control) input and  $\lambda_T$  according to (C.3). The numerical integration procedure is completed by solving this set of equations using a fixed-point iteration procedure. The pseudo-code of the adapted time-stepping algorithm for first-order systems is shown in Algorithm 1.

---

**Algorithm 1** Pseudo-code for the time-stepping procedure for the first-order system (C.1).

---

Initialization:

$t = t_0 : d_t : t_e$ , time vector from  $t_0$  to  $t_e$  with stepsize  $d_t$

$N = \text{length}(t)$

$x_k$  is state at time-instance  $t(k)$  with  $k$  the index of the time-step

Set parameters for time-stepping:

$r$ : parameter in the proximal point description of the set-valued force law

tol: error criterion tolerance for the fixed-point iteration

$T_s$ : maximum value of the set-valued force law (i.e.  $\lambda_T \in [-T_s, T_s]$ , for  $q = 0$ )

Time-stepping method:

**for**  $k = 1 : N - 1$  **do**

$x_A = x_k$

$t_A = t(k)$

    Solve the set of nonlinear algebraic equations (C.5) using a fixed-point iteration, the error criterion is based on the convergence of the friction force  $\lambda_T$

**while** Not converged **do**

$u$  is the control input

$dx = (Ax_A + Bu + G(v_{sm} + \lambda_T)) d_t$

$x_E = x_A + dx$

$q_E = Hx_E$

$v_{sm}(q_E)$  is the smooth part of the nonlinearity  $\varphi$

$\lambda_{T,old} = \lambda_T$

$\lambda_T = \text{PROX}_{C_T}(\lambda_T - rq_E, T_s)$

        error =  $\|\lambda_T - \lambda_{T,old}\|$

        Converged if: error < tol

**end while**

$x_{k+1} = x_E$

**end for**

---

**function**  $\text{PROX}_{C_T}(x, a)$

$y = \min(\max(-a, x), a)$

**return**  $y$

**end function**

---



## Appendix D

---

# Derivation and parameters of the drill-string model including anti stick-slip tool

---

### D.1 Derivation equations of motion

In order to derive the equations of motion for the drill-string model including AST, a Lagrangian approach for systems with constraints is used, that is, the following generic form of the equation of Lagrange with constraints is used:

$$\frac{d}{dt} (T,_{\dot{q}}) - (T,_{q}) + (V,_{q}) = (Q^{nc})^{\top} + (W\lambda)^{\top}, \quad (\text{D.1})$$

with  $T$  the kinetic energy,  $V$  the potential energy,  $Q^{nc}$  the non-conservative generalized forces and  $\lambda$  the generalized constraint force associated with the constraint in (7.8). First, we derive the kinetic energy of the system as follows:

$$T = \frac{1}{2}M\dot{U}^2 + \frac{1}{2}I\dot{\Phi}^2 + \frac{1}{2}M_b\dot{U}_b^2 + \frac{1}{2}I_b\dot{\Phi}^2. \quad (\text{D.2})$$

The potential energy in the system follows from the springs that are present in the system and is given by

$$V = \frac{1}{2}K(U - V_0t)^2 + \frac{1}{2}C(\Phi - \Omega_0t)^2 + \frac{1}{2}K_b(U - U_b)^2. \quad (\text{D.3})$$



The non-conservative forces and torques can be determined to be

$$Q^{nc} = \begin{bmatrix} -D\dot{U} + D_b (\dot{U}_b - \dot{U}) \\ -W - D_b (\dot{U}_b - \dot{U}) \\ 0 \\ -T \end{bmatrix}. \quad (D.4)$$

Next, we rewrite the constraint equation (7.8) in the form  $h(q) = 0$ , with

$$h(q) = U_b - U + \alpha (\Phi - \Phi_b) \quad (D.5)$$

to determine that

$$W = \frac{\partial h}{\partial q} = [-1 \ 1 \ \alpha \ -\alpha]^\top. \quad (D.6)$$

In order to apply the equation of Lagrange as in (D.1), we determine:

$$T_{,q} = 0 \quad (D.7)$$

$$T_{,q} = [M\dot{U} \ M_b\dot{U}_b \ I\dot{\Phi} \ I_b\dot{\Phi}_b] \quad (D.8)$$

$$\frac{d}{dt}(T_{,q}) = [M\ddot{U} \ M_b\ddot{U}_b \ I\ddot{\Phi} \ I_b\ddot{\Phi}_b] \quad (D.9)$$

$$V_{,q} = \begin{bmatrix} K(U - V_0t) + K_b(U - U_b) \\ -K_b(U - U_b) \\ C(\Phi - \Omega_0t) \\ 0 \end{bmatrix}^\top \quad (D.10)$$

$$(W\lambda)^\top = [-\lambda \ \lambda \ \alpha\lambda \ -\alpha\lambda]. \quad (D.11)$$

The application of Lagrange's equations in (D.1) gives the equations of motion for the system:

$$\begin{aligned} M\ddot{U} + D\dot{U} + D_b (\dot{U} - \dot{U}_b) + K(U - V_0t) + K_b(U - U_b) &= -\lambda \\ M_b\ddot{U}_b - D_b (\dot{U} - \dot{U}_b) - K_b(U - U_b) &= -W^c - W^f + \lambda \\ I\ddot{\Phi} + C(\Phi - \Omega_0t) &= \alpha\lambda \\ I_b\ddot{\Phi}_b &= -T^c - T^f - \alpha\lambda \end{aligned} \quad (D.12)$$

with the kinematic constraint that is described by (7.8):

$$U - U_b = \alpha (\Phi - \Phi_b). \quad (D.13)$$

From the constraint equation it follows that

$$\begin{aligned} \Phi &= \frac{U - U_b}{\alpha} + \Phi_b \\ \ddot{\Phi} &= \frac{\ddot{U} - \ddot{U}_b}{\alpha} + \ddot{\Phi}_b. \end{aligned} \quad (D.14)$$

This is used in the third equation of (D.12) to obtain:

$$I \left( \frac{\ddot{U} - \ddot{U}_b}{\alpha} + \ddot{\Phi}_b \right) + C \left( \frac{U - U_b}{\alpha} + \Phi_b - \Omega_0 t \right) = \alpha \lambda, \quad (\text{D.15})$$

and thus the Lagrange multiplier  $\lambda$  satisfies

$$\lambda = \frac{I}{\alpha} \left( \frac{\ddot{U} - \ddot{U}_b}{\alpha} + \ddot{\Phi}_b \right) + \frac{C}{\alpha} \left( \frac{U - U_b}{\alpha} + \Phi_b - \Omega_0 t \right). \quad (\text{D.16})$$

This expression can be used in the equations of motion (D.12) to eliminate the degree of freedom related to  $\Phi$ . This yields the following unconstrained 3-DOF model for the drill-string dynamics with AST:

$$\begin{aligned} \left( M + \frac{I}{\alpha^2} \right) \ddot{U} - \frac{I}{\alpha^2} \ddot{U}_b + \frac{I}{\alpha} \ddot{\Phi}_b + D\dot{U} + D_b (\dot{U} - \dot{U}_b) + K (U - V_0 t) + \\ K_b (U - U_b) + \frac{C}{\alpha^2} (U - U_b) + \frac{C}{\alpha} (\Phi_b - \Omega_0 t) = 0, \end{aligned} \quad (\text{D.17})$$

$$\begin{aligned} -\frac{I}{\alpha^2} \ddot{U} + \left( M_b + \frac{I}{\alpha^2} \right) \ddot{U}_b - \frac{I}{\alpha} \ddot{\Phi}_b - D_b (\dot{U} - \dot{U}_b) - \\ K_b (U - U_b) - \frac{C}{\alpha^2} (U - U_b) - \frac{C}{\alpha} (\Phi_b - \Omega_0 t) = \end{aligned} \quad (\text{D.18})$$

$$\begin{aligned} -na\zeta\varepsilon (U_b(t) - U_b(t - t_n(t))) - nal\bar{\sigma} \frac{1 + \text{sign}(\dot{U}_b)}{2}, \\ \frac{I}{\alpha} \ddot{U} - \frac{I}{\alpha} \ddot{U}_b + (I_b + I) \ddot{\Phi}_b + \frac{C}{\alpha} (U - U_b) + C (\Phi_b - \Omega_0 t) = \\ -\frac{1}{2} na^2 \varepsilon (U_b(t) - U_b(t - t_n(t))) - \frac{1}{2} na^2 \xi \mu l \bar{\sigma} \frac{1 + \text{sign}(\dot{U}_b)}{2}. \end{aligned} \quad (\text{D.19})$$

## D.2 Parameters drill-string model including anti stick-slip tool

The parameters of the drill-string model including AST (7.11)-(7.14) are given in this appendix. The parameters are determined based on the properties of a real drilling system including the AST and (as far as possible) on field measurements of the drilling system under investigation.

In Table D.1, the parameters related to the bit-rock interaction are given. The considered drilling system uses a 12<sup>1</sup>/<sub>4</sub>'' PDC bit with 6 blades, resulting in a drill bit radius of 0.16 m. The remaining bit-rock related parameters could be determined based on (down-hole) measurement data and the approach proposed

Table D.1: Bit parameters for the model with the AST included.

| Parameter                | Symbol         | Value               | Unit  |
|--------------------------|----------------|---------------------|-------|
| Drill bit radius         | $a$            | 0.16                | [m]   |
| Specific energy          | $\varepsilon$  | 60                  | [MPa] |
| Wearflat length          | $l$            | $1.2 \cdot 10^{-3}$ | [m]   |
| Contact stress           | $\bar{\sigma}$ | 60                  | [MPa] |
| Cutting face orientation | $\zeta$        | 0.6                 | [-]   |
| Bit geometry parameter   | $\xi$          | 1                   | [-]   |
| Friction coefficient     | $\mu$          | 0.6                 | [-]   |
| Number of blades         | $n$            | 6                   | [-]   |

in [23]. However, the available (surface) measurement data was not reliable enough to accurately determine these parameters based on field data. Therefore, the parameter values  $\varepsilon$ ,  $l$ ,  $\bar{\sigma}$ ,  $\zeta$ ,  $\xi$  and  $\mu$  are based on the parameter values obtained from other studies (i.e. [6, 37]). Possibly, a better correspondence between field results and the simulation results can be obtained if these parameters can be validated based on suitable (preferably down-hole) field measurements.

The model parameters regarding the mechanical properties of the drill-string model are given in Table D.2. These parameters are based on the drill-string and BHA configuration of the drilling system under investigation and also include the properties of the AST (i.e. lead, leadangle, axial spring stiffness and damping in the tool) that is used in this drilling system.

Table D.2: Drill-string parameters for the model with the AST included.

| Parameter                    | Symbol   | Value                | Unit                 |
|------------------------------|--|----------------------|----------------------|
| Steel density                | $\rho_s$   | 8000                 | [kg/m <sup>3</sup> ] |
| Steel shear modulus          | $G$  | 77                   | [GPa]                |
| Steel elasticity modulus     | $E$  | 200                  | [GPa]                |
| Drill pipe length            | $L_p$  | 8013.5               | [m]                  |
| Length BHA below AST         | $L_b$  | 44.6                 | [m]                  |
| Length BHA above AST         | $L_{hp}$   | 229.2                | [m]                  |
| Drill pipe outer radius      | $r_{po}$   | 0.084                | [m]                  |
| Drill pipe inner radius      | $r_{pi}$   | 0.075                | [m]                  |
| Heavy drill pipe outer rad.  | $r_{hpo}$  | 0.84                 | [m]                  |
| Heavy drill pipe inner rad.  | $r_{hpi}$  | 0.057                | [m]                  |
| AST outer radius             | $r_{bo}$   | 0.106                | [m]                  |
| AST inner radius             | $r_{bi}$   | 0.036                | [m]                  |
| AST helix radius             | $r_h$  | 0.081                | [m]                  |
| Leadangle                    | $\theta$   | $\pi/4$              | [rad]                |
| Lead                         | $p = \tan(\theta) * 2\pi r_h$                                | 0.509                | [m]                  |
| Constraint constant          | $\alpha = \frac{p}{2\pi}$                                    | 0.081                | [m]                  |
| Drill pipe mass              | $M_p = \rho\pi(r_{po}^2 - r_{pi}^2)L_p$                      | $2.88 \cdot 10^5$    | [kg]                 |
| Heavy drill pipe mass        | $M_{hp} = \rho\pi(r_{hpo}^2 - r_{hpi}^2)L_{hp}$              | $2.19 \cdot 10^5$    | [kg]                 |
| BHA below AST mass           | $M_b = \rho\pi(r_{bo}^2 - r_{bi}^2)L_b$                      | $1.11 \cdot 10^4$    | [kg]                 |
| Effective mass               | $M = \frac{4}{\pi^2}M_p + M_{hp}$                            | $1.39 \cdot 10^5$    | [kg]                 |
| Area cross section pipe      | $A_p = \pi(r_{po}^2 - r_{pi}^2)$                             | $4.49 \cdot 10^{-3}$ | [m <sup>2</sup> ]    |
| Area cross section BHA       | $A_{hp} = \pi(r_{hpo}^2 - r_{hpi}^2)$                        | $1.19 \cdot 10^{-2}$ | [m <sup>2</sup> ]    |
| Area cross section AST       | $A_b = \pi(r_{bo}^2 - r_{bi}^2)$                             | $3.12 \cdot 10^{-2}$ | [m <sup>2</sup> ]    |
| Drill pipe inertia           | $I_p = \rho L_p \frac{\pi}{2} (r_{po}^4 - r_{pi}^4)$         | 1827.4               | [kgm <sup>2</sup> ]  |
| BHA above AST inertia        | $I_{hp} = \rho L_{hp} \frac{\pi}{2} (r_{hpo}^4 - r_{hpi}^4)$ | 113.0                | [kgm <sup>2</sup> ]  |
| BHA below AST inertia        | $I_b = \rho L_b \frac{\pi}{2} (r_{bo}^4 - r_{bi}^4)$         | 69.8                 | [kgm <sup>2</sup> ]  |
| Effective inertia            | $I = \frac{4}{\pi^2}I_p + I_{hp}$                            | 853.6                | [kgm <sup>2</sup> ]  |
| Drill pipe torsional stiffn. | $C_p = \frac{GJ_p}{L_p}$                                     | 273.9                | [Nm/rad]             |
| Drill pipe axial spring      | $K_p = \frac{EA_p}{L_p}$                                     | $1.12 \cdot 10^5$    | [N/m]                |
| AST axial spring stiffness   | $K_b$  | $9.5 \cdot 10^5$     | [N/m]                |
| AST axial damping            | $D_b$  | $14.3 \cdot 10^3$    | [Ns/m]               |
| Drill-string axial damping   | $D$  | $67.7 \cdot 10^3$    | [Ns/m]               |

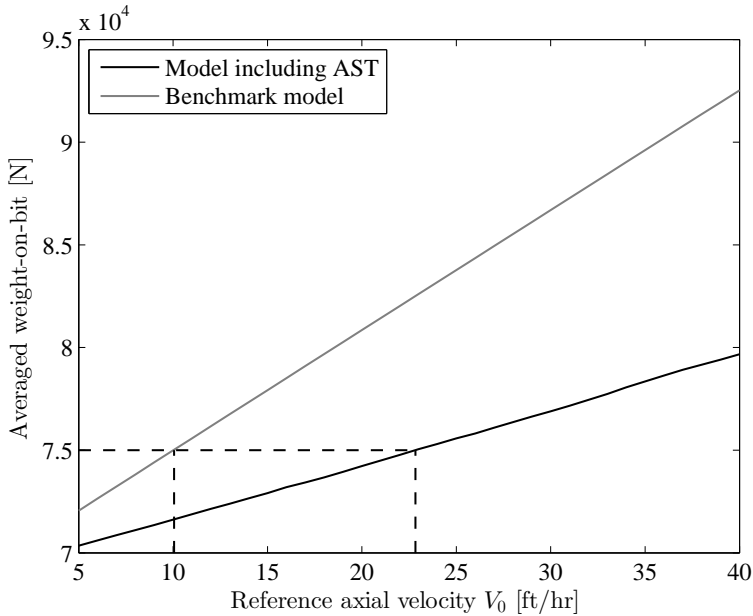


Figure D.1: Averaged value of the total weight-on-bit as function of the prescribed axial velocity at the top of the drill-string with a prescribed rotational velocity of 50 rpm.

### D.3 Investigation of the effect of the tool on the rate-of-penetration: 50 rpm case

The same analysis as presented in Section 7.4.3 for a prescribed rotational velocity of 120 rpm has been performed for a prescribed rotational velocity of 50 rpm. The results are shown in Figures D.1 and D.2. Similar conclusions can be drawn as for the 120 rpm case, that is for the same level of averaged weight-on-bit, a significantly higher rate-of-penetration can be obtained for the system with tool. The difference in ROP between the system with and without AST is even higher compared to the 120 rpm case, as can be seen in Figure D.1. For example, an averaged WOB of 75 kN results in an averaged rate-of-penetration of approximately 10.0 ft/hr for the benchmark model while a rate-of-penetration of approximately 22.8 ft/hr is achieved for the model including AST.

In Figure D.2, again a distinction is made between the contribution of the cutting force and the frictional force, for both models. Also for the 50 rpm case, for the model including the AST the averaged friction forces are decreasing for increasing axial velocity. While for the model without the tool the friction force is close to the maximum value, independently of the prescribed axial velocity.

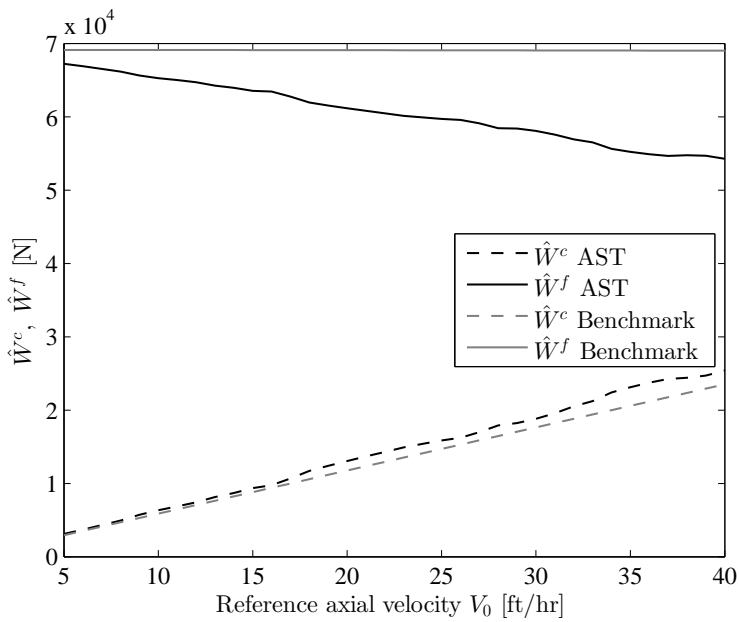


Figure D.2: Averaged value of the cutting force  $\hat{W}^c$  and frictional contact force  $\hat{W}^f$  as result of averaging the response of drill-string dynamics and a prescribed rotational velocity of 50 rpm.



---

# Bibliography

---

- [1] F. Abdulgalil and H. Siguerdidjane. Nonlinear control design for suppressing stick-slip oscillations in oil well drillstrings. In *5th Asian Control Conference*, volume 2, pages 1276–1281 Vol.2, July 2004.
- [2] E. Akutsu, M. Rødsjø, J. Gjertsen, M. Andersen, M. Reimers, N. Granhøy-Lieng, E. Strøm, and K.A. Horvei. Faster rop in hard chalk: Proving a new hypothesis for drilling dynamics. In *SPE/IADC Drilling Conference and Exhibition*, SPE/IADC 173068, London, United Kingdom, March 2015.
- [3] J.J. Bailey and I. Finnie. An analytical study of drillstring vibration. *ASME Journal of Engineering for Industry*, pages 122–128, 1960.
- [4] A.G. Balanov, N.B. Janson, P.V.E. McClintock, R.W. Tucker, and C.H.T. Wang. Bifurcation analysis of a neutral delay differential equation modelling the torsional motion of a driven drill-string. *Chaos, Solitons & Fractals*, 15(2):381 – 394, 2003.
- [5] S.V. Belokobyl'skii and V.K. Prokopov. Friction-induced self-excited vibrations of drill rig with exponential drag law. *Soviet Applied Mechanics*, pages 1134–1138, 1983. Translated from *Prikladnaya Mekhanika*, 18(12):98-101, 1982.
- [6] B. Besselink, N. van de Wouw, and H. Nijmeijer. A semi-analytical study of stick-slip oscillations in drilling systems. *Journal of Computational and Nonlinear Dynamics*, 6(2):021006–1 to 021006–9, 2011.
- [7] B. Besselink, N. van de Wouw, and H. Nijmeijer. Model reduction for nonlinear systems with incremental gain or passivity properties. *Automatica*, 49(4):861 – 872, 2013.
- [8] B. Besselink, T. Vromen, N. Kremers, and N. van de Wouw. Analysis and control of stick-slip oscillations in drilling systems. *IEEE Transactions on Control Systems Technology*, under review, 2015.
- [9] I. Boussaada, H. Mounier, S.-I. Niculescu, and A. Cella. Analysis of drilling vibrations: A time-delay system approach. In *Proceedings of the 20th Mediterranean Conference on Control and Automation*, pages 610–614, Barcelona, Spain, July 2012.



- [10] D. Bresch-Pietri and M. Krstic. Adaptive output-feedback for wave PDE with anti-damping - application to surface-based control of oil drilling stick-slip instability. In *Proceedings of the 53rd IEEE Conference on Decision and Control*, pages 1295–1300, Los Angeles, California, U.S.A., December 2014.
- [11] J. F. Brett. The genesis of torsional drillstring vibrations. *SPE Drilling Engineering*, 7(3):168–174, 1992.
- [12] C. Canudas-de Wit, F.R. Rubio, and M.A. Corchero. D-OSKIL: A new mechanism for controlling stick-slip oscillations in oil well drillstrings. *IEEE Transactions on Control Systems Technology*, 16(6):1177–1191, Nov 2008.
- [13] N. Challamel. Rock destruction effect on the stability of a drilling structure. *Journal of Sound and Vibration*, 233(2):235–254, 2000.
- [14] N. Challamel, H. Sellami, E. Chenevez, and L. Gossuin. A stick/slip analysis based on rock/bit interaction. *Journal of Petroleum Technology*, 52(12):30–31, 2000.
- [15] A. P. Christoforou and A. S. Yigit. Dynamic modelling of rotating drillstrings with borehole interactions. *Journal of Sound and Vibration*, 206(2):243–260, 1997.
- [16] A. P. Christoforou and A. S. Yigit. Fully coupled vibrations of actively controlled drillstrings. *Journal of Sound and Vibration*, 267(5):1029–1045, 2003.
- [17] Copley Controls. Xenus Plus XTL-230-40. Website: <http://www.copleycontrols.com/Motion/Products/Drives/Digital/xenusPlus.html>, July 2015.
- [18] R.A. Cunningham. Analysis of downhole measurements of drill string forces and motions. *ASME Journal of engineering for industry*, pages 208–216, 1968.
- [19] J. C. A. de Bruin, A. Doris, N. van de Wouw, W. P. M. H. Heemels, and H. Nijmeijer. Control of mechanical motion systems with non-collocation of actuation and friction: A Popov criterion approach for input-to-state stability and set-valued nonlinearities. *Automatica*, 45(2):405–415, 2009.
- [20] F. H. Deily, D. W. Dareing, G. H. Paff, J. E. Otrloff, and R. D. Lynn. Downhole measurements of drill string forces and motions. *ASME Journal of Engineering for Industry*, 90(2):217–225, 1968.
- [21] A. Depouhon and E. Detournay. Instability regimes and self-excited vibrations in deep drilling systems. *Journal of Sound and Vibration*, 333(7):2019 – 2039, 2014.
- [22] E. Detournay and P. Defourny. A phenomenological model for the drilling action of drag bits. *International Journal of Rock Mechanics and Mining Sciences and Geomechanics Abstracts*, 29(1):13–23, 1992.
- [23] E. Detournay, T. Richard, and M. Shepherd. Drilling response of drag bits: Theory and experiment. *International Journal of Rock Mechanics and Mining Sciences*, 45(8):1347–1360, 2008.
- [24] A. Doris. Controlling vibrations in a drilling system. *Patent*, WO 2012/084886 A1, 2012.

- [25] A. Doris. Method and system for controlling vibrations in a drilling system. *Patent*, WO 2013/076184 A2, 2013.
- [26] A. Doris, A. L. Juloski, N. Mihajlović, W. P. M. H. Heemels, N. van de Wouw, and H. Nijmeijer. Observer designs for experimental non-smooth and discontinuous systems. *IEEE Transactions on Control Systems Technology*, 16(6):1323–1332, 2008.
- [27] T.T.B. Dorussen. Experimental model and controller validation for drilling systems. Master of Science Thesis, D&C 2015.057, Eindhoven University of Technology, Department of Mechanical Engineering, 2015.
- [28] dSPACE. DS1103 ppc controller board. Website: <https://www.dspace.com/en/inc/home/products/hw/singbord/ppconbo.cfm>, June 2015.
- [29] V. A. Dunayevsky, F. Abbassian, and A. Judzis. Dynamic stability of drillstrings under fluctuating weight on bit. *SPE Drilling and Completion*, 8(2):84–92, 1993.
- [30] S. Dwars. Recent advances in soft torque rotary systems. In *SPE/IADC Drilling Conference and Exhibition*, SPE/IADC 173037, London, United Kingdom, March 2015.
- [31] M. W. Dykstra, D. C.-K. Chen, T. M. Warren, and J. J. Azar. Drillstring component mass imbalance: A major source of downhole vibrations. *SPE Drilling and Completion*, 11(4):234–241, 1996.
- [32] M. A. Elsayed and D. W. Dareing. Coupling of longitudinal and torsional vibrations in a single-mass model of a drillstring. *Developments in Theoretical and Applied Mechanics*, 17:128 – 139, 1994.
- [33] M. A. Elsayed, R. L. Wells, D. W. Dareing, and K. Nagirimadugu. Effect of process damping on longitudinal vibrations in drillstrings. *ASME Journal of Energy Resources Technology*, 116(2):129–135, 1994.
- [34] E. Fridman, S. Mondié, and B. Saldivar. Bounds on the response of a drilling pipe model. *IMA Journal of Mathematical Control and Information*, 27(4):513–526, 2010.
- [35] Georgii Kobold. KTY-F torque motors. Website: <http://www.georgiikobold.de/en/products/Torque-Motors-KTY.b7059.php>, July 2015.
- [36] M. Géradin and D. Rixen. *Mechanical vibrations: theory and application to structural dynamics*. John Wiley & Sons, Ltd, Chichester, England, 2nd edition, 1997.
- [37] C. Germa, V. Denoël, and E. Detournay. Multiple mode analysis of the self-excited vibrations of rotary drilling systems. *Journal of Sound and Vibration*, 325(1-2):362–381, 2009.
- [38] C. Germa, N. van de Wouw, R. Sepulchre, and H. Nijmeijer. Nonlinear drillstring dynamics analysis. *SIAM Journal on Applied Dynamical Systems*, 8(2):527553, 2009.
- [39] R. Grauwman and I. Stulemeijer. Drilling efficiency optimization: vibration study. Presentation Shell Exploration and Production, Rijswijk, the Netherlands, Dec 2009.

- [40] G. W. Halsey, A. Kyllingstad, and A. Kylling. Torque feedback used to cure slip-stick motion. In *SPE Annual Technical Conference and Exhibition*, SPE 18049, Houston, Texas, U.S.A., October 1988.
- [41] D. Hanselman. *Brushless permanent magnet motor design*. Magna Physics Publishing, 2nd edition, 2003.
- [42] F. Hartung and J. Turi. Linearized stability in functional-differential equations with state-dependent delays. In *Proceedings of the International Conference Dynamical Systems and Differential Equations*, pages 416–425, Atlanta, U.S.A., 2000.
- [43] P. O. Haugom and N. Reimers. A torque converter for use when drilling with a rotating drill bit. *Patent*, WO 2006/075921 A1, 2006.
- [44] W.P.M.H. Heemels, A.L. Juloski, and B. Brogliato. Observer design for Lur’s systems with multi-valued mappings. In *Proceedings of the 16th IFAC World Congress on Automatic Control*, Prague, Czech Republic, July 2005.
- [45] Heidenhain. Encoders for servo drives, pages 70-71. Catalog: [http://www.heidenhain.com/de\\_EN/php/documentation-information/brochures/popup/media/media/file/view/file-0040/file.pdf](http://www.heidenhain.com/de_EN/php/documentation-information/brochures/popup/media/media/file/view/file-0040/file.pdf), July 2015.
- [46] Horn international. Website: <http://hornonline.com/tomax-as/>, June 2015.
- [47] L. Hsieh. Small-scale focus yields big value for shell’s rig operational performance. Drilling contractor, January/February 2015.
- [48] T. Insperger, G. Stépán, and J. Turi. State-dependent delay in regenerative turning processes. *Nonlinear Dynamics*, 47(1-3):275–283, 2007.
- [49] J. D. Jansen. Non-linear rotor dynamics as applied to oilwell drillstring vibrations. *Journal of Sound and Vibration*, 147(1):115–135, 1991.
- [50] J. D. Jansen. *Nonlinear Dynamics of Oilwell Drillstring*. PhD thesis, Delft University of Technology, Delft, The Netherlands, 1993.
- [51] J. D. Jansen and L. van den Steen. Active damping of self-excited torsional vibrations in oil-well drillstrings. *Journal of Sound and Vibration*, 179(4):647–668, 1995.
- [52] M. K. Johannessen and T. Myrvoid. Stick-slip prevention of drill strings using nonlinear model reduction and nonlinear model predictive control. Master of Science Thesis, Norwegian University of Science and Technology, Department of Engineering Cybernetics, 2010.
- [53] M. Karkoub, M. Zribi, L. Elchaar, and L. Lamont. Robust  $\mu$ -synthesis controllers for suppressing stick-slip induced vibrations in oil well drill strings. *Multibody System Dynamics*, 23(2):191–207, 2010.
- [54] H. Khalil. *Nonlinear systems*. Prentice-Hall, 3rd edition, 2002.
- [55] Y. A. Khulief and H. Al-Naser. Finite element dynamic analysis of drillstrings. *Finite Elements in Analysis and Design*, 41(13):1270–1288, 2005.
- [56] Y. A. Khulief and F. A. Al-Sulaiman. Laboratory investigation of drillstring vibrations. In *Proceedings of the Institution of Mechanical Engineers, Part C: Journal of Mechanical Engineering Science*, volume 223, pages 2249–2262, 2009.

- [57] Y. A. Khulief, F. A. Al-Sulaiman, and S. Bashmal. Vibration analysis of drill-strings with self-excited stick-slip oscillations. *Journal of Sound and Vibration*, 299(3):540–558, 2007.
- [58] S. Kjølglum. Analysis of down hole tools for drilling optimization. Master of Science Thesis, Norwegian University of Science and Technology, Department of Petroleum Engineering and Applied Geophysics, 2007.
- [59] Y. Kovalyshen. A simple model of bit whirl for deep drilling applications. *Journal of Sound and Vibration*, 332(24):6321 – 6334, 2013.
- [60] Y. Kovalyshen. Experiments on stick-slip vibrations in drilling with drag bits. In *Proceedings of the 48th US Rock Mechanics Geomechanics Symposium*, Minneapolis, Minnesota, USA, June 2014.
- [61] E. Kreuzer and O. Kust. Analysis of long torsional strings by proper orthogonal decomposition. *Archive of Applied Mechanics*, 67(1-2):68–80, 1996.
- [62] E. Kreuzer and M. Steidl. Controlling torsional vibrations of drill strings via decomposition of traveling waves. *Archive of Applied Mechanics*, 82(4):515–531, 2012.
- [63] A. Kyllingstad and G. W. Halsey. A study of slip/stick motion of the bit. *SPE Drilling Engineering*, 3(4):369–373, 1988.
- [64] A. Kyllingstad and P. J. Nessjøen. A new stick-slip prevention system. In *SPE/IADC Drilling Conference and Exhibition*, SPE/IADC 199660, Amsterdam, Netherlands, March 2009.
- [65] R. I. Leine. Literature survey on torsional drillstring vibrations. Technical Report WFW 97.069, Eindhoven university of technology, Department of Mechanical engineering, 1997.
- [66] R. I. Leine and H. Nijmeijer. Dynamics and bifurcations of non-smooth mechanical systems. In *Lecture notes in applied and computational mechanics*, volume 18. Springer Verlag, 2004.
- [67] R. I. Leine, D. H. van Campen, and W. J. G. Keultjes. Stick-slip whirl interaction in drillstring dynamics. *ASME Journal of Vibration and Acoustics*, 124(2):209–220, 2002.
- [68] R. I. Leine and N. van de Wouw. Stability and convergence of mechanical systems with unilateral constraints. In *Lecture notes in applied and computational mechanics*, volume 36. Springer Verlag, 2008.
- [69] B. Lesso, M. Ignova, F. Zeineddine, J. Burks, and B. Welch. Testing the combination of high frequency surface and downhole drilling mechanics and dynamics data under a variety of drilling conditions. In *SPE/IADC Drilling Conference and Exhibition*, SPE/IADC 140347, Amsterdam, Netherlands, March 2011.
- [70] Z. Li and B. Guo. Analysis of longitudinal vibration of drillstring in air and gas drilling. In *Rocky Mountain Oil and Gas Technology Symposium*, SPE 107697, Denver, Colorado, U.S.A., April 2007. Society of Petroleum Engineers.
- [71] J. Löfberg. YALMIP : A toolbox for modeling and optimization in MATLAB. In *Proceedings of the IEEE International Symposium on Computer Aided Control Systems Design*, pages 284 –289, Taipei, Taiwan, September 2004.

- [72] H. Lu, J. Dumon, and C. Canudas-de Wit. Experimental study of the d-  
oskil mechanism for controlling the stick-slip oscillations in a drilling laboratory  
testbed. In *Proceedings of the IEEE Multi-conference on Systems and Control*,  
pages 1551–1556, Saint Petersburg, Russia, July 2009.
- [73] G. Meinsma. Unstable and nonproper weights in  $\mathcal{H}_\infty$  control. *Automatica*,  
31(11):1655 – 1658, 1995.
- [74] W. Michiels and S.-I. Niculescu. *Stability and Stabilization of Time-Delay Sys-  
tems: An eigenvalue based approach*, volume 12 of *Advances in Design and Con-  
trol*. Society for Industrial and Applied Mathematics, 2007.
- [75] N. Mihajlović, N. Van De Wouw, M. P. M. Hendriks, and H. Nijmeijer. Friction-  
induced limit cycling in flexible rotor systems: An experimental drill-string set-  
up. *Nonlinear Dynamics*, 46(3):273–291, 2006.
- [76] N. Mihajlović, N. van de Wouw, P. C. J. N. Rosielle, and H. Nijmeijer. In-  
teraction between torsional and lateral vibrations in flexible rotor systems with  
discontinuous friction. *Nonlinear Dynamics*, 50(3):679–699, 2007.
- [77] N. Mihajlović, A. A. van Veggel, N. van de Wouw, and H. Nijmeijer. Analysis  
of friction-induced limit cycling in an experimental drill-string system. *ASME  
Journal of Dynamic Systems Measurement and Control*, 126(4):709–720, 2004.
- [78] J.J. Moreau. Unilateral contact and dry friction in finite freedom dynamics.  
In J.J. Moreau and P.D. Panagiotopoulos, editors, *Nonsmooth Mechanics and  
Applications*, volume 302 of *International Centre for Mechanical Sciences*, pages  
1–82. Springer Vienna, 1988.
- [79] K. Nandakumar and M. Wiercigroch. Stability analysis of a state dependent  
delayed, coupled two DOF model of drill-stringvibration. *Journal of Sound and  
Vibration*, 332(10):2575 – 2592, 2013.
- [80] E. M. Navarro-López. An alternative characterization of bit-sticking phenom-  
ena in a multi-degree-of-freedom controlled drillstring. *Nonlinear Analysis: Real  
World Applications*, 10(5):3162–3174, 2009.
- [81] E.M. Navarro-López and E. Licéaga-Castro. Non-desired transitions and sliding-  
mode control of a multi-dof mechanical system with stick-slip oscillations. *Chaos,  
Solitons & Fractals*, 41(4):2035 – 2044, 2009.
- [82] P. J. Nessjøen, A. Kyllingstad, P. D’Ambrosio, I. S. Fonseca, A. Garcia, and  
B. Levy. Field experience with an active stick-slip prevention system. In  
*SPE/IADC Drilling Conference and Exhibition*, SPE/IADC 139956, Amster-  
dam, Netherlands, March 2011.
- [83] Y. Nishimatsu. The mechanics of rock cutting. *International Journal of Rock  
Mechanics and Mining Sciences*, 9(2):261–270, 1972.
- [84] T. Oomen, R. van Herpen, S. Quist, M. van de Wal, O. Bosgra, and M. Steinbuch.  
Connecting system identification and robust control for next-generation motion  
control of a wafer stage. *IEEE Transactions on Control Systems Technology*,  
22(1):102–118, 2014.
- [85] P.A. Patil and C. Teodoriu. A comparative review of modelling and controlling  
torsional vibrations and experimentation using laboratory setups. *Journal of  
Petroleum Science and Engineering*, 112(0):227 – 238, 2013.

- [86] D. R. Pavone and J. P. Desplans. Application of high sampling rate downhole measurements for analysis and cure of stick-slip in drilling. In *SPE Annual Technical Conference and Exhibition*, SPE 28324, New Orleans, Louisiana, U.S.A., September 1994.
- [87] PCM. RT2 - rotating torque transducer. Website: <http://www.pcm-uk.com/transducer-torque-rt2.html>, July 2015.
- [88] L. Perneder and E. Detournay. Steady-state solutions of a propagating borehole. *International Journal of Solids and Structures*, 50:1226 – 1240, 2013.
- [89] Printed Motor Works. GN series. Website: <http://www.printedmotorworks.com/wp-content/uploads/GN-Series-Overview.pdf>, July 2015.
- [90] N. Reimers. Antistall tool reduces risk in drilling difficult formations. *Journal of Petroleum Technology*, 64(1):26–29, January 2012.
- [91] N. Reimers. Mitigation of torsional vibrations and stick-slip induced by aggressive, energy efficient drill-bits. In E. Detournay, V. Denoël, N. van de Wouw, and Y. Zhou, editors, *Third International Colloquium on Nonlinear Dynamics and Control of Deep Drilling Systems*, pages 9–14, Minneapolis, Minnesota, U.S.A., May 2014.
- [92] T. Richard. *Self-Excited Stick-Slip Oscillations of Drag Bits*. Ph. D. Thesis, University of Minnesota, Minneapolis, Minnesota, U.S.A., December 2001.
- [93] T. Richard, C. Gernay, and E. Detournay. A simplified model to explore the root cause of stick-slip vibrations in drilling systems with drag bits. *Journal of Sound and Vibration*, 305(3):432–456, 2007.
- [94] T. G. Ritto, C. Soize, and R. Sampaio. Non-linear dynamics of a drill-string with uncertain model of the bit-rock interaction. *International Journal of Non-Linear Mechanics*, 44(8):865–876, 2009.
- [95] J.P. Riva. Petroleum in encyclopaedia britannica. Website: <http://www.britannica.com/science/petroleum>, July 2015.
- [96] D.J. Runia, R. Grauwman, and I. Stulemeijer. A brief history on the Shell “soft torque rotary system” and some recent case studies. In N. van de Wouw and E. Detournay, editors, *Second International Colloquium on Nonlinear Dynamics and Control of Deep Drilling Systems*, pages 69–76, Eindhoven, The Netherlands, May 2012.
- [97] C. Sagert, F. Di Meglio, M. Krstic, and P. Rouchon. Backstepping and Flatness Approaches for Stabilization of the Stick-Slip Phenomenon for Drilling. In *Proceedings of the 5th Symposium on System Structure and Control*, pages 779–784, Grenoble, France, February 2013.
- [98] B. Saldivar, I. Boussaada, H. Mounier, S. Mondié, and S-I. Niculescu. An overview on the modeling of oilwell drilling vibrations. In *proceedings of the 19th IFAC World Congress*, pages 5169–5174, Cape Town, South Africa, August 2014.
- [99] B. Saldivar, S. Mondié, J.-J. Loiseau, and V. Rasvan. Suppressing axial-torsional coupled vibrations in drillstrings. *Journal of Control Engineering and Applied Informatics*, 15(1):3–10, 2013.

- [100] R. Sampaio, M. T. Piovan, and G. V. Lozano. Coupled axial/torsional vibrations of drill-strings by means of non-linear model. *Mechanics Research Communications*, 34(5-6):497–502, 2007.
- [101] A. Schroter and P. Fuchs. As the coil turns, inductive rotary encoders fill the gap between resolvers and optical rotary encoders. Website: <http://machinedesign.com/archive/coil-turns>, May 2002.
- [102] K.S. Selnes, C. Clemmensen, and N. Reimers. Drilling difficult formations efficiently with the use of an antistall tool. *SPE Drilling & Completion*, 24(4):531–536, 2009.
- [103] A. F. A. Serrarens, M. J. G. van de Molengraft, J. J. Kok, and L. van den Steen.  $\mathcal{H}_\infty$  control for suppressing stick-slip in oil well drillstrings. *IEEE Control Systems Magazine*, 18(2):19–30, 1998.
- [104] Sick. DFS60A incremental encoder. Website: [http://www.sick.com/group/EN/home/products/product\\_portfolio/encoders/Pages/rotary\\_incremental.aspx](http://www.sick.com/group/EN/home/products/product_portfolio/encoders/Pages/rotary_incremental.aspx), July 2015.
- [105] Sieb & Meyer. SD2S drive amplifier. Website: [http://www.sieb-meyer.de/products/items/SD2S\\_Servo.html](http://www.sieb-meyer.de/products/items/SD2S_Servo.html), July 2015.
- [106] S. Skogestad and I. Postlethwaite. *Multivariable feedback control*. John Wiley & Sons, Ltd, 2nd edition, 2005.
- [107] E.D. Sontag and Y. Wang. On characterizations of the input-to-state stability property. *Systems and Control Letters*, 24(5):351–259, 1995.
- [108] E.D. Sontag and Y. Wang. New characterizations of input-to-state stability. *IEEE Transactions on Automatic Control*, 41(9):1283–1294, 1996.
- [109] P. D. Spanos, A. M. Chevallier, N. P. Politis, and M. L. Payne. Oil well drilling: A vibrations perspective. *The Shock and Vibration Digest*, 35(2):81–99, 2003.
- [110] L. van den Steen. *Suppressing Stick-Slip-Induced Drillstring Oscillations: a Hyper Stability Approach*. PhD thesis, University of Twente, Enschede, The Netherlands, 1997.
- [111] J. F. Sturm. Using SeDuMi 1.02, A MATLAB toolbox for optimization over symmetric cones. *Optimization Methods and Software*, 11(1-4):625–653, 1999.
- [112] Tomax. Website: <http://www.tomax.no/resources/field-results/field-results-reamer-process-improvement-year/>, June 2015.
- [113] G.E. Totten. A timeline of highlights from the histories of ASTM committee d02 and the petroleum industry. Website: [http://www.astm.org/COMMIT/D02/to1899\\_index.html](http://www.astm.org/COMMIT/D02/to1899_index.html), July 2015.
- [114] R. W. Tucker and C. Wang. An integrated model for drill-string dynamics. *Journal of Sound and Vibration*, 224(1):123–165, 1999.
- [115] R. W. Tucker and C. Wang. On the effective control of torsional vibrations in drilling systems. *Journal of Sound and Vibration*, 224(1):101–122, 1999.
- [116] R.W. Tucker and C. Wang. Torsional vibration control and cosserat dynamics of a drill-rig assembly. *Meccanica*, 38(1):143–159, 2003.

- [117] U.S. Energy information administration. International energy statistics - total oil supply. Website: <http://www.eia.gov/cfapps/ipdbproject/iedindex3.cfm?tid=5&pid=53&aid=1&cid=ww,&syid=1980&eyid=2014&unit=TBPD>, July 2015.
- [118] M.S. Vassiliou. *Historical dictionary of the petroleum industry*. Scarecrow Press, 2009.
- [119] N. Vljajic and B. Balachandran. Nonlinear and delay effects in drilling mechanics. In E. Detournay, V. Denoël, N. van de Wouw, and Y. Zhou, editors, *Third International Colloquium on Nonlinear Dynamics and Control of Deep Drilling Systems*, pages 51–66, Minneapolis, Minnesota, U.S.A., May 2014.
- [120] T. Vromen, Dai C-H., N. van de Wouw, Oomen. T., P. Astrid, and H. Nijmeijer. Robust output-feedback control to eliminate stick-slip oscillations in drill-string systems. In *Proceedings of the 2nd IFAC Workshop on Automatic Control in Offshore Oil and Gas Production*, pages 272–277, Florianópolis, Brazil, May 2015.
- [121] T. Vromen, C-H. Dai, N. van de Wouw, T. Oomen, P. Astrid, and H. Nijmeijer. Mitigation of torsional vibrations in drilling systems: A robust control approach. *To be submitted*, 2015.
- [122] T. Vromen, N. van de Wouw, A. Doris, P. Astrid, and H. Nijmeijer. Observer-based output-feedback control to eliminate torsional drill-string vibrations. In *Proceedings of the 53rd IEEE Conference on Decision and Control*, pages 872–877, Los Angeles, California, U.S.A., December 2014.
- [123] T. Vromen, N. van de Wouw, A. Doris, P. Astrid, and H. Nijmeijer. Nonlinear output-feedback control of torsional vibrations in drilling systems. *To be submitted*, 2015.
- [124] M. Wiercigroch, E. Pavlovskaja, V. Vaziri, and M. Kapitaniak. Resonance enhanced drilling: Modelling, experiments and design. In E. Detournay, V. Denoël, N. van de Wouw, and Y. Zhou, editors, *Third International Colloquium on Nonlinear Dynamics and Control of Deep Drilling Systems*, pages 1–7, Minneapolis, Minnesota, U.S.A., May 2014.
- [125] Z. Wu and W. Michiels. Reliably computing all characteristic roots of delay differential equations in a given right half plane using a spectral method. Technical Report TW 596, K.U. Leuven, Department of Computer Science, 2011.
- [126] A. S. Yigit and A. P. Christoforou. Coupled axial and transverse vibrations of oilwell drillstrings. *Journal of Sound and Vibration*, 195(4):617–627, 1996.
- [127] A. S. Yigit and A. P. Christoforou. Coupled torsional and bending vibrations of drillstrings subject to impact with friction. *Journal of Sound and Vibration*, 215(1):167–181, 1998.
- [128] A. S. Yigit and A. P. Christoforou. Stick-slip and bit-bounce interaction in oilwell drillstrings. *Journal of Energy Resources Technology, Transactions of the ASME*, 128(4):268–274, 2006.
- [129] A. Zakuan, A.J. Abd Aziz, B. Subroto, H. Hermawan, A.F. Othman, A.H.B. Shariff, and S.A. Jahari. Stick slip mitigation plan to improve drilling. In *Proceedings of the SPE Asia Pacific Oil and Gas Conference and Exhibition*, SPE 141988, Jakarta, Indonesia, September 2011.



- [130] K. Zhou, J.C. Doyle, and K. Glover. *Robust and Optimal Control*. Prentice Hall, 1996.
- [131] Xiaohua Zhu, Liping Tang, and Qiming Yang. A literature review of approaches for stick-slip vibration suppression in oilwell drillstring. *Advances in Mechanical Engineering*, 6, 2014.

---

# Acronyms

---

|      |                                  |
|------|----------------------------------|
| AST  | Anti stick-slip tool             |
| BHA  | Bottom hole assembly             |
| DOC  | depth-of-cut                     |
| DOF  | degree-of-freedom                |
| FEM  | Finite-element method            |
| FRF  | Frequency response function      |
| ISS  | Input-to-state-stability         |
| LFT  | Linear fractional transformation |
| LHP  | Left-half-plane                  |
| LISS | Local input-to-state-stability   |
| LMI  | Linear matrix inequality         |
| LTI  | Linear time-invariant            |
| LWD  | Logging while drilling           |
| MWD  | Measurement while drilling       |
| PDC  | Polycrystalline diamond compact  |
| RHP  | Right-half-plane                 |
| ROP  | Rate-of-penetration              |
| TOB  | Torque-on-bit                    |
| WOB  | Weight-on-bit                    |



---

# Summary

---

This thesis considers the design and implementation of controllers for oil-field drilling systems to eliminate (torsional) stick-slip oscillations. These vibrations decrease the drilling efficiency, accelerate bit wear, and may cause drill-string failure due to fatigue. Increasing demands on the operating envelope of drilling systems and a tendency towards drilling deeper and inclined wells impose higher demands on the controllers used in drilling systems. Current industrial controllers are not always able to eliminate stick-slip vibrations under such increasingly challenging operating conditions. Two main reasons for this deficiency are the influence of multiple dynamical modes of the drill-string on torsional vibrations and the uncertainty in the bit-rock interaction. These issues are addressed in this thesis and controllers to eliminate stick-slip vibrations in drilling systems are designed and experimentally validated.

For the design and analysis of the proposed controller design methodologies, modelling of the drill-string dynamics plays an important role. Most existing controller designs rely on one or two degree-of-freedom models for the torsional dynamics only. The resisting torque-on-bit as a result of the interaction torques at the bit-rock interface is typically modelled as a frictional contact with a velocity-weakening effect. In this work, a similar bit-rock interaction model, with severe velocity-weakening effect, is adopted. In contrast to other studies, however, a multi-modal model of the torsional dynamics is employed, as field observations have revealed that multiple torsional resonance modes play a key role in the onset of stick-slip oscillations. A lumped-parameter model, exhibiting the most dominant torsional flexibility modes and based on a finite-element method representation of a realistic drilling system, is proposed as a basis for controller design.

The nominal operating condition for the drill-string system is associated with a constant angular velocity, therewith avoiding stick-slip vibrations. A controller should (locally) stabilize this constant rotational velocity while using only surface measurements, since real-time down-hole information generally cannot be

obtained in practice. Moreover, the controller has to ensure robustness with respect to uncertainty in the nonlinear bit-rock interaction. Two controller design methodologies that meet these requirements have been developed. The first strategy involves a nonlinear observer-based controller synthesis approach for Lur'e-type systems with discontinuities. Particular benefits of this approach are the fact that a realistic multi-modal model of the drill-string dynamics is taken into account and a guarantee for (local) asymptotic stability of the closed-loop system is given for bit-rock interaction laws satisfying a certain sector condition. The second controller design strategy is based on robust  $\mathcal{H}_\infty$ -control techniques. Also this linear controller design methodology guarantees (local) asymptotic stability of the desired operating point based on surface measurements only, and is applicable to multi-modal models of the drill-string dynamics. Moreover, the designed controller is optimized to obtain robustness with respect to uncertainty in the bit-rock interaction and performance specifications regarding measurement noise sensitivity and actuator limitations are integrated in the controller design.

Based on the drill-string models developed, a novel lab-scale oil-field drill-string system has been designed and realized, which exhibits the essential torsional dynamics of a real drilling system. That is, it captures the first three (torsional) resonance modes of the drill-string dynamics and exhibits stick-slip vibrations when an industrial (SoftTorque) velocity controller is used. A linear  $\mathcal{H}_\infty$ -based controller and state-feedback controller have been implemented on the setup. Both controllers successfully stabilize the desired angular velocity and therewith mitigate stick-slip vibrations on the experimental setup. Experimental validation of the designed controllers is an important intermediate step towards field implementation of the controllers.

Besides active control of stick-slip vibrations, passive down-hole tools for stick-slip suppression have been recently introduced in drilling practice. A specific tool that has been developed to eliminate bit-induced torsional vibrations and to improve drilling efficiency is investigated in this work. This tool couples the axial and torsional motion of the bit relative to the drill-string. Motivated by the fact that recent research has shown that the coupling of the axial and torsional drill-string dynamics through the bit-rock interaction is the root cause for stick-slip vibrations, an existing model of the coupling between the axial and torsional drill-string dynamics is extended with a model of the tool. Dynamic analyses of this model are performed to assess the working principle of such a down-hole tool. Indications of a rate-of-penetration increase and a reduction of the destabilizing velocity-weakening effect in the averaged bit-rock interaction have been revealed. However, further investigation is required to prove these claims and to validate the model with field measurements.

The results in this thesis support the design of controllers and passive down-hole tools to eliminate stick-slip vibrations in drilling systems and therewith contribute to meeting the increasing demands on the operating envelope of drilling systems.

---

# Societal summary

---

Drilling systems are used for the exploration and production of oil, gas, mineral resources, and geo-thermal energy. The primary importance of these resources is their large contribution in the total world energy consumption. Moreover, oil is also of great importance for the production of a wide range of products, such as plastics, soaps and detergents, solvents, synthetic fibers and rubbers. To meet the increasing demand for these resources, the production has increased substantially over the last decades. Because the easy-to-access reservoirs became intensively explored, the drilling industry recognizes an increasing need for drilling in harsher and more difficult environments. To reach such unconventional reservoirs, deep and curved borehole geometries need to be drilled. This tendency towards drilling deeper and inclined wells increases the susceptibility to (torsional stick-slip) vibrations of drilling systems. These drill-string vibrations decrease the quality of the borehole, provoke premature wear of drilling equipment resulting in fatigue and induce failures such as drill pipe twist-off; thereby compromising both the efficiency and safety of drilling operations.

In this research, two controller design strategies have been developed for active feedback control of drilling systems in order to mitigate stick-slip vibrations. As a stepping stone towards field implementation, the controllers have been validated on a lab-scale drill-string system, designed and realized in the scope of this thesis. Simulation and experimental results show that the designed controllers are able to mitigate stick-slip vibrations for operating conditions for which current industrial controllers fail to eliminate stick-slip vibrations. Such drilling automation will support the widening of the operational envelope of drilling systems, which, in turn, will be instrumental in making challenging drilling operations more efficient, reliable and safe.



---

# Samenvatting

---

Dit proefschrift beschouwt het ontwerp en de implementatie van regelaars voor boorsystemen om (torsie) stick-slip oscillaties te voorkomen. Dergelijke trillingen verminderen de efficiëntie van het boorproces en kunnen leiden tot slijtage van de boorkop en de boorpijp. Daarnaast leiden toenemende eisen ten aanzien van het werkgebied van boorsystemen en de trend om steeds dieper te boren tot hogere eisen aan regelaars voor boorsystemen. Regelaars die momenteel gebruikt worden in de industrie zijn door deze toenemende eisen niet altijd in staat om stick-slip trillingen te voorkomen. Twee belangrijke redenen voor deze tekortkoming zijn de invloed van meerdere dynamische modes van de drill-string en onzekerheid in de interactie tussen de boorkop en het gesteente ('bit-rock' interactie). In dit proefschrift worden deze effecten onderzocht en worden regelaars die stick-slip trillingen kunnen voorkomen ontworpen en experimenteel gevalideerd.

Voor het ontwerp en de analyse van regelaars speelt het modelleren van de drill-string dynamica een belangrijke rol. De meeste bestaande regelaars maken gebruik van modellen van de torsie dynamica met slechts een of twee vrijheidsgraden. Hierbij wordt het interactie koppel tussen de boorkop en het gesteente meestal gemodelleerd als een wrijvingskarakteristiek met Stribeck ('velocity-weakening') effect. In dit onderzoek wordt een vergelijkbaar model met een sterk velocity-weakening effect gebruikt. In tegenstelling tot andere studies, wordt er in dit werk echter gebruik gemaakt van een model van de torsie dynamica met meerdere dynamische flexibiliteits modes. Uit metingen blijkt namelijk dat meerdere resonantie modes een rol spelen bij het ontstaan van torsie trillingen. Dit model, dat gebaseerd is op een eindige elementen model van een boorsysteem, is gebruikt als basis voor het ontwerpen van de regelaars.

Een boorsysteem dient met een constante snelheid te roteren en daarmee stick-slip trillingen te voorkomen. Een regelaar heeft als doel deze constante snelheid (lokaal) te stabiliseren waarbij alleen metingen aan het oppervlak gebruikt kunnen worden, omdat 'real-time' metingen dieper in het boorgat meestal niet mogelijk zijn in de praktijk. Daarbij dient de regelaar ook robuustheid ten



opzichte van de onzekerheid in de niet-lineaire bit-rock interactie te garanderen. Twee regelaar ontwerp-strategieën, die aan deze eisen voldoen, zijn ontwikkeld in dit proefschrift. De eerste methode betreft een niet-lineaire regelaar waarbij gebruik gemaakt wordt van een waarnemer voor toestands-schatting. Een aantal voordelen van deze aanpak zijn dat er gebruik gemaakt is van een realistisch model van het boorsysteem met meerdere vrijheidsgraden en dat lokale stabiliteit van het gesloten lus systeem is aangetoond voor bit-rock interactie wetten die aan een bepaalde sector conditie voldoen. De tweede methode is gebaseerd op robuuste  $\mathcal{H}_\infty$ -regelaar technieken. Ook met deze lineaire regelaar kan lokale stabiliteit van het gewenste gedrag worden aangetoond. Daarbij is deze regelaar zodanig ontworpen dat de robuustheid voor onzekerheid in de bit-rock interactie geoptimaliseerd kan worden en specificaties met betrekking tot de prestatie van het systeem, zoals gevoeligheid voor meetruis en beperkingen van de actuator, kunnen worden geïntegreerd in het regelaar ontwerp.

Op basis van de ontwikkelde modellen van de dynamica van een boorsysteem is er een lab-opstelling ontworpen en gerealiseerd om de ontworpen regelaars experimenteel te valideren. Experimentele validatie is een belangrijke tussenstap voordat de regelaars kunnen worden toegepast in het veld. De opstelling bevat de essentiële torsie dynamica van een boorsysteem, dat wil zeggen dat de eerste drie torsie resonantie modes van het systeem zijn meegenomen en dat er, zoals in werkelijkheid, stick-slip trillingen optreden wanneer een industriële (SoftTorque) regelaar wordt toegepast. Vervolgens zijn een lineaire  $\mathcal{H}_\infty$ -regelaar en een regelaar gebaseerd op toestands-terugkoppeling geïmplementeerd. Beide regelaars zijn in staat om de gewenste snelheid te stabiliseren en daarmee stick-slip trillingen te voorkomen.

Naast actief regelen van stick-slip trillingen, bestaan er ook passieve gereedschappen die vlak bij de boorkop geplaatst kunnen worden om stick-slip trillingen te onderdrukken. Een specifiek element dat hiervoor is ontwikkeld en daarnaast de efficiëntie van het boorproces verbetert, is onderzocht in dit werk. Dit element koppelt de axiale en torsie beweging van de boorkop ten opzichte van de drill-string. Aangezien recent onderzoek heeft aangetoond dat de koppeling tussen de axiale en torsie dynamica via de bit-rock interactie de oorzaak is van het ontstaan van stick-slip trillingen, is in dit proefschrift een model dat deze koppeling beschrijft uitgebreid met een model van het ontwikkelde gereedschap. Uit analyse van dit model blijkt dat het gereedschap de axiale snelheid van het boorsysteem (de 'rate-of-penetration') kan verhogen en het destabiliserende effect in de gemiddelde bit-rock interactie kan verminderen. Er is echter verder onderzoek nodig om deze resultaten te bevestigen en het model te valideren met behulp van metingen van een realistisch boorsysteem.

De resultaten in dit proefschrift ondersteunen het ontwerp van regelaars en down-hole instrumenten om stick-slip trillingen in boorsystemen te voorkomen. Met deze resultaten wordt een bijdrage geleverd aan de toenemende behoefte om de grenzen van het werkgebied van boorsystemen te verleggen.

---

# Dankwoord

---

De afgelopen vier jaar zijn voorbij gevlogen en in die periode heb ik ontzettend veel geleerd maar ook heel veel plezier gehad. Ook al is het mijn promotie-onderzoek, ik heb niet het gevoel dat ik het alleen gedaan heb en daarom wil ik graag een aantal mensen bedanken.

Op de eerste plaats wil ik mijn promotoren Henk en Nathan bedanken. In de afgelopen vier jaar heb ik met heel veel plezier met jullie samengewerkt. Henk, bedankt dat je me de mogelijkheid hebt gegeven om binnen jouw groep mijn promotie-onderzoek uit te voeren. Ik heb veel waardering voor je betrokkenheid en steun. Ook wil ik je bedanken voor je input tijdens onze discussies over het project.

Nathan, heel erg bedankt voor je bijdrage aan mijn onderzoek en dit proefschrift. Ik heb ontzettend veel van je geleerd, en tijdens onze discussies wist je me altijd weer de juiste richting op te sturen. Daarnaast wil ik je bedanken voor je kritische blik, je gedetailleerde feedback is zeer waardevol geweest voor de kwaliteit van dit proefschrift. Naast je inhoudelijke bijdrage wil ik je ook bedanken voor de gezelligheid tijdens verschillende conferenties en vooral onze reis naar Brazilië.

Daarnaast wil ik ook iedereen bij Shell die bij dit project betrokken is geweest bedanken. Jan, Jan-Jette, Peter, Sicco, Ivo en Djurre bedankt voor jullie tijd en moeite en natuurlijk voor jullie bijdrage tijdens de project meetings. Daarnaast wil ik Wim bedanken voor de hulp met alles wat met de lab-opstelling te maken heeft. Apostolos, I would like to thank you for your help in the starting phase of the project and the fact that you have always been involved in the background. I would particularly like to thank Patricia. I really appreciate all your effort, our discussions about the project and your support, both on scientific level, as well as, with other things in the project.

I would like to thank Emmanuel Detournay, Walter Lacarbonara and Siep Weiland for taking part in my research committee and for the constructive feedback on my thesis.

Part of this research has been performed in collaboration with Tomax in Stavanger, Norway. Nils, thank you for all the information regarding the AST, the discussions about the model and also for inviting me to visit the Ullrig test rig during the drilling test, which was a very valuable and interesting experience.

Tijdens mijn promotie heb ik samengewerkt met vijf afstudeerders en meerdere resultaten in dit proefschrift zijn mede tot stand gekomen door de resultaten van die verschillende projecten. Cam-Hing, Olaf, Tom, Max en Paul bedankt voor de samenwerking.

Een goede werksfeer draagt natuurlijk bij aan de resultaten. Ik wil dan ook alle collega's van de Dynamics & Control en Control Systems Technology groepen bedanken voor de gezelligheid. De dagelijkse lunch en (vele) koffiepauzes zorgen voor een aangename afwisseling op het onderzoek. Daarnaast zal ik de gezelligheid tijdens de uitjes en verschillende conferenties nooit vergeten. Dennis, Jiquan en Bert, bedankt voor de goede sfeer op ons kantoor en met name Dennis bedankt voor onze gesprekken, die lang niet altijd over onderzoek gingen. Bas, bedankt dat de deur van je kantoor altijd open staat (ook nadat Bram weg was) zodat ik altijd even binnen kon lopen voor een praatje. Bram en Joost, bedankt voor jullie vriendschap, ik hoop dat we elkaar nog regelmatig (misschien iets minder dan de afgelopen 10 jaar) blijven zien!

Naast mijn collega's wil ik uiteraard ook mijn vrienden en familie bedanken. Pap en mam, Karien en Ger en Fleur bedankt voor jullie interesse en steun, maar vooral voor alle leuke en gezellige dingen die we samen beleefd hebben en waarvan er hopelijk nog veel zullen volgen. Pap en mam, ik wil jullie niet alleen bedanken voor de afgelopen jaren maar eigenlijk voor alles wat jullie voor ons doen, jullie adviezen en grenzeloze vertrouwen. Bedankt!

En als laatste Loes, bedankt voor je liefde en steun. Je bent er altijd als ik je nodig heb, om dingen weer positief te bekijken als het even tegenzit maar zeker ook om successen en leuke momenten samen te vieren. Bij jou voel ik me thuis!

*Thijs Vromen  
Eindhoven, oktober 2015*

---

# Curriculum vitae

---

Thijs Vromen was born on October 11, 1987 in Heerlen, the Netherlands. In 2005 he finished secondary education at Sint-Janscollege in Hoensbroek. Subsequently, he studied Mechanical Engineering at Eindhoven University of Technology, the Netherlands, where he obtained his Master's degree (*with great appreciation*) in 2011. As part of this curriculum, he performed an international traineeship at Norwegian University of Science and Technology (NTNU), Trondheim, Norway, in 2009. In this project, Thijs investigated parametric roll resonance of container carriers. His master's thesis was entitled "Control of a mobile robot by an electronic brain" and was carried out under the supervision of Erik Steur and Henk Nijmeijer.

In September 2011, Thijs started his Ph.D. research in the Dynamics and Control group at the faculty of Mechanical Engineering at Eindhoven University of Technology, under the supervision of Nathan van de Wouw and Henk Nijmeijer. The results of this research are presented in this thesis and focus on control of stick-slip vibrations in drilling systems. The research was supported by Shell Global Solutions International B.V., Rijswijk, the Netherlands.

